ULTRASONIC IRRADIATION OF CHEMICAL COMPOUNDS IN AQUEOUS SOLUTIONS

Thesis by

Anastassia Kotronarou

In Partial Fulfillment of the Requirements

for the Degree of

Doctor of Philosophy

California Institute of Technology

Pasadena, California

1992

(Submitted August 6, 1991)

Στους γονείς μου Γιώργο - Λίτσα

Dedicated to my parents George – Litsa

Acknowledgments

I would like to thank several persons who have made it possible for me to spend four of the most educating, productive, and fulfilling years of my life at Caltech. A big thanks goes to my advisor, Michael Hoffmann, for offering me the perfect blend of freedom and guidance, for bringing out the chemist in me, and for having faith in me even when I was doubting myself. Jimmy Mills showed me how to get my hands wet in the lab, gave me some of his enthusiasm for chemistry, and has been an invaluable friend and mentor even from a distance. This thesis could have never been the same without him.

Special thanks go to Norman Brooks, Jim Morgan, and Mary Lidstrom for serving in my examination committees, for teaching me many lessons (not only in the classroom), and for being (each on his/her own way) great role models. Several discussions with Chris Brennen and Allan Acosta have contributed to my better understanding of acoustic cavitation; I am indebted to them.

Claudius Kormann, and the "fog squad" (Bruce Daube, Bill Munger, Jeff Collett, and Dieter Gunz) made my life a lot easier during the first year of my studies here, and introduced me to various lab instruments and facilities. Jochen Kraft helped me get started in one of the projects that is part of this work, and showed me what "being organized" means. The fact that I never really managed to follow his example should not take anything away from Jochen; I suspect that my Greek heritage has something to do with it. Isabel Chen, Martha Shaw, Joel Pedersen, Jeff Noelte, Inez Hua, and Joel Adamson were directly involved in some parts of the experimental work. The fact that most of those parts required working with wastewater certainly makes their help even more appreciated.

I want to acknowledge Rayma Harrison and Gunilla Hastrup for being there with a smile when I needed help in the library, Joe Fontana and Rich Eastvedt for their help in the workshop, Gabor for his eagerness to fix my broken glassware, and

Elena Escot for helping me practice my Spanish. Thanks are also due to Elaine Granger, Fran Matzen, Sandy Brooks, and Karen Hodge for all those "small things" that would amount to a mountain if I had to do them myself.

My fellow students in the Keck building have made these past years much more easier and fun for me. Amy Hoffman, Beth Carraway, Mark Schlautman, Wolfgang Rogge, Talal Balaa, Steve Rogak, Sandy Elliot, Mike Scott, Russell Mau, and Simo Pehkonen are the first whose name comes in mind at that moment. Special thanks go to my officemates Stanley Grant, who helped raise my spirits once too often, and Jeremy Semrau, who gave me the chance to see how falling from 12000 feet feels like. Suzan Haney was a great roommate for over a year. I learned a lot more from her than just vegetarian cooking and gardening.

Thanks are also due to the members of the "Greek Mafia" at Caltech. Especially to Spyro Pandi and his wife Angeliki (for being great opponents for tennis doubles and even greater partners for card games), Michael Kariakli (my Toyota owes a lot to him), and Panagioti Pantzika (always available for a cup of coffee and long discussions). Chris Pilinis deserves a special acknowledgment. He earned it by always being there for me: a shoulder to cry on, a tennis partner, a proofreader, a companion for excursions and for many other things.

I would also like to acknowledge my previous academic advisers, Marcos Bonazountas (at the National Technical University of Athens) and Paul Jawitt (at Imperial College), for introducing me to environmental engineering and for inspiring me to pursue further studies in that area.

Above all, I want to offer a big thanks from the heart to my family: my brother *Αλεξη*, and my parents *Γιωργο* and *Λιτσα*. I will not even try to express my feelings for them, or to mention what they have done for me over the years. This thesis would not mean nearly as much to me if it were not for the joy that I know it will bring to them. *Αγαπητη οικογενεια, ευχαριστω για ολα*!

Abstract

The ultrasonic irradiation of para–nitrophenol, S(–II), and parathion is studied in aqueous solutions at 20 kHz and $\simeq$ 75 W·cm^{-2}. Para–nitrophenol was degraded primarily by denitration and secondarily by ·OH radical attack to yield NO_2^-, NO_3^-, benzoquinone, hydroquinone, 4–nitrocatechol, formate and oxalate. These reaction products and the kinetic observations are consistent with a model involving high–temperature reactions of p–nitrophenol in the interfacial region of cavitation bubbles. The average effective temperature of the interfacial region surrounding the cavitation bubbles was estimated to be T $\simeq$ 800 K.

Ultrasonic irradiation of S(–II) is studied in aqueous solutions over the pH range 7 – 12. The reaction of HS^- with ·OH is the principal pathway for the oxidation of S(–II) at pH $\geq$ 10; the oxidation products are SO_4^{2-}, SO_3^{2-}, and $S_2O_3^{2-}$. Upon prolonged sonication, SO_4^{2-} is the only observed product. At pH $\leq$ 8.5, thermal decomposition of H_2S within or near collapsing cavitation bubbles becomes the important pathway and elemental sulfur is found as an additional product of the sonolysis of S(–II). The sonolytic oxidation of H_2S at pH $\geq$ 10 was successfully modeled with an aqueous–phase free–radical chemistry mechanism and assuming continuous and uniform ·OH input into solution from the imploding cavitation bubbles.

Parathion degradation occurred primarily by enhanced hydrolysis and secondarily by direct ·OH radical attack.

The effect of various physical and chemical parameters on sonolytic yields is examined. The observed effects are in qualitative agreement with the sonolysis mechanisms proposed for the chemicals of interest and the existing hydrodynamic

theories of acoustic cavitation.

The formation of iodine upon ultrasonic irradiation of potassium iodide solutions and the sonolysis of S(–II) are used as probes to compare the sonochemical efficiency of different experimental set–ups.

This work elucidates the mechanisms of the ultrasonic decomposition of typical organic and inorganic pollutants. It is shown that ultrasound has the potential to become a viable alternative for the destruction of chemical contaminants in water and wastewater. The current limitation of sonolysis is its low energy utilization efficiency, but there is room for improvement by optimizing reactor design and physical/chemical operation conditions. This work offers some recommendations and insight in that respect.

Table of Contents

Acknowledgments iv
Abstract vi
Table of Contents viii
List of Tables xii
List of Figures xiii
Thesis Overview and Summary xix

Chapter 1

INTRODUCTION 1
Motivation 2
Research objectives 4
References 5

Chapter 2

AN INTRODUCTION TO THE PHYSICS OF SONOCHEMISTRY 9
Background 10
Acoustic cavitation 11
Introduction 11
Initiation of acoustic cavitation 12
Single bubble dynamics 16
Bubble fields – photographic studies 20
Sonochemistry 23
References 28

Chapter 3

ULTRASONIC IRRADIATION OF p–NITROPHENOL
IN AQUEOUS SOLUTION 31
Abstract 32
Introduction 33
Experimental 34
Results 35
Discussion 52

References 70
Appendix 74

Chapter 4
OXIDATION OF HYDROGEN SULFIDE IN AQUEOUS SOLUTIONS BY ULTRASONIC IRRADIATION 78
Absract 79
Introduction 80
Experimental 82
Results 83
Acknowledgments 115
References 116
Appendix 120

Chapter 5
MATHEMATICAL MODELING OF THE FREE RADICAL CHEMISTRY OF THE S(–II) + OH SYSTEM AND APPLICATION TO THE ULTRASONIC IRRADIATION OF S(–II) 122
Abstract 123
Introduction 124
S(–II) + $^{\cdot}OH$ + O_2 system mechanism formulation 124
Model application to ultrasonic irradiation of S(–II) 132
References 153

Chapter 6
ULTRASONIC IRRADIATION OF IODIDE AND PARATHION IN AQUEOUS SOLUTION 154
Ultrasonic irradiation of iodide 155
Introduction 155
Results and discussion 156
Conclusions 168
Ultrasonic irradiation of parathion 170
Introduction 170
Experimental 170

Results and discussion 171
Conclusion 175
References 176

Chapter 7
EFFECT OF PHYSICAL AND CHEMICAL PARAMETERS ON SONOLYSIS OF CHEMICAL COMPOUNDS 178
Introduction 179
Results and discussion 179
Ionic strength and specific ions 179
Input power and temperature 186
Dissolved gases 188
Vessel type 188
Particles 191
Continuous flow experiments 194
Sonication unit 199
Wastewater 211
Conclusions 214
References 215

Chapter 8
CONCLUSIONS 216
Conclusions 217
Recommendations for future research 221

Appendix A
CATALYTIC AUTOXIDATION OF HYDROGEN SULFIDE IN WASTEWATER A–1
Abstract A–2
Introduction A–3
Experimental Section A–5
Preparation of Cobalt(II)–tetrasodium–tetrasulfophthalocyanine A–5
Reagents A–6

Experimental apparatus A–7
Kinetic data A–8
Results and discussion A–10
Water A–10
Kinetic results in wastewater A–20
Mechanism A–30
Conclusions A–34
Acknowledgments A–35
References A–36

APPENDIX B

PEROXYMONOSULFATE: AN ALTERNATIVE TO HYDROGEN PEROXIDE FOR THE CONTROL OF HYDROGEN SULFIDE B–1
Abstract B–2
Introduction B–3
Experimental B–5
Reagents B–5
Apparatus B–6
Results and discussion B–7
Sulfide oxidation in raw wastewater B–7
Peroxymonosulfate experiments B–9
Kinetics B–9
Stoichiometry B–13
Control experiments with iron salts B–16
Combined additions of HSO_5^- and other chemicals B–19
Conclusions B–21
Acknowledgments B–22
References B–24

APPENDIX C

USMODEL AND EPIS COMPUTER CODES C–1
USMODEL C–2
EPIS C–11
PD0 C–41

List of Tables

Table		Page
2.1	Sonication of water at 20 kHz, 75 $W \cdot cm^{-2}$	21
2.2	Reactions involved in water sonolysis	26
3.1	Calculated first–order p–NP thermal decomposition rates and corresponding effective temperatures of the reaction zone	63
5.1	Chemical species	126
5.2	Equilibrium reactions	127
5.3	Sulfur chemistry	128
5.4	Model parameters	131
6.1	Equilibrium reactions	160
6.2	Free radical iodide chemistry	161
6.3	Effect of dissolved gases on KI sonolysis	165
A.1	Pseudo–first–order rate constants (k_{obs}) for the catalytic oxidation of sulfide in oxygen saturated deionized water	A–11
A.2	Pseudo–first–order rate constants (k_{obs}) for Co(II)TSP catalyzed sulfide oxidation in sewage, under air and oxygen saturation	A–21
A.3	Pseudo–frst–order rate constants (k_{obs}) for Co(II)TSP catalyzed sulfide oxidation in raw sewage, and low oxygen concentrations	A–28
B.1	Pseudo–first–order rate constants (k_{obs}) for the oxidation of sulfide in wastewater	B–8
B.2	Sulfide oxidation in the presence of $FeCl_2$	B–17

List of Figures

Figure		Page
2.1	Nuclei distribution from various sources	14
2.2	Growth and collapse of a bubble in water	22
2.3	Schematic representation of the regions of sono–chemical reactions in aqueous sonochemistry	25
3.1	Absorption spectra evolution with sonication time	37
3.2	[p–NP] and [4–NC] versus sonication time at pH 5	38
3.3	First–order plot of [p–NP] decay at pH 5	39
3.4a	NO_2^- and NO_3^- formation during sonication	40
3.4b	First order plot of NO_x^- formation at pH 5	40
3.5	Hydrogen peroxide generation during sonication	42
3.6	$[H^+]$ vs. time during sonication	44
3.7	Formate and oxalate formation during sonication	45
3.8	p–BQ concentration vs. sonication time at pH 5, $[p–NP]_o = 100\ \mu M$	47
3.9a.	Effect of $[p–NP]_o$ on the rate of p–NP degradation	48
3.9b.	Effect of $[p–NP]_o$ on the initial rate of 4–NC formation	48
3.10	Effect of pH on the rate of p–NP degradation	49
3.11	Percentage of p–NP decayed converted to 4–NC	76
4.1	Ultrasonic Apparatus	83
4.2	Sonication of S(–II) at pH = 10, $T_b = 25\ ^oC$, 75 W/cm^2, $[S(–II)]_o = 196\ \mu M$	86
4.3	Hydrogen peroxide formation versus sonication time	87
4.4	NO_y formation during sonication	88
4.5	Dependence of k_o on $[S(–II)]_o$ at pH 10	90
4.6	$S_2O_3^{2-}$ sonication product distribution at pH 10	91
4.7	S(–II) sonication products distribution in borate and phosphate buffer at pH 10.6	92

4.8	S(–II) sonication product distibution at pH 7.4 and $[S(-II)]_o = 82\ \mu M$	94
4.9	SO_4^{2-} measured in H_2O_2–treated S(–II) solutions ($[S(-II)]_o \simeq 92\ \mu M$) before and after sonication at pH 7.4	95
4.10	Effect of sonicated solution volume; pH 10, $[S(-II)]_o = 100\ \mu M$, $t_{son} = 10$ min	97
4.11	Effect of input power on S(–II) sonication; pH 10, $[S(-II)]_o = 100\ \mu M$	99
4.12	Effect of bulk solution temperature on S(–II) sonication; pH 10, $[S(-II)]_o = 100\ \mu M$	101
4.13	Calculated zero–order and first–order rate constants for S(–II) sonolytic oxidation	113
5.1	[S(–II)] profiles for various OH_{input} values; pH 10, $[S(-II)]_o = 196\ \mu M$, $[O_2]_o = 240\ \mu M$	134
5.2	$[O_2]$ profiles for various OH_{input} values; pH 10, $[S(-II)]_o = 196\ \mu M$, $[O_2]_o = 240\ \mu M$	135
5.3	Main pathways for the S(–II) + OH system in the presence of O_2 at alkaline pH	136
5.4	a)[S(–II)] profiles for different oxygen transfer coefficients; pH 10, $OH_{input} = 3.5\ \mu M \cdot min^{-1}$, $[S(-II)]_o = 196\ \mu M$, $[O_2]_o = 240\ \mu M$. b) corresponding $[O_2]$ profiles	138
5.5	Comparison between [S(–II)] decrease predicted by the free–radical chemistry model and that observed upon ultrasonic irradiation of S(–II) at pH 10, $[S(-II)]_o = 196\ \mu M$, $[O_2]_o = 240\ \mu M$	140
5.6	Comparison between [S(–II)] decrease predicted by the free–radical chemistry model and that observed upon ultrasonic irradiation of S(–II) at pH 10, $[O_2]_o = 240\ \mu M$ and two different $[S(-II)]_o$ low values a) 45 μM, and b) 7 μM.	141
5.7	a) Comparison of calculated [S(–II)] profiles with $[O_2]$ kept constant at air saturation (solid line) and with	

	the oxygen transfer coefficient of Table 5.4 (broken line) at pH 10, OH_{input} = 3.5 $\mu M \cdot min^{-1}$, $[S(-II)]_o$ = 300 μM, $[O_2]_o$ = 240 μM. b) corresponding $[O_2]$ profiles.	142
5.8	a) Comparison of sonolysis data with calculated [S(–II)] profiles with $[O_2]$ kept constant at air saturation (solid line) and with the oxygen transfer coefficient of Table 5.4 (broken line) at pH 10, OH_{input} = 3.5 $\mu M \cdot min^{-1}$, $[S(-II)]_o \simeq 450$ μM, $[O_2]_o$ = 240 μM. b) corresponding calculated $[O_2]$ profiles	143
5.9	Comparison of sonolysis data with calculated [S(–II)] profiles with $[O_2]$ kept constant at air saturation (solid line) at pH 10, OH_{input} = 3.5 $\mu M \cdot min^{-1}$, $[S(-II)]_o \simeq 955$ μM, $[O_2]_o$ = 240 μM	144
5.10	Effect of $[S(-II)]_o$ on initial zero–order S(–II) oxidation rate, k_o	145
5.11	[S(–II)] profile and oxidation product distribution at pH 10, $[S(-II)]_o$ = 196 $\mu M \cdot min^{-1}$. Model results and experimental data	147
5.12	[S(–II)] profile and oxidation product distribution at pH 10.6, $[S(-II)]_o$ = 96 $\mu M \cdot min^{-1}$. Model results and experimental data	148
5.13	Comparison between [S(–II)] decrease predicted by the free–radical chemistry model and that observed upon ultrasonic irradiation of S(–II) at pH 9.0, $[S(-II)]_o$ = 91 μM, $[O_2]_o$ = 240 μM	149
5.14	Comparison between [S(–II)] decrease predicted by the free–radical chemistry model and that observed upon ultrasonic irradiation of S(–II) at pH 8.5, $[S(-II)]_o$ = 88 μM, $[O_2]_o$ = 240 μM	150
5.15	Comparison between [S(–II)] decrease predicted by the free–radical chemistry model and that observed upon ultrasonic irradiation of S(–II) at pH 7.4,	

	$[S(-II)]_o \simeq 80\ \mu M$, $[O_2]_o = 240\ \mu M$	151
6.1	"Weissler's solution" before and after sonication at 20 kHz and 75 W/cm^{-2} for $\simeq$ 10 seconds	157
6.2	Absorption at 350 nm with sonication time; 1M KI, 20 kHz, 75 W/cm^{-2}, SS cell, 25 ml, $T_b \simeq 28\ ^oC$	158
6.3	Comparison of I_3^- yields in the presence of borate buffer (pH 10) and in the absence of buffer (pH_{in} 6.9, pH_{final} 8.8)	162
6.4	Effect of dissolved gas on iodine yield; 1M KI, 100 ml glass cell, $T_b \simeq 28\ ^oC$, 20 kHz, 75 W/cm^{-2}	164
6.5	Products of parathion sonication at 75 W/cm^{-2}, $T_b \simeq$ 28 ^oC, $pH_{in} \simeq 6.0$, and initial parathion concentration of $\simeq 82\ \mu M$	172
7.1	Effect of a) NaCl and b) $CaCl_2$ on the sonolysis of S(–II); $[S(-II)]_o \simeq 200\ \mu M$, pH 10, SS cell	180
7.2	Plot of $\log k_o$ vs $\sqrt{I}$, using the data of Figure 7.1	181
7.3	Plot of $\log k_o$ vs $[Cl^-]$, using the data of Figure 7.1	182
7.4	Effect of KI on S(–II) sonolysis at pH 10	184
7.5	Effect of KI on p–NP sonolysis	185
7.6	Effect of CO_3^{2-}/HCO_3^- on the sonolysis of $S_2O_3^{2-}$	187
7.7	Sonoluminescence patterns observed by Reynolds *et al.* and Crum and Reynolds with a direct immersion horn	190
7.8	Comparison between a glass sonication reactor (30 ml) and the stainless steel cell (25 ml)	192
7.9	Effect of silica particles on S(–II) sonication	193
7.10	Schematic representation of the continuous system	195
7.11	Fraction of S(–II) remaining in the holding reservoir; Q=165ml/min,1/2–in. horn, 80W,$[S(-II)]_o$=200μM,pH=10	198
7.12	Continuous flow sonication; comparison of two different sonication units on the fraction of S(–II) remaining in the reservoir	200

7.13	Sonication of 1 M KI solution. Continuous flow and batch operation using two different power supplies	202
7.14	Sonication of 1 M KI using SS/VC1500 at different nominal outpout powers	203
7.15	Rise in temperature of 25 ml water with sonication time; SS/VC1500, different nominal power	204
7.16	Schematic diagram of cup–horn sonicationreactor configuration	205
7.17	KI – CCl_4 – starch solution sonicated inside a flask in the cup horn	207
7.18	Comparison of the I_3^- release during sonication of a 1M KI solution with the direct immersion horn	208
7.19	Continuous flow sonication with Cup–Horn/VC1500 a) $[S(-II)]_o$ = 200 μM, b) 1 M KI	210
7.20	S(–II) sonication in wastewater (20% borate buffer); pH = 9.5, T_b = 39 °C	212
7.21	S(–II) sonication in wastewater; effect of $[S(-II)]_o$ on first–order reaction rate constant	213
A.1	k_{obs} dependence on [Co(II)TSP] for Co(II)TSP–catalyzed sulfide oxidation in water; T=25 °C, pH=6.7 (phosphate buffer), oxygen saturation ($[O_2]=1.2\cdot10^{-3}$ M)	A–13
A.2	k_{obs} dependence on [S(–II)] for Co(II)TSP catalyzed sulfide oxidation in water; T=25 °C, pH=6.7 (phosphate buffer), oxygen saturation , [Co(II)TSP] = 10^{-7} M	A–14
A.3	k_{obs} values for different catalysts; T=25 °C, pH=6.7, oxygen saturation	A–16
A.4	UV/VIS spectra during a kinetic run in water; $[Ni^{2+}]=3\cdot10^{-5}$ M, $[S(-II)]=10^{-3}$ M, $[O_2]=1.2\cdot10^{-3}$ M (oxygen saturation), pH=6.7, T=25 °C.	A–17
A.5	Co(II)TSP–catalyzed sulfide oxidation; comparison between water and wastewater	A–23
A.6	Co(II)TSP–catalyzed sulfide oxidation; comparison between raw and autoclaved wastewater	A–24

A.7 Dependence of k_{obs} on $[O_2]$ for sulfide oxidation in wastewater; T=25 °C, neutral pH, $[S(-II)]_o = 150\ \mu M$ A–26

A.8 UV/VIS spectra of Co(II)TSP in water and wastewater; $[Co(II)TSP] = 10^{-5}$ M A–29

B.1 S(–II) oxidation by HSO_5^- in wastewater. Percentage of $[S(-II)]_o$ oxidized after 2 minutes of HSO_5^- addition; pH ≃ 7.5, $[O_2]_o \leq 1.5$ ppm, $[S(-II)]_o = 200\ \mu M$ B–12

B.2 S(–II) oxidation by HSO_5^- in wastewater. Effect of $[HSO_5^-]_o$:$[S(-II)]_o$ on effective reaction stoichiometry $[HSO_5^-]_o$:$[S(-II)]_{oxidized}$ B–15

B.3 Combined addition of HSO_5^- and H_2O_2 in water; $[S(-II)]_o = 68\ \mu M$, pH = 6.3 B–20

Thesis Overview and Summary

In this work, the ultrasonic irradiation of selected inorganic and organic compounds is studied in aqueous solutions and under controlled laboratory conditions. Based on the observed kinetics and reaction products, mechanisms for the sonochemical degradation of these compounds are proposed. The effect of various physical and chemical parameters and different ultrasonic devices on sonochemical reaction yields is also examined. This research was motivated by the potential application of sonolysis for the elimination of chemical contaminants found in water.

Chapter 2 presents a literature review on acoustic cavitation, bubble dynamics and aqueous sonochemistry. Acoustic cavitation is the phenomenon where small bubbles (cavities) are formed in the solution under sonication in response to the passage of expansion and compression waves. Current hydrodynamic theories can model the dynamics of single bubbles and provide estimates for the high transient temperatures and pressures that result locally upon implosion of the cavities. It is these transient extreme conditions that lead to chemical transformations of the solvent and the chemical species present in the solution. The primary sonochemical reactions are high temperature reactions taking place in the gas phase, but there are also secondary reactions occurring in the liquid phase that involve species escaping from the gas phase into solution.

Unfortunately, the number and size distribution of cavitation bubbles and the physical conditions inside the bubble and its surrounding region upon collapse cannot be predicted. Furthermore, the existing theories cannot handle bubble fields, where many bubbles of different sizes interact with one another as well as with the sound field. Photographic and holographic methods coupled with sonoluminescence can be used to follow bubble dynamics and probe the intensity of

collapse and the spatial and temporal distributions of cavitation events. Applications of these methods indicate that, even though real bubble fields are very complex, overall behavior of bubble clouds agrees qualitatively with that predicted from hydrodynamic theories for single bubbles.

Para–nitrophenol (p–NP) was chosen as model organic compound since phenol and substituted phenols are significant environmental pollutants. Chapter 3 presents kinetic data and selected mechanistic observations for the sonochemical degradation of p–NP in water. In the presence of ultrasound (20 kHz, 84 Watts, $\simeq$ 75 $W \cdot cm^{-2}$) p–NP was degraded primarily by denitration to yield NO_2^-, NO_3^-, benzoquinone, hydroquinone, 4–nitrocatechol, formate and oxalate. These reaction products and the kinetic observations are consistent with a model involving high–temperature reactions of p–nitrophenol in the interfacial region of cavitation bubbles. The main reaction pathway appears to be carbon–nitrogen bond cleavage. Reaction with hydroxyl radical provides a secondary reaction channel. The average effective temperature of the interfacial region surrounding the cavitation bubbles was estimated to be T $\simeq$ 800 K.

Sulfide [S(–II)] was chosen as model inorganic compound since reduced sulfur species are another class of pollutants commonly found in aquatic environment. Chapter 4 presents the results of an investigation of the kinetics and mechanism of the sonolysis of S(–II), where $[S(-II)] = [H_2S] + [HS^-] + [S^{2-}]$, in oxic aqueous solutions over the pH range 7 – 12. Ultrasonic irradiation of S(–II) at 20 kHz and 75 $W \cdot cm^{-2}$ resulted in its rapid oxidation. The reaction of HS^- with $^{\cdot}OH$ is the principal pathway for the oxidation of S(–II) at pH $\geq$ 10; the oxidation products are SO_4^{2-}, SO_3^{2-}, and $S_2O_3^{2-}$. Upon prolonged sonication, SO_4^{2-} is the only observed product. At pH $\leq$ 8.5, thermal decomposition of H_2S within or near collapsing

cavitation bubbles becomes the important pathway and elemental sulfur is found as an additional product of the sonolysis of S(–II). Oxidation of S(–II) by ultrasonic irradiation may present an alternative method for the control of H_2S in water and wastewater systems.

In Chapter 5, a comprehensive aqueous phase mechanism that describes the free radical chemistry of the S(–II) + hydroxyl radical ($^{\cdot}OH$) system in the presence of oxygen is developed. The oxidation of S(–II) is initiated by reaction with $^{\cdot}OH$ but it is further propagated by a free–radical chain sequence involving O_2. This chemical mechanism is used to model the ultrasonic irradiation of S(–II); $^{\cdot}OH$ input from the imploding cavitation bubbles into the aqueous phase is assumed to be continuous and uniform.

This simplified approach can model adequately the observed sonolytic degradation of S(–II) in air saturated aqueous solutions at high pH but underpredicts the rate of S(–II) disappearance at pH $\leq$ 8.5. These results are in agreement with the pathways for S(–II) sonolysis proposed in Chapter 4 and they indicate that the action of ultrasonic waves on aqueous solutions containing species that are not susceptible to thermal decomposition can be predicted based on the knowledge of the free–radical chemistry of the species. It is also shown that even though aqueous–phase sonochemical reactions are initiated by $^{\cdot}OH$ transfer into the aqueous phase from the cavities, molecular oxygen present in the solution can be the main oxidant if it can propagate a free–radical chain reaction. This observation is important with respect to the application of ultrasound for the control of chemicals in trace amounts in water and wastewater systems.

Chapter 6 presents the results of ultrasonic irradiation of iodide and parathion. The main motivation behind the iodide experiments was to perform a

visual inspection of the ultrasonic field to detect possible inhomogeneities and to obtain all the background information needed for later use of KI as a dosimeter for different ultrasonic apparatus. It is concluded that the mechanism of KI sonolysis could be more complicated than the simple reaction of I^- with $^{\cdot}OH$. Molecular oxygen clearly plays an important role in this free radical oxidation. High temperature reactions of I_2 in the gas phase were suspected but the effect of dissolved gases on I_2 yield seems to indicate otherwise. Potassium iodide can be used as an overall sonochemical dosimeter but a closed system is necessary, since considerable amounts of I_2 produced can be lost through evaporation. The I_2 yield is independent of pH in the neutral to alkaline region.

Parathion is a commonly used organophosphate pesticide that is fairly persistent in natural systems ($\tau_{1/2}$ = 108 days at 20 °C and pH 7.4). Its chemical structure is similar to that of many nerve gases. Ultrasonic irradiation of a parathion–saturated aqueous solution at 20 kHz and 75 W/cm^2 resulted in complete destruction of parathion within 2 hours. The observed products include inorganic species (sulfate, nitrate, phosphate) and simpler organic compounds (mainly p–NP and organic acids) that are known to degrade further under the action of ultrasound. Clearly, ultrasonic irradiation (US) has an advantage versus catalyzed hydrolysis of organophosphates; US results in harmless products, while many of the hydrolytic products (e.g., substituted phenols) may be toxic or cause taste and odor problems in water systems.

Chapter 7 presents the effects of different parameters on the sonolysis yields of the above mentioned chemicals. The observed effects are in agreement with the sonolysis mechanisms proposed in the previous chapters and the existing acoustic cavitation theory. It is shown that specific ions (e.g., halogens) can have significant

catalytic or inhibitory effects for the sonolysis of chemicals. These effects are attributed to high temperature reactions at or near the interfacial region, or reactions with ·OH.

Sonolysis is relatively inefficient with respect to the input energy. It is calculated that only a small portion of the total energy supplied to the direct immersion horn system results in "useful" free–radical reactions. Different commercial ultrasonic apparatus is tested and continuous flow operation is compared to batch experiments. It is suggested that sonication units with larger radiating surfaces (e.g., cup–horn type) are a better choice than localized application of high intensity ultrasound (direct immersion horn type). The operation of both types of sonicators in the flow–through mode does not greatly decrease the sonochemical efficiency of the unit. Sonication of S(–II) in wastewater indicates that sonochemical free–radical reactions are not significantly affected by the complex wastewater matrix.

The main conclusions of this work are summarized in Chapter 8. It is concluded that ultrasound has the potential to be a viable alternative for the destruction of chemical contaminants in water and wastewater. Its low energy utilization efficiency would currently limit its potential use to applications where higher cost could be offset by one or more of the advantages that this novel treatment method presents (e.g., rapid decomposition of otherwise persistent organics, harmless decomposition products, relatively "clean" and "easy" operation). For instance, application of sonolysis for groundwater remediation, or for low–flow pretreatment of industrial wastes could be envisioned for the near future. Furthermore, there is room for improvement of sonolysis by optimizing reactor design and physical/chemical operation conditions.

Appendix A and Appendix B present the results of investigations for novel chemical reagents for the control of S(–II) in water and wastewater. The motivations for this work were *i*) the existing need for new cost–effective methods for the control of hydrogen sulfide in water and wastewater systems, and *ii*) the desire to compare ultrasonic degradation of S(–II) to improved chemical methods for the oxidation of that chemical.

The catalytic effectiveness of cobalt(II)–4,4',4'',4'''–tetrasulfophthalocyanine [Co(II)TSP] for the autoxidation of hydrogen sulfide, S(–II), is presented in Appendix A. At pH 7 and 25°C the rate of S(–II) oxidation is first–order with respect to [S(–II)]. A fractional order on the catalyst is observed. At oxygen concentrations 15 to 200 μM the oxygen dependence can be described by simple Michaelis–Menten kinetics with K = 63 μM. The uncatalyzed oxidation of sulfide by molecular oxygen is found to be faster in wastewater than in clean water. This difference is attributed to microbial oxidation of S(–II) and to catalytic action of transition metals present in wastewater.

Appendix B presents the results of S(–II) oxidation in wastewater by an alternative oxidant, peroxymonosulfate. Peroxymonosulfate, HSO_5^-, is found to be a more rapid and efficient oxidant of S(–II) than either H_2O_2 or Fe(II). The combination of peroxymonosulfate and hydrogen peroxide is additive in terms of S(–II) oxidation, while the combination of peroxymonosulfate and Fe(II) results in a decrease in the effectiveness of Fe(II) as an oxidant. Peroxymonosulfate is shown to be a viable alternative to H_2O_2 for the control of sulfide–induced corrosion in concrete sewers.

The computer code of the mathematical model discussed in Chapter 5 is presented in Appendix C.

CHAPTER 1

INTRODUCTION

Motivation

The elimination and control of chemical contaminants in the environment have become a major regulatory issue in recent years. In order to address this problem, there has been a continuous search for innovative technologies for the removal of inorganic and organic pollutants from water and wastewater. In some situations urgent problems require fast, practical, and cost–effective solutions. The application of ultrasonic irradiation may provide a convenient method for the elimination of problematic pollutants.

Ultrasound is the name given to sound waves with frequencies higher than those to which the human ear can respond (> 16 kHz). The chemical effects of ultrasonic irradiation have been known for more than 50 years[1]. But it is only in recent years that a considerable interest in sonochemistry has arisen. Several books[2-4] and numerous review papers[5-9] have appeared during the last few years. The similarities of sonochemistry to radiation and combustion chemistry have been recognized, and ultrasound has been used to induce or accelerate a variety of chemical reactions[10-19]. Nevertheless, the mechanisms involved in sonochemical reactions are not fully understood. Even though ultrasound has currently a wide range of industrial applications[2-3], its potential as an alternative water and wastewater treatment method has only been explored at a preliminary level so far[20-23].

In this work, the ultrasonic irradiation of selected inorganic and organic compounds is studied in aqueous solutions under controlled laboratory conditions. Based on the observed kinetics and reaction products, mechanisms for the sonochemical degradation of these compounds are proposed. The effect of various

physical and chemical parameters and different commercial ultrasonic apparatus on sonochemical reaction yields is also examined. The motivation for this work is the potential application of ultrasound for the pyrolytic and oxidative control of hazardous chemicals in water systems. However, the primary focus is directed toward the fundamental chemistry of the sonolysis of chemicals.

Para–nitrophenol (p–NP) was chosen as model organic compound since phenol and substituted phenols are significant environmental pollutants. Small amounts of phenolic compounds can cause taste and odor problems in water supplies, especially after chlorination[23]. Phenolic compounds are also relatively difficult to remove by conventional wastewater treatment methods, particularly when present at high concentrations. Phenols have been often used as model compounds for wastewater in experimental studies on the feasibility of wastewater treatment methods[20,23]. There are data available in the literature on the degradation of phenolic compounds by thermal decomposition[24] and radiolysis[25-27]. Furthermore, information exists about the oxidation of phenol in an ultrasonic field[28]. Even though this information is rather qualitative, it definitely suggests that phenolic compounds can be degraded sonochemically.

Sulfide [S(–II)] was chosen as model inorganic compound since reduced sulfur species are another class of pollutants commonly found in aquatic environment. They have both natural (geochemical and biological) and anthropogenic (fossil fuel refining and combustion) sources. Hydrogen sulfide (H_2S) and mercaptans (RSH) have characteristically unpleasant odors and very low threshold concentrations (<1 ppbv). Even in very low concentrations, these compounds may create odor and taste problems in drinking water supplies[29]. In natural waters, sulfides and mercaptans are toxic to many aquatic organisms[30]. Odor and corrosion problems

associated with the presence of hydrogen sulfide are often encountered in geothermal power plants[31] and oil refineries[32]. Hydrogen sulfide is also a major contributor to objectionable odors and corrosion in wastewater collection and treatment facilities, and it represents a significant safety hazard to plant personnel[33,34]. Despite extensive research that covers both laboratory and field scale[35-46], there is still an urgent need for novel cost–effective methods for the control of hydrogen sulfide in water and wastewater systems[33,47].

Research objectives

The main research objectives of this thesis were:

- To select model chemicals of environmental importance and examine their behavior in aqueous solution when exposed to ultrasonic irradiation.
- To understand the mechanisms of the sonolytic decomposition of the selected model chemical compounds.
- To study the effect of various physical and chemical parameters on the sonochemical reaction yields and attempt to correlate the experimental results with existing acoustic theory.
- To evaluate the feasibility of the use of ultrasound as an alternative for the destruction of chemicals in water and wastewater.

References

1. Richards, W. T.; Loomis, A. L. *J. Am. Chem. Soc.*, 49, 3086–3100 (1927).
2. Suslick, K. S. (ed.). Ultrasound: Its Chemical, Physical and Biological Effects, VCH, New York (1988).
3. Mason, T. J.; Lorimer, J. P. Sonochemistry. Theory, applications and uses of Ultrasound in Chemistry. Ellis Horwood, Ltd. (1988).
4. Shutilov, V. A. Fundamental Physics of Ultrasound; Gordon & Breach Science Publishers: New York (1988).
5. Suslick, K. S. *Modern Synthetic Methods*, 4, 1–60 (1986).
6. Lorimer, J. P.; Mason, T. J. *Chem. Soc. Rev.*, 16, 239–274 (1987).
7. Henglein, A. *Ultrasonics*, 25, 6–16 (1987).
8. Margulis, M. A. *Russ. J. Phys. Chem.*, 50, 1–11 (1976).
9. Suslick, K. S. *Scientific American*, 80–86, Feb (1989).
10. (a) Hart, E. J.; Fischer, C–H.; Henglein, A. *J. Phys. Chem.*, 94, 284–290 (1990).

    (b) Gutierrez, M.; Henglein, A. *ibid.*, 92, 2978–2981 (1988).

    (c) Fischer, Ch.–H.; Hart, E. J.; Henglein, A. *ibid.*, 90, 1954–1956 (1986).

    (d) Hart, E. J.; Fischer, C–H.; Henglein, A. *ibid.*, 90, 5989–5991 (1986).

    (e) Henglein, A; Gutierrez, M. *Int. J. Radiat. Biol.*, 50, 3, 527–533 (1986).

    (f) Hart, E. J.; Henglein, A. *J. Phys. Chem.*, 89, 4342–4347 (1985).

    (g) Henglein, A.; Kormann, C. *Int. J. Radiat. Biol.*, 48, 251–258 (1985).

    (h) Hart, E. J; Henglein, A. *J. Phys. Chem.*, 89, 4342–4347 (1985).

    (i) Gutierrez, M.; Henglein, A.; Fischer, Ch.–H. *Int. J. Radiat. Biol.*, 50, 313 (1986).
11. (a) Alegria, A. E.; Lion, Y.; Kondo, T.; Riesz, P. *J. Phys. Chem.*, 93,

4908–13 (1989).

(b) Murali Krishna, C.; Kondo, T.; Riesz, P. *ibid.*, 93, 5166–5172 (1989).

(c) Murali Krishna, C.; Lion, Y.; Kondo, T.; Riesz, P. *ibid.*, 91, 5847–5850 (1987).

(d) Kondo, T.; Murali Krishna, C.; Riesz, P. *Radiat. Res.*, 118, 211 (1989).

(e) Murali Krishna, C.; Kondo, T.; Riesz, P. *Radiat. Phys. Chem.*, 32, 121 (1988).

(f) Kondo, T.; Murali Krishna, C.; Riesz, P. *Int. J. Radiat. Biol.*, 53, 891 (1988).

12. (a) Margulis, M. A. *Russ. J. Phys. Chem.*, 50, 9, 1358–1360 (1976).

(b) Margulis, M. A. *Russ. J. Phys. Chem.*, 50, 9, 1361–1363 (1976).

(c) Margulis, M. A. *Russ. J. Phys. Chem.*, 50, 4, 534–537 (1976).

13. (a) Suslick, K. S.; Hammerton, D. A.; Cline, D. E., Jr. *J. Am. Chem. Soc*, 108, 5641–5642 (1986).

(b) Suslick, K. S.; Hammerton, D. A. *IEEE Trans. UFFC–33*, 2, 143–147 (1986).

14. (a) Makino, K.; Massoba, M. M.; Riesz, P. *J. Phys. Chem.*, 87, 1369–1377 (1983).

(b) Makino, K.; Massoba, M. M.; Riesz, P. *J. Am. Chem. Soc.*, 104, 3537 (1982).

15. (a) Sehgal, C. M.; Wang, S. Y. *IEEE Trans. SU–30*, 37, 374–379 (1983).

(b) Sehgal, C. M.; Wang, S. Y. *J. Am. Chem. Soc.*, 103, 6606–6611 (1981).

16. Mead, E. L.; Sutherland, R. G.; Verall, R. E. *Can. J. Chem.*, 54, 1114–1120, (1975).

17. Todd, J. H. *Ultrasonics*, 234–238, Oct (1970).

18. Anbar, M.; Pecht, I. *J. Phys. Chem.*, 71, 5, 1246–1249 (1986).

19. Cauwet, G.; Coste, C. M.; Knoche, H.; Longuemard, J. P. *Bull. Soc. Chim. Fr.*, 1–2, 45–48 (1976).

20. Turai, L. L.; Rosario, F. *Appita*, 35, 5, 407–411 (1982).

21. Dahi, E. *Wat. Research*, 10, 677–684 (1976).

22. Masschelein, W. (ed.). Ozonation Manual for Water & Wastewater Treatment, 92–102 (1982).

23. Chen, J. W.; Chang, J. A.; Smith, G. V. *Chem. Eng. Prog. Symp. Ser.*, 67, 109, 18–26 (1971).

24. Dearson, W. R.; Kderner, W. E.; Munch, R. H. *Ind. Eng. Chem.*, 51, 1001–1004 (1959).

25. Hashimoto, S; Miyata, T.; Washino, M.; Kawakami, W. *J. Am. Chem. Soc.*, 13, 1, 71–75 (1979).

26. O'Neil, P.; Steenken, S.; VanDerLinde, H.; Schulte–Frohlinde, D. *Radiat. Phys. Chem.*, 12, 13–17 (1987).

27. Suarez, C.; Louys, F.; Gunther, K.; Eiben, K. *Tetrahedron Letters*, 8, 575–578 (1920).

28. Lur'e, Y. Y.; Kandzas, P. F.; Mokina, A. A. *Russ. J. Phys. Chem.*, 36, 12, 1422–1425 (1962).

29. Chen, K. Y.; Morris, J. C. *Environ. Sci. Technol.*, *6*, 529–537 (1972).

30. O'Brien, D. J.; Birkner, F. B. *Environ. Sci. Technol.*, *11*, 1114–1120 (1977).

31. Weres, O.; Tsao, L.; Chatre, R. M. *Corrosion*, *41*, 307–316 (1985).

32. Snavely, E. S.; Blount, F.E. *Corrosion*, *25*, 397–404 (1969).

33. ASCE, Manuals and reports on Engineering Practice, 69 (1989).

34. National Research Council. Hydrogen Sulfide, University Park Press,

Baltimore (1979).

35. Millero, I. J. *Marine Chemistry*, 18, 121–147 (1986).

36. Kuhn, A. T.; Kelsall, G. H.; Chana, M. S. *J. Chem. Tech. Biotechnol.*, 33A, 406–414 (1983).

37. Chen, K. Y.; Gupta, S. K. *Environmental Letters,* 4,3, 187–200 (1973).

38. Millero, F. J.; Hershey, J. P. in *ACS Symp.*, New Orleans, Sept. (1987).

39. Wilmot P. D.; Cadee, K.; Katinic, J. J.; Kavanagh, B. V. *Journal WPCF, 60*, 7, 1264–1270 (1988).

40. Pomeroy, R.; Bowlus, F. D. *J. Sewage Works*, 18, 4, 597–640 (1946).

41. (a) Hoffmann, M. R.; Lim, B. C. H. *Environ. Sci. Technol., 13*, 1406–1414 (1979).

(b) Hong, A. P.; Boyce, S. D.; Hoffmann, M. R. *Environ. Sci. Technol., 23*, 533–540 (1989).

(c) Leung, K.; Hoffmann, M. R. *Environ. Sci. Technol., 22*, 275–281 (1988).

42. Dohnalek, D. A.; FitzPatrick, J. A. *J. Am. Water Works Assoc., 65*, 298–308 (1983).

43. (a) Ueno, Y. *J. WPCF*, 46, 12, 2778–2784 (1984).

(b) Ueno, Y. *Water Research*, 10, 317–321 (1976).

44. Chen, K. Y.; Morris, J. G. *J. of the San. Eng. Div., Proc. ASCE, SA1*, 215–227 (1972).

45. Cadena, F.; Petres, R. *J. WPCF*, 60, 7, 1259–1263 (1988).

46. Hoffmann, M. R. *Environ. Sci. Technol., 11*, 61–66 (1977).

47. Borgarello, E.; Pappa, R.; Serpone, N.; Pelizzetti, E. In: Photocatalysis and Environment, M. Schiavello (ed.), Kluwer Academic Publ., pp 567–581 (1988).

CHAPTER 2

AN INTRODUCTION TO THE PHYSICS OF SONOCHEMISTRY

Background

Ultrasound is the name given to sound waves having frequencies higher than those to which the human ear can respond (>16 kHz). The upper limit of ultrasonic frequency is not sharply defined but is usually taken to be 5 MHz for gases and 500 MHz for liquids and solids[1].

When a sound wave passes through a liquid or a gas the molecules of the medium vibrate longitudinally in the direction of the wave propagation. Pressure variations (rarefaction and compression cycles) are associated with the movement of the molecules. For a sinusoidal sound source, the acoustic pressure at any time t is given by $P(t) = P_a \cdot \sin 2\pi ft$, where P_a = maximum pressure amplitude, f = frequency of the sound wave. The following relationship exists between the intensity of the sound source (I = energy per unit area per unit time) and P_a:

$$I = P_a^2/2\rho c \qquad (2.1)$$

where ρ = density of the medium, c = velocity of sound in that medium ($c = f\lambda$, where λ is the wavelength of the sound wave; $c \simeq 1450$ m/s for water). For water ($\rho = 1$ kg/m^3), equation (2.1) gives $P_a \simeq 1.7\ I^{0.5}$, where P_a is in atm and I in W/cm^2.

The intensity decreases with distance traveled by the wave (sound attenuation) due to energy losses. For the one–dimensional case, the intensity at a distance, l, from the source is given by[1]:

$$I = I_o\, e^{-2\alpha l} \qquad (2.2)$$

where I_0 is the intensity at the source and α is an overall attenuation coefficient that includes frictional losses, thermal conduction losses, and other energy losses represented by the bulk viscosity. For constant T, α is proportional to f^2, and a value of $\alpha/f^2 = 21.5 \times 10^{-17}$ $sec^2 \cdot cm^{-1}$ was observed experimentally for a wide variety of frequencies in water[1]. On the basis of this value, 1% loss in the intensity will be noticed in $\simeq$ 600 m, 23 m and 23 cm at 20 kHz, 100 kHz and 1 MHz, respectively. Therefore, higher frequency ultrasound is associated with higher energy losses. For 20 kHz sound waves, energy losses are negligible for short distances.

Following the existing nomenclature, the terms sonication, insonation, and ultrasonic irradiation are used in this work interchangeably, and they all refer to the introduction of ultrasound into a medium.

Acoustic cavitation

Introduction

The term cavitation refers to the formation and the subsequent dynamic life of bubbles in liquids. These bubbles will be filled with vapor and/or gases present in the liquid. Cavitation is brought about by tension produced by pressure variations and may be of hydrodynamic, thermal or acoustic origin. It can occur in many fluids such as water, organic solvents, biological fluids, liquid helium and molten metals[2].

Acoustic cavitation, i.e., cavitation taking place when a medium is subjected to ultrasonic irradiation is accepted to be the most important physical mechanism involved in sonochemistry[1-4]. This section focuses on acoustic cavitation in water.

Initiation of acoustic cavitation

The tensile strength of a pure liquid is determined by the attractive intermolecular forces which maintain its liquid state. In order for a cavity to form during sonication of a pure liquid, the total pressure during the rarefaction cycle must overcome the tensile strength of the medium. The tensile strength of water in the complete absence of impurities has been calculated to be in excess of 1000 atm[3]. However, cavitation thresholds (i.e., acoustic pressure amplitudes to which the liquid is exposed when cavitation is first detected) of the order of 1 atm are measured for water without protracted purification[2].

It is generally accepted that inhomogeneities in water serve as preferential sites for liquid rupture[1-6]. Furthermore, free gas bubbles present in a liquid in small numbers (i.e., not near gas saturation) are not accepted as the main source of nucleation sites[1,2], since theoretical calculations show that small bubbles will dissolve very fast due to surface tension[7] while large bubbles will rise to the surface[8]. Therefore, mechanisms that prevent dissolution of microbubbles have been postulated and they have been reviewed by Crum[6] and more recently by Atchey & Crum[8]. The two main models are: *i*) the organic skin model, that assumes that surface–active–organic molecules form "skins" on the surface of the gas bubbles preventing them from dissolving, and *ii*) the crevice model that accepts the existence of gas pockets in crevices of hydrophobic solid impurities present in water; during the rarefaction cycle (and if a critical "vacuum" threshold is exceeded) the gas pocket grows releasing small free bubbles into the solution or, it undergoes violent collapse itself. A mathematical description of the crevice model where the acoustic cavitation threshold is primarily a function of surface tension

and dissolved gas concentration has been presented[6].

Atchley & Crum[8] have summarized the results of a number of cavitation threshold measurements in water. The observed cavitation threshold decreases with increasing amount of dissolved gases and increasing number and size of solid contaminants, is directly proportional to the hydrostatic pressure applied to the liquid and varies inversely with surface tension and temperature.

Assuming ideal gas behavior, the following expression can be calculated[3-4] for the minimum rarefaction pressure (i.e., "vacuum"), P_b, that must be applied in order to create a bubble of radius R_o (refs. 1, 2, and 3 among others) :

$$P_b = P_h + \frac{2}{3}\left[\frac{(2\sigma/R_o)^3}{3(P_h - P_v + 2\sigma/R_o)}\right]^{0.5} \qquad (2.3)$$

where σ = surface tension (76 dynes/cm for pure water, $\simeq$ 72 dynes/cm for tap water), P_h = ambient pressure, and P_v = saturation vapor pressure ($\simeq$ 0.03 atm at 25 °C for water). P_b is known as Blake's threshold pressure since it was first introduced by Blake[9] (with $P_v = 0$).

In most sonochemical experiments a gas saturated solution is used, and the question of inception of cavitation does not arise since enough nuclei are present to initiate bubble formation. Figure 2.1 is reproduced from Katz & Acosta[10] and summarizes measured nuclei distributions from various sources. The term nuclei is used here to denote free–gas bubbles; sometimes "nuclei" is used as a generic term and includes all inhomogeneities that can result in the formation of a cavity. The number density distribution function, N(R), is defined so that the total number of nuclei with sizes between R_o and $R_o + dR$ is $N(R_o)dR_o$ per unit volume. Gavrilov[11]

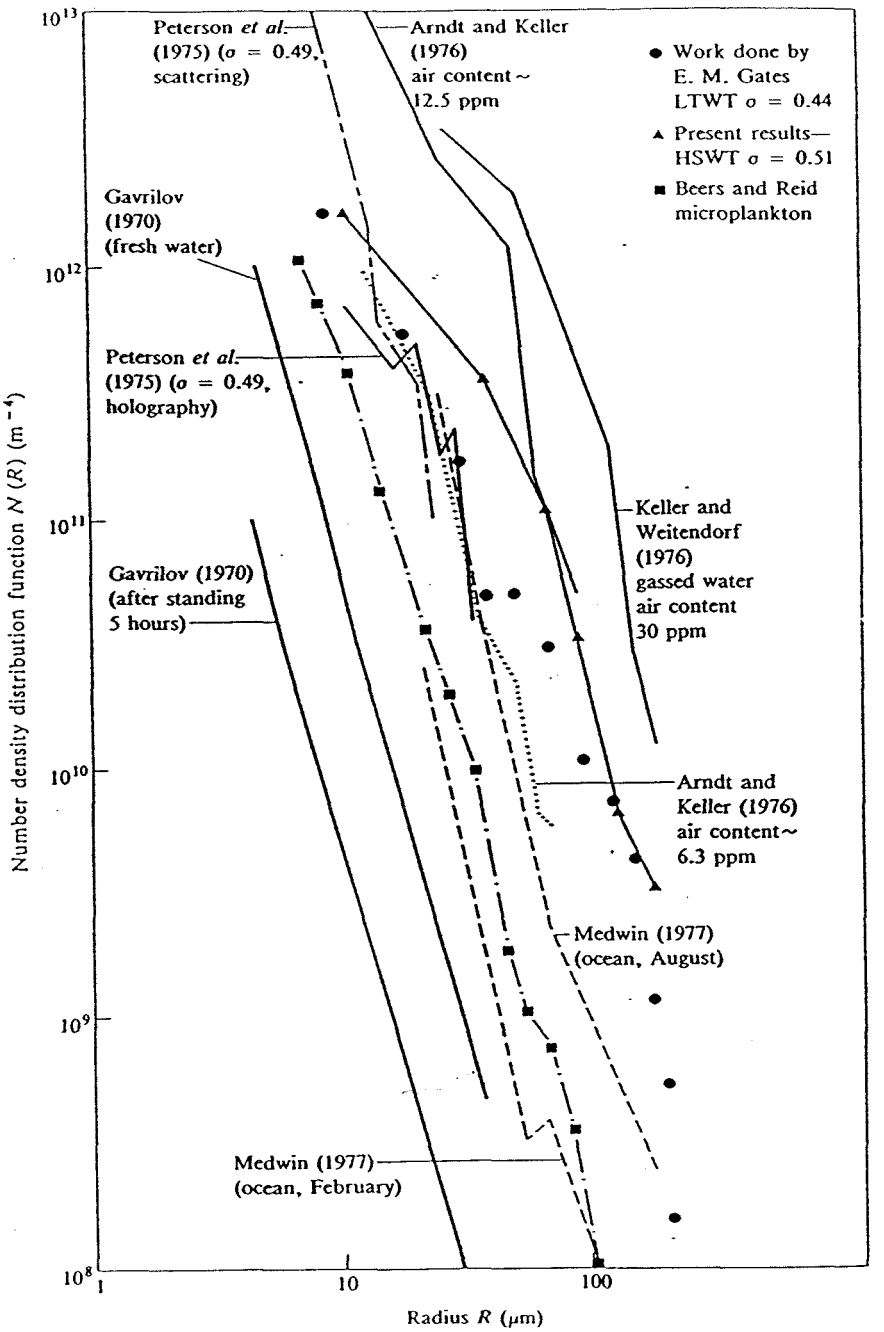

Figure 2.1 Nuclei distribution from various sources. Figure is reproduced from Ref. 12 and was presented originally by Katz and Acosta (1982)

used thermodynamic arguments to conclude that N(R) must be proportional to R^{-3}. As it can be seen in Fig. 2.1, the experimental data of various investigators can be represented by

$$N(R) = A/R^n \tag{2.4}$$

where A is a constant and the value of n is around 3. Gavrilov[11] suggested the use of eq. (2.4) with $A = 10^{-9}$ cm^{-4} and $n = 3$ (R in cm) for water allowed to settle for a long time. It is noted that various acoustical, optical and electrical methods have been used in order to perform measurements of the number and size distribution of gas bubbles. A review of those methods can be found in Ref. 12.

After the onset of cavitation, imploding bubbles will also contribute to the number of available nucleation sites by adding smaller bubbles into the solution. It is expected that the number of nuclei is increased by several orders[13] and that the relative distribution changes too. However, there are no experimental data that give N(R) under sonication. Hansson *et al.*[14] have presented numerical calculations of the expected total number and average diameter of bubbles during sonication with an ultrasonic probe at 20 kHz near a solid surface. Their analysis assumes a continuum of single size bubbles (all bubbles present in the solution before sonication are assumed to be of the same size, and that size changes with sonication). Such an assumption may be justified when the total volume of gas is of interest, e.g., for determining the compressibility of the medium. However, the actual bubble size distribution is important for sonochemical applications since the size of a bubble will determine its fate and, consequently, the type and intensity of the resulting chemical phenomena.

Single bubble dynamics

The formulation of the general hydrodynamic problem of a single bubble in a liquid exposed to a time variable pressure involves: *i*) writing the equations of conservation of mass, momentum, and energy for both the gas and the liquid phases, *ii*) matching of these equations at the interface between the gas and the liquid, and *iii*) using the proper equations of state for the gas and the liquid. The pressure and velocity fields and the motion of the bubble wall could then be determined by solving the system of the non–linear differential equations. However, the general problem is too complicated to solve and the use of simplifying assumptions is necessary in order to arrive to a system that is amenable to numerical or even analytical solution.

The following equation for the motion of the bubble wall is commonly used for bubble cavitation:

$$RR+(3/2)R^2=(1/\rho)[(P_o+2\sigma/R_o-P_v)(R_o/R)^{3k}-P_o-P_a\sin\omega t-2\sigma/R-(4\mu R)/R] \quad (2.5)$$

where: R = bubble radius, R_o = initial radius, ρ = liquid density, P_o = ambient pressure, $P_a\sin\omega t$ = acoustic pressure, P_v = vapor pressure, σ = surface tension, μ = viscocity, κ = polytropic exponent [between 1 (isothermal) and γ (adiabatic)], and dots indicate differentiation with respect to time.

This equation is usually referred to as the Rayleigh–Plesset equation, but the name R.P.N.N.P. used by Neppiras[15] seems more appropriate since it refers to all of the basic contributors: Rayleigh[16], Plesset[17], Nolting & Neppiras[18,19], and Poritsky[20]. It assumes incompressible liquid, constant gas content, sound

wavelength large compared with bubble dimensions, ρ, κ of liquid small compared with that of gas, and spatially uniform conditions within the bubble, and neglects damping (because of thermal conduction or acoustic radiation), heat and mass transfer, body forces (e.g., gravity), and loss of spherical shape.

There is a generally accepted division of cavitation phenomena in homogeneous liquids into[2]: *i*) stable cavitation, in which a bubble oscillates many times with limited change about its equilibrium radius, and *ii*) *transient* cavitation, in which a short lived small bubble undergoes violent radial pulsations in a few acoustic cycles and may terminate in violent collapse. Both forms of cavitation may occur simultaneously in a solution and a bubble undergoing stable cavitation may change to transient cavitation.

Stable cavitation is commonly the case for low sound intensities (1–3 W/cm^2) and bubbles are believed to contain mainly gas (since they live long enough for gases to diffuse into them). The resonance frequency, f_{res}, of a bubble of radius R is given by[15]:

$$f_{res} = [\ 1/(2\pi R)\ ]\ \{[3\kappa(P_o+(2\sigma/R))-(2\sigma/R)]/\rho\}^{0.5} \qquad (2.6)$$

where ρ, κ, and P_o are as for equation (2.5). It can be calculated that at 20 kHz and 1 MHz the resonance size of cavities is $\simeq$ 170 μm and 3.3 μm respectively. If surface tension is neglected (large bubble), equation (2.6) is simplified to :

$$f_{res} = [\ 1/(2\pi R)\ ]\ (3\gamma P/\rho)^{0.5} \qquad (2.7)$$

where P = pressure inside the bubble. For air bubbles in water at 1 atm, eq. (2.6)

gives $f_{res} \cdot R \simeq 3$ (f_{res} in Hz, R in m).

Transient cavitation is believed to occur in liquids exposed to high sound intensities (>10 W/cm^2)[4] and transient gas bubbles are mostly filled with vapor; this leads to violent collapse since there is not much gas present to cushion the impact of the implosion. Assuming adiabatic conditions upon collapse, the following equations have been developed for the time of collapse, τ, the maximum pressure, P_{max}, the maximum temperature, T_{max}, and the maximum Mach number, M_{max} [15]:

$$\tau = 0.915\, R_{max}(\rho/P_m)^{0.5}(1+Q/P_m) \tag{2.8}$$

$$P_{max} = Q\left[\frac{P_m(k-1)}{Q}\right]^{\frac{k}{k-1}} = Q\, Z^k \tag{2.9}$$

$$T_{max} = T_o\left[\frac{P_m(k-1)}{Q}\right] = T_o\, Z^{k-1} \tag{2.10}$$

$$M_{max} = (0.015\,(R_{max}/R_{min})^{1.5}(P_m/Q), \text{ for } R_{max}/R_{min} \geq 4 \tag{2.11}$$

where: R_{max}, R_{min} = maximum and minimum bubble radius (at start and end of collapse), P_m = liquid pressure at collapse, Q = initial gas pressure, k = polytropic exponent, Z = volume compression ratio = $(R_{max}/R)^3$.

The polytropic exponent is again used in the place of γ (ratio of specific heats). The assumptions of eq. (2.5) are also implied. The incompressibility assumption is valid for $M \leq \sim 0.2$, that corresponds to $(P_m/Q) \leq \sim 100$ [15]. The above equations should only be used as an approximation to get the order of magnitude for T, P upon bubble collapse. However, they demonstrate the importance of the dissolved gas (γ is 5/3, 7/5, and 4/3 for monoatomic, diatomic,

and triatomic gases), and of the vapor pressure (affects Q; P_v increases with increasing temperature and gas solubility).

Modifications of eq. (2.5) have been proposed where some of the assumptions have been relaxed (and usually replaced by others that are more justified). For example, Gilmore[21] included the compressibility of the liquid by using the Kirkwood–Bethe approximation[22] (wave propagates with velocity equal to the sum of the sound and the fluid velocity) and neglected the effect of surface tension and viscocity. Heat conduction was added by Hickling & Plesset[23], who showed that Gilmore's approximation is in general justified. Margulis & Dmitrieva recently included heat exchange[24] and presented calculations for cavitation bubbles containing air, Ar, He, and water vapor[25]. The overall collapse time did not differ much from that given from eq. (2.8). However, rate of collapse and maximum temperature were shown to be about twofold lower than those calculated from eqs. (2.9) and (2.10), and the minimum R attained is about twofold higher than that of adiabatic collapse.

The growth of small microbubbles to bubbles of larger size can be explained by the mechanism of rectified diffusion, i.e., unequal mass transfer across the gas–water interface during bubble oscillation. Not all bubbles initially present in the solution will cavitate. Furthermore, cavitating bubbles will be either stable or transient, or will go from one type of cavitation to the other. Cavitation thresholds can be found by setting criteria for the onset of transient cavitation and with the use of eq. (2.5) or even a more simplified non–linear equation of motion. The increase of the radius of the bubble to approximately double its original size, or wall velocity approaching the velocity of sound in water are the two most commonly used criteria for the onset of transient cavitation. Apfel[26] has presented

cavitation prediction charts that combine thresholds for gas nucleation [Blake threshold, eq. (2.1)], rectified diffusion (using Safar's analysis[27]), and transient cavitation ($R_{max} = 2.3 \cdot R_o$ is used as the threshold condition). The expressions used for the minimum and maximum rectified diffusion threshold, and the maximum radius controlled by inertia are given in Table 2.1.

Table 2.1 summarizes the parameters that are relevant to sonication in water at 20 kHz and 75 $W \cdot cm^{-2}$ (conditions used in most of the experiments presented in the following chapters). It can be seen that only bubbles between 40 nm and 460 μm are expected to contribute in transient cavitation under these conditions.

Bubble fields – photographic studies

The dynamics of a single bubble are relatively well understood and can be modeled mathematically. However, many bubbles of different sizes are present in bubble fields encountered in practice. High speed photography, cinematography and holography have been used to visually observe the dynamics of single bubbles and bubble fields.

Ellis[28] did pioneering work using a drum camera and a Kerr Cell as the shutter. Lauterborn and co–workers[29-32] have reported observations of cavities that are produced by focusing an intense light beam from a ruby laser. They have studied stable and transient bubbles and bubble fields, and they reported interesting features of bubble–bubble interactions (e.g., bubbles of similar size coalesce, bubbles of significantly different sizes develop jets before coalescence), bubble–wall interactions, and the dynamics of clouds originating from the collapse of a single bubble. Figure 2.2 presents the recorded growth and collapse of a bubble in water. Several other researchers have also used similar techniques to study

Table 2.1
Sonication in water at 20 kHz, 75 W·cm^{-2}

Variable	value	formula used
sound wavelength	7.25 cm	$\lambda = c/f$
resonant radius	165 μm	$\omega^2 = \left[\frac{3k(P_o+2\sigma/R_r)-2\sigma/R_r}{\rho R_r^2}\right]$
min radius corresponding to Blake's threshold	0.04 μm	$P_a = P_o+8\sigma/9\left[\frac{3\sigma}{2(P_o+2\sigma/R_b)R_b^3}\right]$
RD min threshold	0.06 μm	$\frac{P_a}{P_o} = \frac{(3k(1+X)-X)\,(1-(f/f_a)^2)(1-C-X)^{0.5}}{6\,(1+X)^{0.5}}$
RD max threshold	830 μm	$(\frac{4}{3\omega})(P_a-P_o)(\frac{2}{\rho P_a})^{0.5}[1+\frac{2}{3P_o}(P_a-P_o)]$
Max inertial R	460 μm	$0.3/f(\Delta P/\rho)^{0.5}$
collapse time	4 μs	$0.915R_{max}(\rho/P)^{0.5}$

where: $\Delta P = 2/3P_o(P_a-1)$, $X = 2\sigma/(P_oR)$, $P = P_a+P_o$, C = gas saturation (0–1), f_b = resonance frequency of bubble, P_a, P_o, and f as defined in the text values used: $\sigma = 7.25\cdot10^{-2}$ N/m, $\kappa = 1.4$ (air), $\rho = 1$ kg/m^3, c = 1450 m/s, $P_o = 1$ atm, $P_a = 14.7$ atm.

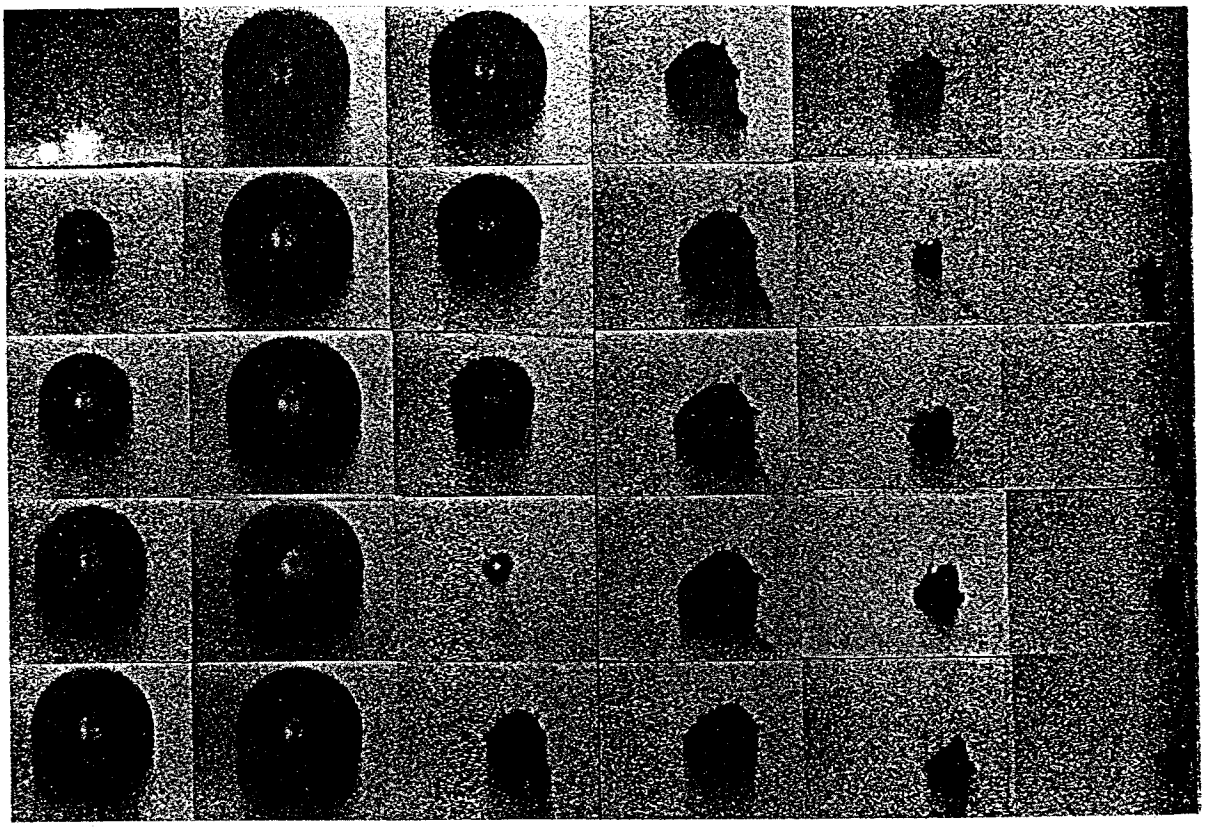

Figure 2.2 Growth and collapse of a bubble in water. Photographs taken at 20,000 frames/s (time between consecutive photographs = 50 μs). Frame sequence from top to bottom and from left to right. (Reproduced from ref. 30; Lauterborn, 1974)

bubble dynamics. Recently, Sanada *et al.*[33] used holography in order to observe the interaction of a small air bubble with a shock wave and obtained an estimate of about 4000 atm for the impact pressure induced by the collapse of a 1.7 mm bubble.

In general, these type of studies have revealed surface deformations and loss of spherical shape of individual bubbles (sometimes followed by release of microbubbles into solution), complex interactions between bubbles, and the existence of bubble clouds, streamers, shock waves, and jets. On the other hand, overall behavior of bubble clouds has been observed to be similar qualitatively to that of single bubbles, at least with reference to collapse and rebound[31], or cavitation noise[32].

The need for mathematical description of the complex dynamics of bubble fields has become apparent, and considerable efforts are under way in that area (e.g., refs. 14, 34–37).

Sonochemistry

The term sonochemistry includes all chemical effects that occur upon ultrasonic irradiation of a medium. Sonochemistry is attributed to the high temperatures and pressures associated with acoustic cavitation[1,2]. Transient cavitation is considered to be the main contributor to the observed sonochemical effects, but stable cavitation may also be important[4].

Sonochemical reactions could be categorized as: *i*) primary reactions, involving thermal decomposition of solvent, solute, or gases present in solution as a result of the high temperatures and pressures attained upon bubble collapse, and *ii*) secondary reactions, involving radicals from primary reactions and other species;

reactions of those radicals may occur in the gas phase within the hot bubble, the bubble/water interface, or the bulk aqueous phase.

A schematic representation of the regions of sonochemical reactions is given in Figure 2.2. It is noted that conflicting estimates of the temperatures attained upon collapse exist currently. The temperature estimates shown in Fig. 2.2 have been reported for sonication of metal carbonyls in mixtures of hydrocarbons[38]. It is reasonable to expect that these temperatures will be lower in the case where water is the solvent (because of the lower vapor pressure and the higher thermal conductivity of water). An average effective temperature of $\simeq$ 800 K is estimated for the interfacial region during sonication in water at 20 kHz in this work (see Chapter 3). It is also stressed that Fig. 2.2 is only an idealization since cavitation bubbles will loose their spherical shape upon collapse.

It is noted that the observed destructive, cleaning, or mixing action of sonication on various systems (e.g., macromolecules, organometallic chemistry, catalysis) is partly due to hydrodynamic phenomena, such as jets and shock waves, that take place during sonication. However, hydrodynamic phenomena could not account for sonochemistry, since they could not result in direct breaking of chemical bonds[2].

Spin trapping methods combined with ESR have provided evidence for the formation of H atoms and $^{\cdot}$OH radicals in the cavitation bubbles produced by ultrasound in Ar saturated water[39]. The formation of H and $^{\cdot}$OH is attributed to thermal dissociation of water vapor present in the cavities during the compression phase[1-4]. Table 2.2 shows the principal reactions that appear to be involved in water sonolysis in the presence of Ar, O_2, N_2, and air[2]. These reactions have been proposed by analogy to combustion and shock tube chemistry following evidence

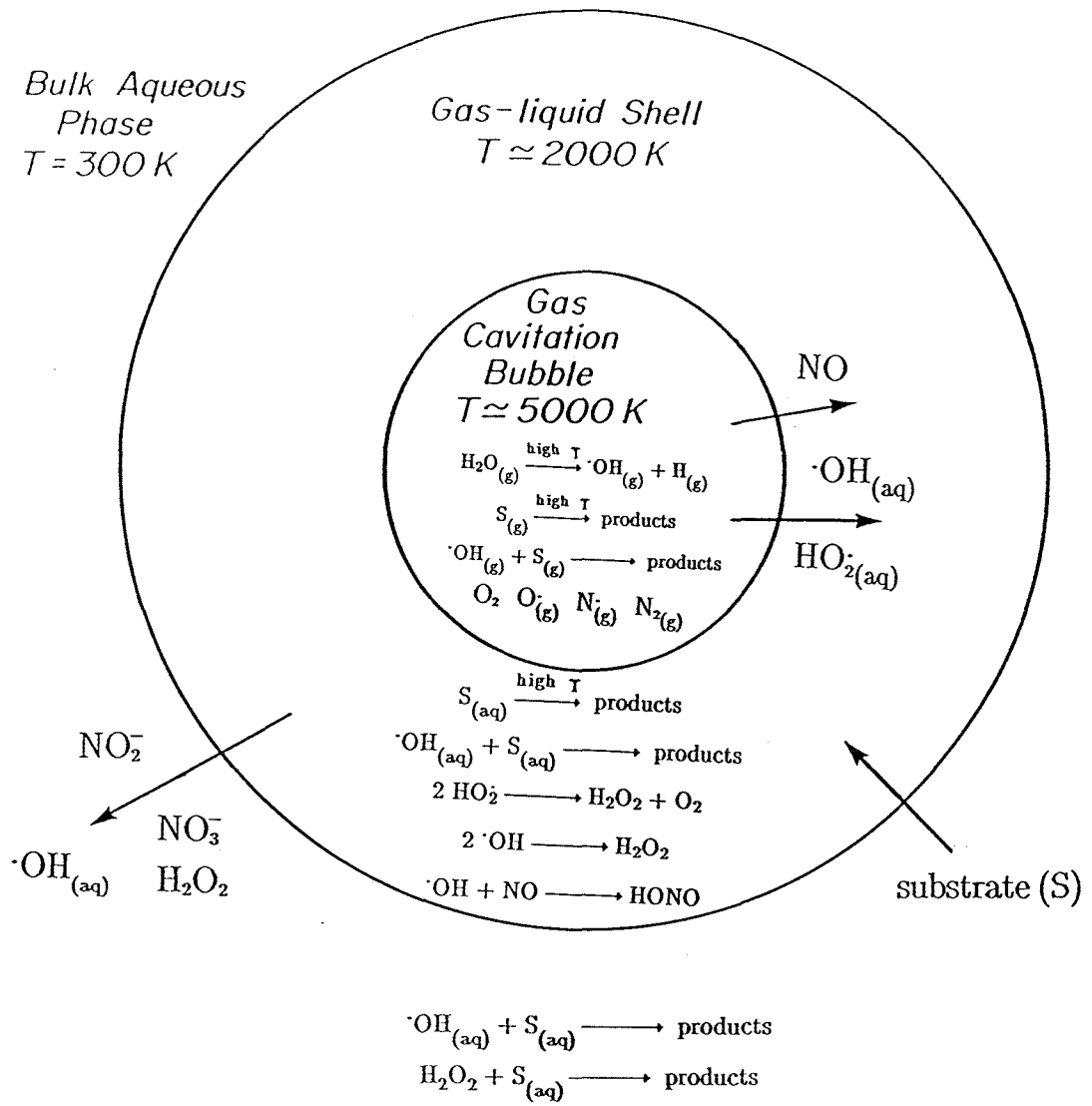

Figure 2.3 Schematic representation of the regions of sonochemical reactions in aqueous sonochemistry (see text for comments).

Table 2.2
Reactions involved in water sonolysis

1) Under Ar:

$$H_2O \xrightarrow{US} H^{\cdot} + OH^{\cdot}$$

$$^{\cdot}OH + {}^{\cdot}H \xrightarrow{M} H_2O$$

$$2\ {}^{\cdot}OH \rightleftharpoons {}^{\cdot}O + H_2O$$

$$2\ {}^{\cdot}OH \xrightarrow{M} H_2O_2$$

$$2\ H^{\cdot} \xrightarrow{M} H_2$$

$$2\ O^{\cdot} \xrightarrow{M} O_2$$

$$O_2 + H^{\cdot} \longrightarrow HO_2^{\cdot}$$

$$HO_2^{\cdot} + H^{\cdot} \longrightarrow H_2O + O^{\cdot}$$

2) Under O_2:

$$O_2 \longrightarrow 2\ O^{\cdot}$$

$$O_2 + H^{\cdot} \longrightarrow HO_2^{\cdot}\ (\text{or } {}^{\cdot}OH + O)$$

$$2\ HO_2^{\cdot} \longrightarrow H_2O_2 + O_2$$

$$O^{\cdot} + HO_2^{\cdot} \rightleftharpoons 2\ {}^{\cdot}OH$$

3) Under N_2:

$$N_2 + {}^{\cdot}OH \longrightarrow N_2O + H^{\cdot}$$

$$N_2 + O^{\cdot} \overset{M}{\rightleftharpoons} N_2O$$

$$N_2 + O^{\cdot} \rightleftharpoons NO + N^{\cdot}$$

$$N_2O + O^{\cdot} \longrightarrow N_2 + O_2$$

$$NO + H^{\cdot} \longrightarrow N^{\cdot} + {}^{\cdot}OH$$

4) Under air:

as in 2 and 3 plus $N_2 + O_2 \longrightarrow 2\ NO$

provided by isotopic scrambling (e.g., refs. 40, 41). In the absence of ·OH scavengers the main product of the sonolysis of water is H_2O_2.

No direct studies on the conditions inside and in the vicinity of cavitating bubbles exist (e.g., measurements of temperature, pressure, or concentrations of chemical species). This is due to the dynamic nature of acoustic cavitation and the small time and length scales involved in the collapse of the cavities (see Table 2.1). Indirect methods such as sonoluminescense (SL) and comparative rate thermometry[42] have been used to probe the intensity of collapse and the spatial and temporal distribution of cavitation events. An excellent review article on the phenomenon of SL and its use as sonication probe has been presented by Walton & Reynolds[43]; a more recent review of SL was presented by Verral & Sehgal[2].

Sonoluminescence (SL) refers to the emission of light when a liquid is sonicated. It is now accepted that SL originates from recombination of free radicals (e.g., $H^{\cdot} + OH^{\cdot} \longrightarrow H_2O$) and de–excitation of excited species[44] (e.g., H_2O^*, OH*). Its intensity and spectrum depend on the factors that affect cavitation, i.e., nature of solvent and solute (including dissolved gas), sound frequency, temperature, pressure (ambient, acoustic)[43]. SL can be detected with the use of photomultipliers or image intensifiers. Luminol (o–aminophthalhydrazide) can be used to enhance the natural water SL[43] (because of its reaction with H_2O_2). A high–gain image intensifier system has been used to obtain visual observations of ultrasonic fields[45,46].

In conclusion, sonochemistry can be seen as a third–order phenomenon of ultrasonic irradiation. The introduction of sound waves into the system results in cavitation. Conditions "suitable for chemistry" develop in a small fraction of the total number of cavities (e.g., high T, P upon collapse of transient cavities). These conditions then result in various tertiary chemical effects.

References

1. Mason, T. J.; Lorimer, J. P. Sonochemistry. Theory, applications and uses of Ultrasound in Chemistry. Ellis Horwood, Ltd. (1988).
2. Suslick, K. S. (ed.) Ultrasound: Its Chemical, Physical and Biological Effects, VCH, New York (1988).
3. Crum, L. A. *IEEE Ultrasonics Symp*, 1–11 (1982).
4. Henglein, A. *Ultrasonics*, 25, 6–16 (1987).
5. Apfel, R. *J. Acoust. Soc. Am.*, 49, 145 (1971).
6. Crum, L. A. *Appl. Sci. Res.*, 38, 101 (1982).
7. Epstein, P. S.; Plesset, M. *J. Chem. Phys.*, 18, 1505 (1950).
8. Atchley, A. A.; Crum, L. In reference 2, Chapter 1.
9. Blake, F. G., Jr. The Onset of Cavitation in Liquids, Technical Memo No. 12, Acoustics Research Laboratory, Harvard University (1949).
10. Katz, J.; Acosta, A. *Appl. Sci. Res.*, 38, 123 (1982).
11. Gavrilov, L. R. In Physical principles of ultrasonic technology, Rozenberg (ed.), Vol. 2, Part VI, Plenum Press, New York (1973).
12. Young, F. R. Cavitation, Chapter 7, McGraw–Hill, London (1989).
13. Sirotyuk, M. G. In Power Ultrasonic fields, Part 5, Nauka, Moscow (1968).
14. Hansson, I.; Kedrinskii, V.; Morch, K. A. *J. Phys. D; Appl. Phys.*, 15, 1725 (1982).
15. Neppiras, E. A. *Physics Reports*, 61, 159 (1980).
16. Lord Rayleigh. *Phil. Mag.*, 34, 94 (1917).
17. Plesset, M. S. *J. Appl. Phys.*, 25, 96 (1954).
18. Nolting, B.; Nepirras, E. *Proc. Phys. Soc. B (London)*, 63 B, 674 (1950).

19. Nepirras, E.; Nolting, B. *Proc. Phys. Soc B (London)*, 64 B, 1032 (1957).

20. Poritsky, H. *Proc. 1st US Nat. Congress in Appl. Mechanics (ASME)*, 813 (1952).

21. Gilmore, F. R. California Institute of Technology, Hydrodynamics Laboratory Report, No. 26–4 (1952).

22. Kirkwood, J. G.; Bethe, H. A. Office of Science Research and Development Report No 558, USA (1942).

23. Hickling, R.; Plesset, M. S. *Phys. Fluids*, 7, 7 (1964).

24. Margulis, M. A.; Dmitrieva, A. F. *Russ. J. Phys. Chem*, 56 (4), 530 (1982).

25. Margulis, M. A.; Dmitrieva, A. F. *Russ. J. Phys. Chem*, 56 (2), 198 (1982).

26. Apfel, R. E. *J. Acoust. Soc. Am.*, 69, 1624 (1981).

27. Safar, M. H. *J. Acoust. Soc. Am.*, 43, 1188 (1968).

28. Ellis, A. T. California Institute of Technology Hydrodynamics Laboratory, Report No. 21–12 (1952).

29. Lauterborn, W. *Appl. Phys. Lett.*, 21, 27 (1972).

30. Lauterborn, W. *Acoustica*, 31, 51 (1974).

31. Lauterborn, W.; Ebeling, K. J. *Appl. Phys. Lett.*, 31, 663 (1977).

32. Lauterborn, W. *Appl. Sci. Res.*, 38, 165 (1982).

33. Sanada, N.; Takayama, K; Onodera, O.; Ikeuchi, J. In Shock Waves and Shock Tubes, Bershader, D.; Hanson, R. (ed.), Stanford University Press, Stanford (1986).

34. Morch, K. A. *Appl. Sci. Res.*, 38, 313 (1982).

35. d'Agostino, L.; Brennen, C. E. *J. Fluid Mechanics*, 199, 155 (1988).

36. d'Agostino, L.; Brennen, C. E.; Acosta, A. J. *J. Fluid Mechanics*, 192, 485 (1988).

37. Kumar, S.; Brennen, C. E. *J. Acoust. Soc. Am.*, 89, 707 (1991).

38. Suslick, K. S.; Hammerton, D. A. *IEEE Trans.*, *UFFC–33*, 143 (1986).

39. Makino, K.; Mossoba, M. M.; Riesz, P. *J. Phys. Chem.*, 87, 1369 (1983).

40. Fischer, C–H.; Hart, E. J.; Henglein, A. *J. Phys. Chem.*, 90, 1954 (1986).

41. Hart, E. J.; Henglein, A. *J. Phys. Chem.*, 90, 5992 (1986).

42. Suslick, K. S.; Hammerton, D. A.; Cline, R. E., Jr. *J. Am. Chem. Soc.*, 108, 5642 (1986).

43. Walton, A. J.; Reynolds, G. T. *Adv. Phys.*, 33, 595 (1984).

44. Sehgal, C.; Sutherland, R. G.; Verall, R. E. *J. Phys. Chem.*, 84, 388 (1980).

45 Reynolds, G. T.; Walton, A. J. *Rev. Sci. Instrum.*, 53, 1673 (1982).

46. Crum, L. A.; Reynolds, G. T. *J. Acoust. Soc. Am.*, 78, 137 (1985).

CHAPTER 3

ULTRASONIC IRRADIATION OF p–NITROPHENOL IN AQUEOUS SOLUTION

(*The Journal of Physical Chemistry*, 1991, *95*, 3630)

ABSTRACT

The kinetics and mechanism of the sonochemical reactions of p–nitrophenol have been investigated in oxygenated aqueous solutions. In the presence of ultrasound (20 kHz – 84 Watts) p–nitrophenol was degraded primarily by denitration to yield NO_2^-, NO_3^-, benzoquinone, hydroquinone, 4–nitrocatechol, formate and oxalate. These reaction products and the kinetic observations are consistent with a model involving high–temperature reactions of p–nitrophenol in the interfacial region of cavitation bubbles. The main reaction pathway appears to be carbon–nitrogen bond cleavage. Reaction with hydroxyl radical provides a secondary reaction channel. The average effective temperature of the interfacial region surrounding the cavitation bubbles was estimated to be $T \simeq 800$ K.

Introduction

The action of ultrasonic waves in liquids can induce or accelerate a wide variety of chemical reactions.[1] The chemical effects of ultrasound have been explained in terms of reactions occurring inside, at the interface or at some distance away from cavitating gas bubbles.[1–3] In the interior of a collapsing bubble, extreme but transient conditions are known to exist. Temperatures approaching 5000 K have been determined[4] and pressures of several hundred atmospheres have been calculated.[5] Temperatures on the order of 2000 K have been determined for the interfacial region.[4] These and other important results such as the direct observation of cavitation dynamics[6] and the ESR[7] detection of H· and ·OH radicals from the thermal decomposition of water have generated an increasing interest in sonochemistry. Much of the current interest in sonochemistry has arisen because of the utilization of sonolysis in catalysis[1] and synthesis.[8]

Sonochemical reactions are characterized by the simultaneous occurrence of pyrolysis and radical reactions especially at high solute concentrations.[9] Any volatile solute will participate in the former reactions because of its presence inside the bubbles during the oscillations or collapse of the cavities.[9–11] In the solvent layer surrounding the hot bubble, both combustion and free radical reactions (e.g. involving ·OH derived from the decomposition of H_2O) are possible. Pyrolysis (i.e. combustion) in the interfacial region is predominant at high solute concentrations,[11a,12] while at low solute concentrations free radical reactions are likely to predominate.[12] In the bulk solution phase the reaction pathways are similar to those observed in aqueous radiation chemistry.[11a,12,13] However, evidence for combustion reactions at low solute concentrations with non–volatile

surfactants and polymers has been presented.[14]

In this paper we present kinetic data and selected mechanistic observations for the sonochemical degradation of para–nitrophenol (PNP) in water. We were motivated in part by the potential application of sonolysis for the elimination of chemical contaminants found in water.

Experimental

The ultrasonic irradiation of aqueous solutions of PNP was carried out with a Branson 200 sonifier that was operated at 20 kHz and with an output of electrical power–to–converter equal to 84 W. Reactions were performed in a stainless–steel continuous–flow reaction cell operated in the batch mode (Sonics & Materials). The total volume of the cell was 50 ml; the sonicated volume was 25 ml. The reactor was encased in a self–contained water jacket and was cooled with water at 15 °C. The measured reaction temperature inside the cells was 30 °C. All reactions were carried out with air–saturated solutions. Two openings on the upper part of the reactor allowed for a continuous exposure to air during the course of sonication. Unless otherwise stated experiments were performed with aqueous solutions adjusted to an initial pH of 5.

Quantification of PNP and 4–nitrocatechol (4–NC) was achieved by the measurement of their respective absorbancies in alkaline solution (0.1 M NaOH) at λ = 401 nm (ϵ = 19200 $M^{-1}cm^{-1}$ for PNP) and 512 nm (ϵ = 12300 $M^{-1}cm^{-1}$ for 4–NC).[15] The measured absorbance of PNP was corrected for the small contributions due to 4–NC at 401 nm (ϵ = 6500 $M^{-1}cm^{-1}$).[15] The concentration of p–benzoquinone (p–BQ) was determined spectrophotometrically in a solution

containing 20% n–butylamine at λ = 345 nm.[16] The measured absorbance at 345 nm was corrected for the contributions due to PNP and 4–NC (extinction coefficients in 20% n–butylamine: p–BQ, ϵ_{345} = 26400 $M^{-1}cm^{-1}$; p–NP, ϵ_{345} = 3800 $M^{-1}cm^{-1}$; 4–NC, ϵ_{345} = 3300 $M^{-1}cm^{-1}$).

Nitrite, nitrate, formate and oxalate were determined with a Dionex 2020i ion chromatograph and a Dionex AS4–A column. The IC eluents were 2.2 mM CO_3^{2-}, 2.8 mM HCO_3^- and 5 mM $B_4O_7^{2-}$. The concentration of H^+ was determined with a Radiometer autotitration system. Ionic strength was adjusted after sonication to 1 mM with Na_2SO_4. Hydrogen peroxide was determined iodometrically and fluorometrically as described previously.[17] Kinetic runs were carried out by sonication of a sample for a desired length of time. At that time an aliquot was withdrawn for complete chemical analysis. Kinetic experiments were continued after cleaning the cell thoroughly and filling it with fresh solution. Before analysis all samples were filtered with 0.2 μm HPLC filters (from Gelman) to remove Ti particles produced during sonication by erosion of the Ti tip of the sonication horn. Loss of PNP or its degradation products by adsorption to the HPLC filters was not observed. The water employed in all preparations was purified by a Milli–Q/RO system (18 Mohm resistivity) produced by Millipore. Absorption spectra were measured with a Shimadzu MPS–2000 UV–VIS spectrophotometer and fluorescence analyses were performed with a Shimadzu RF–540 spectrofluorimeter.

Results

Exposure of 25 ml solutions of 100 μM p–NP to ultrasound in the presence of

air resulted in a decrease in the absorption due to PNP at 401 nm and the subsequent formation of a new absorption band at 512 nm corresponding to 4–NC. The evolution of the absorption spectra with time is presented in Figure 3.1. Two near (but not exact) isosbestic points were observed at ~ 460 and ~ 335 nm. At sonication times longer than 40 min. these apparent isosbestic points were lost. Figure 3.2 shows the concentration vs. irradiation time profiles for PNP and 4–NC. The initial increase in the [4–NC] was linear with time. A maximum concentration of 4–NC was observed after 40 min. of sonication. The concentration of PNP decreased exponentially with sonication time.

Figure 3.3 shows a first–order plot of ln [PNP] vs. time. The ultrasonic degradation of PNP followed apparent first–order kinetics for at least four half–lives. A first–order rate constant of $k_1 = 3.7 \times 10^{-4}$ s^{-1} was determined from the slope of this plot.

Nitrite and nitrate were found as primary nitrogen–containing products of the degradation of PNP. The time–dependent variations in the concentrations of these ions are shown in Figure 3.4a. NO_2^- appears to be the main product at short sonication times; it reached a maximum concentration of 57 μM after 42 min. of sonication. The concentration of NO_3^- increased continuously with time. The results of Figure 3.4a were obtained by analyzing the samples immediately after sonication. However, if the IC analysis were repeated on the same sample aliquot after several hours, NO_3^- was found as the main product and only traces (~ 6 μM) of nitrite were detected. These results suggest that NO_2^- is the principal product of the decay of PNP by ultrasound.

It is well known that nitrite and nitrate are generated by the ultrasonic oxidation of N_2 in air–saturated aqueous solutions[1]. Sonication of pure water under

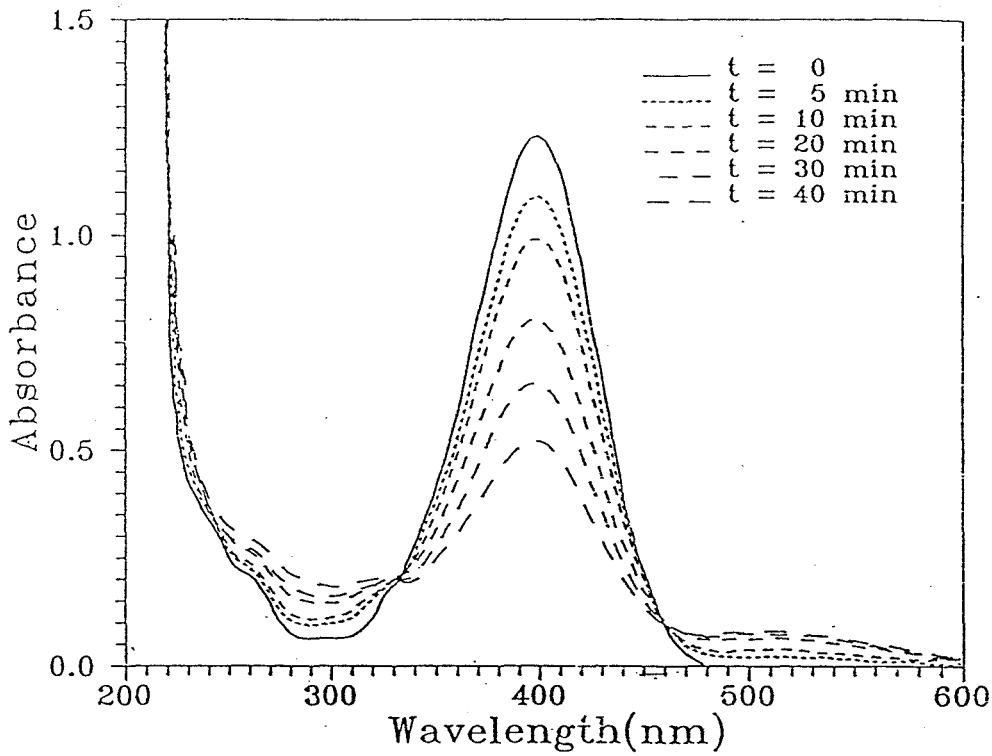

Figure 3.1 Absorption spectra evolution with sonication time where peak at 401 nm corresponds to p–NP while the broad band at 512 nm corresponds to 4–NC.

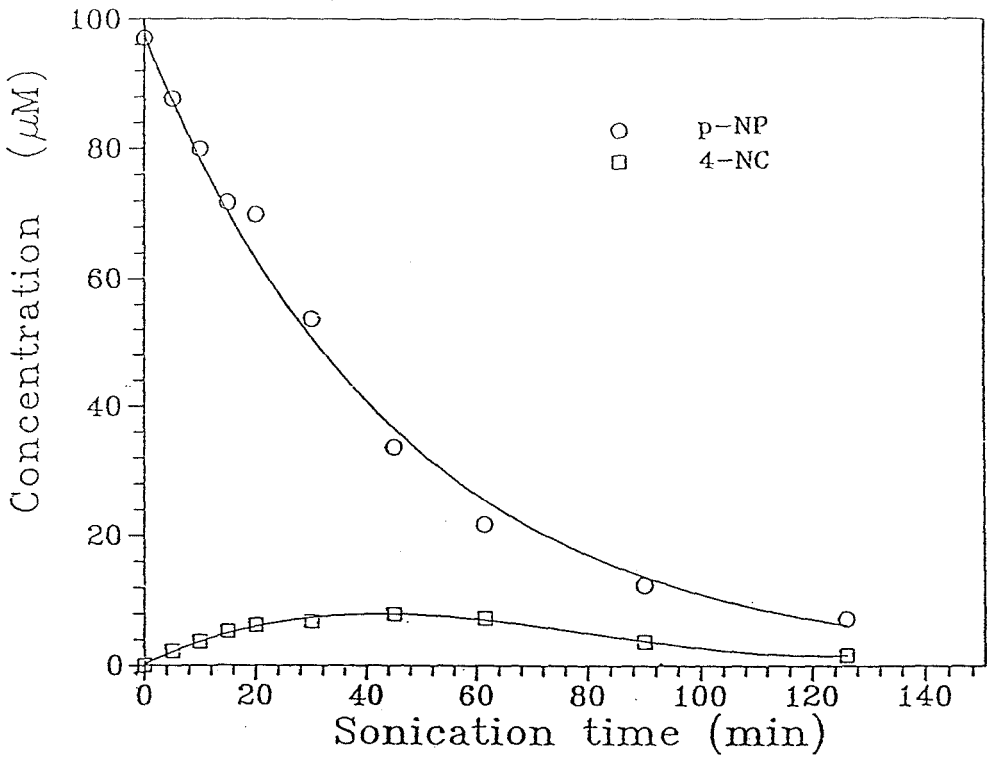

Figure 3.2 [p–NP] and [4–NC] versus sonication time at pH 5

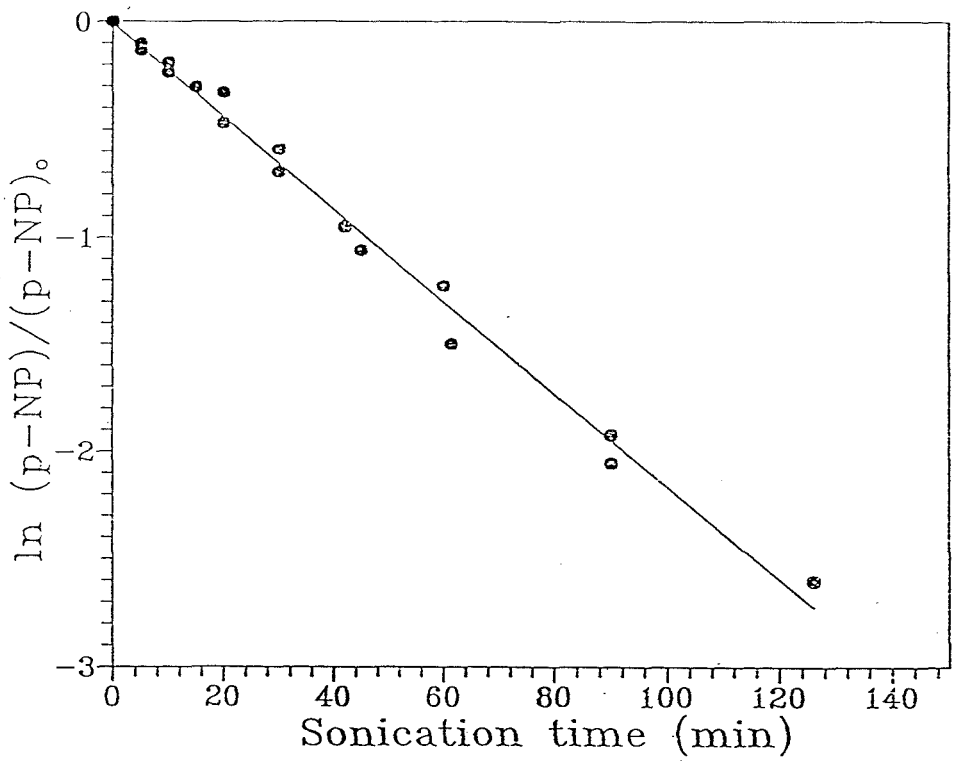

Figure 3.3 First–order plot of ln[p–NP] vs. time for the sonochemical decay of p–NP at pH 5.

A)

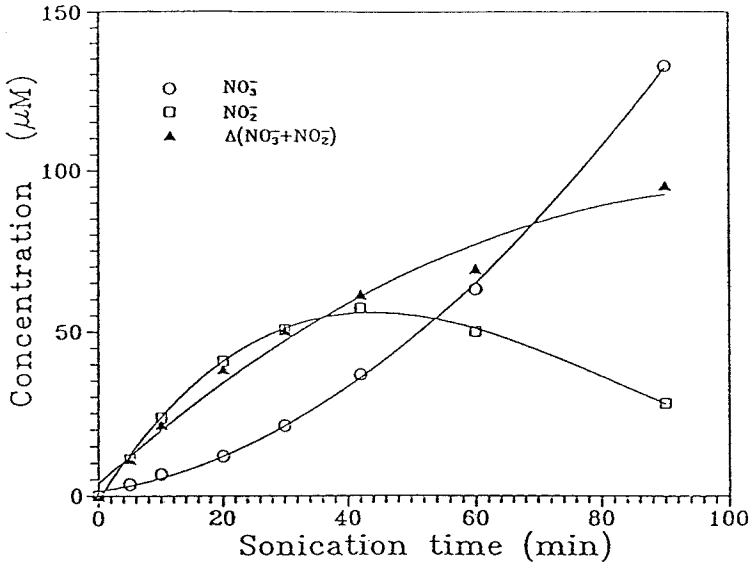

B)

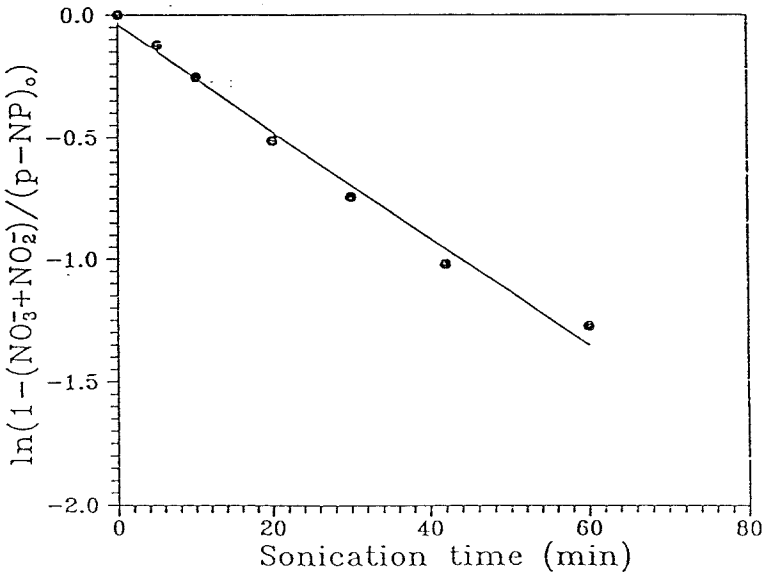

Figure 3.4 (a, top) NO_2^- and NO_3^- formation during sonication of p–NP. (b, bottom) First–order plot of NO_x^- formation at pH 5.

the same experimental conditions used for the PNP solutions produced substantial concentrations of these ions. The determination of the $[NO_3^-] + [NO_2^-]$ produced by the decay of PNP was possible by subtracting $[NO_3^-] + [NO_2^-]$ produced in the control reaction with purified water from the sum of the concentrations of these ions in the PNP solutions, for each irradiation time as follows:

$$\left([NO_3^-]^t_{PNP} + [NO_2^-]^t_{PNP}\right) - \left([NO_3^-]^t_{H_2O} + [NO_2^-]^t_{H_2O}\right) = \left(NO_3^- + NO_2^-\right) \quad (3.1)$$

where $[NO_x^-]^t_{PNP}$ represents the amount of NO_x^- produced by sonication of PNP solutions and $[NO_x^-]^t_{H_2O}$ represents the amount of NO_x^- formed by sonication of water at time = t. The results of this calculation are included in Figure 3.4a. From these results we see that NO_x^- (i.e. $NO_3^- + NO_2^-$) increased exponentially with irradiation time between 0 and 60 min. The corresponding first–order plot of these results is shown in Figure 3.4b. A first–order rate constant for the formation of $(NO_2^- + NO_3^-)$ of $k_1 = 4 \times 10^{-4}\ s^{-1}$ was obtained from these data (Fig. 3.4b).

As shown in Figure 3.5, H_2O_2 was produced during the decay of PNP by sonication. These results were obtained by analyzing the PNP solutions immediately after sonication. Lower peroxide concentrations were detected when irradiated samples were left in the dark for several hours and then reanalyzed. The decrease of $[H_2O_2]$ during the post–irradiation period can be attributed to the reaction of H_2O_2 with NO_2^- to yield NO_3^-.[20] No organic peroxides were detected with the iodide–difference method of Kormann *et al.*[17] Both analytical methods for H_2O_2 gave identical results. Henglein[1] has shown that H_2O_2 is generated by the action of ultrasonic waves on pure water. Under our experimental conditions sonolysis of the solvent alone led to a linear increase of $[H_2O_2]$ vs. irradiation time

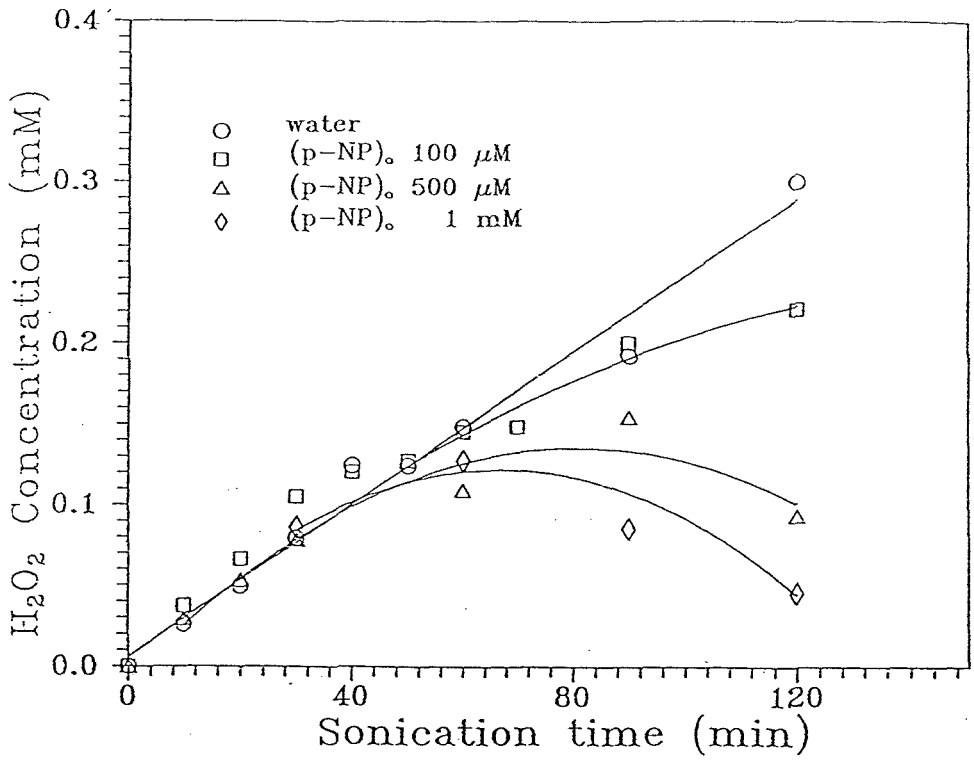

Figure 3.5 Hydrogen peroxide generation during sonication.

with a rate constant of 4×10^{-8} M s^{-1}. Sonication of solutions containing PNP yielded initially the same result as shown in Figure 3.5. At longer irradiation times the observed concentrations of H_2O_2 were lower in PNP solutions than in pure water. The deviation from the results obtained with water alone increased with increasing initial concentrations of PNP. Also, this deviation occurred at earlier stages of the reaction in solutions containing high concentrations of nitrophenol. However, the initial rate of formation of H_2O_2 was the same as in pure water alone, regardless of the [PNP].

Hydrogen ions were formed by the action of ultrasound on a 100 μM PNP solution. Figure 3.6 shows the increase of proton concentrations in a PNP solution and in pure water as a function of sonication time. The increase of $[H^+]$ was initially slow in both systems. However, after 10 minutes of irradiation, $[H^+]$ increased. The sonolysis of pure water produced a linear increase of $[H^+]$ as a function of time with an apparent zero–order rate constant of 8.3×10^{-9} M min^{-1}. At sonication times $\geq$ 20 min., $[NO_2^-] + [NO_3^-]/[H^+] = 1$. On the other hand, in sonicated PNP solutions the increase of $[H^+]$ (at $t \geq 10$ min.) appeared to be first–order with an apparent first–order rate constant of $k_1 = 3 \times 10^{-4}$ s^{-1} after correction of the $[H^+]$ in manner analogous to the correction made for $NO_3^- + NO_2^-$ (*vide supra* eq. 3.1).

Since the rate of production of H^+ was less than the rate of generation of NO_3^- and NO_2^- in PNP solutions, a pH–buffering effect by some of the products was indicated. IC analyses of the sonicated PNP solutions showed clearly that HCO_2^- and $C_2O_4^{2-}$ were formed as a function of time (Figure 3.7). The $[HCO_2^-]$ increased linearly with sonication time with an apparent zero–order rate constant of 4.2×10^{-9} M s^{-1}. After an induction period of ~ 10 min., oxalate was produced with an

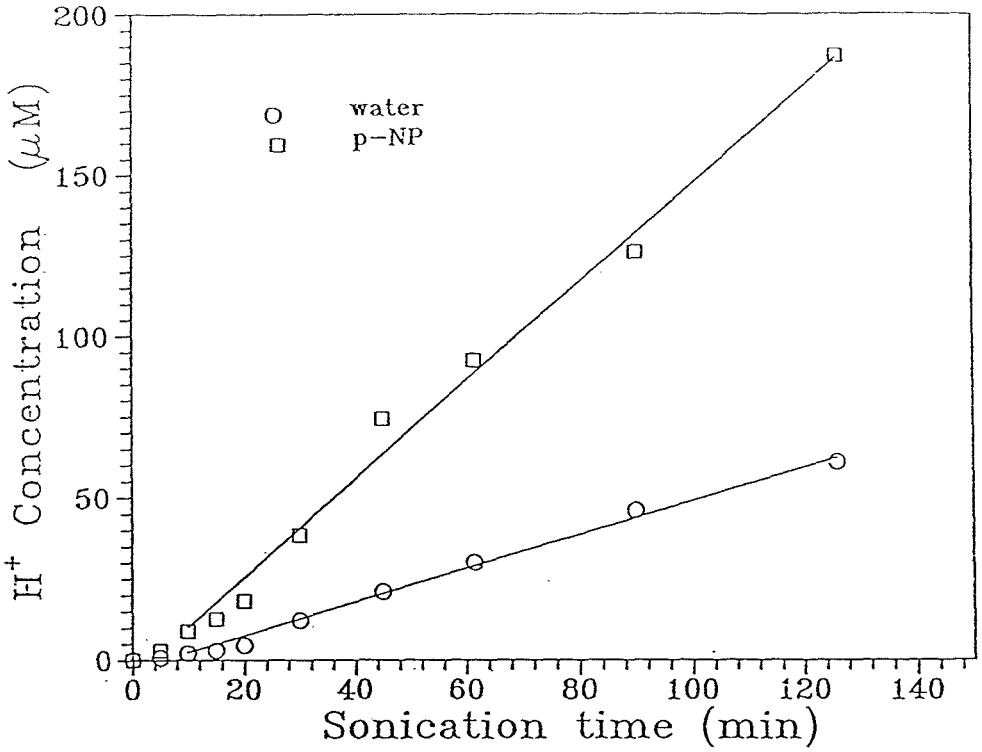

Figure 3.6 $[H^+]$ vs. time during sonication.

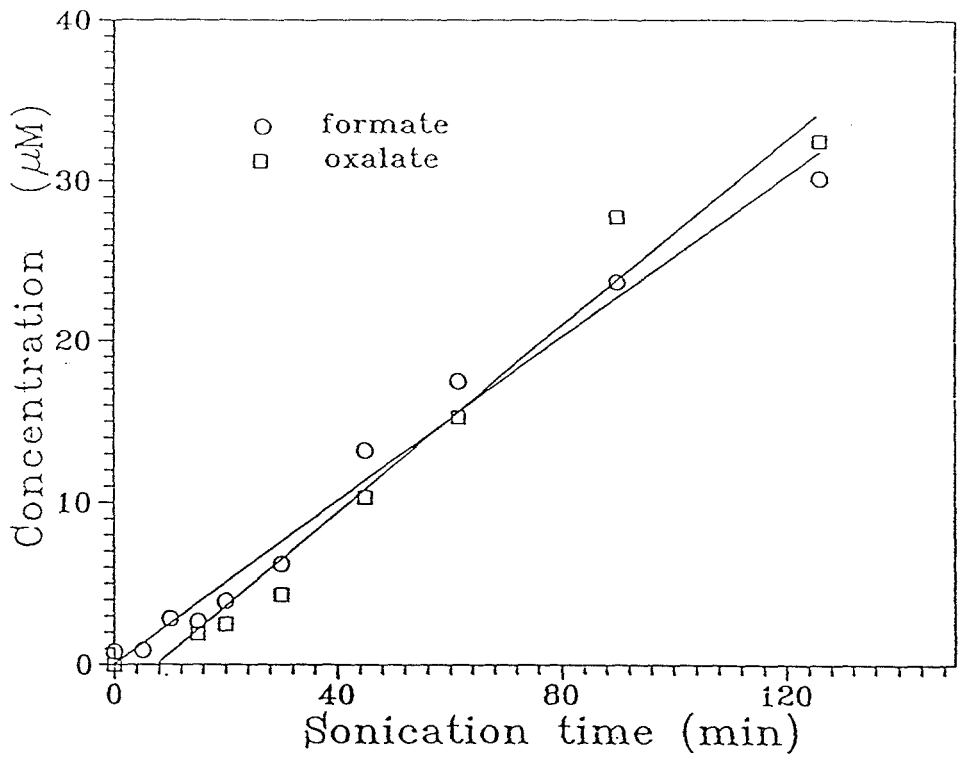

Figure 3.7 Formate and oxalate formation during sonication of 10^{-4} M p–NP.

apparent zero–order rate constant of 5×10^{-9} M s^{-1}.

Para–benzoquinone (p–BQ) was also formed upon exposure of PNP solutions to ultrasound. The [p–BQ] vs. sonication time profile is shown in Figure 3.8. Concentrations of p–BQ increased during the first 30 min. of sonication to about 17 μM and remained nearly constant at longer reaction times. It should be noted that the n–butylamine method responds to p–BQ. However, hydroquinone is oxidized rapidly in air to p–BQ in alkaline n–butylamine solutions.[16] Hence, the results depicted in Figure 3.8 correspond to summation of p–BQ and hydroquinone.

As mentioned above, PNP decayed in the presence of ultrasound via apparent first–order kinetics. However, the rate of PNP decay by sonication was found to be dependent on the initial concentration of PNP ($[PNP]_i$) as shown in Figure 3.9a. While PNP decayed exponentially with time irrespective of the PNP concentration, the apparent first–order rate constant decreased from 1.37×10^{-2} s^{-1} at $[PNP]_i = 10$ μM to 6.17×10^{-5} s^{-1} at $[PNP]_i = 1$ mM. A plot of log k_1 vs. log $[PNP]_i$ yielded a straight–line ($r^2 = 0.99$) relationship from which the following empirical equation, $k_1 = 3.83 \times 10^{-7} [PNP]_i^{-0.7}$, was obtained.

The formation of 4–NC from PNP followed zero–order kinetics at short sonication times (Figure 3.2, $[PNP]_i = 100$ μM) with an apparent rate constant of $k_o = 6.17 \times 10^{-9}$ M s^{-1}. However, the rate of formation increased with increasing $[PNP]_i$. These results are illustrated in Figure 3.9b. The initial zero–order rate constant varied from $k_o = 3.0 \times 10^{-9}$ M s^{-1} at $[PNP]_i = 10$ μM to $k_o = 1.7 \times 10^{-8}$ M s^{-1} at $[PNP]_i = 1$ mM.

Changes in the initial pH (pH_i) of the PNP solutions also affected the decay of PNP as shown in Figure 3.10. PNP decayed exponentially with time at all pH values. The apparent first–order rate constant decreased from $k_1 = 3.67 \times 10^{-4}$ s^{-1}

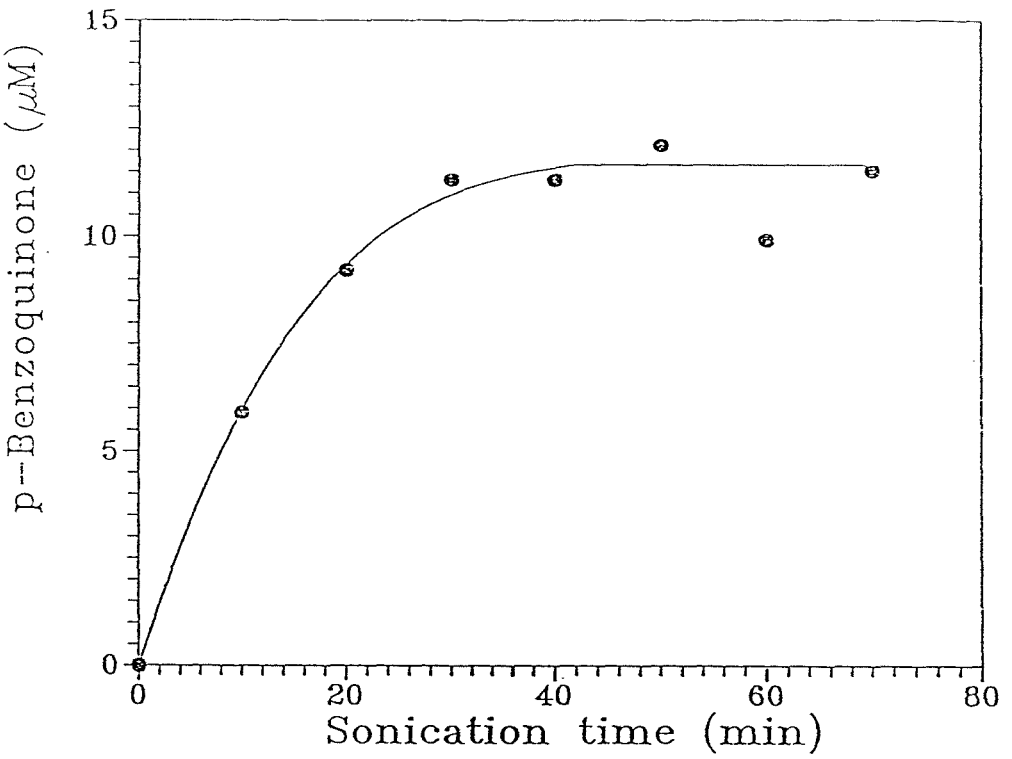

Figure 3.8 [p–BQ] vs. sonication time at pH 5 with $[p\text{–}NP]_o = 100\ \mu M$.

A)

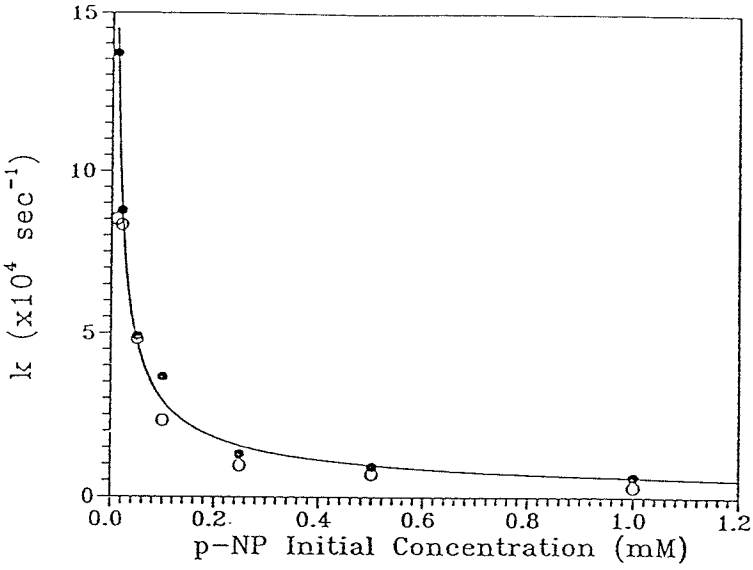

B)

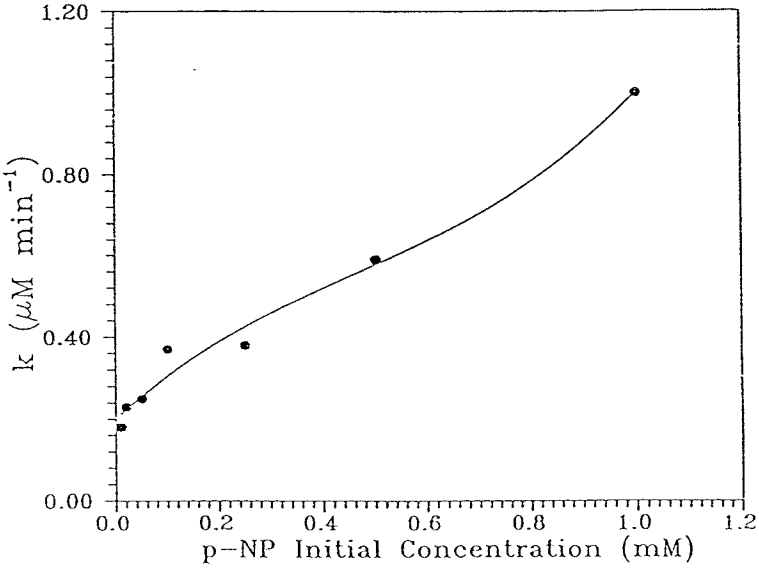

Figure 3.9 (a, top) Effect of $[p\text{–}NP]_o$ on the rate of p–NP degradation. (b, bottom) Effect of $[p\text{–}NP]_o$ on the initial rate of 4–NC formation.

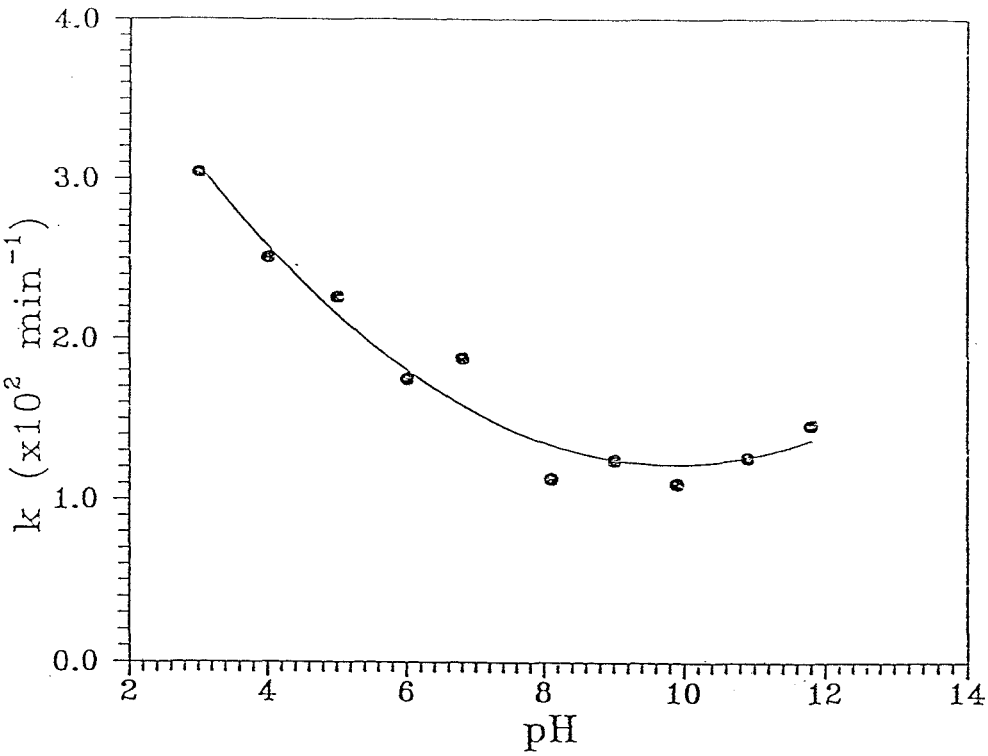

Figure 3.10 Effect of pH on the rate of p–NP degradation.

at $pH_i = 5$ to $k_1 = 2.0 \times 10^{-4}\ s^{-1}$ at $pH_o = 8$ and remained constant up to $pH_o = 10$.

At $pH_o > 10$ the apparent first–order rate constant increased slightly because of the slow thermal reaction between PNP and the products of the base–catalyzed decomposition of H_2O_2. This thermal reaction was detected as a post–irradiation decay of PNP in alkaline solutions, which extended for several hours. The post–irradiation effect was detected in all sonicated PNP solutions that were made alkaline for the analysis of the nitrophenoxide ion at 401 nm. No post–irradiation decay of PNP was observed in solutions that were acidified to pH = 1 immediately after sonication. The latter solutions were analyzed spectrophotometrically for PNP at $\lambda = 317$ nm ($\epsilon = 10190\ M^{-1}cm^{-1}$). In the experiments at high pH, only borax and phosphate buffers were used. This procedure was adopted to avoid possible interference from the buffers due to the scavenging of $H^{\cdot}$ and $^{\cdot}OH$ radicals. Similar results were obtained when experiments carried out in the presence of phosphate buffers were repeated with borax buffers.

A modest increase of k_1 was noticed when the pH was lowered with H_2SO_4 from pH = 5 to pH = 4 (Figure 3.10). At pH < 4 the apparent first–order rate constant increased to $5.0 \times 10^{-4}\ s^{-1}$ (pH = 3). However, at $[H^+] > 1$ mM results were not reproducible. The increase of k_1 with increasing acid concentrations cannot be explained by ionic strength effects, since sonication of PNP solutions at pH = 5 in the presence of 0.5 mM Na_2SO_4 or 1 mM $NaNO_3$ gave identical results to those obtained in the absence of these electrolytes

4–NC was formed with an apparent zero–order rate of $k_o = 6.17 \times 10^{-9}\ M\ s^{-1}$ which was found to be independent of pH over pH range of 4 to 10. At pH = 3 the rate of formation decreased to $k_o = 1.67 \times 10^{-9}\ M\ s^{-1}$. A similar effect was noticed in alkaline solutions where $k_o = 1 \times 10^{-9}\ M\ s^{-1}$ at pH = 10.9 and $k_o = 6.67 \times 10^{-10}$

M s^{-1} at pH = 11.8.

Several experiments were performed in order to evaluate the sonochemical reactivity of some of the reaction products and their influence in the reactions of PNP. For this purpose, air–saturated solutions containing 20 μM 4–NC were exposed to ultrasound. The concentration of 4–NC decreased exponentially with time with an apparent first–order rate constant of $k' = 9.83 \times 10^{-4}$ s^{-1}. This result is very close to the rate constant obtained in a solution containing 20 μM PNP ($k_1 = 8.83 \times 10^{-4}$ s^{-1}). Sonication of a mixture containing 100 μM PNP and 20 μM 4–NC resulted in an apparent first–order rate constant for the decay of PNP equal to $k_1 = 2.5 \times 10^{-4}$ s^{-1}. The concentration of 4–NC decreased continuously with sonication time. Under these conditions the decay of 4–NC was faster at all sonication times than its formation from PNP. However, 4–NC decayed in the presence of 100 μM PNP with an apparent first–order rate constant of 2.83×10^{-5} s^{-1}; a value significantly lower than that obtained in the absence of PNP.

While NO_3^- did not interfere with the sonochemical reactions of PNP, NO_2^- appeared to affect the decay of p–nitrophenol. Irradiation of a solution containing 100 μM PNP and 100 μM $NaNO_2$ with ultrasound resulted in a slower disappearance of PNP ($k_1 = 2.0 \times 10^{-4}$ s^{-1}) when compared to a kinetic run in the absence of NO_2^- ($k_1 = 3.67 \times 10^{-4}$ s^{-1}). In addition, we found that the formation of 4–NC was slower in the presence of NO_2^-. The apparent zero–order rate constant for the formation of nitrocatechol was about one half ($k_o = 3.0 \times 10^{-9}$ M s^{-1}) of the rate constant obtained in the absence of NO_2^- ions ($k_o = 6.2 \times 10^{-9}$ M s^{-1}).

On several occasions the spectrophotometric determination of PNP at 401 nm in alkaline solutions was verified by measurements of [PNP] in acid solution at 317 nm ($\epsilon = 10200$ $M^{-1}cm^{-1}$). Excellent agreement (derivation < 5%) between the

two methods was obtained after correcting the absorption at 317 nm for the small contributions of 4–NC (ϵ = 5700 $M^{-1}cm^{-1}$). No absorption at λ = 348 nm was detected in PNP solutions acidified to pH = 1 after sonication. Knowing that in acid solution neither PNP nor 4–NC absorb at this wavelength and that the absorption of 4–nitroresorcinol at low pH is strongest at λ = 348 nm (ϵ = 8850 $M^{-1}cm^{-1}$),[18] it can be concluded that the concentration of nitroresorcinol was smaller than 5 μM at all sonication times. Products of the nitration of PNP such as 2,4–dinitrophenol were not detected in concentrations above the limit of detection of 7 μM.

The rate of disappearance of PNP was found to be independent of the volume of sonicated solution (20–40 ml). Sonication of air–saturated solutions, which were not exposed to air during the course of sonication, produced the same results as those obtained with air–equilibrated solutions. Furthermore, identical results were obtained by using continuous sonication or pulsed sonication (0.5 s. sonication per every second). The comparison was made using the net sonication times in the case of pulse experiments. No significant effects due to tip erosion were found.

Discussion

We have shown clearly that the action of ultrasound on PNP in aqueous solutions resulted in its degradation with the formation of NO_2^-, NO_3^- and H^+ as primary products and with HCO_2^-, $C_2O_4^{2-}$, 4–NC and H_2O_2 as secondary products. Several reaction mechanisms can be postulated to account for these observations. Since PNP boils at T $\geq$ 166 °C,[21] high temperature reactions of PNP vapor inside the cavitating bubbles can be discounted due to its low vapor pressure. Processes

leading to the denitrification of PNP are more likely to occur in the hot solvent layer surrounding the gas bubbles or in the bulk of the solution. A degradation mechanism that involves ·OH radical attack on PNP appears plausible.[22] Results of radiation–chemistry investigations have shown that ·OH reacts rapidly with PNP to produce 4–NC, p–BQ and NO_2^-.[23–25] A plausible mechanism for the reaction of hydroxyl radicals with PNP is as follows:

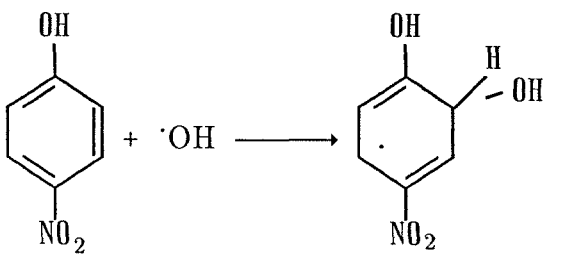

(1)

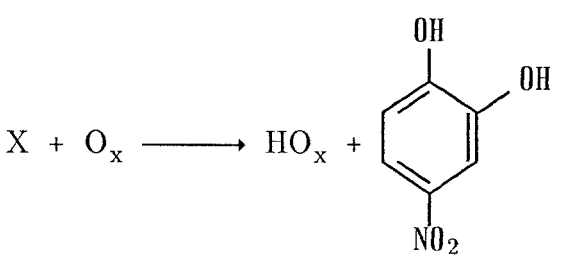

(2)

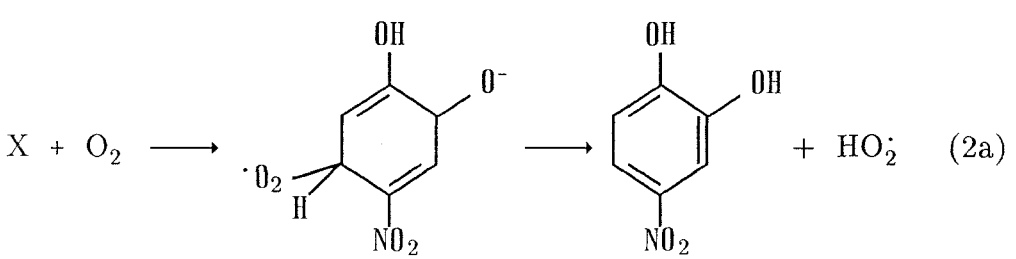

(2a)

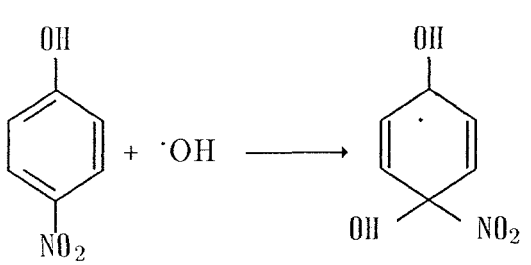

(3)

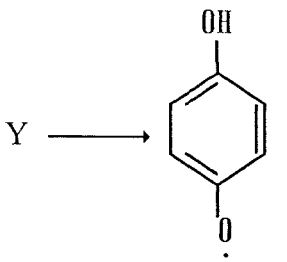

$$+ \ HNO_2 \qquad (4)$$

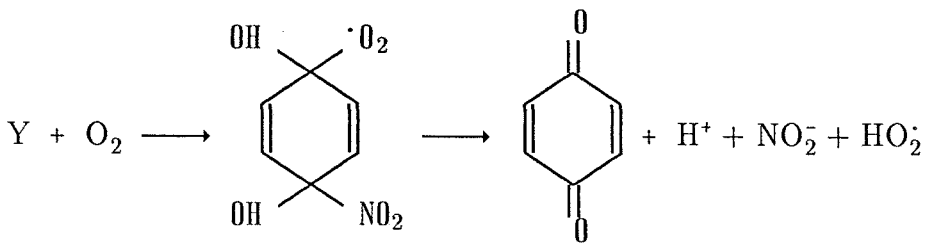

$$+ \ H^+ + NO_2^- + HO_2^{\cdot} \qquad (4a)$$

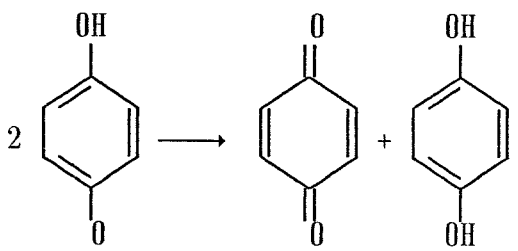

$$(5)$$

where O_x in eq. 2 is an oxidant and HO_x is the reduced form of O_x. Both radicals X and Y have been identified by ESR as the major products of ·OH attack on PNP.[26] The unknown oxidant O_x could be the benzoquinone radical produced by eq. 4 or products from the attack of ·OH in positions ortho (at the carbon atom of the ring bonded to the hydroxyl function) or meta. At pH = 5, about 15% of the ·OH radicals attack PNP via eqs. 1b through 5 to produce NO_2^-, whereas 70% of ·OH radicals react with formation of 4–NC according to eqs. 1a to 3.[23a,24] The ratio of yields for the products is p–BQ (+ hydroquinone):NO_2^-:4–NC = 1:1:4.7. At pH $\geq$ 8, however, 30% of the hydroxyl radicals react to produce nitrite and 5% of

the ·OH radicals reacts with PNP to form 4–NC.[23a,24] Under these conditions, the ratio of yields for the different products is p–Bq (+ hydroquinone):NO_2^-:4–NC = 1:1:1.8.

In aerated solutions the products, X and Y, react with oxygen ($k = 1.7 \times 10^6$ $M^{-1}s^{-1}$ [25]) via eqs. 2a and 4a to yield the same products (and ratio of products) produced by eqs. 1 to 5 with the exception of hydroquinone. Instead, only p–BQ is produced, which is equivalent to the oxidation of hydroquinone by O_2 to produce hydrogen peroxide. In aerated solutions, the peroxy radicals formed by eqs. 2a and 4a will decay with generation of H_2O_2[27]:

$$2\ HO_2^{\cdot} \longrightarrow H_2O_2 + O_2 \qquad (6)$$

For every pair of ·OH radicals which react with PNP one molecule of H_2O_2 is produced. This means that in PNP solutions, the same amounts of peroxide are produced from hydroxyl radical reactions as by sonolysis of pure water. In the absence of PNP, ·OH recombines to form hydrogen peroxide[22]:

$$2\ {}^{\cdot}OH \longrightarrow H_2O_2 \qquad (7)$$

Hydrogen atoms are known to react with PNP but the rate constant of this reaction has not been measured.[25] ·OH and ·H will react preferentially with scavengers present in the cavition bubbles. The main scavenger for H atoms in the gas phase of the bubbles is oxygen. The reaction between H and O_2 at high temperatures is believed to produce oxygen atoms and OH radicals[11b]:

$$H + O_2 \longrightarrow {}^{\cdot}OH + {}^{\cdot}O \qquad (8)$$

According to this reaction, hydrogen atoms are converted to hydroxyl radicals and oxygen atoms before they can reach the solution and react with PNP. Oxygen atoms and hydroxyl radicals are expected to be partially scavenged by nitrogen in the gas bubbles.[11a] These reactions lead to the formation of NO_2^- and NO_3^- in the sonolysis of air–saturated water. Only those radicals which escape into solution without reacting with N_2 will be scavenged by PNP. This argument implies that nitrate and nitrite are produced by two independent mechanisms during the sonolysis of PNP solutions: ***a)*** via the same gas phase reaction which takes place in pure water and ***b)*** from the decay of PNP molecules. The basic assumption that PNP did not interfere with the gas phase chemistry taking place inside the hot cavities is confirmed by the close agreement of k_1 calculated from the decay of PNP and the rate constants derived from the formation of NO_2^- and NO_3^- as well as from the H^+ results.

However, a closer inspection of the results reveals that the sonochemical decay of PNP in aqueous solution cannot be explained only on the basis of reactions between ·OH and PNP in the bulk solution phase. For example, PNP decreased exponentially with sonication time, while PNP attack by ·OH in homogeneous solution follows zero–order kinetics.[24,25] First–order kinetics have been observed in the sonication of thymine[2] and phenol.[28] In both cases the concentration decreased exponentially with time at initial concentrations of substrate $\leq$ 1 mM, whereas at higher concentrations the reactions followed zero–order kinetics.[2,28] These results have been explained by assuming that thymine and phenol react preferentially in the interfacial region with free radicals.[2] At low substrate concentrations ($\leq$ 1 mM)

the rate–limiting step was considered to be the diffusion of substrate to the reaction zone, while the reaction of free radicals and substrate was assumed to occur very fast (diffusion controlled).[2] At high solute concentrations (> 1 mM) the reactive radicals will be scavenged as they reach the interface; thus zero–order kinetics are observed.[2] This model is only correct if the radical concentrations at the interface are very high, otherwise low concentrations of solute would be sufficient to scavenge most of the free radicals.

However, this model presents a simplified version of the events that occur during sonolysis. For example, solute–radical reactions in the bulk solution[11a,12,13] are not considered. Also, no allowance is made for thermal decomposition reactions of the solute in cavities as well as reactions in the hot surroundings of the cavities.

It is, therefore, not surprising that several observations made in sonolysis experiments with PNP solutions remained unexplained. The unexplained results are as follows:

1) According to the above model, the first–order decay of substrate is related to diffusion of substrate to the reaction zone. In the case of PNP this assumption implies that diffusion of the PNP molecules to the interface was highest at the lowest [PNP], since k_1 increased with decreasing concentration of the substrate (Figure 3.9a). Obviously, such a conclusion is not correct.

2) If p–BQ is formed exclusively via the sequence of eqs. 3 and 4a the measured concentrations of quinone represent only 13% of the products produced by reaction of ·OH with PNP. We observed that after 10 min of sonication [p–BQ] = 5.9 μM. The free–radical model predicts a change of [PNP] equal to Δ[PNP] = 45 μM for the same reaction time. The predicted value of Δ[PNP] does not agree with the experimental value of 17 μM.

3) The initial ratio of products from the sonolysis of PNP was p–BQ:NO_2^-:4–NC = 1:3.6:0.7. In contrast, the observed products of ·OH attack on PNP were formed initially with a ratio of p–BQ:NO_2^-:4–NC of 1:1:4.7.[23a,24] Note that in the case of phenol the ratio of products, at short reaction times, was the same at high[29] as well as at low[30] ·OH concentrations. By analogy, the initial ratio of products from hydroxyl radical attack on PNP is not expected to vary with changing [·OH]. The differences in the ratio of products suggest that the mechanism of reaction in the sonolysis of PNP is different from the mechanism represented by reactions 1 to 5. It might be argued that the different ratio of products in the sonolysis reflects a different selectivity of the ·OH attack at high temperatures. However, extensive investigations on high temperature reactions of ·OH with aromatic compounds have demonstrated that at T $\geq$ 400 K the main reaction pathway is hydrogen atom abstraction instead of addition to the aromatic ring.[31] Thus, the denitrification of PNP initiated by reaction 1 is not expected to be the main reaction pathway in the high temperature regions of the interface.

The relatively fast decay of PNP can be explained by the thermal decomposition of PNP in the near vicinity region of the hot collapsing gas cavities. The thermal instability of nitroaromatic compounds, which forms the basis for their use as explosives, is well documented.[21,32,33] As mentioned above, PNP is known to decay thermally at T $\geq$ 166 °C (439 K). While no kinetic information is available for PNP, closely related compounds such as nitrobenzene (NB) and p–nitrotoluene (p–NT) have been recently studied by shock–tube experiments.[33] Both compounds are decomposed at high temperatures by cleavage of the C–NO_2 bond. The analogous reactions for PNP are:

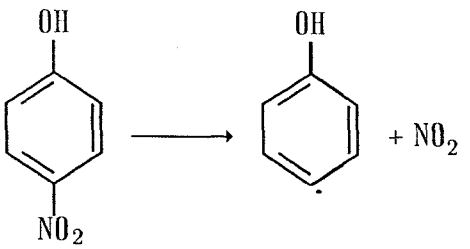

(9)

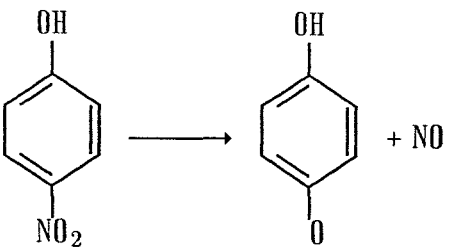

(10)

Assuming that NO and NO_2 are the precursors of NO_2^- (*vide infra*), the unimolecular decay of PNP via eqs. 9 and 10 provides a plausible explanation for the observed first–order denitrification of PNP by the action of ultrasound. In order to understand the formation of 4–NC it has to be assumed that PNP decays by parallel zero– and first–order processes:

$$-\frac{d[PNP]}{dt} = k_0' + k_1[PNP]_t \qquad (11)$$

There k_1 represents $k_9 + k_{10}$ and k_0' is the zero–order rate constant for the reaction between ·OH and PNP, which produces mainly 4–NC. The solution to eq. 11 is :

$$[PNP]_t = \frac{-k_0'}{k_1} + \left(\frac{-k_0'}{k_1} + [PNP]_0\right)e^{-k_1 t} \qquad (12)$$

Since approximately 70% of the ·OH radicals that react with PNP yield

4–NC, the value of $k_0' \simeq k_0/0.7$. Given the experimental values of k_0 shown in Figure 3.9b, the values of k_0' for different initial concentrations of PNP can be estimated. Using these results and the measured concentrations of PNP at different sonication times, the apparent first–order rate constants at different concentrations of PNP were calculated using a non–linear fitting procedure and are presented in curve 2 of Figure 3.9a. The calculated values of k_1 agree closely with the experimental values for k_1 Only kinetic data obtained at short sonication times [i.e. at low fractions of PNP destroyed (1–F ≤ 20%)] were used for this analysis. It can be concluded that the exponential decay of [PNP] via eqs. 9 and 10 is the dominant process and that ·OH radical reactions contribute to PNP decay only at short reaction times. If this interpretation is correct, 4–NC is formed via a zero order process represented by reactions 1 and 2a and decays exponentially with time via reactions analogous to eqs. 9 and 10.

The present model can also account for the unusually high ratio of p–BQ to 4–NC of 1:0.7 observed from sonolysis compared to the ratio obtained from radiolysis of PNP (i.e. p–BQ:4–NC = 0.19:1).[23a,24] Tsang et al.[33] identified two different reaction channels for the pyrolysis of NB and p–NT; they were identified as *1)* the direct loss of NO_2 and *2)* the isomerization of bound NO_2 followed by elimination of NO. In our case these two reaction pathways are represented by eqs. 9 and 10, respectively. For NB and p–NT Tsang et al. estimated that the ratio of rate constants was $k_{elimination}:k_{isomerization} = 2:1$. Hence, the fraction of products formed by the isomerization channel is simply $k_{isomerization}/(k_{elimination} + k_{isomerization}) = 1/3$. Assuming a similar mechanism in our case, it appears that a reaction path involving first eq. 9 followed by eq. 5 contributed to the formation of p–BQ. From the pyrolysis mechanism it is predicted that $[p\text{–}BQ]t \times (\Delta[PNP]t)^{-1}$

= 1/3 provided that the decay of p–BQ is negligible. After correcting both [p–BQ] and Δ[PNP] for the contributions from the ·OH radical reactions, the experimental ratio is 1/2.2 (at t = 10 min). The difference between the expected ratio and the experimental value can be explained by assuming that a fraction of the $NO_2^{\cdot}$ reacted with the aromatic hydroxy radical generated via eqs. 9 and 13 followed by reaction 5.

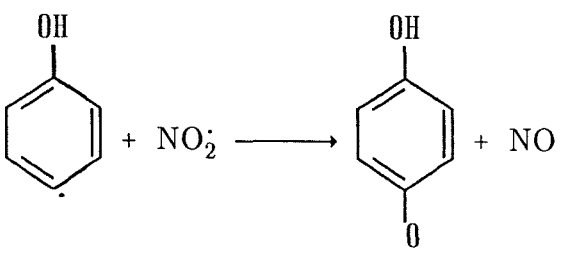

(13)

Reaction 13 is analogous to the postulated mechanism for the attack of $NO_2^{\cdot}$ on hydroxy–cyclohexadieryl radicals.[34] Thus, according to our model, p–BQ is produced mainly by pyrolysis of PNP while the formation of p–BQ by ·OH radical attack is of minor importance.

The proposed mechanism for the decomposition of PNP based on pyrolysis reactions not only explains our kinetic observations, but enables us to estimate the reaction temperatures in the interfacial region. Using the known rate expressions for model compounds and assuming a similar rate expression for the case of PNP, the average temperature in the reaction zone can be evaluated. This method, which is called chemical thermometry, has been used previously to estimate the temperature inside and in the surroundings of collapsing bubbles in hydrocarbon solvents.[4] From the values of k_1 shown in Figure 3.9a and using $k(C_6H_5NO_2 \longrightarrow C_6H_5^{\cdot} + NO_2^{\cdot}) = 1.9 \times 10^{15} e^{-3306/T}\ s^{-1}$,[33] the temperature of the interfacial region

was found to vary between T = 740 – 790 K (see Table 3.1). The same results were obtained by using the rate expression for p–NT.[33] Higher temperatures (~ 2000 K) were estimated for the interface of bubbles in hydrocarbon solvents.[4] The difference in temperature between water and hydrocarbons can be explained by considering the different thermal conductivities of each solvent. Because of the higher thermal conductivity of H_2O, heat will move faster in this water and the peak interfacial temperature is expected to be lower.[35] The results presented in Table 3.1 are considered to be lower limits for the average temperature in the interfacial region, since k_1 is only an apparent first–order rate constant for the reaction.

In order to explain the chemical processes, which take place at the interface, it is necessary to understand, at least qualitatively, the sequence of events occurring in that region. The local temperature in the solvent surrounding the bubble will be a time–dependent spatial gradient during the collapse of the cavity as proposed earlier for hydrocarbon solvents.[4] Thus, heat will move from the surface of the bubble toward the solution bulk. It is further assumed that ·OH generated in the hot bubbles will diffuse to the solvent interface and subsequently through it at a speed similar to that of the front of the heat wave. In the solvent, ·OH reacts with PNP. The OH–adducts will increase in thermal energy as the temperature of the solvent increases. At the same time PNP molecules situated at the interface having a thermal energy equivalent to or greater than 439 K will react by denitration via eqs. 9 and 10. However, this reaction is not restricted to PNP molecules. Addition of OH radicals to the ring of PNP is not expected to increase the strength of the C–NO_2 bond. Therefore, all OH–adducts with sufficient thermal energy will undergo denitrification via an analogous mechanism. The

Table 3.1

Calculated first-order p–NP thermal decomposition rates and corresponding effective temperatures of the reaction zone.

[p–NP] (μM)	$10^4 \cdot k$ (s^{-1})	T (K)[a]
10	8.50	782
20	8.33	781
50	4.83	771
100	2.33	758
250	0.96	743
500	0.70	738
1000	0.30	724

[a] Calculated assuming $k_1 = 1.9 \times 10^{15} e^{-33026/T}$

threshold temperature for the loss of NO_2 from "OH–PNP" adducts is expected to be similar to the minimum temperature for PNP.

The fate of the resulting OH adducts can be predicted from results gained in high temperature studies on hydroxyl radicals with aromatics.[31] These studies indicate that at $T \leq 325$ K the addition reaction (eq. 14) dominates.

$$\cdot OH + \text{aromatic} \longrightarrow (OH - \text{aromatic}) \qquad (14)$$

For $T \geq 400$ K dissociation of the OH–adduct is very fast:

$$(OH - \text{aromatic}) \longrightarrow \cdot OH + \text{aromatic} \qquad (15)$$

At $T \simeq 1000$ K hydroxyl radicals and hydrogen atoms react predominantly with phenol via hydrogen atom abstraction from the hydroxy group.[31a] In the case of PNP, the resulting phenoxyl radicals are strong oxidants ($E^o = 1.2$ V vs NHE)[36] and will probably reform PNP after oxidizing other products. The reaction of eq. 15 is very interesting because it implies that, after the release of the hydroxyl radical from the aromatic ring, the radical can further diffuse to colder regions of the solvent and react again with solute molecules. The temperature dependence of k_{15} has been measured for benzene, bromobenzene and aniline.[37] For direct comparison with our results with PNP, aniline appears to be the most appropriate since the electron–donating properties of the $-NH_2$ and –OH are similar. Using the corresponding temperature dependence, $k_{15} = 6 \times 10^{11} e^{-8400/T}\ s^{-1}$ [37], a half–life of 48 ns is calculated for eq. 15 at 790 K ($k_{15} = 1.5 \times 10^7 s^{-1}$). This short half–life implies that PNP and probably most of the hydroxylated aromatic products

produced by the decay of PNP are relatively non–reactive toward ·OH in the high–temperature regions of the interface. This argument leads to the conclusion that formation of 4–NC and denitration of PNP via ·OH radical attack (reactions 2a and 4a) occurred in the cooler region of the interface (T < 439 K).

Products of eqs. 9 and 10 are expected to decay further by pyrolysis and/or free radical reactions. The preferential formation of nitrite at short sonication times is an indication that the reaction between NO_2 and ·OH (eq. 16) to form nitric acid is not important. Nitrous acid (i.e. nitrite) is produced via eq. 17.[38]

$$NO_2 + {}^{\cdot}OH \longrightarrow HNO_3 \qquad (16)$$

$$NO + OH \longrightarrow HNO_2 \qquad (17)$$

Since eq. 9 is considered to be the main decay pathway for PNP, it appears that NO_2 was rapidly converted to NO presumably by combination of NO_2 with organic radicals produced by pyrolysis reactions in a reaction similar to eq. 10:

$$R^{\cdot} + NO_2 \longrightarrow RO^{\cdot} + NO \qquad (18)$$

While ·OH reaction with aromatics followed by O_2 addition can lead to ring opening and formation of polycarboxylic acids,[31b] formation of formate from these acids would require a concerted attack by several hydroxyl radicals. Thus, the generation of formate is consistent with a pyrolysis pathway. Oxalate was detected only after an induction period of about 10 min. Oxalate could be produced by OH radical attack on formate as has been found in the sonolysis of aqueous formate

solutions under Ar.[11c] However, the sonolysis of oxygenated formate solutions generates CO_2 and not oxalate.[11c] Reaction of ·OH with formic acid at high temperatures also leads to CO_2 in the absence of O_2.[31b] Since at short sonication times only 50% of the degraded PNP is accounted for by the appearance of 4–NC, p–BQ and HCO_2^-, the remainder could be postulated to be polycarboxylic acids formed as intermediates. The delayed formation of oxalate can be explained if the polycarboxylic acids are formed as precursors.

According to our model PNP was denitrated mainly by pyrolysis reactions but the detected products resulted from pyrolysis and free radical reactions. The concentration of PNP near the surface of the bubbles, which is the zone of the interface where pyrolysis is expected to take place, is assumed to increase with increasing PNP concentration in solution. However, once the interface is saturated with PNP molecules, no further increase of [PNP] in this region will result upon increasing [PNP] in the solution. It seems that the limiting concentration of PNP at the interface is achieved at $[PNP]_i \simeq 500$ μM, since P (percentage of PNP converted to 4–NC) was nearly independent of concentration in the range $10 \leq [PNP]_i \leq 500$ μM (see Figure 3.11; Appendix). At $[PNP]_i = 1$ mM the fraction P increased abruptly to 30%, indicating that [PNP] was still increasing in regions far away from the bubble surface. This in turn allowed PNP to compete successfully with pyrolysis products for ·OH. The decrease of k_1 in solutions containing PNP and 4–NC or NO_2^- is explained, in part, assuming that 4–NC and NO_2^- were able to displace some PNP molecules from the interface. In addition, both NO_2^- and 4–NC decay at the interface with formation of NO_2. Nitrite is oxidized by OH radicals to NO_2 according to eq. 19:[22]

$$NO_2^-/HNO_2 + {}^{\cdot}OH \longrightarrow NO_2 + OH^-/H_2O \qquad (19)$$

The additional formation of NO_2 at the interface by reactions other than eq. 9 will increase the probability of the reverse reaction (eq. –9). This second–order reaction will become faster with increasing $[NO_2]$ resulting in the apparent retardation of PNP decay. The same explanation holds for the results shown in Figure 9a. At low concentrations of PNP only small amounts of NO_2^-, 4–NC and products from eq. 9 are generated by sonication. Thus, the back reverse reaction of eq. 9 is expected to be very slow and the unimolecular decay of PNP dominates. As $[PNP]_i$ increased k_1 decreased due to the increasing amounts of products from eq. 9 and from the increasing concentrations of NO_2^- and 4–NC; which produced higher $[NO_2]$ and accelerated the reverse of eq. 9.

The concentration of PNP in the high temperature zone of the interface is expected to depend also on solution pH. Evidence gathered in earlier studies suggests that the bubbles are hydrophobic and that hydrophobic compounds can accumulate in the hot surroundings of the interfacial region where they undergo high temperature reactions. The hydrophobic nature of the aromatic ring should drive PNP molecules to the interfacial zone, whereas the polar NO_2 and OH groups will be repelled from the interface. At pH > pK_a the [PNP] at the interface is expected to be smaller than the concentrations attained at lower pH values, due to the increased repulsion from the interface generated by the phenoxide ion. Furthermore, delocalization of electrons from the deprotonated hydroxyl groups into the aromatic ring will increase the stability of the C–NO_2 bond by increasing the sp^2 character of that bond:

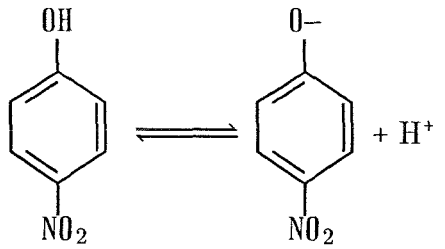

(20)

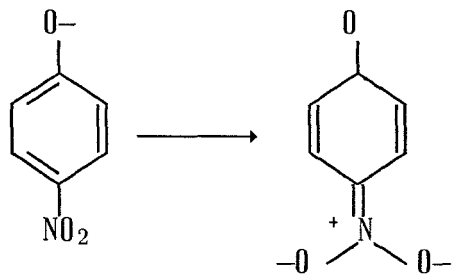

(21)

An increase in the stability of the C–NO_2 bond will lead to an increase in the thermal stability of PNP. The decrease of [PNP] at the interface at pH > 7 (pK_a of PNP = 7.05), together with the increased stability of the nitrophenoxide ion explains the low values of k_1 found in alkaline solutions. The fact that k_1 is relatively constant between $8 \leq pH \leq 11.8$ and is independent of the nature of the buffer (phosphate or borax) provides support for our interpretation.

In conclusion, the application of ultrasound for the control of oxidizable trace contaminants in water has the potential to become a competitive technology with semiconductor photodegradation.[39] For example, the relative efficiency of ultrasound in terms of the total power consumed per mole of p–nitrophenol degraded per liter of water is far superior to photolysis.[39] In our investigation of the ultrasonic oxidation of H_2S, we have found a direct linear relationship between the applied power at a fixed frequency and the observed rate of loss of S(–II). Thus, a continuous–flow stirred–tank (CSTR) probe reactor can attain significant conversion efficiencies at relatively high volumetric flow rates. Our initial tests

indicate that the use of large high–powered sonicators in the CSTR mode can result in viable degradation efficiencies.

An attractive alternative to the flow–through probe system is the high intensity flat–plate reverberatory sonicator or the near–field acoustical processor (NAP).[40] The NAP reactor system consists of two sonicated metal plates that form two sides of a rectangular flow–through pipe; one plate has a set of transducers operated at 16 kHz while the opposing plate has a similar set of transducers operated at 20 kHz. In this configuration, a liquid flowing between the plates, which may be as large as 0.5 m × 3 m with a plate separation of 0.08 m, is exposed to an ultrasonic intensity that is greater than that expected from a simple doubling of a single plate due to reverberation of the ultrasound. This technology has already been used on a large scale for the extraction of oil from oil shale.[40] In the near future, we plan to explore the feasibility of a NAP system for high capacity water purification. Commercial systems have been constructed to handle process streams with volumetric flow rates approaching 265 L min^{-1}.[40]

References

1. Suslick, K. S., in ***Ultrasound: Its Chemical, Physical and Biological Effects***; Suslick, K. S., Ed., VCH: New York, **1988**, pp. 126–163.
2. Sehgal, C. M.; Wang, S. Y. *J. Am. Chem. Soc.* **1981**, *103*, 6606.
3. Henglein, A. *Ultrasonics* **1987**, *25*, 6.
4. Suslick, K. S.; Hammerton, D. A.; Cline, D. E., Jr. *J. Am. Chem. Soc.* **1986**, *108*, 5641.
5. Shutilov, V. A. In ***Fundamental Physics of Ultrasound***; Gordon & Breach Science Publishers: New York, 1988.
6. Lauterborn, W. *Acustica* **1974**, *31*, 51.
7. (a) Makino, K.; Massoba, M. M.; Riesz, P. *J. Phys. Chem.* **1983**, *87*, 1369.
   (b) Makino, K.; Massoba, M. M.; Riesz, P. *J. Am. Chem. Soc.* **1982**, *104*, 3537.
8. Suslick, K. S. In ***Modern Synthetic Methods***; Sheffold, R., Ed., Springer–Verlag: New York, 1986, Vol. 4.
9. Henglein, A.; Kormann, C. *Int. J. Radiat. Biol.* **1985**, *48*, 251.
10. (a) Murali Krishna, C.; Kondo, T.; Riesz, P. *J. Phys. Chem.* **1989**, *93*, 5166.
    (b) Murali Krishna, C.; Lion, Y.; Kondo, T.; Riesz, P. *ibid.*, **1987**, *91*, 5847.
11. (a) Hart, E. J.; Fischer, Ch.–H.; Henglein, A. *J. Phys. Chem.* **1986**, *90*, 5989.
    (b) Fischer, Ch.–H.; Hart, E. J.; Henglein, A. *ibid.*, **1986**, *90*, 1954.
    (c) Hart, E. J.; Henglein, A. *ibid.*, **1985**, *89*, 4342.
12. (a) Kondo, T.; Murali Krishna, C.; Riesz, P. *Radiat. Res.* **1989**, *118*, 211.
    (b) Gutierrez, M.; Henglein, A.; Fischer, Ch.–H. *Int. J. Radiat. Biol.* **1986**,

50, 313.

13. (a) Murali Krishna, C.; Kondo, T.; Riesz, P. *Radiat. Phys. Chem.* 1988, *32*, 121.

(b) Kondo, T.; Murali Krishna, C.; Riesz, P. *Int. J. Radiat. Biol.* 1988, *53*, 891.

14. (a) Alegria, A. E.; Lion, Y.; Kondo, T.; Riesz, P. *J. Phys. Chem.* 1989, *93*, 490.

(b) Gutierrez, M.; Henglein, A. *J. Phys. Chem.* 1988, *92*, 2978.

15. Kortum, G. *Z. Physik. Chem.* [B] 1939, *42*, *39*.

16. Lacoste, R. J.; Covington, J. R.; Frisone, G. *Anal. Chem.* 1960, *32*, 990.

17. Kormann, C.; Bahnemann, D. W.; Hoffmann, M. R. *Environ. Sci. Technol.* 1988, *22*, 798.

18. (a) Sunkel, J.; Staude, H. *Ber. Bunsenges. Phys. Chem.* 1969, *73*, 203.

(b) Sunkel, J.; Staude, H. *ibid.*, 1968, *72*, 567.

19. Mead, E. L.; Sutherland, R. G.; Verral, R. *Can. J. Chem.* 1976, *54*, 1114.

20. Bhattacharyya, P. K; Veeraghavan, R. *Int. J. Chem. Kinetics* 1977, *9*, 629.

21. Deason, W. R.; Koerner, W. E.; Munch, R. H. *Ind. Eng. Chem.* 1959, *51*, 1001.

22. Buxton, G. V.; Greestock, C. L.; Helman, W. P.; Ross, A. B. *J. Phys. Chem. Ref. Data* 1988, *17*, 513.

23. (a) O'Neil, P.; Steenken, S.; Van Der Linde, H.; Schulte–Frohlinde, D. *Radiat. Phys. Chem.* 1978, *12*, 13.

(b) Volkert, O.; Termens, G.; Schulte–Frohlinde, D. *Z. Phys. Chem.* N. F. 1967, *56*, 261.

(c) Grasslin, D.; Merger, F.; Schulte–Frohlinde, D.; Volkert, O. *Z. Phys.*

Chem. N. F. **1966**, *51*, 84.

24. Suarez, C.; Louys, F.; Gunter, K.; Eiben, K. *Tetrahedron Lett.* **1970**, 575.

25. Cercek, B.; Ebert, M. *Adv. Chem. Ser.* **1968**, *81*, 210.

26. Eiben, K.; Schulte–Frohlinde, D.; Suarez, C.; Zorn, D. *Int. J. Radiat. Phys. Chem.* **1971**, *3*, 409.

27. Bielski, H. J.; Cabelli, D. E.; Arudi, R. L.; Ross, A. B. *J. Phys. Chem. Ref. Data* **1985**, *14*, 1041.

28. (a) Chen, J. W.; Chang, J. A.; Smith, G. V. *Chem. Eng. Prog. Symp. Ser.* **1971**, *67*, 18.

(b) Lure, Yu. Yu.; Kandzas, P. F.; Mokina, A. A. *Russ. J. Phys. Chem.* **1962**, *36*, 1422.

29. Hashimoto, S.; Miyata, T.; Washino, M.; Kawakami, W. *Environ. Sci. Technol.* **1979**, *13*, 71.

30. Raghavan, N. V.; Steenken, S. *J. Am. Chem. Soc.* **1980**, *102*, 3495.

31. (a) He, Y. Z.; Mallard, W. G.; Tsang, W. *J. Phys. Chem.* **1988**, *92*, 2196.

(b) Atkinson, R. *Chem. Rev.* **1985**, *85*, 69.

32. Maksimov, Yu. Ya. *Russ. J. Phys. Chem.* **1972**, *46*, 990.

33. Tsang, W.; Robaugh, D.; Mallard, W. G. *J. Phys. Chem.* **1986**, *90*, 5968.

34. Zellner, R.; Fritz, B.; Preidel, M. *Chem. Phys. Letters* **1985**, *121*, 42.

35. Weast, R. C. (Ed.) ***CRC Handbook of Chemistry and Physics***, 1st Student Edition; CRC: Boca Raton, 1988, pp. E–4, E–10.

36. Lind, J.; Shew, X.; Eriksen, T. E.; Merenyi, G. *J. Am. Chem. Soc.* **1990**, *112*, 47.

37. Witte, F.; Urbanik, E.; Zetzsch, C. *J. Phys. Chem.* **1986**, *90*, 325.

38. (a) Seddow, W. A.; Fletcher, J. W.; Sopchyshyn, F. C. *Can. J. Chem.* **1973**,

51, 1123.

(b) Burkholder, J. B.; Hammer, P. D.; Howard, C. J. *J. Phys. Chem.* 1987, *91*, 2136.

39. Mills, G.; Chew, B.; Hoffmann, M. R. *J. Phys. Chem.* **1990**, "Photocatalytic Degradation of Pentachlorophenol on TiO_2," in revision.

40. Mason, T. J.; Lorimer, J. P. ***Sonochemistry***, Ellis Horwood Limited: Chichester, England, 1988; pp. 226–227.

Appendix

The action of 20–kHz ultrasound on aqueous solutions of p–NP resulted in an exponential decrease of [PNP] as shown in Figures 3.1, 3.2 and 3.3. Small amounts of 4–NC were produced as the result of the decay of PNP. The formation of 4–NC led to the quasi isosbestic point at about 460 nm (Figure 3.1). The presence of isosbestic points in the absorption spectra of products and reactants implies that, after a certain reaction time, the absorption of unreacted PNP plus the absorption of all products is, at a particular wavelength, equal to the initial absorption of the PNP solution. This condition is represented by eq. a1 (for $\ell = 1$ cm).

$$\left([\mathrm{PNP}]_o - [\mathrm{PNP}]_t\right) \epsilon^{460}_{\mathrm{p\text{-}np}} = \sum_i \left([\mathrm{P_i}]_t \, \epsilon^{460}_{\mathrm{P_i}}\right) \qquad \text{(a1)}$$

where $[\mathrm{PNP}]_o$ and $[\mathrm{PNP}]_t$ are the concentrations of PNP at reaction times 0 and t, respectively; and $\epsilon^{460}_{\mathrm{P_i}}$ is the extinction coefficient of PNP at 460 nm. Similarly, $[\mathrm{P_i}]_t$ represents the concentration of the product i after a reaction time t and $\epsilon^{460}_{\mathrm{P_i}}$ is the extinction coefficient of product i at 460 nm. Since identical [PNP]'s were obtained from analyses in basic and in acid solutions (at 401 and 317 nm respectively), it can be assumed that 4–NC is the only product which absorbs above 400 nm in alkaline solutions. If the term in parenthesis on the left hand side of eq. a1 is substituted by $\Delta[\mathrm{PNP}]_t$, then equation can be rearranged to eq. a2:

$$100 \frac{\epsilon^{460}_{\mathrm{PNP}}}{\epsilon^{460}_{\mathrm{4-NC}}} = 100 \frac{[\mathrm{4-NC}]_t}{\Delta[\mathrm{PNP}]_t} = \mathrm{P} \qquad \text{(a2)}$$

In eq. a2, $\Delta[\mathrm{PNP}]_t$ is the amount of PNP which has disappeared after a sonication

time t and $[4\text{–NC}]_t$ represents the concentration of 4–NC formed after the same period of time. Hence, the term on the right hand side of this equation corresponds to the percentage (P) of decomposed PNP which has been converted into 4–NC, after a reaction time t. According to eq. a2, this percentage should remain constant with reaction time if an isosbestic point is to be observed. From $\epsilon^{460}_{PNP} = 1600$ $M^{-1}cm^{-1}$ and $\epsilon^{460}_{4\text{–NC}} = 7300$ $M^{-1}cm^{-1}$ (in 0.1 M NaOH) it is calculated by eq. a2 that about 22% of the reacted PNP was converted to 4–NC in a 100 μM solution of PNP sonicated at pH = 5. In order to verify the validity of the assumptions which led to eq. a2, calculation of P was made from the known concentrations of 4–NC and PNP at different reaction times. To allow for an easy comparison of results obtained under different conditions, the values of P were plotted as function of the fraction of PNP destroyed (F) instead of sonication time (Figure 3.11). Line 1 in Figure 3.11 shows the evolution of P with reaction times for a 100 μM solution of PNP sonicated at pH = 5. P decreased slightly with increasing F; when only small amounts of PNP have decayed (F = 0.13) the fraction P is 24.5% whereas after one half life (F = 0.5) P amounts to 19%. The results presented in line 1 of Figure 3.11 help to explain the small shifts towards longer λ, with increasing sonication times, of the point where the spectrum of the unsonicated solution is intersected by the spectrum of the sonicated solution. As P decreased slightly with increasing F, equation a2 predicts a shift of the intersection point towards longer wavelengths, since ϵ^{460}_{PNP} decreases but $\epsilon^{\lambda}_{4\text{–NC}}$ increases with increasing λ. Because of the large difference in the extinction coefficients of PNP and 4–NC the shifts in the intersection points were very small, resulting in a broad ($\Delta\lambda \simeq 2$ nm) isosbestic point centered at 460 nm. Note that the "mean" value of P in line 1 of Figure 3.11 is 22%, in good agreement with the calculation using eq. a2. The quasi–isosbestic

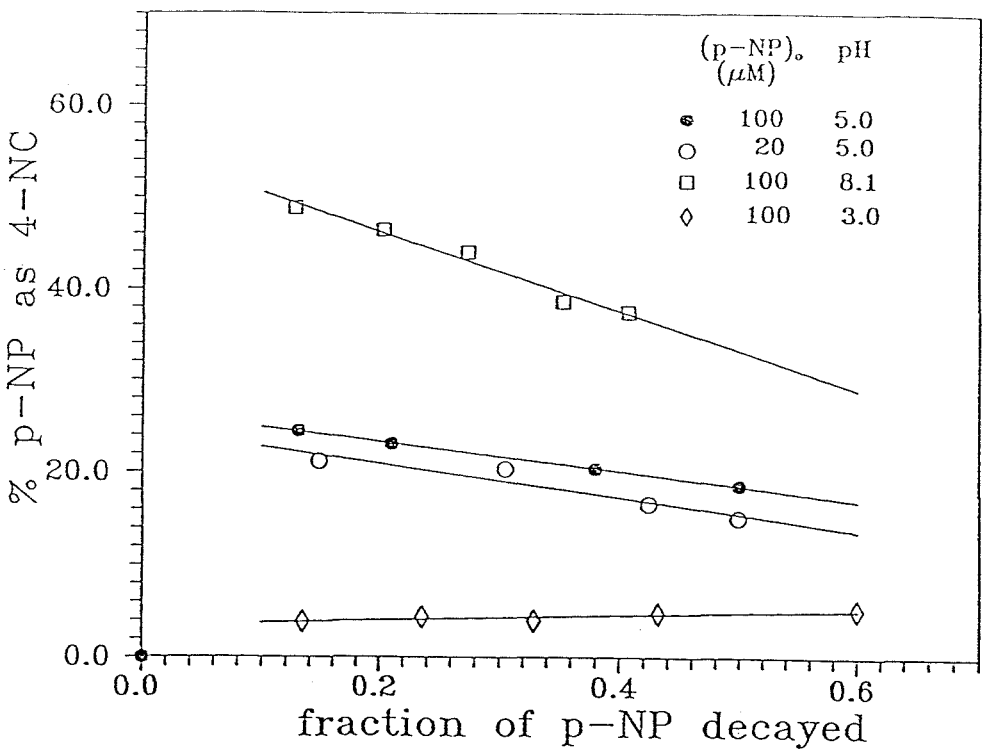

Figure 3.11 Percentage of p–NP decayed converted to 4–NC.

points were close to 460 nm for the experiments carried out at pH = 5. This is not surprising since, at $[PNP]_i < 1$ mM, the dependence of P on F did not change appreciably by changing $[PNP]_i$. An example of this is the result obtained by sonication of a 20 μM solution of PNP (line 2 in Figure 3.11). Only at $[PNP]_i = 1$ mM the quasi isosbestic point shifted to shorter wavelengths because P increased to about 30%. Sonication of PNP solutions at pH = 8.1 led to an isosbestic point at $\lambda \simeq 455$ nm. From the extinction coefficients at that wavelength ($\epsilon_{PNP} = 2700$ $M^{-1}cm^{-1}$ and $\epsilon_{4-NC} = 6400$ $M^{-1}cm^{-1}$) it is calculated that P = 42%, whereas the mean value of P in Figure 3.11 is about 43%. At pH = 3, P is essentially independent of F and P $\simeq$ 5% (Figure 3.11, line 4). From the extinction coefficients at the quasi–isosbestic point at 370 nm ($\epsilon_{PNP} = 530$ $M^{-1}cm^{-1}$, $\epsilon_{4-NC} = 8700$ $M^{-1}cm^{-1}$) a mean value of P = 6% is derived. These examples are a further confirmation of our explanation of the isosbestic points and provide support for the assumption that no product other than 4–NC interfered with the spectrophotometric determinations of [PNP]. This conclusion, in turn, implies that the exponential decay of PNP with sonication time is not an artifact of the analytical methods. The exponential increase of $[NO_2^-]$ with sonication time (Figure 3.4, curve 1) is also consistent with this conclusion.

CHAPTER 4

OXIDATION OF HYDROGEN SULFIDE IN AQUEOUS SOLUTIONS BY ULTRASONIC IRRADIATION

(Submitted to *Environmental Science & Technology*, July 1991)

ABSTRACT

The kinetics and mechanism of the sonolysis of S(–II), where [S(–II)] = [H_2S] + [HS^-] + [S^{2-}], have been investigated in oxic aqueous solutions over the pH range 7 – 12. Ultrasonic irradiation of S(–II) at 20 kHz and 75 $W \cdot cm^{-2}$ results in its rapid oxidation. The reaction of HS^- with $^{\cdot}OH$ is the principal pathway for the oxidation of S(–II) at pH $\geq$ 10; the oxidation products are SO_4^{2-}, SO_3^{2-}, and $S_2O_3^{2-}$. Upon prolonged sonication, SO_4^{2-} is the only observed product. At pH $\leq$ 8.5, thermal decomposition of H_2S within or near collapsing cavitation bubbles becomes the important pathway and elemental sulfur is found as an additional product of the sonolysis of S(–II). Oxidation of S(–II) by ultrasonic irradiation may present an alternative method for the control of H_2S in water and wastewater systems.

Introduction

In 1933, Flosdorf and Chambers (1) reported that metal sulfides were oxidized in the presence of audible sound (1–15 kHz) while investigating the bactericidal action of audible sound. However, Schmitt *et al.* (2) were the first researchers to observe the rapid oxidation of dissolved H_2S gas to colloidal sulfur during sonication at 750 kHz with a 250 W power source. They reported that an increase in the total pressure of the system (P_{O_2}) led to higher oxidation rates up to a limiting pressure. This critical pressure depended on the amount of dissolved H_2S gas and the intensity of irradiation.

Wawrzyczek *et al.* (3) observed the oxidation of H_2S dissolved in water containing Ar or O_2 at 27 kHz and an ultrasonic intensity of 5 W/cm^2. The primary oxidation product was found to be elemental sulfur (i.e., S_8). The reaction yield in their experiments was found to be 25% higher in the presence of Ar as compared to that obtained in oxygenated solutions. The overall reaction was thought to proceed via reactions of HS^- with OH radicals and $HO_2^{\cdot}$ or H_2O_2. A secondary pathway involving the direct decomposition of H_2S to $HS^{\cdot}$ and $H^{\cdot}$ was also proposed.

Cauwet *et al.* (4) studied the ultrasonic decomposition of H_2S into H_2 and S^o at various frequencies up to 600 kHz and at a voltage amplitude of 40 V. They found a continuous increase in H_2 production during sonication of H_2S with increasing ultrasonic power and they found that the yield of H_2 doubled in solutions containing 10% diethanolamine (a possible surface tension effect).

The chemical effects of ultrasound result from the phenomenon of acoustic cavitation (5–7). Sound waves with frequencies higher than 16 kHz traveling through a liquid can force the growth and subsequent collapse of small bubbles in

response to the passage of expansion and compression waves. In the interior of the collapsing bubbles (cavities) extreme transient conditions exist; temperatures approaching 5000 K have been determined experimentally (8) and pressures of several hundred atmospheres have been calculated (5,9). At 20 kHz and typical ultrasonic immersion–horn intensities (10–100 W/cm^2) the radius of the bubble prior to collapse can be estimated to be on the order of several hundred μm (400–500 μm) (10). The time scale for the collapse of the bubble is <100 ns and the time scale for heat diffusion in the surrounding liquid is a few microseconds with a corresponding diffusion length of a few hundred nanometers (8).

The primary chemical effects are realized during and immediately after collapse of the cavity as a result of the transient high pressures and temperatures. For instance, when the solvent is water, water vapor present in the cavities undergoes thermal dissociation to give hydrogen atoms ($H^{\cdot}$) and hydroxyl radicals ($^{\cdot}OH$) (11). Solutes present near the bubble/water interface can also undergo thermal decomposition (12). Secondary reactions take place in the liquid phase between solute molecules and excited species, mainly $^{\cdot}OH$ in the case of aqueous solutions, escaping from the gas phase into solution. $^{\cdot}OH$ is a powerful and efficient chemical oxidant in both the gas and liquid phase. In the aqueous phase, $^{\cdot}OH$ has a one–electron oxidation potential of $E^{o} = +1.8$ V in neutral solution ($^{\cdot}OH + e^{-} \longrightarrow OH^{-}$) and 2.7 V in acidic solution ($^{\cdot}OH + H^{+} + e^{-} \longrightarrow H_2O$) (13). Reactions of $^{\cdot}OH$ with inorganic and organic substrates are often near the diffusion–controlled rate (14).

Although ultrasound has currently a number of industrial uses (5), its potential for water and wastewater treatment has not been fully explored. A few preliminary studies have indicated that ultrasonic irradiation is effective for the

oxidation of organics and the disinfection of water and wastewater either as the sole means of treatment (15), or in combination with ozonation (16) and UV irradiation (17).

In this paper we present the results of an investigation of the ultrasonic irradiation of S(–II) in oxic aqueous solutions over the pH range 7 – 12 at 20 kHz over a range of applied power. Our work was motivated in part by the potential application of sonolysis for the treatment of H_2S in wastewater. The ultrasonic decomposition of H_2S may prove to be an efficient way for the removal of this gas from fossil fuel refining wastes or geothermal power plants with commercial applications similar to that of the Claus process (18).

Experimental

The ultrasonic irradiation of aqueous sulfide solutions was conducted with a Branson 200 sonifier, operating at 20 kHz. The ultrasonic intensity at the titanium tip of the 1/2–in. sonication probe was about 75 W/cm^2 (corresponding power input $\simeq$ 85 W). Reactions were performed in a water–jacketed–stainless steel cell from Sonics & Materials. The cell is shown schematically in Fig. 4.1; its total volume is 50 ml and it is similar to ultrasonic reactors used in other studies (5–6). The temperature inside the reaction vessel was kept constant at 25 ^{o}C. All irradiations were carried out in air saturated solutions at t = 0. The sample ports of the stainless steel reactor were sealed with rubber septa during the course of sonication and no attempt was made to control the pressure in the headspace (volume of headspace = volume of sonicated solution = 25 ml, initial headspace pressure = atmospheric).

Sulfide concentrations were measured with a sulfide ion specific electrode,

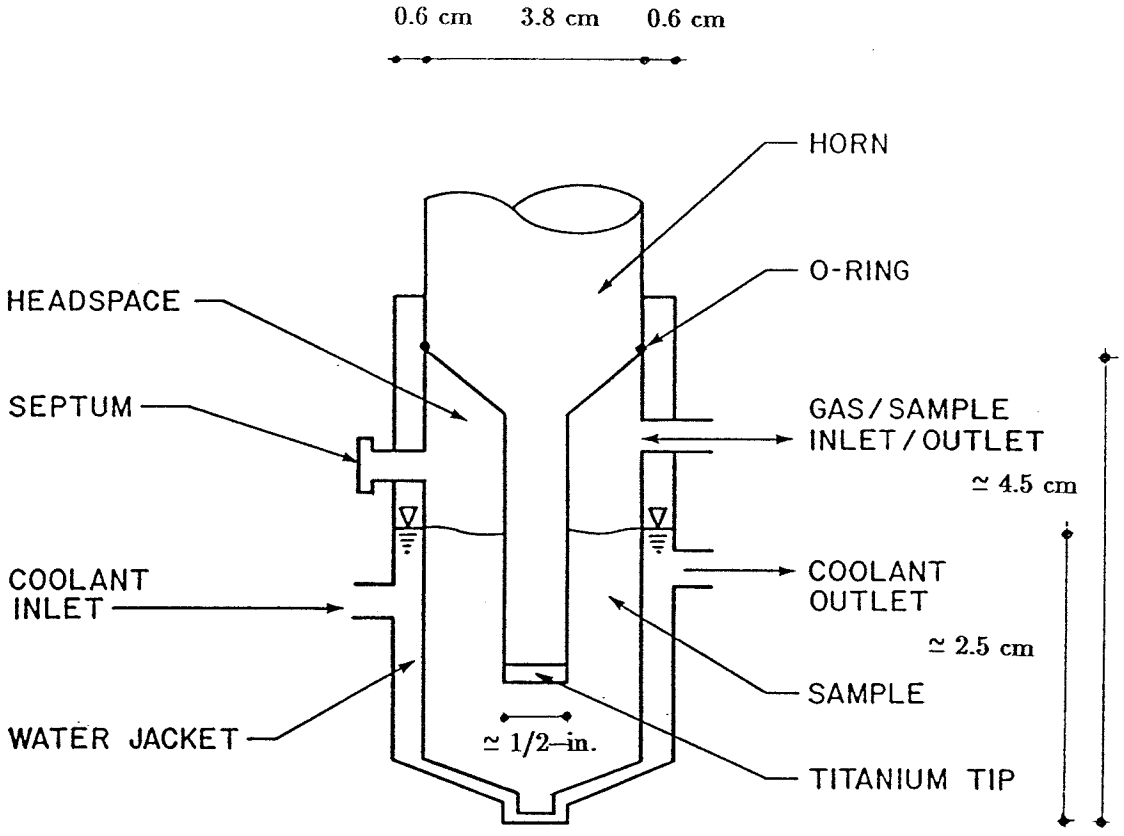

Figure 4.1 Ultrasonic apparatus (Direct immersion horn/SS cell)

ISE (ORION 94–16 Ag/Ag_2S with double junction reference electrode), coupled to an ORION 801–A ion analyzer. Oxygen concentrations were measured with an ORION 97–08–00 oxygen electrode, and pH measurements were performed with a RADIOMETER pH electrode and a PHM84 pH meter. A K–type thermocouple connected to a FLUKE 75 multimeter via a FLUKE 80TK thermocouple module was used for temperature measurements. A HAAKE A80 water circulation and temperature controlling system was used for temperature control. Spectrophotometric measurements were performed on an HP 8450A UV/VIS spectrophotometer. Nitrite, nitrate, sulfate, sulfite and thiosulfate ions were determined with a Dionex 2020i ion chromatograph and a Dionex AS4–A column. The eluent consisted of a mixture of 2.2 mM carbonate and 2.8 mM bicarbonate. Hydrogen peroxide was analyzed fluorometrically as described earlier (19).

Kinetic runs were carried out by sonication of a sample for the desired length of time, followed by sample withdrawal and multiple analysis. Experiments were continued after cleaning the cell thoroughly and filling it with fresh solution. Prior to any analysis, all samples were filtered with 0.2 μ HPLC filters (from Gelman) to remove Ti particles produced during sonication by erosion of the Ti tip of the sonifier. No adsorption of S(–II) or any of the sonication products on the HPLC filters was observed. The water employed in all preparations was purified by a Milli–Q/RO system from Millipore. Mono and disodium phosphate salts (Mallinckrodt) or sodium borate (Spectrum) were used for the preparation of the buffers.

Results

Ultrasonic irradiation of 25 ml solutions of bivalent sulfur at pH 10 (borate

buffer, I=0.06 M) resulted in a linear decrease of [S(–II)] with sonication time. Figure 4.2a shows the concentration of S(–II), where $[S(-II)] = [H_2S] + [HS^-] + [S^{2-}]$, remaining vs sonication time for an experiment at pH 10 and $[S(-II)]_o \simeq 200$ μM. The zero–order rate for this particular experiment was 7.5 $\mu M \cdot min^{-1}$. The rate of [S(–II)] disappearance was also followed spectrophotometrically ($\epsilon_{230} = 7950$ $M^{-1}cm^{-1}$ for HS^-) and the zero–order rate constants obtained using the absorbance data were in agreement with those obtained from the ISE measurements. The products of S(–II) sonolysis at pH 10 were found to be SO_4^{2-} (sulfate), SO_3^{2-} (sulfite) and $S_2O_3^{2-}$ (thiosulfate) as shown in Figure 4.2b. These products were initially formed in the mole ratio 2.2:2.7:1, respectively. An overall mass balance (i.e. $[S(-II)]_t = [S(-II)]_o - [SO_4^{2-}]_t - [SO_3^{2-}]_t - 2 \cdot [S_2O_3^{2-}]$) was achieved within the limits of analytical error.

A post–irradiation oxidation of sulfite to sulfate was observed and was attributed to the subsequent thermal reaction of HS^- with H_2O_2. Hydrogen peroxide is known to form during the sonolysis of water (5). In order to verify this hypothesis, sonicated S(–II) solutions were analyzed for H_2O_2. These concentrations were compared to those measured in sonicated Milli–Q water buffered at pH 10. In the control experiments a linear increase of $[H_2O_2]$ vs sonication time was observed with a zero–order rate constant of 2.52 $\mu M \cdot min^{-1}$. This measured rate of H_2O_2 production during sonolysis of deionized water agreed with our previously reported results (20). However, $[H_2O_2]$ was found to be lower for the S(–II) sonicated solutions as shown in Figure 4.3. The difference can be attributed to the thermal reactions of HS^-, SO_3^{2-} and $S_2O_3^{2-}$ with H_2O_2.

NO_2^- and NO_3^- were also found as products of the sonolysis of water. Figure 4.4 shows the total concentrations of these ions ($[NO_2^-]+[NO_3^-] = [NO_y]$) in

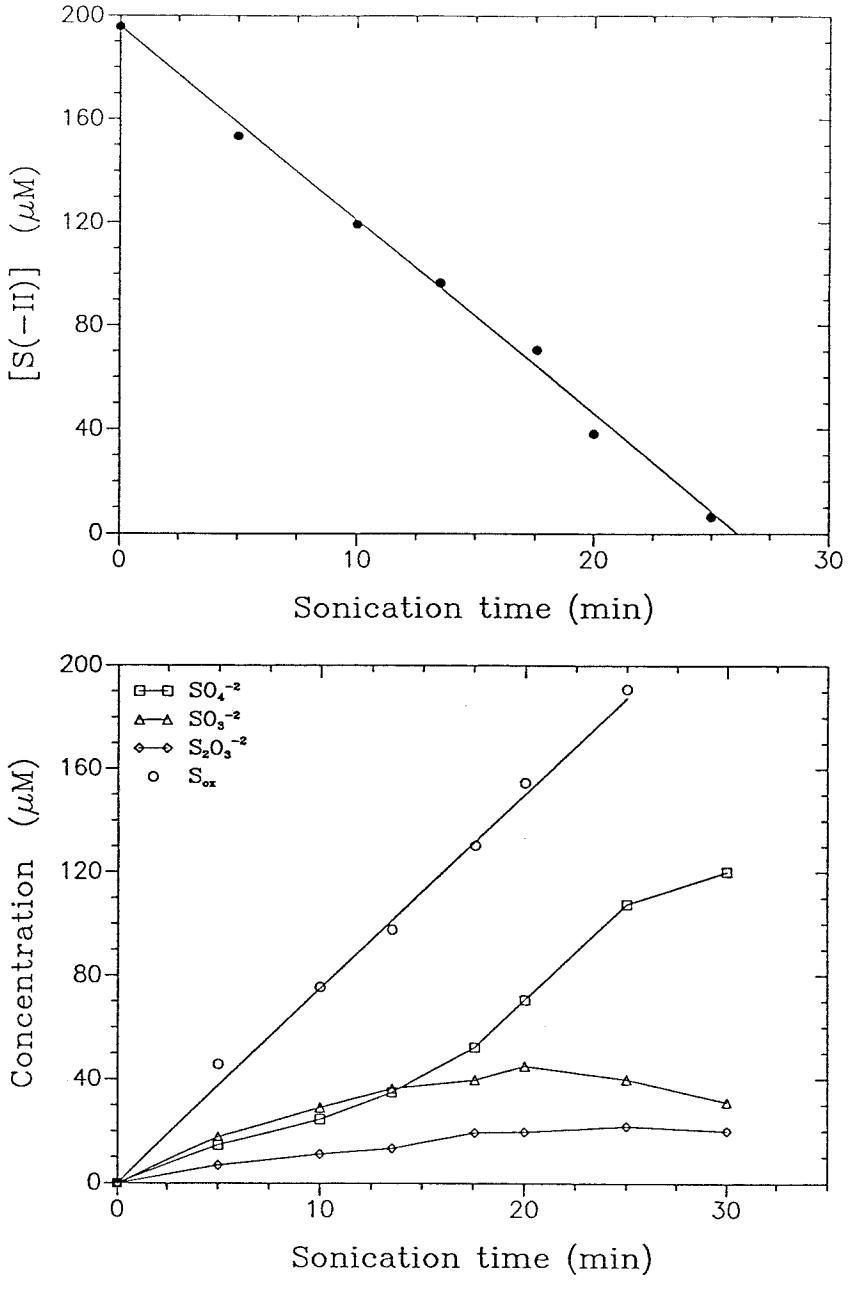

Figure 4.2 Sonication of S(–II) at pH 10, T_b = 25 °C, 75 W/cm², $[S(-II)]_o$ = 196 μM. (a, top) S(–II) decrease with sonication time. (b, bottom) Sonication products distribution; $S_{ox} = [SO_4^{2-}] + [SO_3^{2-}] + 2\cdot[S_2O_3^{2-}]$.

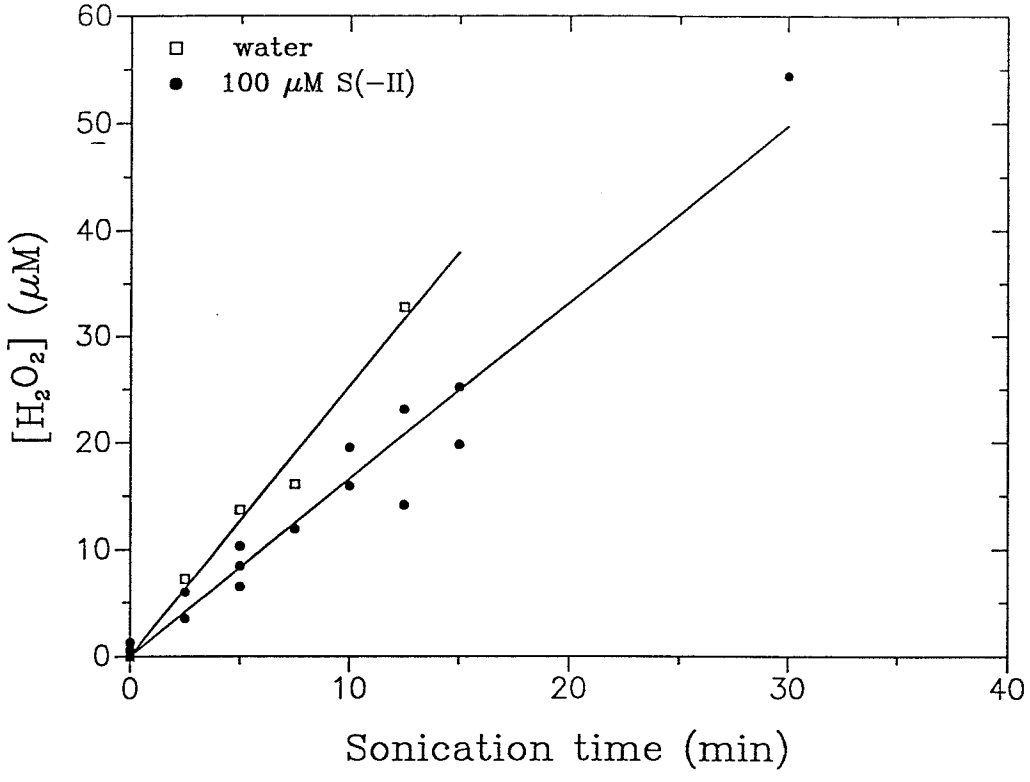

Figure 4.3. Hydrogen peroxide formation versus sonication time.

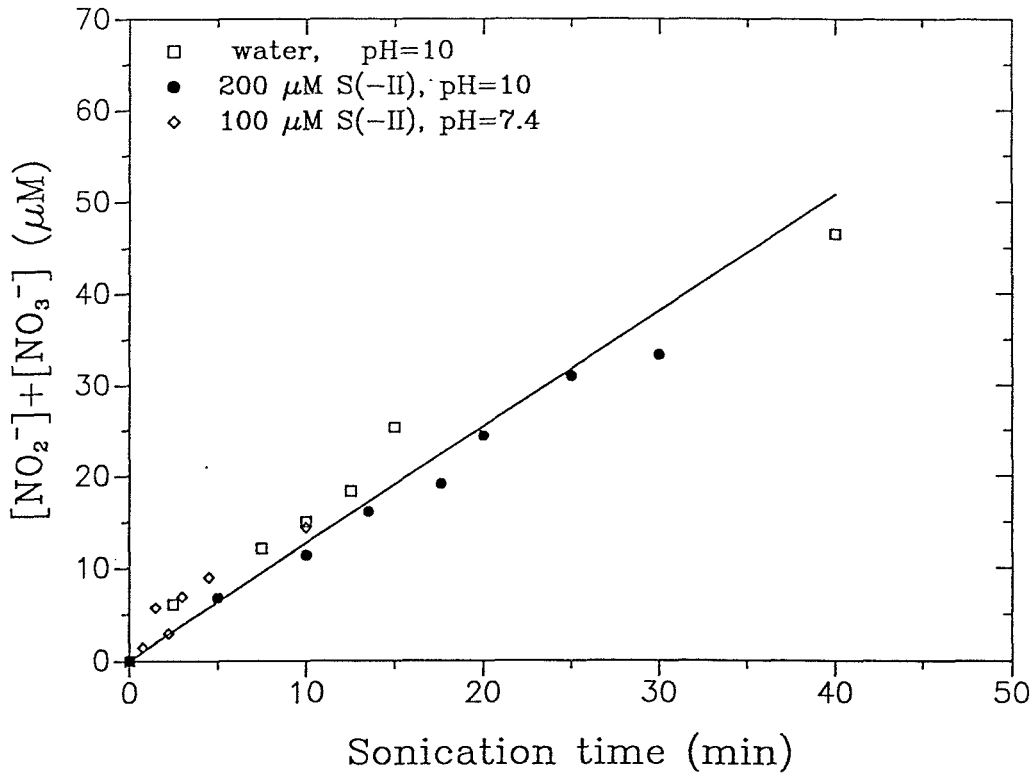

Figure 4.4 NO_y formation during sonication.

sonicated solutions as a function of time. From these results it can be seen that the presence of S(–II) did not affect the rate of NO_y formation which was found to be 1 $\mu M \cdot min^{-1}$.

As mentioned above, the oxidation of S(–II) at pH 10 was found to be zero–order with respect to [S(–II)]. However, the zero–order rate constant, k_o, was found to depend on the initial concentration of S(–II) as shown in Figure 4.5. It can be seen that k_o increased linearly with $[S(-II)]_o$ up to $[S(-II)]_o \simeq 450$ μM and then remained practically constant for higher [S(–II)]. This behavior of k_o vs $[S(-II)]_o$ is quite interesting and will be discussed further in the discussion part of this paper.

In order to determine the sonochemical reactivity of the intermediate product $S_2O_3^{2-}$, thiosulfate solutions were sonicated at pH 10 under the same conditions used for S(–II). A linear decrease of $[S_2O_3^{2-}]$ vs time was observed, and the oxidation products were found to be SO_4^{2-} and SO_3^{2-}. Those products were initially formed with a stoichiometry 1:1, but SO_3^{2-} was later oxidized to SO_4^{2-}. Figure 4.6 shows the distribution of the products for $[S_2O_3^{2-}]_o = 100$ μM. A limited number of experiments showed that the zero–order rate for $S_2O_3^{2-}$ oxidation, k_{ot}, had a dependency on $[S_2O_3^{2-}]_o$ similar to that described above for S(–II) (i.e., k_{ot} increased with $[S_2O_3^{2-}]_o$).

Additional experiments were performed at pH > 10 (with a phosphate buffer) and $[S(-II)]_o = 100$ μM. As in the earlier experiments described above the ultrasonic oxidation of S(–II) followed apparent zero–order kinetics and the oxidation products were found to be SO_4^{2-}, SO_3^{2-} and $S_2O_3^{2-}$. The zero–order rate decreased from 5.4 $\mu M \cdot min^{-1}$ at pH 10 to 4.0 $\mu M \cdot min^{-1}$ at pH 11 and remained constant thereafter. Figure 4.7 presents the results of two experiments performed

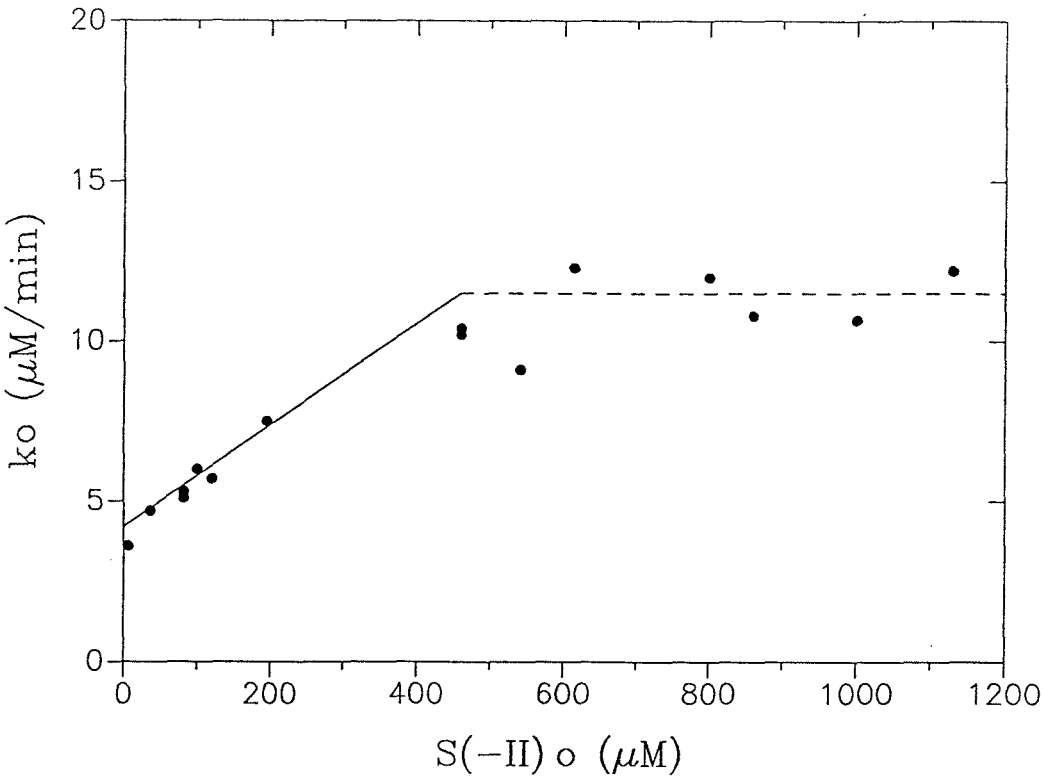

Figure 4.5 Dependence of k_o on $[S(-II)]_o$ at pH 10.

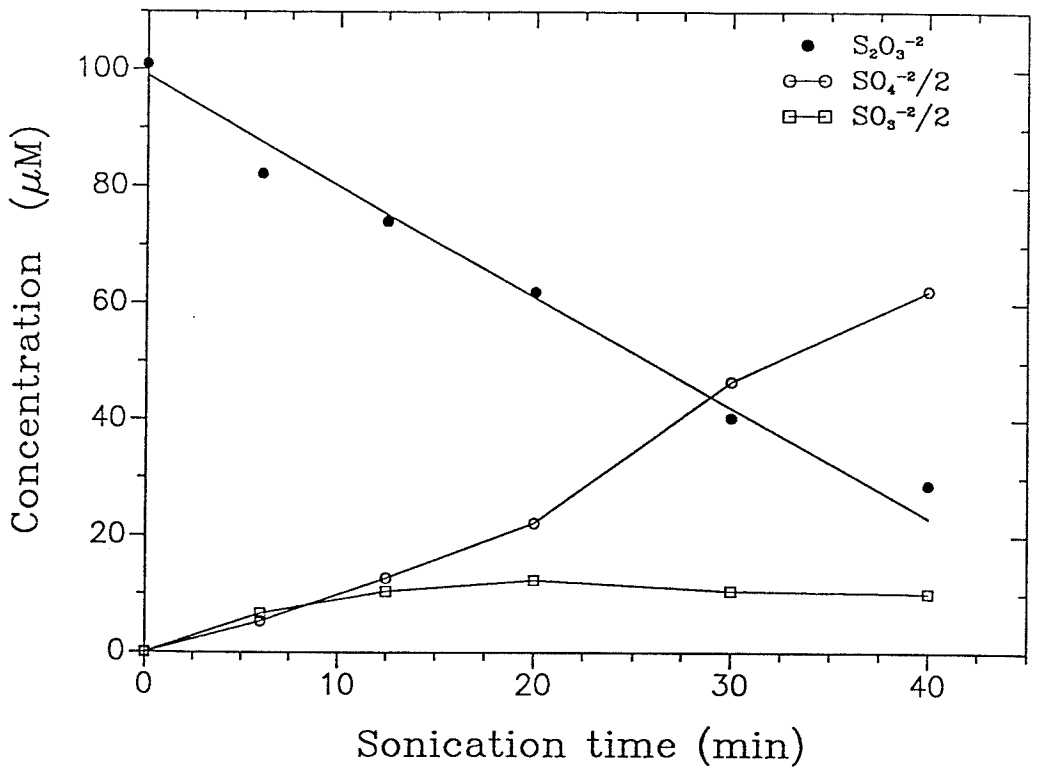

Figure 4.6 $S_2O_3^{2-}$ sonication product distribution at pH 10.

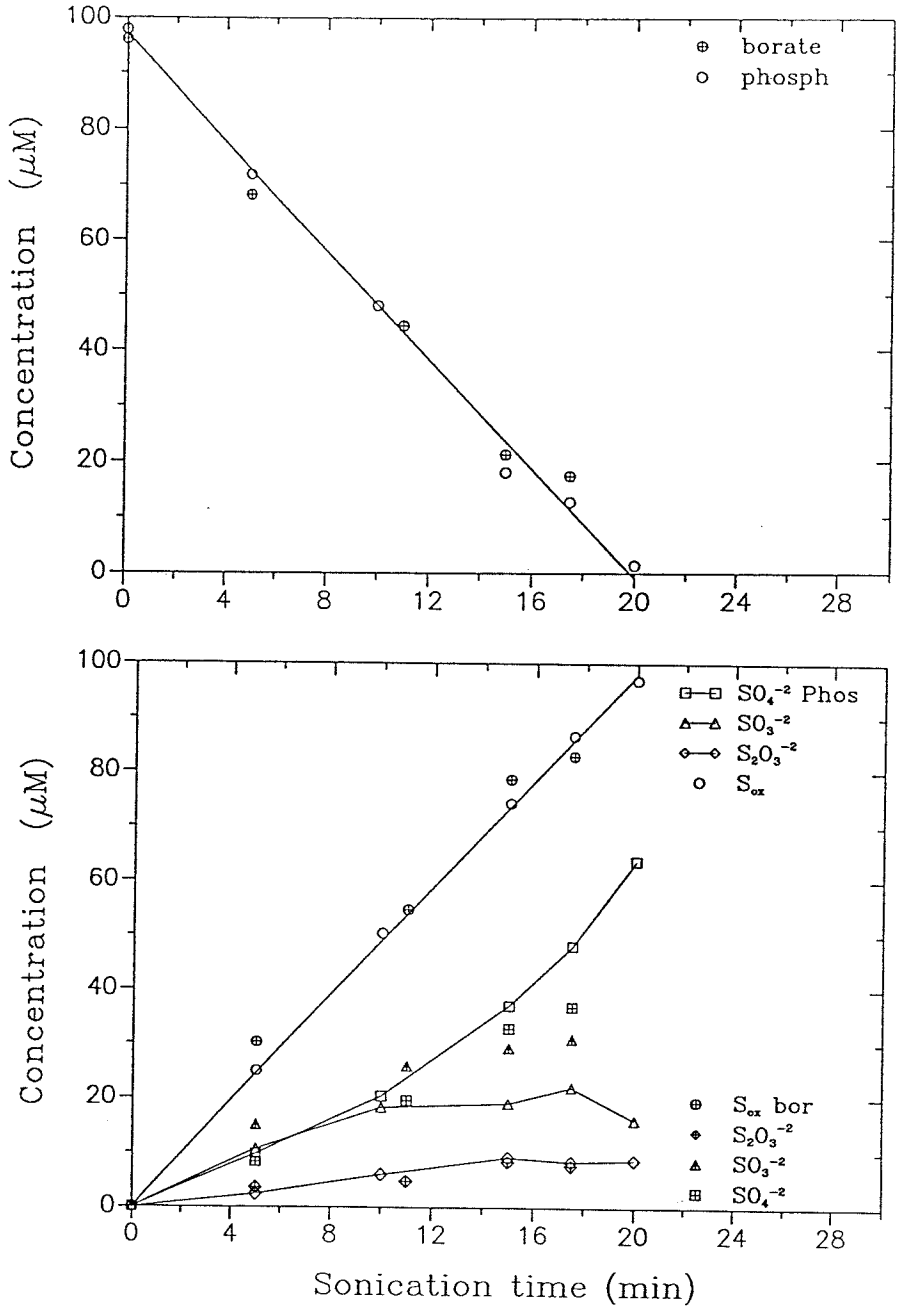

Figure 4.7 S(–II) sonication products distribution in borate and phosphate buffer at pH 10.6. (a, top) S(–II) vs time. (b, bottom) Products.

at pH 10.6, $[S(-II)]_o$ = 100 μM, and with different buffers. It can be seen that the overall rate of the ultrasonic oxidation of S(–II) is the same in both borate and phosphate buffers (Figure 4.7a). The distribution of the products (Figure 4.7b) indicates a catalytic effect of the phosphate buffer on the oxidation of SO_3^{2-} to SO_4^{2-}. Phosphate buffer catalysis has been reported previously by Hoffmann and Edwards (21) and Mader (22).

Experiments performed at pH < 10 revealed an apparent change in the observed reaction kinetics. The rate of ultrasonic oxidation of S(–II) was found to be first–order with respect to [S(–II)] at pH ≤ 8.5. The rate of oxidation of S(–II) increased with decrease in pH. However, the measured concentrations of SO_4^{2-}, SO_3^{2-} and $S_2O_3^{2-}$ could not account for the total observed decrease in S(–II), especially at short sonication times. This difference is shown in Fig. 4.8 where [S(–II)], $[S_{ox}]_{identified}$ (= $[SO_4^{2-}]+[SO_3^{2-}]+2\cdot[S_2O_3^{2-}]$) and $[S_{un}]$ (= $[S(-II)]_o-[S(-II)]-[S_{ox}]_{id}$) are plotted vs sonication time for a typical experiment at pH 7.4. In subsequent experiments H_2O_2 (in excess of $4\cdot[S(-II)]_o$) was added in samples from the sonicated S(–II) solutions and was allowed to react with the reduced sulfur present in the samples before analyzing for S_{ox}. As expected, only SO_4^{2-} was present in the H_2O_2–treated samples. In Fig. 4.9 the $[SO_4^{2-}]$ measured in H_2O_2–treated sonicated solutions at pH 7.4 and $[S(-II)]_o$ = 92 μM is compared to that measured in H_2O_2–treated blanks taken out from the cell before sonication (control). Even though both sets of data showed some scatter compared to the expected value of 92 μM (solid line in Fig. 4.9) (this is attributed to poor pH control during H_2O_2 addition) no significant difference was found between the sonicated samples and the control case. Therefore, the possibility of H_2S degassing, at least in considerable amounts, during sonication was discounted; this conclusion

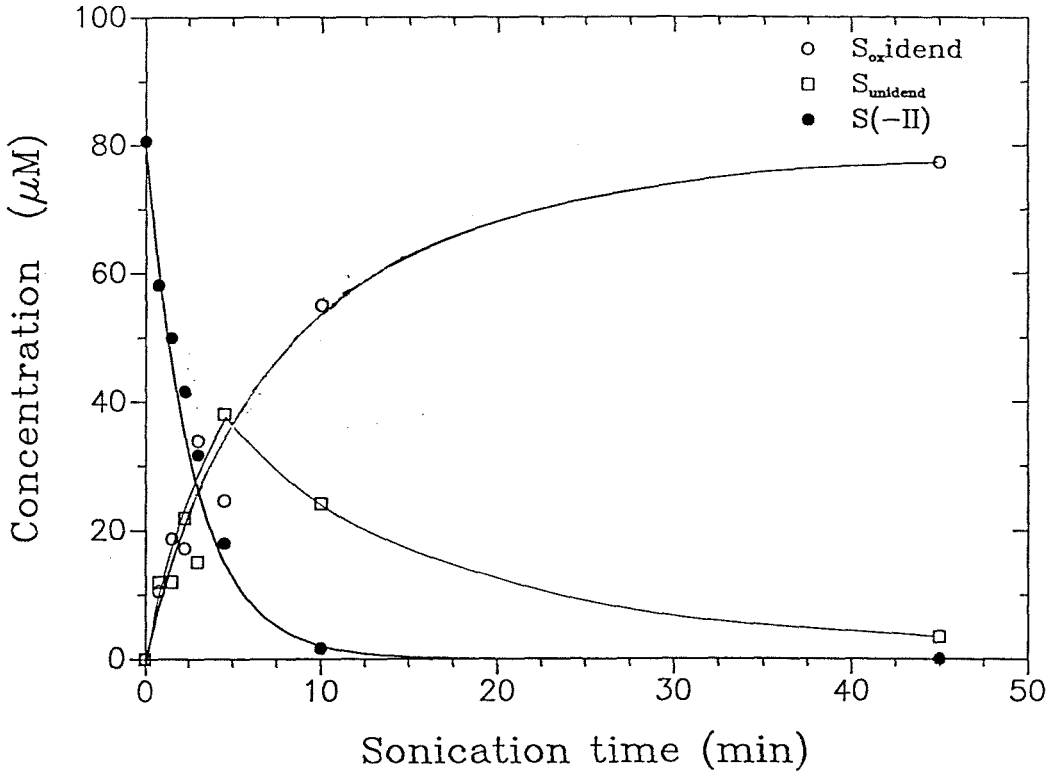

Figure 4.8 S(–II) sonication product distribution at pH 7.4, and $[S(-II)]_o$ = 82 μM.

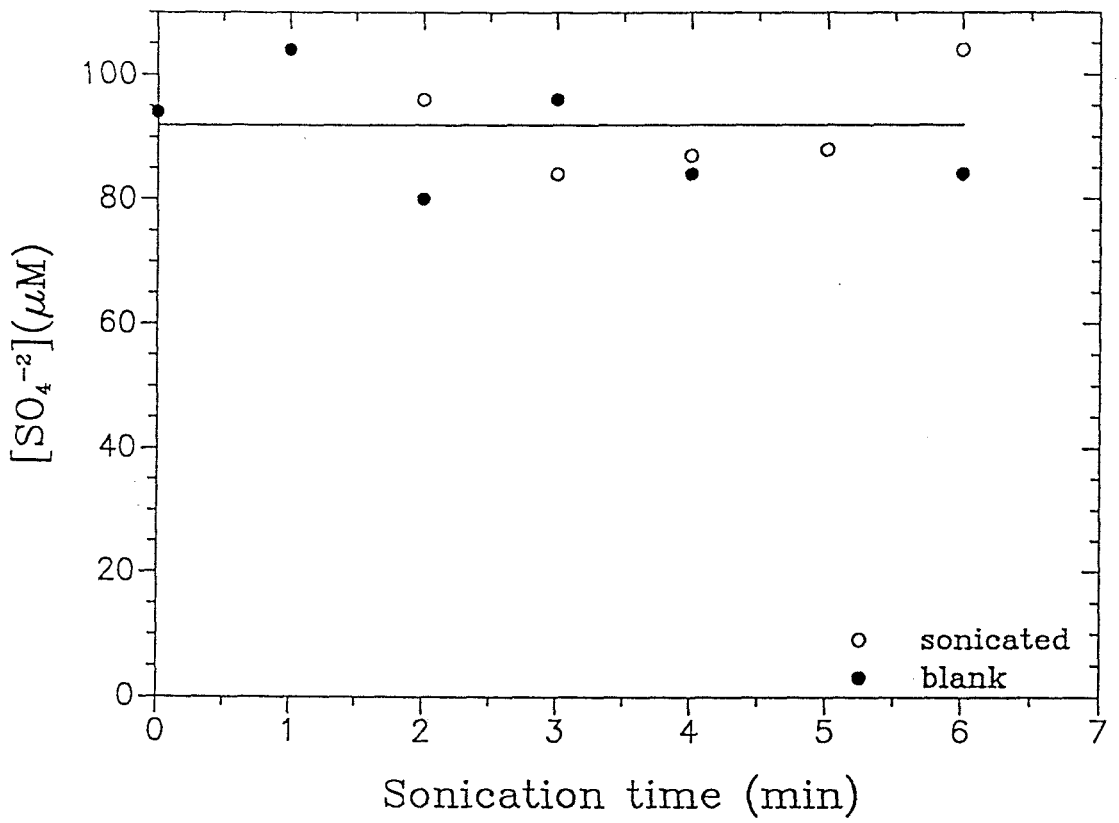

Figure 4.9 SO_4^{2-} measured in H_2O_2 treated S(–II) solutions ($[S(-II)]_o \simeq 82$ μM) before and after sonication at pH 7.4.

is also supported by calculations based on the known gas–transfer rates for H_2S that show that a negligible change in [S(–II)] in solution (in the order of 1 μM) is expected due to H_2S gas escaping into the headspace during the course of the experiment. Thus, the discrepancy between the $[S_{ox}]$ measured and $[S_{ox}]$ expected is attributed to the formation of elemental sulfur (S_8) which was not determined analytically but was observed qualitatively as an increased turbidity of the solution.

The rate of the sonolysis of low S(–II) concentrations was found to be independent of the volume of solution between 20 and 35 ml and showed some decrease for solution volume of 40 ml (this volume is close to the reactor cell capacity). Fig. 4.10 shows the fraction of $[S(-II)]_o$ remaining after 10 min. of sonication as a function of solution volumes (20–40 ml) at pH 10 and $[S(-II)]_o$ = 100 μM. The total input power (as measured by calorimetry; see below) increased from $\simeq$ 65 W to $\simeq$ 103 W for sonication of 20 ml and 35 ml, respectively and remained at $\simeq$ 103 W for solution volume 40 ml. It was calculated that the amount of S(–II) oxidized per unit energy offered to the system was similar for all sonicated volumes; a maximum efficiency of $3.9 \cdot 10^{-11}$ moles/J corresponded to 35 ml sonication volume, and the efficiency for 20, 25, 30, and 40 ml was $3.3 \cdot 10^{-11}$, $3.4 \cdot 10^{-11}$, $3.7 \cdot 10^{-11}$, and $3.6 \cdot 10^{-11}$ moles/J, respectively.

Fig. 4.10 also shows the agreement between [S(–II)] values calculated from the sulfide ISE measurements and the absorbance data. Identical results were obtained with continuous or pulsed sonication with duty cycles (% of time that sonicator is on every second) ranging from 30% to 70%. The comparison was made using the net sonication time in the case of pulsed experiments.

A series of experiments were conducted in which the output power was varied

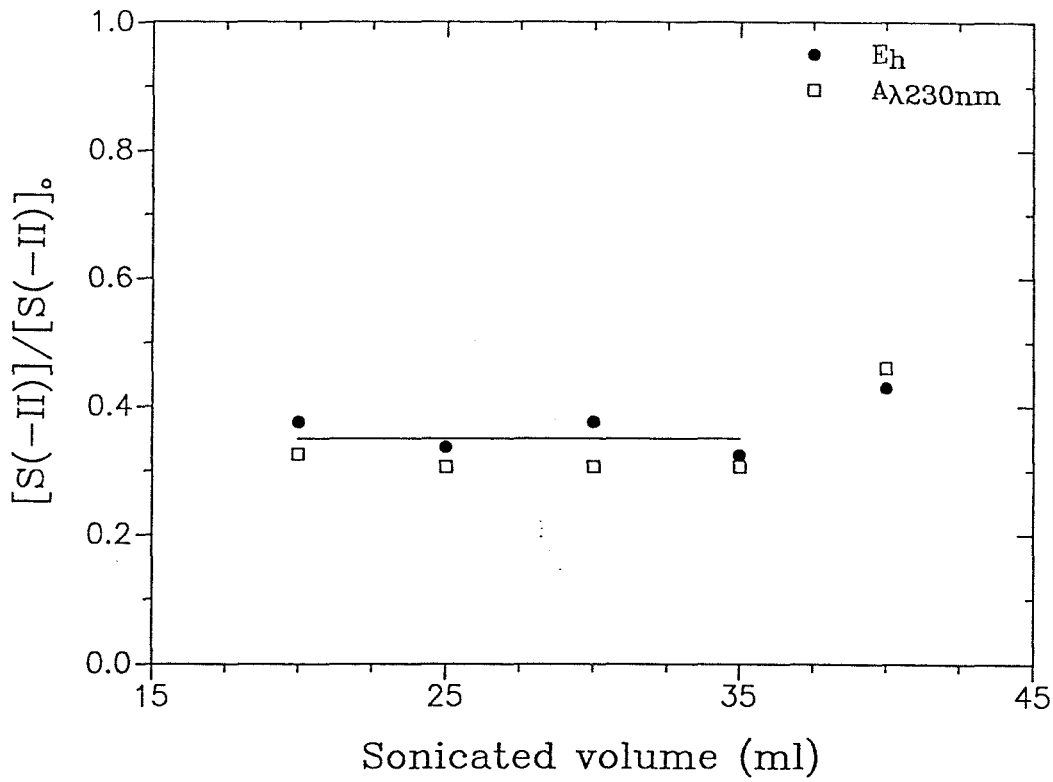

Figure 4.10 Effect of sonicated solution volume; pH 10, $[S(-II)]_o$ = 100 μM, t_{son} = 10 min.

within the limitations of the power unit. Power values were determined from the rise in temperature, T, of a known volume of water with sonication time, t, in the absence of cooling. Using a simplified heat transfer analysis, the rate of energy input to the system (power = Q, in Watts) is given by

$$Q = M \cdot C_P \cdot dT/dt + U \cdot A_w \cdot (T - T_{amb}) \qquad (4.1)$$

where T_o and T_{amb} are the initial temperature of the solution and the ambient temperature respectively, A_w is the wetted area (total wall area of the reaction vessel that is wetted by the sonicated liquid; 43 cm^2 for our SS cell at 25 ml), M is the mass of sonicated water, C_P is the specific heat of water (4.18 J/gr/K), and U is a bulk heat loss coefficient (units of Watts/m^2/K). Integrating eq. (4.1) we obtain:

$$T=\{T_o - T_{amb} - Q/(U \cdot A_w)\} \cdot \exp\{- U \cdot A_w \cdot t/(M \cdot C_P)\} + T_{amb} + Q/(U \cdot A_w) \quad (4.2)$$

and Q and U can be calculated by fitting the temperature data numerically.

If heat losses are neglected, power Q can be calculated from

$$Q = M \cdot C_P \cdot dT/dt \qquad (4.3)$$

where dT/dt is the initial slope of the T vs t curve. Analysis of the data showed that Q values obtained using eq. (4.3) differ less than 10% from the values obtained using eq. (4.2). The ultrasonic intensity at the titanium tip is equal to Q/A_t, where A_t (= 1.2 cm^2) is the surface area of the tip. Figure 4.11 shows that the

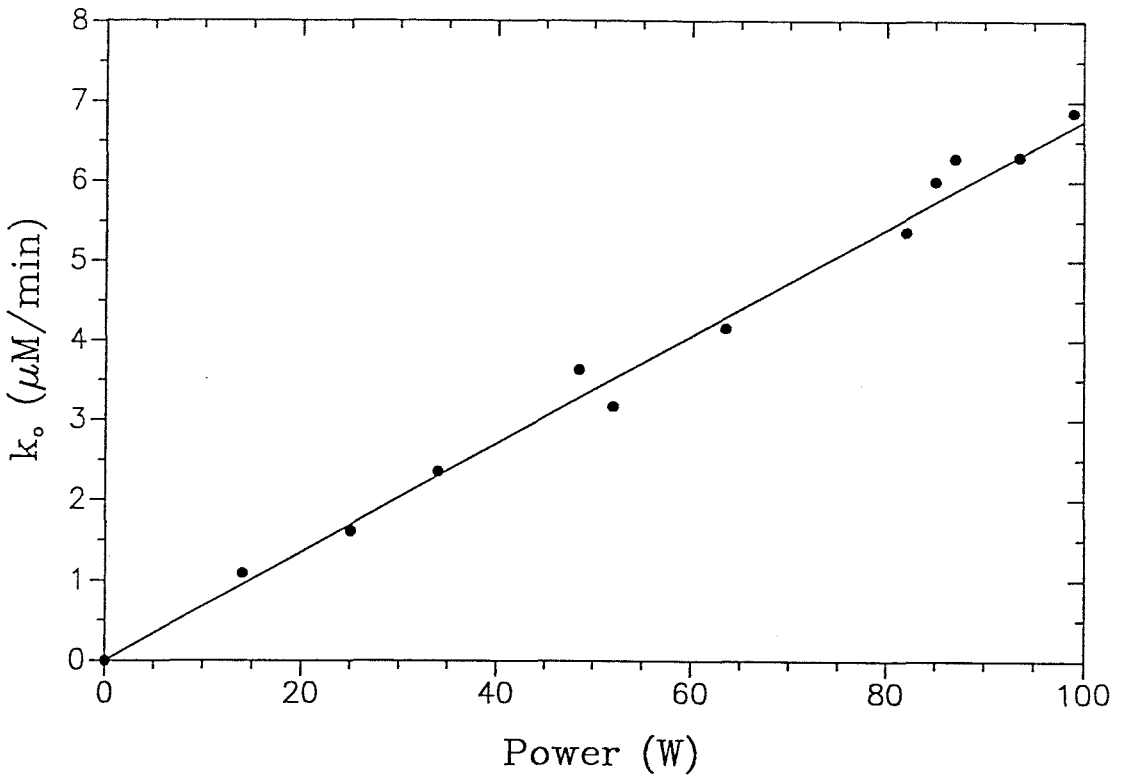

Figure 4.11 Effect of input power on S(–II) sonication; pH 10, $[S(-II)]_o$ = 100 μM.

observed zero–order rate (k_o, in $\mu Mmin^{-1}$) for sonication of 25 ml solution at pH 10 increased linearly with Q in the range studied (i.e. up to 100 W).

The rate of S(–II) oxidation at alkaline pH was found to be practically independent of bulk solution temperature, T_{bulk}. Figure 4.12 shows the observed k_o as a function of T_{bulk} for three different values of power input.

Potassium iodide (KI) has been used by other investigators as a 'sonochemical dosimeter' (23–26). It has been proposed that I^- reacts in the liquid phase with products of the sonolysis of water (mainly $^{\cdot}OH$) and possibly with oxygen atoms coming from the thermal decomposition of O_2 (24) and produces I_2 which can be detected spectrophotometrically in the form of I_3^- [$I_2 + I^- \rightleftharpoons I_3^-$, K = 770 (25); $\epsilon_{350} = 2.6 \cdot 10^4\ M^{-1}sec^{-1}$ for I_3^- (19,24)]. When starch is added to the KI solution, this system can be used for qualitative inspection of a sonochemical reactor system (if the system produces a field that is enough to 'do chemistry' there will be a rapid change in the color of the solution: the initially clear liquid will become deep blue). Sonication of a 1 M solution of KI using the same experimental set–up as for S(–II) sonication resulted in a linear increase in I_3^- of $d[I_3^-]/dt = 13.9\ \mu M \cdot min^{-1}$.

The oxidation of ferrous sulfate to ferric sulfate, known as the Fricke dosimeter, has been also used to probe ultrasonic cavitation activity (28–31). Acidic solutions of 1 mM $Fe(NH_4)_2(SO_4)_2$ (0.8 N H_2SO_4, pH $\simeq$ 0.5) were sonicated and formation of Fe^{3+} was followed spectrophotometrically [$\epsilon_{305} = 2197\ M^{-1}cm^{-1}$ (30)]. The linear increase in [Fe^{3+}] with time was found to be $d[Fe(III)]/dt = 24.4\ \mu Mmin^{-1}$.

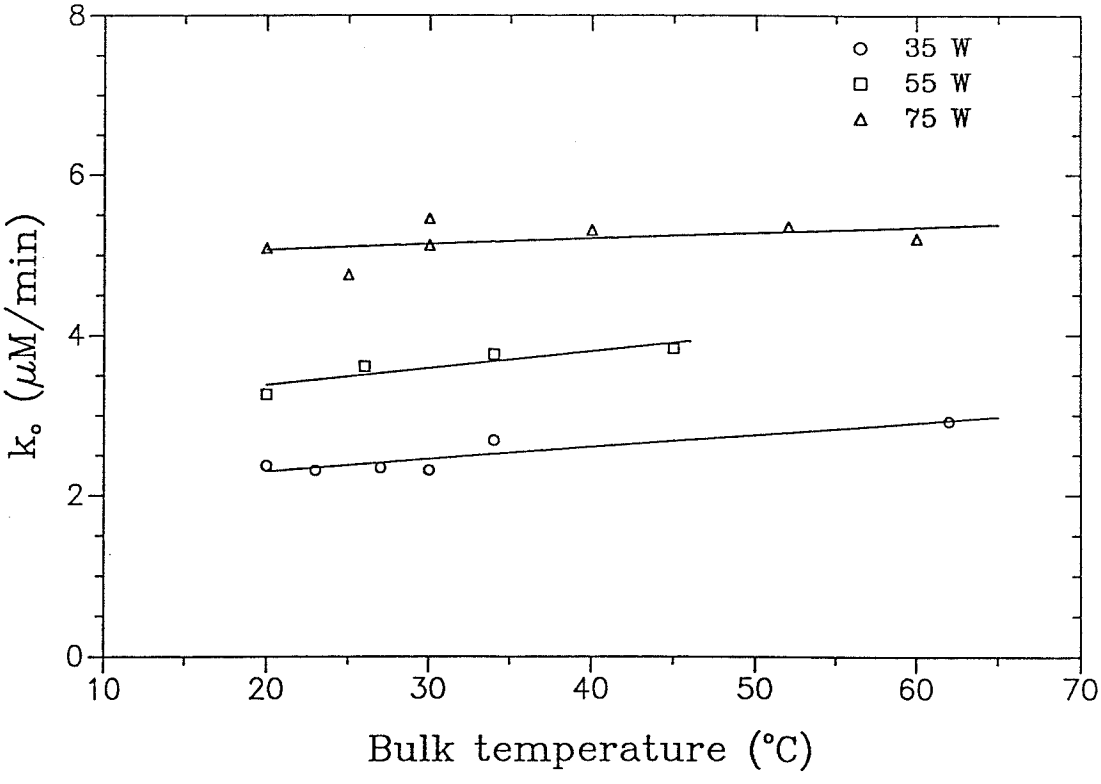

Figure 4.12 Effect of bulk solution temperature on S(–II) sonication; pH 10, $[S(-II)]_o = 100\ \mu M$.

Discussion

The total sulfide, S(–II), is present in the form of H_2S, HS^- or S^{2-}. The relative amounts of these three species depend on the pH of the solution based on the acid/base sulfide equilibria:

$$H_2S \underset{\pm\ H^+}{\overset{pK_{a1}}{\longleftrightarrow}} HS^- \underset{\pm\ H^+}{\overset{pK_{a2}}{\longleftrightarrow}} S^{2-} \qquad (4.4)$$

where K_{a1}, K_{a2} are the first ($pK_{a1} \simeq 7.00$) and second ($pK_{a2} \simeq 17$) acid–dissociation constants for H_2S, respectively. The value of pK_{a2} was previously accepted to be ~ 14 (32), but a later spectrophotometric study (33) reported it as 17.00. It now seems clear that pK_{a2} is much higher than 14 and that S^{2-} is not present at appreciable concentrations even in basic solutions (34). Therefore, the species S^{2-} can be neglected for all practical purposes, and the concentrations of H_2S and HS^- are given by:

$$[H_2S] = \alpha_0[S(-II)] \qquad (4.5)$$

$$[HS^-] = \alpha_1[S(-II)] \qquad (4.6)$$

where

$$\alpha_0 = \frac{[H^+]^2}{([H^+]^2 + K_{a1}[H^+] + K_{a1}K_{a2})} \simeq \frac{[H^+]}{[H^+] + K_{a1}} \qquad (4.7)$$

$$\alpha_1 = \frac{K_{a1}[H^+]}{([H^+]^2 + K_{a1}[H^+] + K_{a1}K_{a2})} \simeq \frac{K_{a1}}{[H^+] + K_{a1}} \qquad (4.8)$$

Therefore, the fraction of the total sulfide, [S(–II)], that is in the form of HS^- increases with increasing pH. At pH around neutral, 50% of the total S(–II) is

present in the form of HS^-, and at pH $\geq$ 9 practically all [S(–II)] is present in the form of HS^- [HS^- represents 99.9% of the total S(–II) at pH 10].

Natroshvili *et al.* (35) have studied the γ–radiolysis of Na_2S at 10^{16}eV/ml·sec at pH 11.8 in the presence of air. They found SO_3^{2-} and $S_2O_3^{2-}$ to be the products of the oxidation of HS^- by ·OH radicals; these two products had practically the same G values (i.e. they were formed with a mole ratio of 1:1). The same investigators also studied the products of the γ–radiolysis of $S_2O_3^{2-}$ in the presence of air; SO_4^{2-}, S and SO_3^{2-} were formed with a mole ratio of 5:3.5:1. Under their experimental conditions they observed the complete scavenging of ·OH radicals by HS^- and $S_2O_3^{2-}$. They did not observe the formation of H_2O_2.

Our results in alkaline solution are in good agreement with the above results from radiation chemistry. The higher SO_4^{2-} ratios that we observed can be explained by further oxidation of the reaction intermediates by H_2O_2. Hoffmann (36) reported the following rate law for the oxidation of S(–II) by H_2O_2 : $d[S(-II)]/dt = k_1[H_2S][H_2O_2]+k_2[HS^-][H_2O_2]$ where $k_1 = 0.5\ M^{-1}s^{-1}$, $k_2 = 29\ M^{-1}s^{-1}$. Based on this expression the half life for [S(–II)] at $[H_2O_2] = 20\ \mu M$ and at pH 10 is 1.2 min. It is also known that in alkaline solutions the main product of S(–II) oxidation by $[H_2O_2]$ is SO_4^{2-}.

It is therefore reasonable to assume that ultrasonic oxidation of S(–II) in alkaline solutions is the result of the direct reaction of HS^- with ·OH. The generation of ·OH during water sonolysis has been established (5–6, 11) and the second–order reaction constants for the reaction of ·OH with reduced sulfur compounds are known to be extremely fast (14): $k(OH+HS^-) = 9\times10^9\ M^{-1}s^{-1}$ [or $5.5\times10^9\ M^{-1}s^{-1}$ (39)], $k(OH+SO_3^{2-}) = 5.5\times10^9\ M^{-1}s^{-1}$, $k(OH+S_2O_3^{2-}) = 7.8\times10^9\ M^{-1}s^{-1}$, $k(OH+H_2S) = 1.5\times10^{10}\ M^{-1}s^{-1}$. These rate constants are comparable to the

self–reaction rate constant for ·OH radical recombination [5×10^9 $M^{-1}s^{-1}$ (38)].

The apparent zero–order dependence on [S(–II)] suggests that the rate–determining step in the overall reaction is the availability of ·OH radicals (i.e. ·OH is scavenged by HS^- and the oxidation intermediates in the liquid phase as soon as it diffuses out of the cavitation bubbles). This interpretation of the experimental results is in line with our observation that the reaction rate was the same in both the borax and the phosphate buffered systems. The second–order reaction constants $k[OH+B(OH)_4^-] < 10^6$ $M^{-1}s^{-1}$ and $k(OH+PO_4^{3-}) < 10^7$ $M^{-1}s^{-1}$ (14) are much lower than 10^9 $M^{-1}s^{-1}$ and thus neither of these ions is expected to interfere with the reactions of ·OH with the reduced sulfur species. On the other hand, a decrease in the rate of $S_2O_3^{2-}$ sonolysis was observed in the presence of high concentrations (> 1 mM) of carbonate/bicarbonate buffer which is in line with the relatively high value of $k(OH+CO_3^{2-}) = 4\cdot10^8$ $M^{-1}s^{-1}$ (14).

The dependence of the zero–order rate on $[S(-II)]_o$ is similar to what has been reported for the ultrasonic oxidation of ferrous sulfate (28). The oxidation of Fe^{2+} to Fe^{3+} during sonolysis has been shown to be zero–order; the zero–order rate, however, increased with increasing initial Fe^{2+} concentration up to $[Fe^{2+}]_o \simeq 0.5$ mM and remained constant thereafter. This phenomenon is also similar to what was observed by Makino *et al.* (11) during experiments designed to spin–trap ·OH and ·H radicals during aqueous solution sonolysis at 50 kHz and 0.06 $W\cdot cm^{-2}$. DMPO (5,5–dimethyl–1–pyrroline 1–oxide) was used to trap ·OH with the formation of the adduct ·OH–DMPO. In air–saturated solutions, the concentration of [·OH–DMPO] increased linearly with time. However, the rate of the formation of [·OH–DMPO] increased with increasing $[DMPO]_o$ reaching a plateau at $[DMPO]_o \simeq 1$ mM.

A standard free radical competition model (see for example reference 39) for the scavenging of OH radicals by HS^- and by $^{\cdot}OH$ (recombination) would lead to the following relationship between the initial zero–order rate constant, k_o, and $[S(-II)]_o$:

$$k_o = \frac{k_s\,[S(-II)]_o}{k_s[S(-II)]_o + k_r[OH]_{ss}}\,k_{rf} \qquad (4.9)$$

where k_s and k_r are the second–order rate constants for reaction of $^{\cdot}OH$ with S(–II) and $^{\cdot}OH$ respectively, and k_{rf} is the rate at which $^{\cdot}OH$ is made available for solution reactions.

Using the experimental data of Figure 4.5, a plot of $1/k_o$ vs $1/[S(-II)]_o$ can be approximated by a straight line ($r^2 = 0.96$) and the following empirical relationship is obtained:

$$k_o = \frac{13.7\,[S(-II)]_o}{[S(-II)]_o + 121.1} \qquad (4.10)$$

Comparing equations (4.9) and (4.10) and using $k_r/k_s = 0.56$ (5×10^9 $M^{-1}s^{-1}/9\times10^9$ $M^{-1}s^{-1}$), we get: $k_{rf} = 13.7\ \mu M\cdot min^{-1}$ and $[^{\cdot}OH]_{ss} \simeq 218\ \mu M$. This calculated steady–state concentration for $^{\cdot}OH$ radical is extremely large and cannot be explained by the calculated k_{rf}. This fact suggests that the oxidation of S(–II) proceeds via a chain reaction that is initiated by $^{\cdot}OH$ and involves an additional oxidant (e.g., O_2).

It is known that the mechanism for the reaction of S(–II) with $^{\cdot}OH$ in the aqueous phase is initiated as follows (14):

$$HS^- + {}^{\cdot}OH \longrightarrow HSOH^- \quad (4.11)$$

$$H_2S + {}^{\cdot}OH \longrightarrow HS^{\cdot} + H_2O \quad (4.12)$$

The subsequent intermediate steps may include a variety of radical reactions. Some of the reactions of $HS^{\cdot}$ have been studied by pulse radiolysis (37) and electron spin resonance (40). In these studies the formation of the transients $SO_2^{\cdot-}$ and $O_2^{\cdot-}$ has been observed in the presence of oxygen. Information also exists about the mechanisms of the oxidation of sulfite, S(IV), by ·OH, H_2O_2 and O_2 because of its importance in aqueous–phase atmospheric chemistry (41–43). The main reaction species involved in the free–radical chemistry of sulfite are $SO_3^{\cdot-}$, $SO_5^{\cdot-}$ and $SO_4^{\cdot-}$ (41–44). Although no data could be found in the literature concerning reaction of these radicals with S(–II), it is reasonable to believe that $SO_3^{\cdot-}$ and $SO_4^{\cdot-}$ will react with HS^- very fast with the formation of $HS^{\cdot}$ and SO_3^{2-} and SO_4^{2-}, respectively.

Based on the above, we propose that the main reactions involved in the oxidation of S(–II) by ·OH in the presence of O_2 are as follows:

$$2\ {}^{\cdot}OH \longrightarrow H_2O_2 \quad (4.13)$$

$$HSOH^{\cdot-} + HS^- \longrightarrow H_2S_2^{\cdot-} + OH^- \quad (4.14)$$

$$HS^{\cdot} + HS^- \rightleftharpoons H_2S_2^{\cdot-} \quad (4.15)$$

$$HSOH^{\cdot-} + O_2 \longrightarrow SO_2^{\cdot-} + H_2O \quad (4.16)$$

$$HS^{\cdot} + O_2 \longrightarrow HSO_2^{\cdot} \quad (4.17)$$

$$HSO_2^{\cdot} \rightleftharpoons H^+ + SO_2^{\cdot-} \quad (4.18)$$

$$H_2S_2^{\cdot-} + O_2 \longrightarrow H_2S_2 + O_2^{\cdot-} \quad (4.19)$$

$$H_2S_2 \rightleftharpoons H^+ + HS_2^- \quad (4.20)$$

$$HS_2^- + O_2 \longrightarrow SO_2^{\cdot-} + HS^- \quad (4.21)$$

$$SO_2^{\cdot-} + O_2 \longrightarrow SO_2 + O_2^{\cdot-} \quad (4.22)$$

$$SO_2^{\cdot-} + HS^- \xrightarrow{O_2} SO_4^{2-} + HS \quad (4.23)$$

$$SO_2 + H_2O \rightleftharpoons SO_2 \cdot H_2O \quad (4.24)$$

$$SO_2 \cdot H_2O \rightleftharpoons H^+ + HSO_3^- \quad (4.25)$$

$$HSO_3^- \rightleftharpoons H^+ + SO_3^{2-} \quad (4.26)$$

$$HS_2^- + SO_3^{2-} \longrightarrow HS^- + S_2O_3^{2-} \quad (4.27)$$

$$SO_3^{2-} + {}^{\cdot}OH \longrightarrow SO_3^{\cdot-} + OH^- \quad (4.28)$$

$$SO_3^{\cdot-} + HS^- \longrightarrow SO_3^{2-} + HS \quad (4.29)$$

$$SO_3^{\cdot-} + O_2 \longrightarrow SO_5^{\cdot-} \quad (4.30)$$

$$SO_5^{\cdot-} + SO_5^{\cdot-} \not\longrightarrow SO_4^{\cdot-} + SO_4^{2-} + O_2 \quad (4.31)$$

$$SO_4^{\cdot-} + HS^- \longrightarrow SO_4^{2-} + HS \quad (4.32)$$

$$3\ O_2^{\cdot-} + HS^- \not\longrightarrow SO_4^{2-} + 2\ OH^- \quad (4.33)$$

$$HSO_3^- + H_2O_2 \longrightarrow HSO_4^- + H_2O \quad (4.34)$$

$$HS^- + 4\ H_2O_2 \not\longrightarrow SO_4^{2-} + 4\ H_2O + H^+ \quad (4.35)$$

It must be noted that some of the above reactions are not elementary steps. Furthermore, since we are primarily interested in the neutral to alkaline pH region, species with low pK_a values are shown only in the deprotonated form and S(–II) appears in the form of HS^-. Equations 4.14, 4.15, 4.23, 4.29, 4.32, 4.33, and 4.35 can also be written for H_2S, with an additional proton appearing in the right hand side.

A more detailed mechanism involving a set of 47 reactions and 22 species has been developed and is presented in Chapter 5. Rate constants for most of the reactions were found in the literature (mainly references 14, 37, 41–43, 45) and in the few cases where no data were available estimates of the rate constants based on

kinetic/thermodynamic considerations were used. The set of the 22 stiff ODE's was solved numerically using an Ordinary Differential Equation System Solver (EPISODE, 46) to find the concentrations of the different species with time. It was assumed that there is a continuous constant input of ·OH in the system (from the cavities), k_{rf}. The experimental results at alkaline pH can be modeled with k_{rf} = 3.5 $\mu M \cdot min^{-1}$ and the corresponding average bulk liquid steady–state concentration is low ($[\cdot OH]_{ss} \leq 0.1\ \mu M$).

The observed dependence of the initial zero–order rate constant, k_o, on $[S(-II)]_o$ (Figure 4.5) is in line with the above described S(–II) oxidation mechanism. A qualitative explanation is as follows: Because of the low [·OH] reaction (4.13) is negligible, and initially, all of the ·OH introduced into solution reacts with S(–II) (eqs. 4.11 and 4.12). The $[\cdot OH]_{ss}$ is then inversely proportional to $[S(-II)]_o$ (i.e., $[\cdot OH]_{ss} \simeq (k_{rf})/(k[S(-II)]_o)$, where $k = k_{11}\alpha_1 + k_{12}\alpha_o$ and α_1, α_o are given by eqs. 4.8 and 4.7 respectively. The steady–state concentration of radical species that react with S(–II) in the free–radical S(–II) oxidation chain is practically independent of $[S(-II)]_o$ and depends mainly on the available oxygen. If oxygen is not depleted, the expected dependence of k_o $(= d[S(-II)]/dt \mid_{t=0})$ on $[S(-II)]_o$ is of the form: $k_o = A + B\ [S(-II)]_o$, where A depends on the ·OH input to the system (k_{rf}) and B depends on $[O_2]$. Assuming that $[O_2]$ is continuously replenished so that it remains constant at the air saturation value (i.e., $[O_2] \simeq 240\ \mu M$) the following values were found using our free–radical mechanism and k_{rf} = 3.5 $\mu M \cdot min^{-1}$: A = 4.4 $\mu M \cdot min^{-1}$, B = 0.016 min^{-1}. These values were used to draw the solid line in Figure 4.5, and it can be seen that the experimental data fall on this line for low $[S(-II)]_o$. Above $[S(-II)]_o \simeq 400\ \mu M$ the rate of S(–II) oxidation is limited by O_2.

It is noted that, even though our reaction vessel was sealed from the atmosphere during the experiments, we had a significant volume of headspace (headspace volume $\simeq$ solution volume = 25 ml). In order to explain the experimental results, it is necessary to assume oxygen transfer from the headspace to solution during sonication. If an overall reaeration coefficient, K_{LO_2}, is used the rate of O_2 addition to the system is $K_{LO_2}([O_2]_{sat}-[O_2])$, where $[O_2]_{sat}$ is the oxygen saturation concentration at the given temperature and pressure and $[O_2]$ is the actual oxygen concentration in solution. The reaeration coefficient that explains our experimental results is $3.7 \cdot 10^{-4}$ s^{-1} = 32 d^{-1} (assuming constant $[O_2]_{sat}$, i.e., neglecting the depletion of O_2 in the headspace; see also Chapter 5). The oxygen transfer coefficient was measured experimentally for sonication of 35 ml of water in a glass vessel open to the atmosphere. The surface area of the vessel was similar to that of the stainless steel (SS) reaction cell used for the S(–II) sonication experiments ($\simeq$ 10 cm^2). The procedure commonly used for measuring oxygen tranfer from aeration equipment and described in Standard Methods (47) was used. The value of K_{LO_2} in that vessel was found to be $4.5 \cdot 10^{-3}$ s^{-1}, i.e., about 10 times higher than the above theoretically derived value for the SS cell. Nevertheless, this discrepancy can be attributed to the differences in geometry, bulk solution temperature and pressure between the two cells, and the fact that the SS cell was not open to the atmosphere and therefore the oxygen of the headspace was depleted with time. It is also interesting to note that the oxygen tranfer coefficient measured for the glass vessel during sonication was about 5 times higher than the oxygen transfer coefficient determined for a similar glass vessel for simple mixing with a stirrer. This enhancement of oxygen transfer upon sonication could be very important for practical applications of ultrasound for treatment and has been

previously reported by Dahi (16). In his experiments, where ultrasound was used in combination with ozonation, he observed a 15–45% increase in the overall aeration constant for oxygen injection during sonication.

The observed decrease in the apparent zero–order rate constant at pH > 10 can be partly explained by the dissociation of OH in alkaline solutions:

$$\cdot OH + OH^- \rightleftharpoons O^{\cdot -} + H_2O \qquad (4.36)$$

where $k_f=1.2\times10^{10}$ $M^{-1}s^{-1}$, $k_b=9.3\times10^7 s^{-1}$. O^- reacts more slowly with the same substrates than $\cdot OH$ (14, 38, 39). It is also possible that the deprotonation of HS_2^- decreases the rate of reaction of that species with oxygen (eq. 4.21). The pK_a's of H_2S_2 are $pK_{a1} = 5$, $pK_{a2} = 9.7$ (36) and S_2^{2-} is the principal H_2S_2 species at pH $\geq$ 10.

The free–radical mechanism presented above underpredicts the rate of S(–II) disappearance at pH $\leq$ 8.5. Near pH 7, H_2S present in the liquid phase will readily go into the gas phase upon formation of vapor cavities. Combustion reactions inside the collapsing cavities are known to occur during sonication of volatile solutes or dissolved gases (5). Thus we propose that thermal decomposition of H_2S occurs within the collapsing cavitation bubbles or within the gas–liquid interface [where temperatures on the order of 800 K have been previously calculated for our experimental conditions (20) at low pH]. The thermal decomposition of H_2S at high temperatures (> ~ 1700 K) (48–50) is first–order process with respect to [H_2S] and the main products are H_2 and S_2 (or SO_2 in the presence of O_2). Thus the thermal decomposition of H_2S can be invoked to explain the observed increase in the oxidation rate of [S(–II)] with decreasing pH, the change in the apparent

reaction kinetics from zero–order to first–order with respect to [S(–II)], and the appearance of S_8 at pH < 9.

The possible elementary reactions involved in the high–temperature pyrolysis of H_2S within the collapsing bubble or within the interfacial region of the bubble are as follows:

$$H_2S \longrightarrow H^{\cdot} + HS^{\cdot} \tag{4.37}$$

$$HS^{\cdot} + HS^{\cdot} \longrightarrow H_2 + S_2 \tag{4.38}$$

$$HS^{\cdot} + S \longrightarrow H^{\cdot} + S_2 \tag{4.39}$$

$$H_2S + H^{\cdot} \longrightarrow H_2 + HS^{\cdot} \tag{4.40}$$

$$H^{\cdot} + O_2 \longrightarrow HO_2^{\cdot} \tag{4.41}$$

$$H_2S + {}^{\cdot}OH \longrightarrow HS^{\cdot} + H_2O \tag{4.42}$$

$$H_2S + O^{\cdot} \longrightarrow HS^{\cdot} + {}^{\cdot}OH \tag{4.43}$$

$$HS^{\cdot} + O_2 \longrightarrow HSO_2^{\cdot} \tag{4.44}$$

$$HSO_2^{\cdot} + {}^{\cdot}OH \longrightarrow SO_2 + H_2O \tag{4.45}$$

$$HSO_2^{\cdot} + O_2 \longrightarrow HSO_4^{\cdot} \tag{4.46}$$

$$HSO_4^{\cdot} + H^{\cdot} \longrightarrow H_2SO_4 \tag{4.47}$$

$$SO_2 + H_2O \rightleftharpoons SO_2 \cdot H_2O \tag{4.48}$$

$$SO_2 \cdot H_2O + {}^{\cdot}OH \longrightarrow HSO_3^{\cdot} + H_2O \tag{4.49}$$

$$HSO_3^{\cdot} + {}^{\cdot}OH \longrightarrow SO_3 + H_2O \tag{4.50}$$

$$HSO_3^{\cdot} + HO_2^{\cdot} \longrightarrow SO_3 + H_2O_2 \tag{4.51}$$

$$SO_3 + H_2O \longrightarrow 2\,H^{+} + SO_4^{2-} \tag{4.52}$$

Since S(–II) is destroyed via two different pathways during sonication, i.e., oxidation by ·OH (rate constant k_o) and thermal decomposition (rate constant k_1),

the overall rate of [S(–II)] disappearance with time can be written as:

$$\frac{d[S(-II)]}{dt} = -k_o - k_1 [S(-II)] \qquad (4.53)$$

Integration of eq. (4.53) yields:

$$[S(-II)] = \left[[S(-II)]_o + \frac{k_o}{k_1}\right] e^{-k_1 t} - \frac{k_o}{k_1} \qquad (4.54)$$

The experimental data for $[S(-II)]_o = 100\ \mu M$ as a function of pH were analyzed using eq. (4.10) to obtain values of k_o and k_1. Figure 4.13 shows the calculated rate constants over the pH range of 7.4 to 12.0. As expected, k_1 is near zero between pH 12 and 10 and increases with decreasing pH. The solid line in Fig. 4.13 represents α_o (eq. 4.7). Since the values of k_1 qualitatively follow this curve, the relationship between k_1 and H_2S is strengthened. k_o values were found to decrease with decreasing pH. This may be partly due to the decrease in the concentration of total sulfide available for free–radical solution reactions and to lower concentrations of $OH^{\cdot}$ radical. As H_2S fills the gas–phase within the bubbles, it will 'cushion' the implosion resulting in lower temperatures upon bubble collapse and thus lower $[OH^{\cdot}]$ (5).

In conclusion, the ultrasonic irradiation of S(–II) in water results in its rapid oxidation. Reaction of $HS^{\cdot}$ with $OH^{\cdot}$ is the main pathway for the oxidation of S(–II) at pH $\geq$ 10. When O_2 is present, the rate of S(–II) oxidation increases linearly with initial sulfide concentration. At pH $\leq$ 8.5, thermal decomposition of H_2S within or near collapsing cavitation bubbles becomes the important pathway.

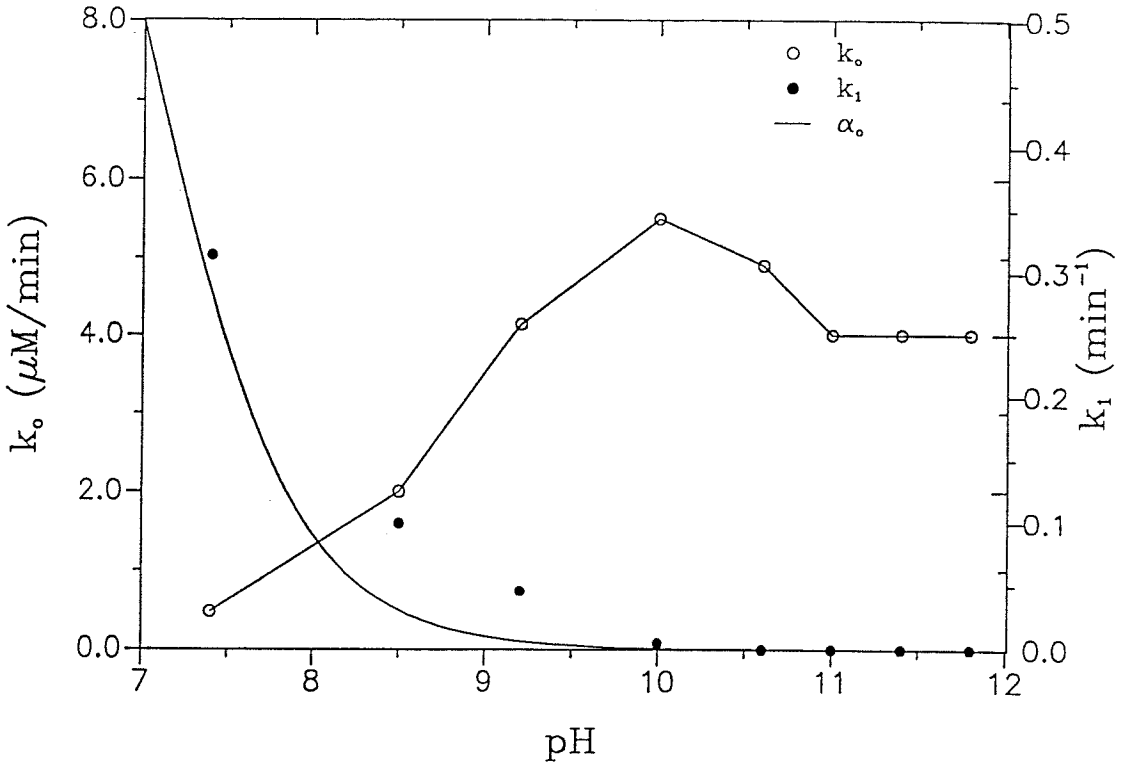

Figure 4.13 Calculated zero–order and first–order rate constants for S(–II) sonolytic oxidation.

The limitation of sonolysis for the control of H_2S and other trace contaminants in water is that it is relatively inefficient with respect to the input energy. Calculations presented in the Appendix show that only a small portion of the total energy supplied to the system results in "useful" free–radical reactions. The formation of free–radicals upon sonication has been traditionally used to define the "chemicoacoustic" or "sonoacoustic" efficiency (29–31, 51, 52) of ultrasonic irradiation. Since our previous (20) and current work showed that the ultrasound–induced elimination of trace contaminants in water is the result of free–radical reactions *and* thermal decomposition it seems that it would be more appropriate to define the efficiency of sonication for the control of chemicals (i.e., the percentage of the total energy supplied to the system that is effectively used in the decomposition of each particular chemical compound) as a "sonolytic" efficiency. The sonolytic efficiency would then depend on the chemical compound of interest and could be higher than the "chemicoacoustic" efficiency as defined previously (e.g., in the case of S(–II) decomposition at low pH). Nevertheless, since both the above mentioned sonolytic mechanisms result from the transient high temperatures that result from cavitation, chemicoacoustic efficiency should still be a good estimate for the order of magnitude of the overall sonolytic efficiency of an ultrasonic irradiation system.

In this regard we point out that the commercial immersion–horn sonifier that was used in this study is not the optimum reactor configuration for the efficient generation of transient cavitation. The high intensity sound waves generated at the tip of the horn result in intense local cavitation (53) as can be seen visually using sonoluminescence (54) but the large number of bubbles formed can cause a 'blanketing effect' (55) that reduces the sonication efficiency. Preliminary

experiments with a larger 3–in. diameter surface radiating at 20 kHz showed that free–radical H_2S oxidation proceeds at a faster rate even at ultrasonic intensities that are one order of magnitude lower than those used with the direct–immersion horn. These results are in agreement with the findings of a recent study (27) where the rate of I_2 formation was shown to be about fivefold higher using a quartz plate oscillating at 1 MHz as compared to a commercial 20 kHz immersion–horn with a tenfold higher intensity. Our current research is focused on a study of the optimum reactor configurations for sonolytic degradations.

Acknowledgments

This work was funded in part by the County Sanitation Districts of Los Angeles County (contract No. 3082) and by the U.S. EPA (Exploratory Research Office R815041–01–0). We are grateful for their support.

References

1. Flosdorf, E. W.; Chambers, L. A. *J. Am. Chem. Soc.* 1933, *55*, 3051.
2. Schmitt, F. O.; Johnson, C. H.; Olson, A. R. *J. Am. Chem. Soc.* 1927, *51*, 370.
3. Wawrzyczek, W.; Jacyk, A.; Przybylski, A. *Naturwissenschaften* 1964, *51*, 335.
4. Cauwet, G.; Coste, C. M.; Knoche, H.; Longuemard, J. P. *Bull. Soc. Chim. Fr.* 1976, *1–2*, 45.
5. Suslick, K. S. in *Ultrasound: Its Chemical, Physical and Biological Effects.* Suslick, K. S., Ed., VCH: New York, 1988.
6. Mason, T.; Lorimer, J. P. *Sonochemistry: theory, applications and uses of ultrasound in Chemistry*, E. Horwood Ltd, 1988.
7. Henglein, A. *Ultrasonics* 1987, *25*, 6.
8. Suslick, K. S.; Hammerton, D. A.; Cline, D. E. *J. Am. Chem. Soc.* 1986, *108*, 5641.
9. Shutilov, V. A. in *Fundamental Physics of Ultrasound*, Gordon & Breach Science Publishers: New York, 1988.
10. Apfel, R. E. *J. Acoust. Soc. Am.* 1981, *69*, 1624.
11. Makino, K.; Massoba, M. M.; Riesz, P. J. *J. Phys. Chem.* 1983, *87*, 1369.
12. Henglein, A.; Kormann, C. *Int. J. Radiat. Biol.* 1985, *48*, 251.
13. Klaning, U. K.; Sehested, K.; Holcman, J. *J. Phys. Chem.* 1985, *89*, 760.
14. Buxton, G. V.; Greestock, C. L.; Helman, W. P.; Ross, A. B. *J. Phys. Chem. Ref. Data* 1988, *17*, 513.
15. Chen, J. W.; Chang, J. A.; Smith, G. V. *Chem. Eng. Prog. Symp. Ser.* 1971,

67, *109*, 18.

16. Dahi, E. *Wat. Res.* 1976, *10*, 677.
17. Sierka, R. A.; Amy, G. L. *Ozone Science & Eng.* 1985, *7*, 47.
18. Kohl, A. L.; Riesenfeld, F. C. *Gas Purification*, 3rd Ed., Gulf Publishing Co., Houston, 1979.
19. Kormann, C.; Bahnemann, D. W.; Hoffmann, M. R. *Environ. Sci. Technol.* 1988, *22*, 798.
20. Kotronarou, A.; Mills, J.; Hoffmann, M. R. *J. Phys. Chem.* 1991, *95*, 3631.
21. Hoffmann, M. R.; Edwards, J. O. *J. Phys. Chem.* 1975, *79*, 2096.
22. Mader, P. M. *J. Am. Chem. Soc.* 1958, *80*, 2634.
23. Suslick, K. S.; Schubert, P. F.; Goodale, J. W. *IEEE Ultrasonics Symposium*, 1981, 612.
24. Hart, E. J.; Henglein, A. *J. Phys. Chem.* 1985, *89*, 4342.
25. Henz, R. R.; Clarence, G. J. *J. Chem. Phys.*, 1969, *51*, 3, 1236.
26. Gutierrez, M.; Henglein, A. *J. Phys. Chem.* 1990, *94*, 3625.
27. Henglein, A.; Gutierrez, M. *J. Phys. Chem.* 1990, *94*, 5169.
28. Miller, N. *J. Amer. Chem. Soc.* 1950, 546.
29. Todd, J. H. *Ultrasonics*, 1970, 234.
30. Margulis, M. A. *Russ. J. Phys. Chem.* 1976, *50*, *9*, 1358.
31. Sehgal, C. M.; Wang, S. Y. *IEEE Trans. Sonics Ultrason.* 1983, *SU–30,* 374.
32. Smith, R. M.; Martell, A. E. *Critical Stability Constant, vol 4: Inorganic complexes*, Plenum, New York, 1976.
33. Giggenbach, W. *Inorg. Chem.* 1971, *10, 7*, 1333.
34. Myers, R. J. *J. Chem. Educ.*, 1986, *63*, *8*, 687.

35. Natroshvili, G. R.; Panchvidze, M. V.; Nanobashvili, H. M. In *Proc. Tihany Symp. Radiat. Chem.*, *3rd*, *2*, Dobo (ed.), 1972, pp. 1281–1291.

36. Hoffmann, M. R. *Env. Sc. Technol.* 1977, *11*, 61.

37. Mills, G.; Schmidt, K. H.; Matheson, M. S.; Meisel, D. *J. Am. Chem. Soc.* 1987, *91*, 1590.

38. Buxton, G. V. in *Radiation Chemistry, Principles and Applications*; Farhataziz; Rodgers, M. A. J., Ed., VCH: New York, 1987, p. 339.

39. Draganic, I. G.; Draganic, Z. D. *The Radiation Chemistry of Water*, Association Press, 1971.

40. Zhu, J.; Petit, K.; Colson, O.; DeBolt, S.; Sevilla, M. D. *J. Phys. Chem.* 1991, *95*, 3676.

41. Jacob, D. J.; Hoffmann, M. R. *J. Geophys. Res.* 1983, *88*, 6611.

42. Jacob, D. J. *J. Geophys. Res.* 1986, *91*, 9807.

43. Pandis, S. N.; Seinfeld, J. H. *J. Geophys. Res.* 1989, *94*, 1105.

44. Neta, P.; Huie, R. E. *Environ. Health Persp.* 1985, *64*, 209.

45. Neta, P.; Huie, R. E.; Ross, A. B. *J. Phys. Chem. Ref. Data* 1988, *17*, 1027.

46. Byrne, G. D.; Hindmarsh, A. C. *ACM Trans. Math. Software* 1975, 71.

47. Standard Methods for the Examination of Water and Wastewater, 14th Ed, 1975, APHA–AWWA–WPCF, pp. 82–86.

48. Higashihara, T.; Saito, K.; Yamamura, H. *Bull. Chem. Soc. Jap.* 1976, *49*, 956.

49. Bradley, J. N.; Dobson, D. C. *J. Phys. Chem.* 1976, *46*, 2865.

50. Roth, P.; Lohr, R.; Barner, U. *Combust. Flame* 1982, *45*, 273.

51. Rozenberg, L. D. *Sov. Phys.–Acoustics* 1965, *11*, 100.

52. Margulis, M. A. *Sov. Phys.–Acoustics* 1969, *13*, 135.

53. Goodwin, T. J. in *Chemistry With Ultrasound, Critical Reports on Applied Chemistry*, Vol. 28, Mason, T. J, Ed., Elsevier Applied Science: New York, 1990.

54. Reynolds, G. T.; Walton, A. J.; Gruner, S. M. *Rev. Sci. Instrum.* 1982, *53*, 1673.

55. Berliner, S. *American Biotechnology Laboratory* 1984.

Appendix

Our experimental conditions ($\simeq$ 3.2 $W.ml^{-1}$) are equivalent to total energy input of 2×10^{19} $eV \cdot ml^{-1} \cdot sec^{-1}$ (or a delivered dose of 3.2×10^{5} $rad \cdot s^{-1}$). At pH 11–12 the ultrasonic oxidation of S(–II) is attributed to the reaction of HS^- with $^{\cdot}OH$ radical and the zero–order rate is 4 $\mu M \cdot min^{-1} = 2 \times 10^{-7}$ $M \cdot s^{-1}$. Natroshvili *et al* (35) working at 10^{16} $eV \cdot ml^{-1}$ sec^{-1} and at pH 11.8 found a $G(-HS^-) = 0.37$ (i.e. 0.37 molecules of HS^- were destroyed per 100 eV) for the γ–radiolysis of S(–II). This G value translates to a zero–order rate of 6.1×10^{-8} $M \cdot s^{-1}$. Therefore, it can be seen that under our experimental conditions a three–fold higher rate was achieved but at the expense of a 2000–fold higher energy input. The higher energy input is due to low acoustic efficiency [i.e. a small amount of the total ultrasonic energy is transformed to cavitation power W_{cav} (29)]. Using the above mentioned $G(HS^-)$ value we can calculate a "sonoacoustic efficiency" (51, 52) of 0.054%. This sonoacoustic efficiency represents the portion of the total energy supplied to the system that was used in bulk solution free–radical reactions similar to those observed in radiation chemistry. The zero order rate of Fe^{+3} formation during irradiation of Fe^{+2} (24.4 $\mu M min^{-1}$) gives a sonoacoustic efficiency of 0.03% if a $G(Fe^{+3})$ value of 3.9 (29) is used. The above estimates of the sonoacoustic efficiency of our system are of the same order of magnitude as those reported by other investigators (31, 52) working under different sonication conditions. This is in agreement with Todd's (29) finding that the yields of water sonolysis depended only on the total energy deposited and were independent of the frequency and intensity distribution of the ultrasonic field. Using a sonochemical efficiency of 0.05% and the estimate for the rate of $^{\cdot}OH$ release into solution calculated in the

main text (3.5 $\mu M \cdot min^{-1}$) a G(OH) = 0.14 can be found for our experimental conditions. This value is in general agreement with the G(OH) = 0.35 ± 0.15 reported by Todd (29).

CHAPTER 5

MATHEMATICAL MODELING OF THE FREE RADICAL CHEMISTRY OF THE S(–II) + OH SYSTEM AND APPLICATION TO THE ULTRASONIC IRRADIATION OF S(–II)

ABSTRACT

A comprehensive mechanism for aqueous–phase oxidation of S(–II), where $[S(-II)] = [H_2S] + [HS^-] + [S^{2-}]$, by ·OH radical in the presence of oxygen is developed. The oxidation of S(–II) is initiated by reaction with ·OH but it is further propagated by a free–radical chain sequence involving O_2. This mechanism can model adequately the observed oxidation of S(–II) in air saturated aqueous solutions sonicated at 20 kHz and 75 $W \cdot cm^{-2}$ at pH $\geq$ 10. At this pH range, practically all S(–II) is present in the form of HS^- and cannot undergo thermal decomposition. Thus, it is shown that the action of ultrasonic waves on aqueous solutions containing species that are not susceptible to thermal decomposition can be predicted based on the knowledge of the free–radical chemistry of the species. It is also shown that even though aqueous phase sonochemical reactions are initiated by ·OH escaping in the aqueous phase from the cavities, molecular oxygen present in the solution can be the main oxidant if it can sustain a free–radical chain reaction. This observation is important with respect to the application of ultrasound for the control of chemicals in trace amounts in water and wastewater systems.

Introduction

As discussed in Chapter 4, ultrasonic irradiation of alkaline oxic aqueous solutions of bivalent sulfur, S(–II), at 20 kHz resulted in the rapid, linear decrease in S(–II) concentration. The observed distribution of the oxidation products was similar to that reported for γ–radiolysis of S(–II). The ultrasound–induced oxidation of S(–II) in alkaline solutions was attributed to the reaction of HS^- with $OH^{\cdot}$. Although the experimental results appear to be qualitatively consistent with our proposed mechanism, there are questions that still remain unanswered. They concern the amount of $^{\cdot}OH$ released into the aqueous phase and the existence and relative importance of additional oxidants.

In order to address these questions, a comprehensive aqueous phase mechanism that describes the free radical chemistry of the S(–II) + $^{\cdot}OH$ + O_2 system has been developed. This mechanism has been subsequently used to model the ultrasonic oxidation of S(–II) in alkaline pH.

S(–II) + $^{\cdot}OH$ + O_2 system mechanism formulation

The free radical chemistry of the sulfur system is very complicated and includes a variety of species and reactions. In this work, we tried to develop a mechanism that can accurately model the overall behavior of the S(–II) + $^{\cdot}OH$ + O_2 system with the minimum number of intermediates. Furthermore, we limited our interest in the neutral to alkaline pH region that is the region where the ultrasonic irradiation of S(–II) experiments were performed.

The chemical species that are included in the mechanism are shown in Table

5.1. It is noted that S(–II), S(–I) and S(IV) are 'group species', representing the sum of reactant species that are in rapid acid/base equilibrium. Equilibrium reactions relevant to our system are shown in Table 5.2. Only the upper part (above the broken line) of this table is actually used in the mathematical model. The pK values for the reactions of the remaining part of the table are considerably outside the pH region of interest, thus allowing us to neglect one of the two species involved in these equilibria (e.g., S^{2-}, $SO_2 \cdot H_2O$).

The 47 reactions that are included in the mathematical modeling of the system are shown in Table 5.3. Broken arrows indicate multistep (i.e., nonelementary) reactions. In the few cases where no data were available estimates of the rate constants based on kinetic/thermodynamic considerations were used.

By analogy with the reactions of $^{\cdot}OH$ with H_2S and HS^-, the rate constant for the reaction of $HS^{\cdot}$ with H_2S (R5) is expected to be of the same order of magnitude as the rate constant for $HS^{\cdot} + HS^-$ (R6); a value of $5.5 \cdot 10^9$ $M^{-1}s^{-1}$ is therefore used. The choice of k_{r5} is not critical for our application since H_2S is not the main S(–II) species at alkaline pH.

The rate constant for the reaction of $HSOH^{\cdot -}$ with O_2 (R11) is expected to be of the same order of magnitude as for the reaction of $HSOH^{\cdot -}$ with HS^- (R9) and lower than the rate constants for the reaction of $HS^{\cdot}$ with those species (R7, R6); the value of 10^9 $M^{-1}s^{-1}$ is therefore used for (R11). The overall rate of S(–II) oxidation does not seem to be sensitive to k_{r11}. At pH 10 and $[S(-II)]_o = 200$ μM, the kinetics and product distribution remained the same even when k_{r11} was set to $5 \cdot 10^9$ $M^{-1}s^{-1}$.

Although $S_2O_3^{2-}$ is a known product of the radiolysis of S(–II) (14), no pathways that lead to its formation have been proposed. We included two possible

Table 5.1
Chemical species

Non–radical species	Radicals
$S(-II) = H_2S + HS^-$	$^{\cdot}OH$
O_2	$HS^{\cdot}$
$S(-I) = H_2S_2 + HS_2^- + S_2^{2-}$	$H_2S_2^{\cdot-}$
$S(IV) = HSO_3^- + SO_3^{2-}$	$HSOH^{\cdot-}$
$S_2O_3^{2-}$	$SO_2^{\cdot-}$
SO_4^{2-}	$^{\cdot}S_2O_3OH^{2-}$
H_2O_2	$^{\cdot}S_4O_6^{3-}$
NO_2^-	$O_2^{\cdot-}$
NO_3^-	$SO_3^{\cdot-}$
	$SO_4^{\cdot-}$
	$HS_2^{\cdot}$
	$H_2S_2O^{\cdot}$
	$NO_2^{\cdot}$

Table 5.2
Equilibrium reactions

Equilibrium Reaction	pK	ΔH	Reference
$H_2O(l) \rightleftharpoons H^+ + OH^-$	14.00	13.34	(1)
$H_2S \rightleftharpoons H^+ + HS^-$	7.02	–5.30	(1)
$HSO_3^- \rightleftharpoons H^+ + SO_3^{2-}$	7.18	3.00	(1)
$HS_2^- \rightleftharpoons H^+ + S_2^{2-}$	9.70		(2)
$H_2S_2 \rightleftharpoons H^+ + HS_2^-$	5.00		(2)
$HS^- \rightleftharpoons H^+ + S^{2-}$	17.1	–12.00	(3)/(1)
$SO_2 \cdot H_2O \rightleftharpoons H^+ + HSO_3^-$	1.91	4.00	(1)
$HSO_4^- \rightleftharpoons H^+ + SO_4^{2-}$	1.99	5.40	(1)
$HS_2O_3^- \rightleftharpoons H^+ + S_2O_3^{2-}$	1.60		(1)
$H_2O_2 \rightleftharpoons H^+ + HO_2^-$	11.65	–7.40	(1)
$HNO_2 \rightleftharpoons H^+ + NO_2^-$	3.15	–2.00	(1)
$HO_2 \rightleftharpoons H^+ + O_2^{\cdot -}$	4.46		(4)
$HSO_2^{\cdot} \rightleftharpoons H^+ + SO_2^{\cdot -}$	≤ 2		(5)
$HSO_3^{\cdot} \rightleftharpoons H^+ + SO_3^{\cdot -}$	≤ 2		(5)
$HSO_4^{\cdot} \rightleftharpoons H^+ + SO_4^{\cdot -}$	≤ 2		(5)

Table 5.3
Sulfur chemistry

id#	Reaction	k $M^{-1}s^{-1}$	Reference
R1	$^{\cdot}OH + {}^{\cdot}OH \longrightarrow H_2O_2$	$5.5 \cdot 10^9$	(6)
R2	$H_2S + {}^{\cdot}OH \longrightarrow HS^{\cdot} + H_2O$	$1.5 \cdot 10^{10}$	(6)
R3	$HS^- + {}^{\cdot}OH \longrightarrow HSOH^{\cdot -}$	$9.0 \cdot 10^9$	(6)
R4	$HS^{\cdot} + HS^{\cdot} \longrightarrow H_2S_2$	$6.5 \cdot 10^9$	(7)
R5	$HS^{\cdot} + H_2S \longrightarrow H_2S_2^{\cdot -} + H^+$	$5.5 \cdot 10^9$	EST*
R6	$HS^{\cdot} + HS^- \longrightarrow H_2S_2^{\cdot -}$	$5.4 \cdot 10^9$	(7)
R7	$HS^{\cdot} + O_2 \longrightarrow HSO_2^{\cdot}$	$7.5 \cdot 10^9$	(7)
R8	$HS^{\cdot} + H_2S_2^{\cdot -} \longrightarrow H_2S_2 + HS^-$	$9.0 \cdot 10^9$	(7)
R9	$HSOH^{\cdot -} + HS^- \longrightarrow H_2S_2^{\cdot -} + OH^-$	$2.0 \cdot 10^9$	(7)
R10	$HSOH^{\cdot -} + H_2S \longrightarrow H_2S_2^{\cdot -} + H_2O$	$3.0 \cdot 10^9$	(7)
R11	$HSOH^{\cdot -} + O_2 \longrightarrow SO_2^{\cdot -} + H_2O$	$1.0 \cdot 10^9$	EST
R12	$H_2S_2^{\cdot -} + H_2S_2^{\cdot -} \longrightarrow H_2S_2 + 2\,HS^-$	$9.5 \cdot 10^8$	(7)
R13	$H_2S_2^{\cdot -} + O_2 \longrightarrow H_2S_2 + O_2^{\cdot -}$	$4.0 \cdot 10^8$	(7)
R14	$HS_2^- + SO_3^{2-} \longrightarrow S_2O_3^{2-} + HS^-$	$1.0 \cdot 10^7$	EST
R15	$HS_2^- + O_2 \longrightarrow SO_2^{\cdot -} + HS^-$	$5.0 \cdot 10^7$	EST
R16	$SO_2^{\cdot -} + O_2 \longrightarrow SO_2 + O_2^{\cdot -}$	$1.0 \cdot 10^8$	(6)
R17	$SO_3^{2-} + {}^{\cdot}OH \longrightarrow SO_3^{\cdot -} + OH^-$	$5.5 \cdot 10^9$	(6)
R18	$HSO_3^- + {}^{\cdot}OH \longrightarrow SO_3^{\cdot -} + H_2O$	$4.5 \cdot 10^9$	(6)
R19	$S_2O_3^{2-} + {}^{\cdot}OH \longrightarrow S_2O_3OH^{2-}$	$7.8 \cdot 10^9$	(8)
R20	$S_2O_3OH^{2-} + S_2O_3^{2-} \longrightarrow S_4O_6^{3-} + OH^-$	$6.0 \cdot 10^8$	(8)
R21	$S_4O_6^{3-} + \frac{3}{4}\,H_2O \;-\!/\!/\!\rightarrow \frac{1}{2}\,SO_3^{2-} + \frac{7}{4}\,S_2O_3^{2-} + \frac{3}{2}\,H^+$	$2.5 \cdot 10^{6\ddagger}$	(8)
R22	$O_2^{\cdot -} + {}^{\cdot}OH \longrightarrow O_2 + OH^-$	$1.0 \cdot 10^{10}$	(6)
R23	$SO_3^{\cdot -} + O_2 \longrightarrow SO_5^{\cdot -} \;-\!/\!/\!\rightarrow \frac{1}{2}\,SO_4^{\cdot -} + \frac{1}{2}\,SO_4^{2-} + O_2$	$1.0 \cdot 10^8$	(9)
R24	$SO_4^{\cdot -} + HSO_3^- \longrightarrow SO_4^{2-} + SO_3^{\cdot -} + H^+$	$1.3 \cdot 10^9$	(10)

Table 5.3 (continued)

id#	Reaction	k $M^{-1}s^{-1}$	Reference
R25	$SO_4^{\cdot-} + SO_3^{2-} \longrightarrow SO_4^{2-} + SO_3^{\cdot-}$	$2.0 \cdot 10^9$	(5)
R26	$SO_4^{\cdot-} + O_2^{\cdot-} \longrightarrow SO_4^{2-} + O_2$	$5.0 \cdot 10^9$	(10)
R27	$SO_4^{\cdot-} + OH^- \longrightarrow SO_4^{2-} + {}^{\cdot}OH$	$7.0 \cdot 10^7$	(5)
R28	$SO_4^{\cdot-} + H_2O_2 \longrightarrow SO_4^{2-} + O_2^{\cdot-} + 2\,H^+$	$1.2 \cdot 10^7$	(5)
R29	$S(IV) + O_2^{\cdot-} + H_2O \longrightarrow SO_4^{2-} + {}^{\cdot}OH + OH^-$	$1.0 \cdot 10^5$	(4)
R30	$S(IV) + H_2O_2 \longrightarrow SO_4^{2-} + H_2O$	0.2	(11)
R31	$S(-II) + H_2O_2 \not\longrightarrow SO_4^{2-} + 4\,H_2O + H^+$	0.483	(2)
R32	$S_2O_3^{2-} + 4H_2O_2 \not\longrightarrow 2SO_4^{2-} + 3H_2O + 2H^+$	0.025	(12)
R33	$S(-II) + 3\,O_2^{\cdot-} \not\longrightarrow SO_4^{2-} + 2\,OH^-$	$1.5 \cdot 10^6$	(6)
R34	$2SO_3^{\cdot-} \longrightarrow S_2O_6^{2-} \longrightarrow SO_4^{2-} + SO_3^{2-} + 2H^+$	$5.3 \cdot 10^8$	(5)
R35	$OH + H_2O_2 \longrightarrow O_2^{\cdot-} + H_2O$	$2.7 \cdot 10^7$	(6)
R36	$NO_2^- + {}^{\cdot}OH \longrightarrow NO_2 + OH^-$	$1.0 \cdot 10^{10}$	(4)
R37	$NO_2 + {}^{\cdot}OH \longrightarrow NO_3^- + H^+$	$1.3 \cdot 10^9$	(4)
R38	$2NO_2 + S(IV) + H_2O \longrightarrow 2NO_2^- + SO_4^{2-} + 3H^+$	$1.7 \cdot 10^7$	(13)
R39	$SO_4^{\cdot-} + S(-II) \longrightarrow SO_4^{2-} + HS^{\cdot}$	$1.0 \cdot 10^9$	EST
R40	$H_2S_2^{\cdot-} \longrightarrow HS^{\cdot} + HS^-$	$5.3 \cdot 10^5$‡	(7)
R41	$SO_2^{\cdot-} + HS^- \xrightarrow{O_2} SO_4^{2-} + HS$	$1.0 \cdot 10^8$	EST
R42	$SO_3^{\cdot-} + HS^- \longrightarrow SO_3^{2-} + HS$	$1.0 \cdot 10^8$	EST
R43	$S_2O_3^{2-} + 2\,O_2^{\cdot-} \not\longrightarrow SO_4^{2-} + SO_3^{2-}$	$1.0 \cdot 10^5$	EST
R44	$HS_2^{\cdot-} + {}^{\cdot}OH \longrightarrow HS_2 + OH^-$	$1.0 \cdot 10^9$	EST
R45	$HS_2 + OH \longrightarrow H_2S_2O$	$1.0 \cdot 10^9$	EST
R46	$HS_2 + HSOH^{\cdot-} \longrightarrow H_2S_2O + HS^{\cdot}$	$1.0 \cdot 10^9$	EST
R47	$H_2S_2O + 4\,{}^{\cdot}OH \not\longrightarrow S_2O_3^{2-} + 2\,OH^- + 4\,H^+$	$1.0 \cdot 10^9$	EST

*EST: estimated (see text); ‡ rate constant in s^{-1}

pathways: a) reaction of HS_2^- with SO_3^{2-} (R14) and b) oxidation of HS_2^- by $^{\cdot}OH$ (R44) followed by successive addition and abstraction reactions (R45 and multistep R47). The rate constant of R14 is not expected to be higher than the rate constant for the reaction of SO_3^{2-} with $NO_2^{\cdot}$ (R38) and was therefore set at 10^7 $M^{-1}s^{-1}$. The rate constants for reactions R44–R47 are expected to be near the diffusion–controlled limit and were set at 10^9 $M^{-1}s^{-1}$. Even if $k_{r14} = 10^8$ $M^{-1}s^{-1}$ and $k_{r44\text{-}47} = 5 \cdot 10^9$ $M^{-1}s^{-1}$, the above mentioned reactions cannot account for the observed formation of $S_2O_3^{2-}$; but the values of these rate constants are not critical for the overall rate of S(–II) oxidation.

The rate constant for the reaction of HS_2^- with O_2 (R15) is expected to be higher than the rate constant for the reaction of HS_2^- with SO_3^{2-} (R14); a value of $5 \cdot 10^7$ $M^{-1}s^{-1}$ was therefore used for k_{r15}. Sulfate radical is a very strong oxidant and is expected to react with S(–II) near the diffusion–controlled limit; the value of k_{r39} was set at 10^9 $M^{-1}s^{-1}$. Sulfur dioxide and sulfite radicals are expected to react with S(–II) slower than $SO_4^{\cdot-}$ and a value of 10^8 $M^{-1}s^{-1}$ was used for k_{r41} and k_{r42}.

The model parameters are shown in Table 5.4. The model accepts a constant and continuous input of $^{\cdot}OH$, H_2O_2, and NO_2^- (OH_{input}, H_2O_{2input}, and NO_{2input}) so that it can simulate the continuous release of those species from the collapsing bubbles during sonication. Provision has been made for reaeration of the solution; an overall oxygen transfer coefficient [$K_l(O_2)$] is used, and the rate of O_2 addition to the system is $K_l(O_2) \cdot ([O_2]_{sat} - [O_2])$, where $[O_2]_{sat}$ is the oxygen saturation concentration at the given temperature and pressure and $[O_2]$ is the actual oxygen concentration in solution.

The values of the model parameters shown in Table 5.4 are those that were found to represent the conditions of our sonication experiments. Their selection is

Table 5.4
Model Parameters

Fixed Model Parameters	Value
OH_{input}	3.5 μM/min
H_2O_{2input}	2.0 μM/min
NO_{2input}	1.0 μM/min
$K_1(O_2)$	$3.7 \cdot 10^{-4}$ s^{-1}
T	298 K
P	1 atm
pH	10.0

discussed in the next section of this chapter.

Since activation energies for most of the reactions of Table 5.3 were not available, T and P are fixed at standard conditions. The pH is also treated as a fixed variable in order to simulate our buffered sonication experiments. The computer code can be modified to correct the rate constants for different T or P (assuming that the necessary thermodynamic data for the reactions of Table 5.3 become available), or to treat pH as a variable species (by including H^+ as a 23rd chemical species).

Given the initial conditions (concentrations of the 22 chemical species at t=0), the concentrations of the chemical species with time are found by solving numerically the set of the 22 stiff ODE's. An Ordinary Differential Equation System Solver (EPISODE, 15) is used. The method chosen for the numerical solution of the system includes variable–step size, variable–order backward differentiation and a chord or semi–stationary Newton method with an internally computed finite difference approximation to the Jacobian.

The computer program (USMODEL) was written in FORTRAN 77 and the code can be found in Appendix C. The ODE Solver subroutine (EPIS) is also included in Appendix C. This is the modification of the original EPISODE code prepared by Warren (16).

Model Application to Ultrasonic Irradiation of S(–II)

During ultrasonic irradiation of aqueous solutions, ·OH radicals are produced from dissociation of water vapor upon collapse of cavitation bubbles. A fraction of these radicals that are initially formed in the gas phase diffuse into solution.

Cavitation is a dynamic phenomenon and the number and location of bursting bubbles at any time cannot be predicted a priori. Nevertheless, the time scale for bubble collapse and rebound is orders of magnitude smaller than the time scale for the macroscopic effects of sonication on chemicals (i.e., nanoseconds to microseconds vs minutes to hours). Therefore, a simplified approach for modeling the liquid–phase chemistry resulting from sonication of a well mixed solution is to view the $^{\cdot}OH$ input into the aqueous phase as continuous and uniform. The implicit assumption in this approach is that the kinetics of the aqueous phase chemistry are not controlled by diffusion limitations of the substrates reacting with $^{\cdot}OH$.

The mathematical model that is presented above was first used to simulate the oxidation of S(–II) at pH=10, $[S(-II)]_o$ = 196 μM, and $[O_2]_o$ = 240 μM (air saturation). These initial conditions correspond to the conditions of the sonication experiment shown in Figure 4.2. The rates of H_2O_2 and NO_2 input to the system (i.e., H_2O_{2input} and NO_{2input}) were set at the experimentally observed zero–order formation rates for those species in deionized water buffered at pH 10 (see Chapter 4). Various runs were performed with different values of OH_{input}.

Figure 5.1 shows the evolution of total sulfide with time for six different $^{\cdot}OH$ input values. As expected, the initial S(–II) oxidation rate increases with increasing OH_{input}. But that initial linear decrease of [S(–II)] is 'halted' at [S(–II)] $\simeq$ 55 μM in all cases. Figure 5.2 explains why: the main oxidant in our system turns out to be molecular oxygen present in the solution. The ratio of $[O_2]_{depleted}$:$[S(-II)]_{oxidized}$ is about 1.7 in all cases, showing that most of the oxygen contained in the oxidized forms of sulfur that are the final products (i.e., SO_4^{2-}, SO_3^{2-} and $S_2O_3^{2-}$) comes from O_2 and not $^{\cdot}OH$. Figure 5.3 shows schematically

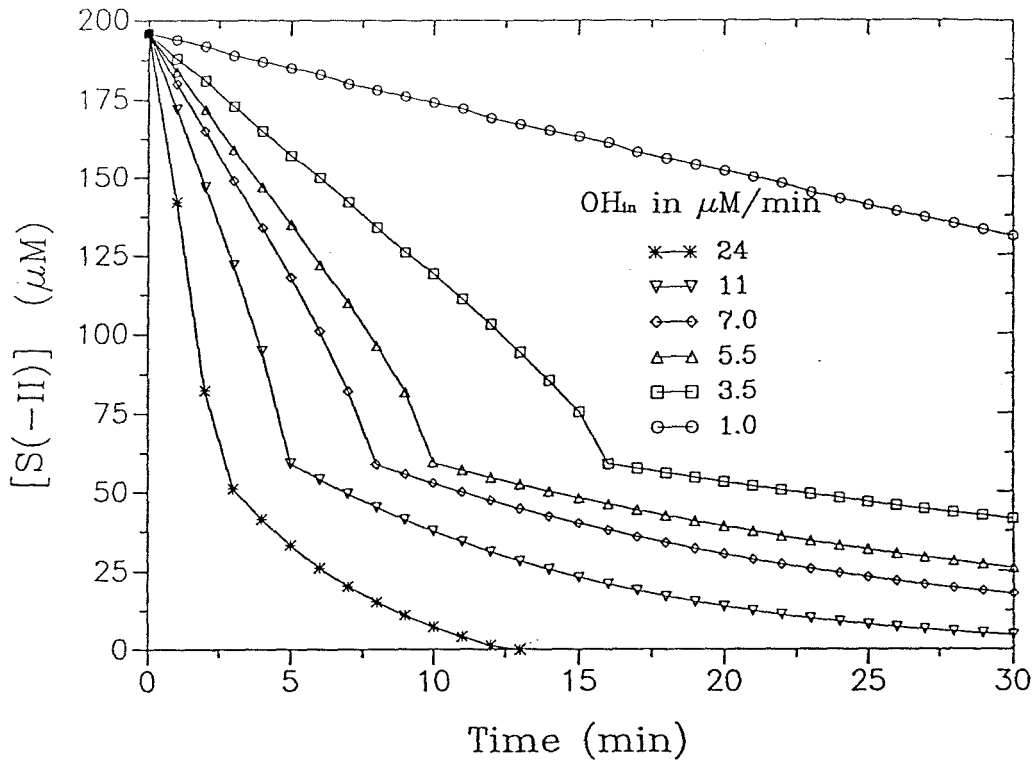

Figure 5.1 [S(–II)] profiles for various OH_{input} values; pH 10, $[S(-II)]_o$ = 196 μM, $[O_2]_o$ = 240 μM.

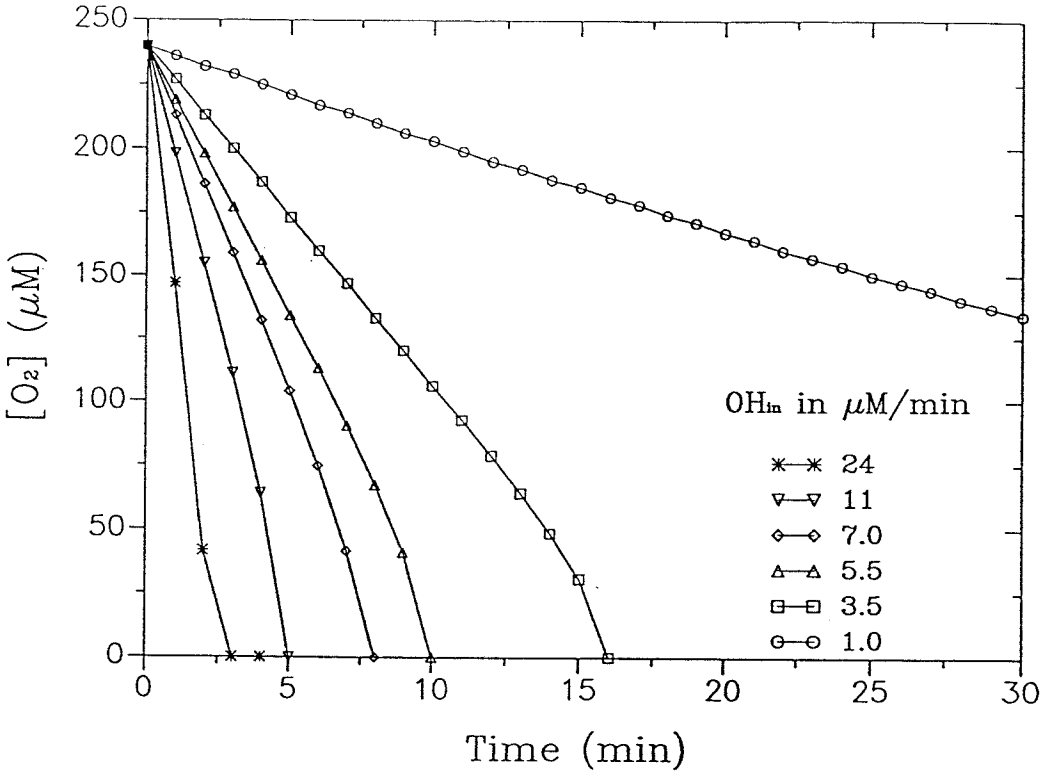

Figure 5.2 $[O_2]$ profiles for various OH_{input} values; pH 10, $[S(-II)]_o$ = 196 μM, $[O_2]_o$ = 240 μM.

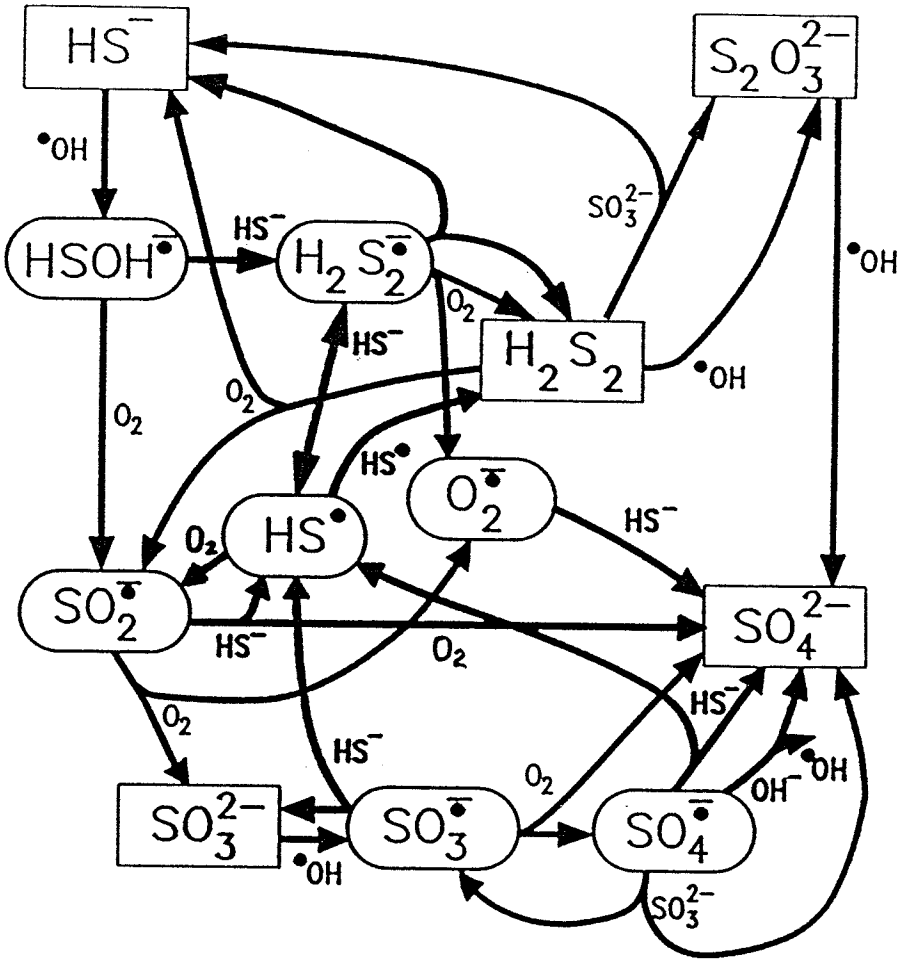

Figure 5.3 Main pathways for the S(–II) + OH system in the presence of O_2 at alkaline pH.

the reactions and species that proved to be the most significant. The oxidation of S(–II) is initiated by reaction with ·OH but is further propagated by a free–radical chain reaction sequence involving O_2.

The value of $\cdot OH_{input}$ that results in an initial rate of S(–II) oxidation equal to the experimentally observed oxidation rate at the above mentioned conditions (i.e., 7.5 $\mu M \cdot min^{-1}$ at $[S(-II)]_o$ = 196 μM and pH = 10) is 3.5 $\mu M \cdot min^{-1}$. In order to explain the experimentally observed linear S(–II) decrease even after all of the initial O_2 should have been depleted, it is necessary to assume oxygen transfer from the headspace to solution during sonication. Figure 5.4 shows the calculated [S(–II)] and [O_2] profiles for $\cdot OH_{input}$ = 3.5 $\mu M \cdot min^{-1}$ and 6 different values of the overall oxygen transfer coefficient $Kl(O_2)$. It can be seen that the value of $Kl(O_2)$ does not affect the initial oxidation rate but determines the subsequent form of the [S(–II)] curve. If not enough oxygen is added into solution, oxygen is depleted before all of the initial sulfide is oxidized resulting in a sudden decrease in the oxidation rate. If a lot of oxygen is added to the system, [O_2] near the end of the reaction is constantly higher than [S(–II)] and a slow–down of the rate of [S(–II)] oxidation occurs [the intermediate species involved in the chain mechanism will react preferably with O_2 and less with S(–II)]. The value of $Kl(O_2)$ that results in a continuous linear [S(–II)] decrease is $3.7 \cdot 10^{-4}$ s^{-1} = 32 d^{-1}.

Subsequent experiments with the same direct–immersion horn that was used in S(–II) sonication but in a different vessel and at different conditions (higher T, vessel open to the atmosphere as opposed to the mere existence of headspace) determined oxygen transfer coefficient values that were even higher than that (see Chapter 4). Therefore, this value of $K_l(O_2)$ was accepted to be reasonable and was used in all subsequent modeling work. It must be noted that the value of $K_l(O_2)$ is

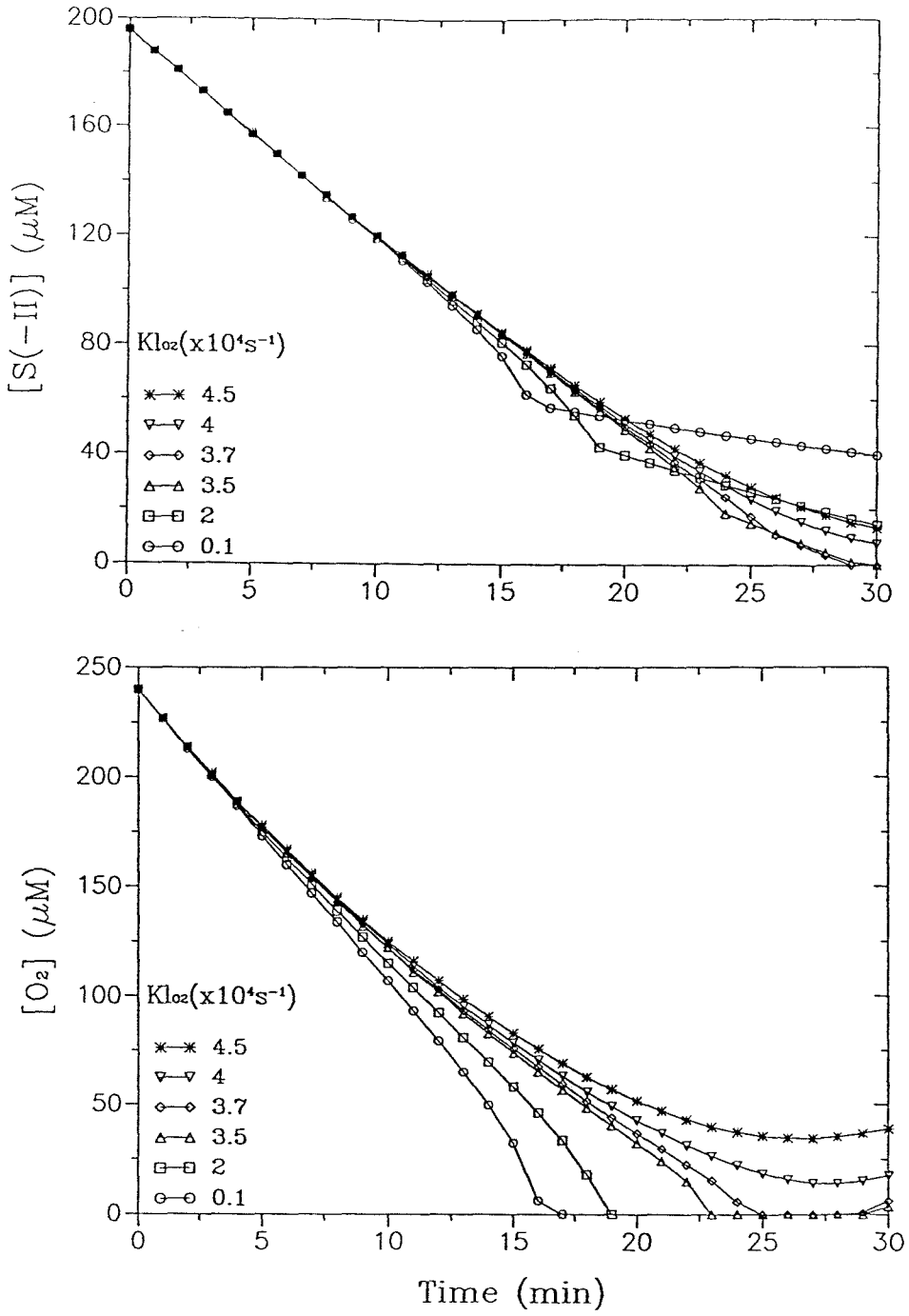

Figure 5.4 (a, top)[S(–II)] profiles for different oxygen transfer coefficients; pH 10, OH_{input} = 3.5 $\mu M \cdot min^{-1}$, $[S(-II)]_o$ = 196 μM, $[O_2]_o$ = 240 μM. (b, bottom) corresponding $[O_2]$ profiles.

vessel–specific, since reaeration will depend on the mixing pattern and the ratio of the surface area to the total volume of the solution.

Figure 5.5 compares the experimentally observed [S(–II)] profile (Figure 4.2a) with the model results using the parameter values shown in Table 5.4. It is noted that, in agreement with the experimental results, the values of H_2O_{2input} and NO_{2input} are not critical for the rate of S(–II) oxidation. Therefore, the initially chosen values (i.e., 2.5 and 1.0 $\mu M \cdot min^{-1}$ respectively) were not changed.

The parameters of Table 5.4 were then used to model the oxidation of S(–II) at pH 10 and different initial sulfide concentrations, $[S(-II)]_o$. The agreement with the experimental data was very good at low $[S(-II)]_o$; the calculated S(–II) profiles for $[S(-II)]_o$ 7 μM and 45 μM are shown in Figure 5.6 together with the experimental S(–II) profiles. As $[S(-II)]_o$ increases, oxygen gets depleted before complete oxidation of the initial sulfide is achieved. Oxygen depletion results in a sudden decrease in the overall oxidation rate. Figure 5.7 shows the calculated [S(–II)] and $[O_2]$ profiles for $[S(-II)]_o$ = 300 μM and two different values of the oxygen transfer coefficient; the solid line represents the case where $[O_2]$ is fixed at the initial air saturation value [by providing a very high $Kl(O_2)$ value], and the broken line is expected to represent our experimental conditions (see above). For that value of $[S(-II)]_o$, continuous aeration of the solution does not improve the S(–II) oxidation rate significantly. The same is shown to be true up to $[S(-II)]_o \simeq$ 450 μM (Figure 5.8). At higher $[S(-II)]_o$, the observed S(–II) oxidation rate is lower than the rate at $[O_2]$ = constant = 240 μM; Figure 5.9 illustrates that point for $[S(-II)]_o$ = 955 μM.

Figure 5.10 shows the agreement between the experimentally determined effect of $[S(-II)]_o$ on the initial sulfide oxidation rate, k_o, for $[S(-II)]_o \leq$ ~450 μM.

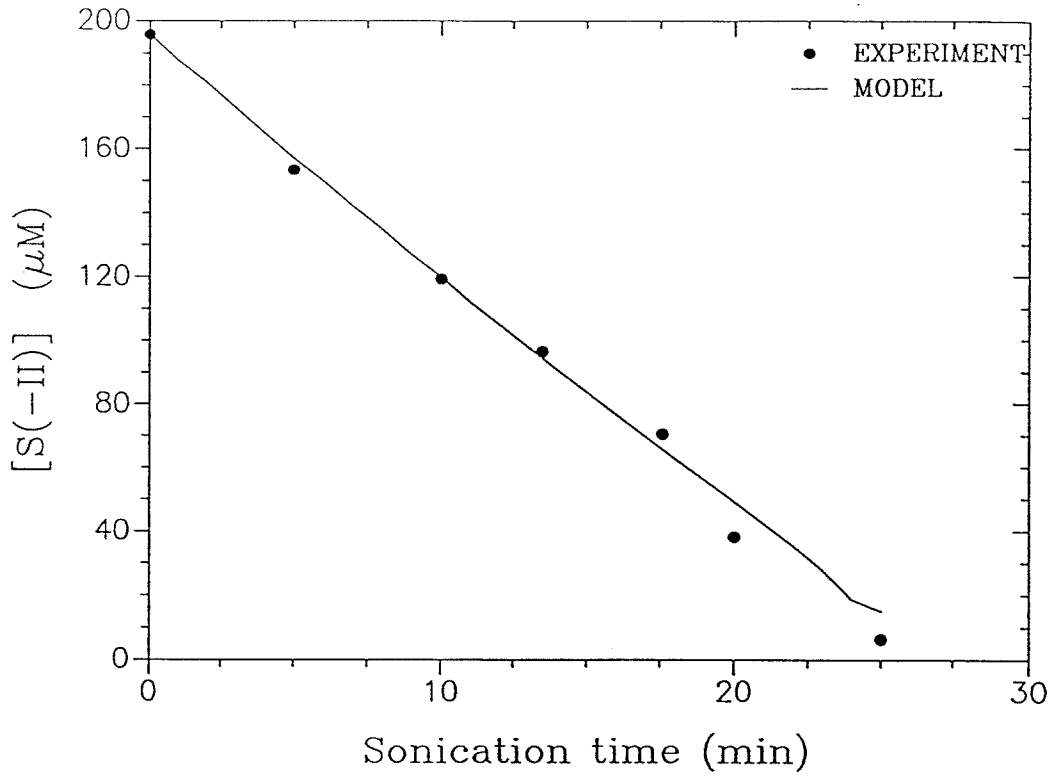

Figure 5.5 Comparison between [S(–II)] decrease predicted by the free–radical chemistry model and that observed upon ultrasonic irradiation of S(–II) at pH 10, $[S(-II)]_o$ = 196 μM, $[O_2]_o$ = 240 μM.

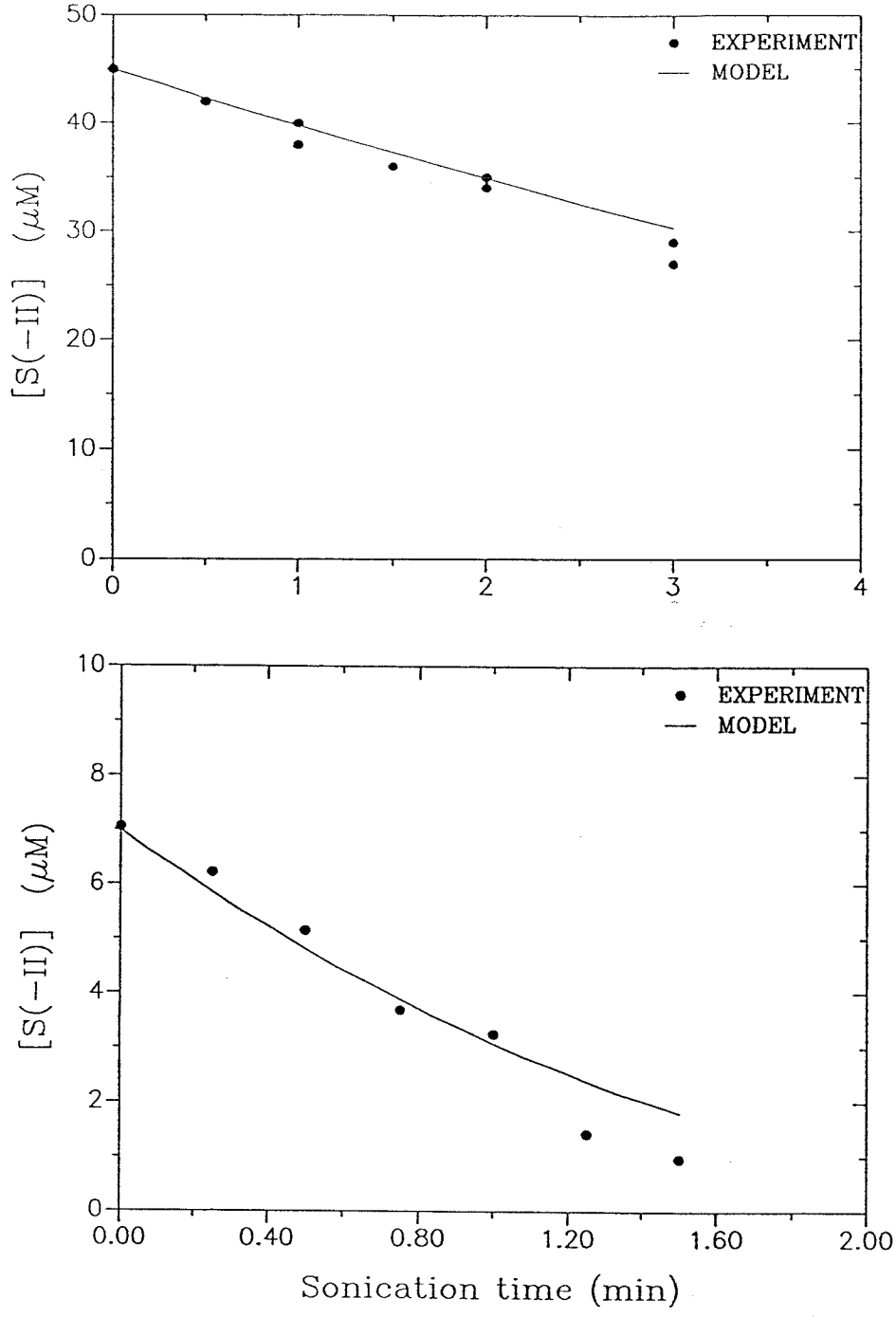

Figure 5.6 Comparison between [S(–II)] decrease predicted by the free–radical chemistry model and that observed upon ultrasonic irradiation of S(–II) at pH 10, $[O_2]_o$ = 240 μM and two different $[S(-II)]_o$ low values (a, top) 45 μM, and (b, bottom) 7 μM.

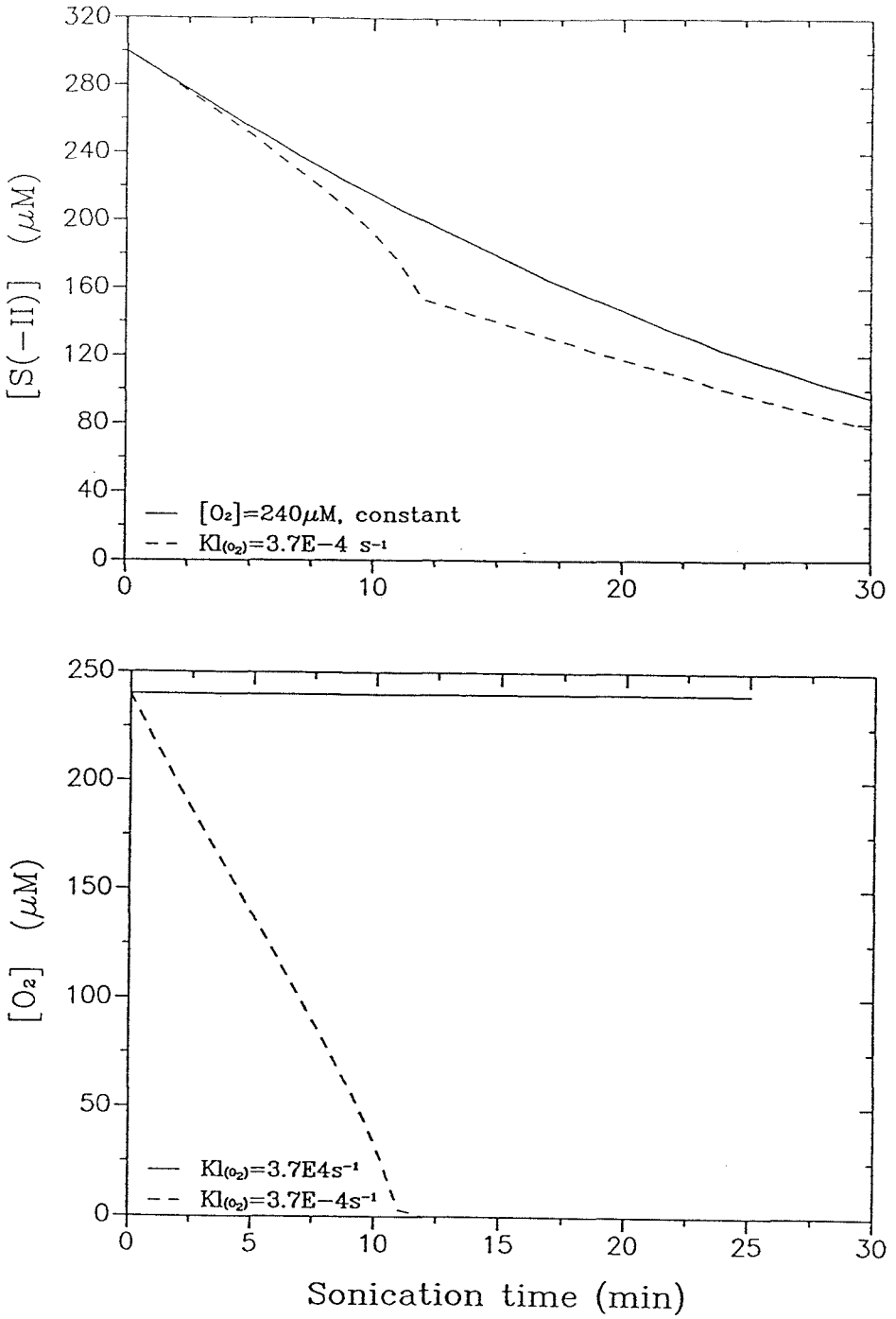

Figure 5.7 (a, top) Comparison of calculated [S(–II)] profiles with $[O_2]$ kept constant at air saturation (solid line) and with the oxygen transfer coefficient of Table 5.4 (broken line) at pH 10, OH_{input} = 3.5 $\mu M \cdot min^{-1}$, $[S(-II)]_o$ = 300 μM, $[O_2]_o$ = 240 μM. (b, bottom) corresponding $[O_2]$ profiles.

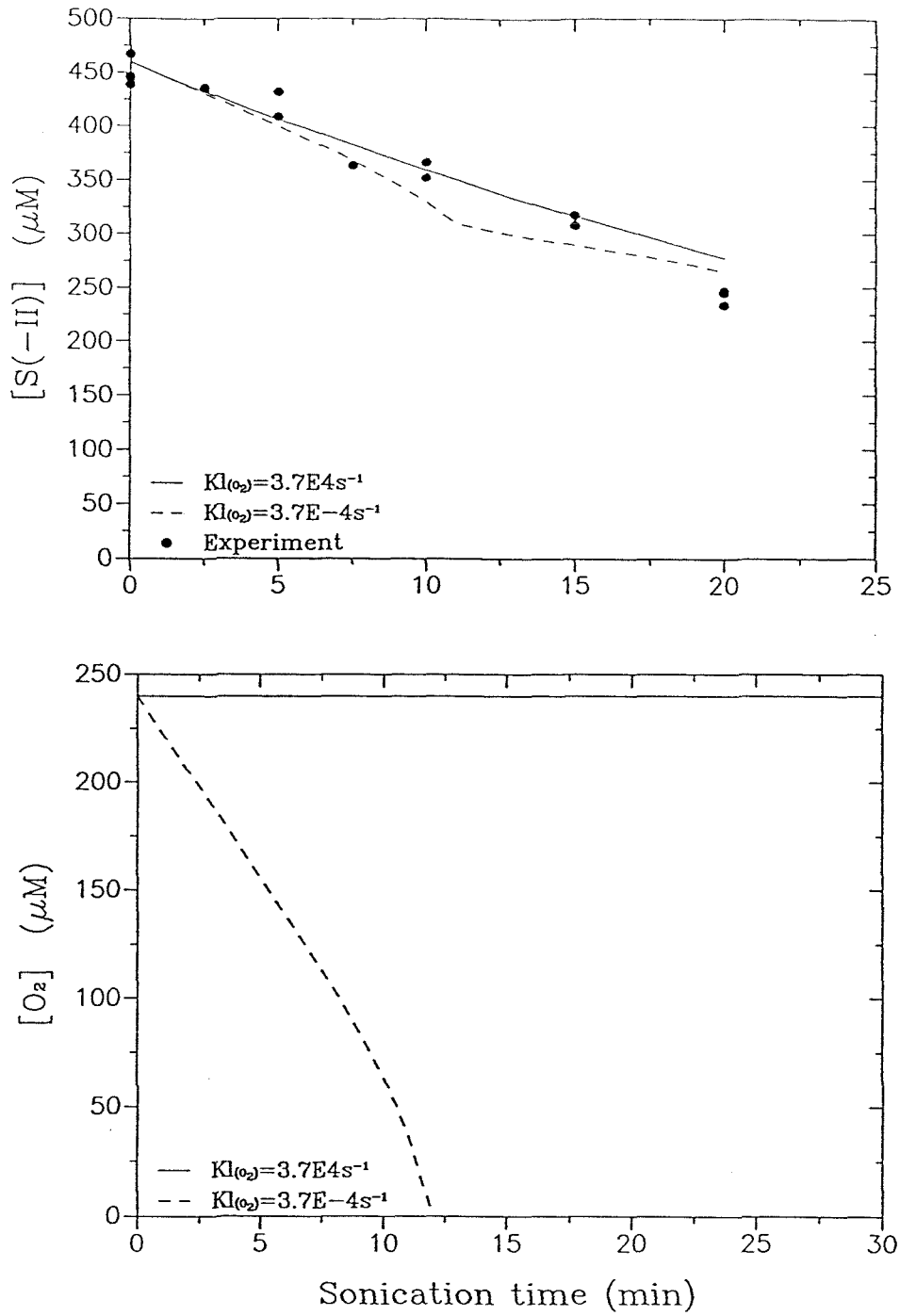

Figure 5.8 (a, top) Comparison of sonolysis data with calculated [S(–II)] profiles with $[O_2]$ kept constant at air saturation (solid line) and with the oxygen transfer coefficient of Table 5.4 (broken line) at pH 10, $OH_{input} = 3.5\ \mu M \cdot min^{-1}$, $[S(-II)]_o \simeq 450\ \mu M$, $[O_2]_o = 240\ \mu M$. (b, bottom) corresponding calculated $[O_2]$ profiles.

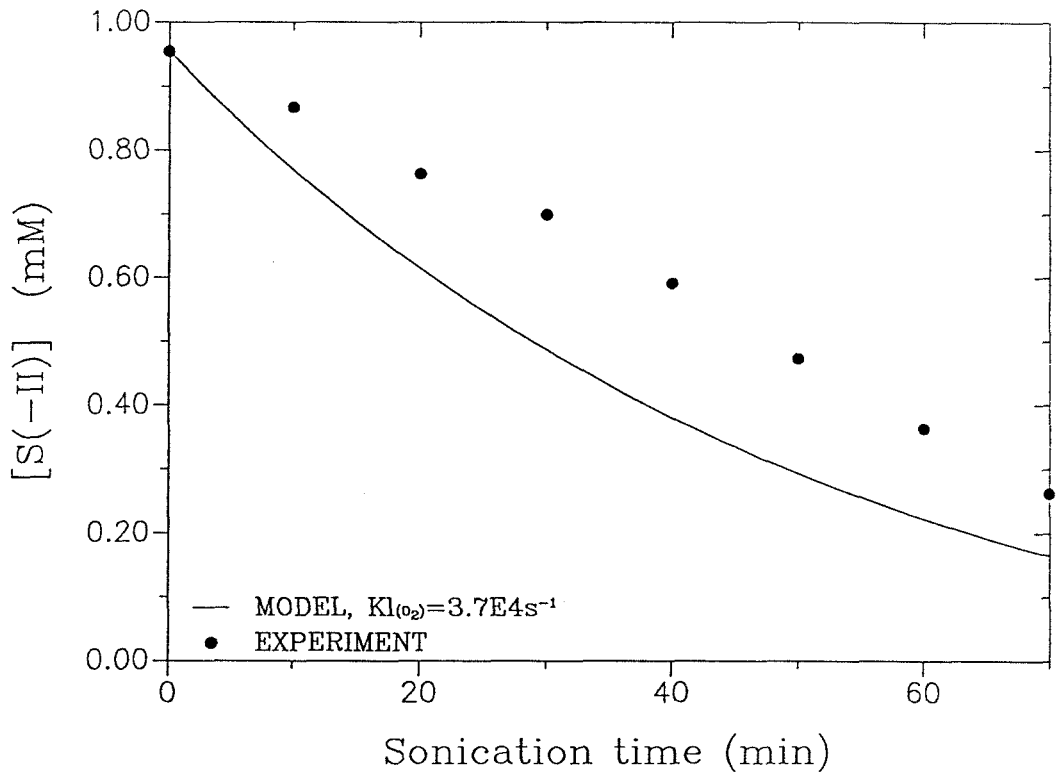

Figure 5.9 Comparison of sonolysis data with calculated [S(–II)] profiles with $[O_2]$ kept constant at air saturation (solid line) at pH 10, $OH_{input} = 3.5\ \mu M \cdot min^{-1}$, $[S(-II)]_o \simeq 955\ \mu M$, $[O_2]_o = 240\ \mu M$.

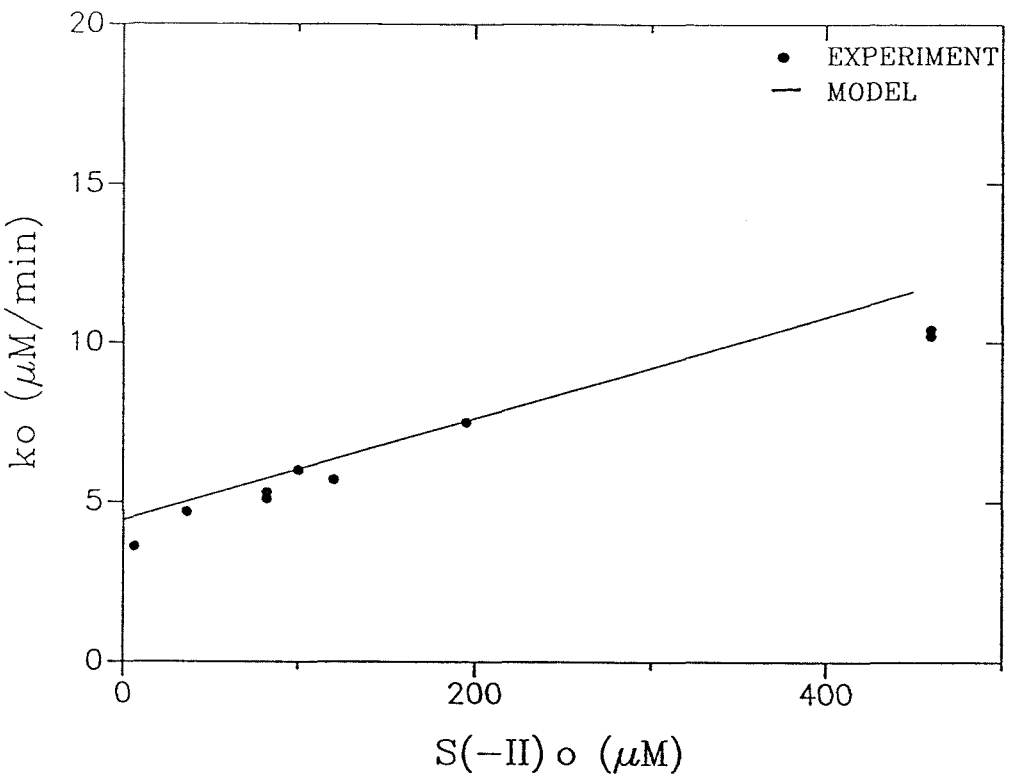

Figure 5.10 Effect of $[S(-II)]_o$ on initial zero–order S(–II) oxidation rate, k_o.

In both cases, k_o increases linearly with $[S(-II)]_o$. The following linear relationship was found from the model:

$$k_o = 4.4 + 0.016\ [S(-II)]_o \qquad (5.1)$$

where, k_o in $\mu M \cdot min^{-1}$, and $[S(-II)]_o$ in μM. As discussed in Chapter 4, the value of the intercept represents the contribution of $^{\cdot}OH$ while the slope is due to the free–radical chain sequence. For $[S(-II)]_o \geq \simeq 300\ \mu M$ the latter term exceeds the former (i.e., O_2 becomes the principal oxidant).

It must be noted that the two pathways that are used to model $S_2O_3^{2-}$ formation cannot outcompete the reaction of H_2S_2 with O_2. This results in an underprediction of $[S_2O_3^{2-}]$ as can be seen in Figure 5.11. Sulfite, on the other hand is modeled rather well as can be seen also in Figure 5.12 where the profiles of [S(–II)] and its oxidation products are presented for pH 10.6. Nevertheless, the free–radical chemistry mechanism describes adequately the overall oxidation of S(–II) upon sonication at alkaline pH.

Figures 5.13, 5.14, and 5.15 present the S(–II) and S_{ox}, where $S_{ox} = [SO_4^{2-}]+[SO_3^{2-}]+2[S_2O_3^{2-}]$, profiles observed upon sonication of S(–II) aqueous solutions at pH 9.0, 8.5, and 7.4 respectively. The broken lines represent the corresponding concentrations of those species predicted by the free–radical chemistry mechanism. It can be seen that the free–radical mechanism underpredicts the rate of S(–II) disappearance at pH $\leq$ 8.5. Nevertheless, the total amount of the oxidized S(–II) that was found in the form of the three species that form S_{ox} is not much higher than the calculated S_{ox}. It must be noted that S_{ox} represents the total amount of sulfide that has been oxidized in the case of the chemical model (since the three species from which S_{ox} comprises of are the only final oxidation products), while in the case of the experimental data S_{ox} represents

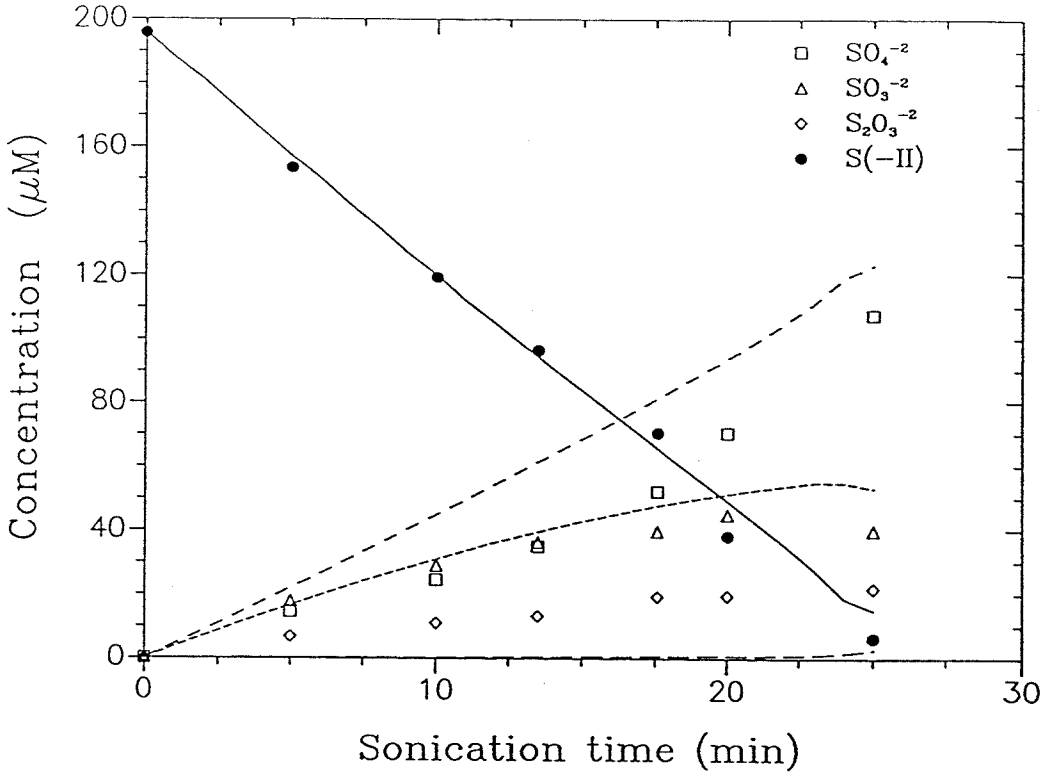

Figure 5.11 [S(–II)] profile and oxidation product distribution at pH 10, $[S(-II)]_o = 196\ \mu M \cdot min^{-1}$. Model results (solid and broken lines) and experimental data (symbols).

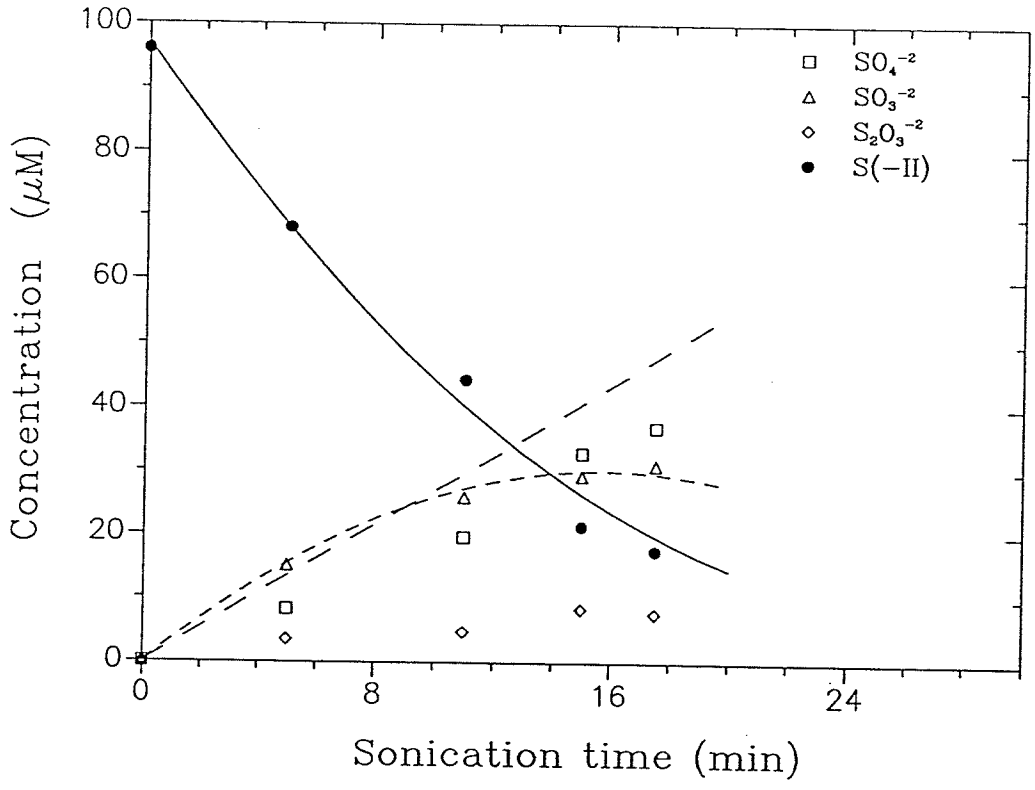

Figure 5.12 [S(–II)] profile and oxidation product distribution at pH 10.6, $[S(-II)]_o = 96\ \mu M \cdot min^{-1}$. Model results (solid and broken lines) and experimental data (symbols).

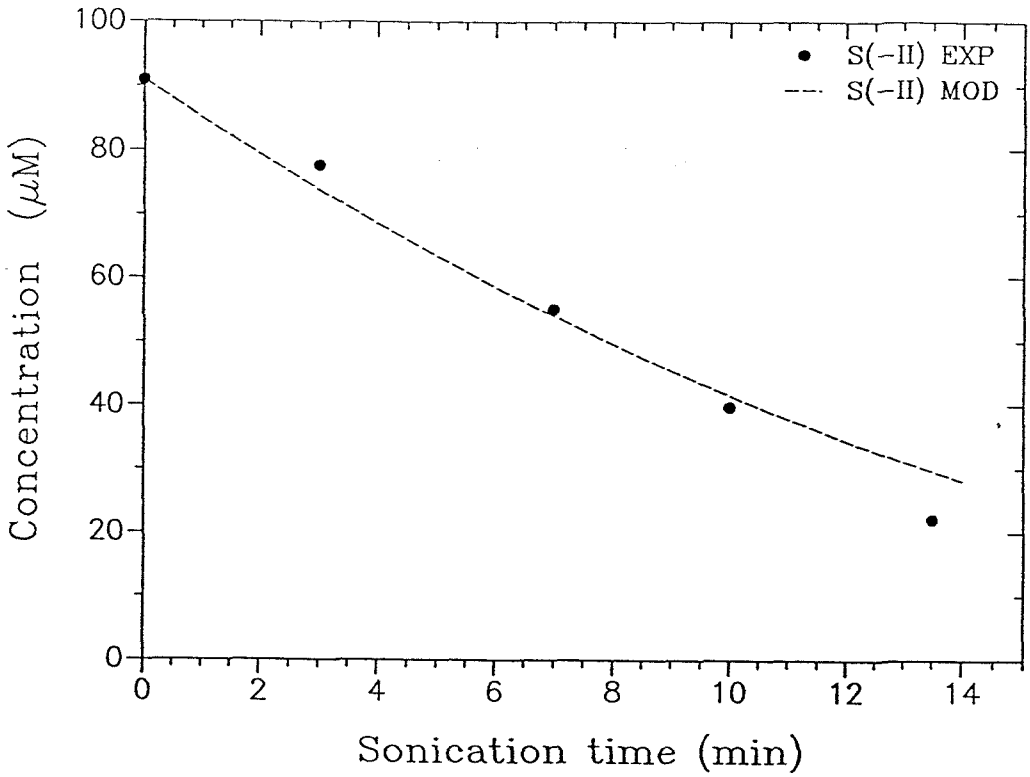

Figure 5.13 Comparison between [S(–II)] decrease predicted by the free–radical chemistry model and that observed upon ultrasonic irradiation of S(–II) at pH 9.0, $[S(-II)]_o$ = 91 μM, $[O_2]_o$ = 240 μM.

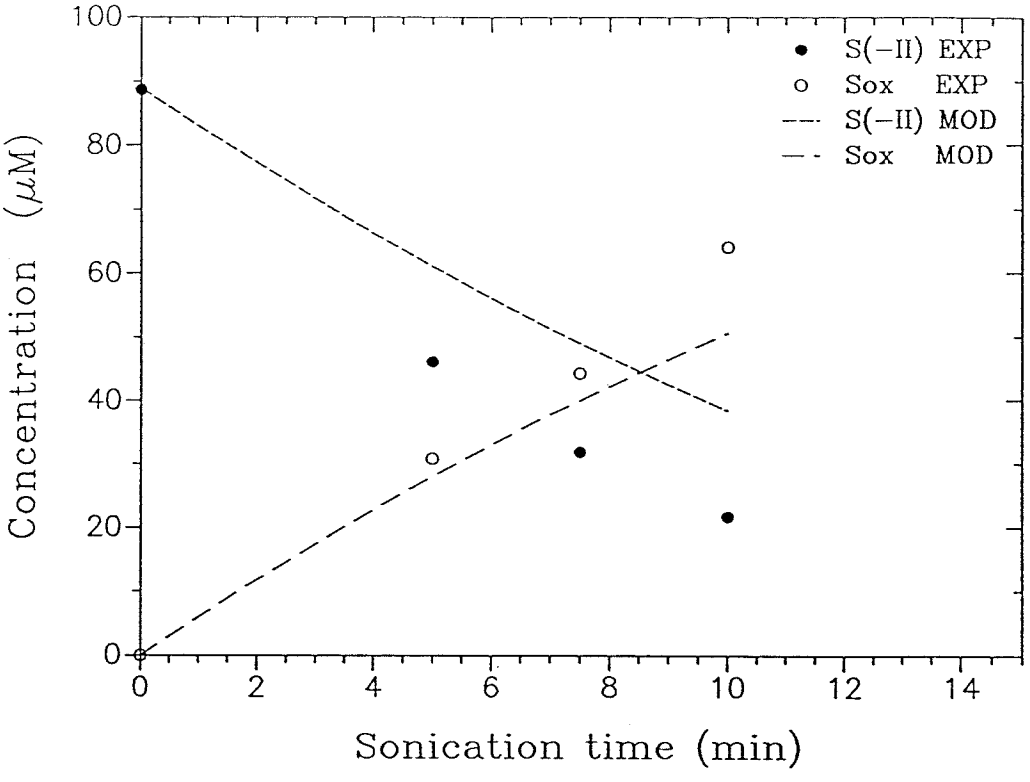

Figure 5.14 Comparison between [S(–II)] decrease predicted by the free–radical chemistry model and that observed upon ultrasonic irradiation of S(–II) at pH 8.5, $[S(-II)]_o$ = 88 μM, $[O_2]_o$ = 240 μM.

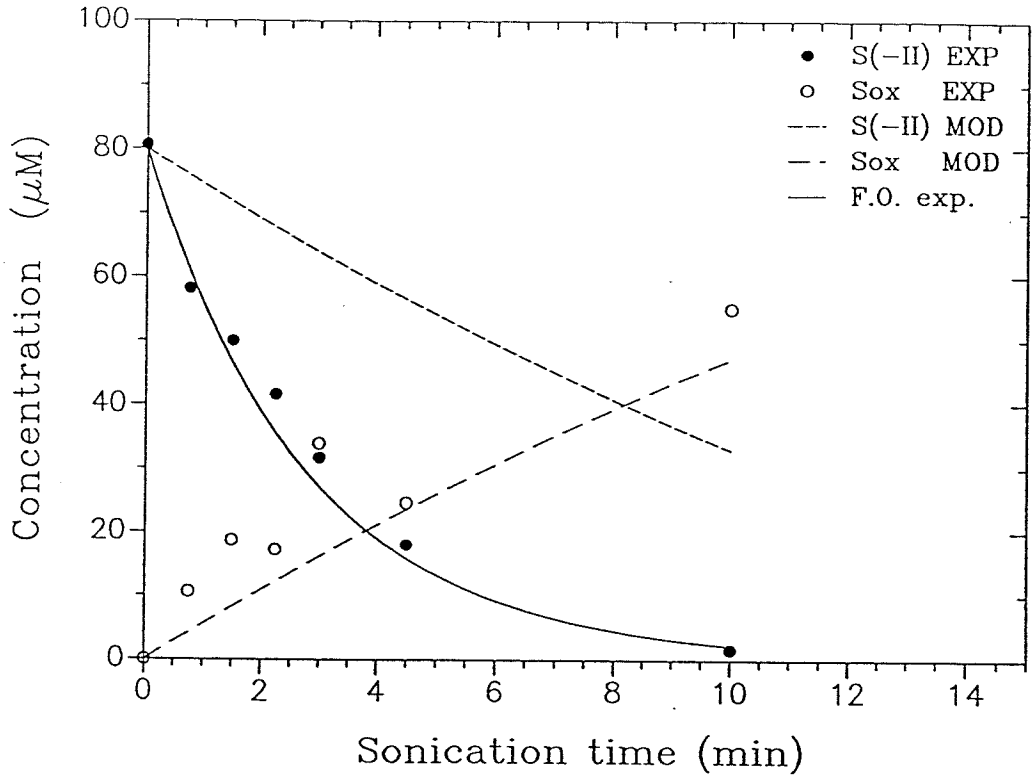

Figure 5.15 Comparison between [S(–II)] decrease predicted by the free–radical chemistry model and that observed upon ultrasonic irradiation of S(–II) at pH 7.4, $[S(-II)]_o \simeq 80$ μM, $[O_2]_o = 240$ μM.

only a part of the oxidation products (Chapter 4).

These results provide further evidence that an important pathway for S(–II) sonolysis at pH $\leq$ 8.5 is thermal decomposition of H_2S within the cavitation bubbles or within the gas–liquid interface. Furthermore, they seem to suggest that elemental sulfur in the main product of that alternative sonolysis pathway.

In conclusion, it has been shown that the sonolysis of S(–II) in the pH range where that species is primarily in the form of HS^- and is not expected to undergo thermal decomposition can be modeled with an aqueous free–radical chemical mechanism and a continuous constant release of $^{\cdot}OH$ into solution. This simplified approach is not valid at the pH range ($\leq$ 8.5) where a significant part of the total sulfide is in the form of H_2S that can participate in the gas phase high temperature chemistry that takes place inside and near collapsing cavitation bubbles. An extended chemical mechanism that would include both gas and liquid phase chemistry is needed in order to model S(–II) sonolysis in the general case. However, the development of next level model is not feasible at this stage because of the lack of enough information about the number and the size distribution of cavitation bubbles. In addition, little is known about the physical conditions inside the bubble and its surrounding region upon collapse.

It has also been shown that molecular oxygen is important for the sonolysis of S(–II) at alkaline pH because it propagates a free–radical chain reaction that is initiated by $^{\cdot}OH$. Furthermore, the enhancement of oxygen transfer upon sonication with a direct–immersion horn has been shown to be considerable. These results may have important implications for the application of ultrasonic irradiation for the destruction of chemical contaminants in water systems.

References

1. Smith, R. M.; Martell, A. E. *Critical Stability Constants, vol 4: Inorganic complexes*, Plenum, New York, 1976.
2. Hoffmann, M. R. *Env. Sc. Technol.* 1977, *11*, 61.
3. Giggenbach, W. *Inorg. Chem.* 1971, *10,* 1333.
4. Pandis, S. N.; Seinfeld, J. H. *J. Geophys. Res.* 1989, *94*, 1105.
5. Neta, P.; Huie, R. E.; Ross, A. B. *J. Phys. Chem. Ref. Data* 1988, *17*, 1027.
6. Buxton, G. V.; Greestock, C. L.; Helman, W. P.; Ross, A. B. *J. Phys. Chem. Ref. Data* 1988, *17,* 513.
7. Mills, G.; Schmidt, K. H.; Matheson, M. S.; Meisel, D. *J. Am. Chem. Soc.* 1987, *91*, 1590.
8. Mehnert, R.; Brede, O. *Radiat. Phys. Chem.* 1984, *23*, 463.
9. Chameides, W. L.; Davis, D. D. *J. Geophys. Res.* 1982, *87*, 4863.
10. Jacob, D. J. *J. Geophys. Res.* 1986, *91*, 9807.
11. Mader, P. M. *J. Am. Chem. Soc.* 1958, *80*, 2634.
12. Hoffmann, M. R.; Edwards, J. O. *Inorg. Chem.* 1977, *16*, 3333.
13. Clifton, C. L.; Altsein, N.; Huie, R.E. *Env. Sc. Techol.* 1988, *22*, 586.
14. Natroshvili, G. R.; Panchvidze, M. V.; Nanobashvili, H. M. In *Proc. Tihany Symp. Radiat. Chem., 3rd, 2*, Dobo (ed.), 1972, pp. 1281–1291.
15. Byrne, G. D.; Hindmarsh, A. C. *ACM Trans. Math. Software* 1975, 71.
16. Warren, D. R. Nucleation and growth of aerosols, PhD thesis, California Institute of Technology, 1986.

CHAPTER 6

ULTRASONIC IRRADIATION OF IODIDE AND PARATHION IN AQUEOUS SOLUTION

Ultrasonic Irradiation of Iodide

Introduction

The formation of iodine when potassium iodide solutions are subjected to ultrasonic irradiation was one of the first sonochemical observations (1). Various investigators have since studied the chemical effects of ultrasonic waves on potassium iodide solutions in an attempt to elucidate the nature of sonochemistry (e.g., 2–5). Following the discovery that carbon tetrachloride greatly accelerates the formation of iodine (6,4), iodide solutions with traces of carbon tetrachloride (known as "Weissler's solution") were used as chemical dosimeters for sonochemical apparatus (7,8). With the advances in modern spectrophotometry the addition of CCl_4, that used to be a source for irreproducibility, seems no longer necessary (9).

It is accepted currently that iodide oxidation upon sonication is due to free–radical reactions initiated by the thermal decomposition of solvent or solute molecules in compressed cavitation bubbles (10). Nevertheless, open questions remain as to the precise chemical mechanisms of KI sonolysis and the importance of additional oxidants (e.g., O_2) (4). No direct information exists on the effect of pH on the iodine yield; even the related effect of pH on H_2O_2 formation upon water sonication has only been studied in the acidic pH region (4). No mention is found in the literature concerning the importance of I_2 evaporation from the aqueous solutions, except of the suggestion that care should be taken to minimize it (9). The effect of dissolved gases on I_2 yields has not been satisfactory resolved (2, 5, 11).

In this section, experimental results obtained when potassium iodide solutions were exposed to 20 kHz ultrasound are presented. The motivations for

performing these experiments were: *a*) perform a visual inspection of the ultrasonic field to detect possible inhomogeneities, *b*) address some of the above stated open questions so as to feel confident in using the KI system as a dosimeter to compare the sonochemical efficiency of different experimental set–ups.

Results and discussion

The formation of the blue color iodine–starch complex when starch is added in the KI–CCl_4 solution was used for visual inspection of the action of ultrasound (8). Figure 6.1 shows the rapid change in the color of a 0.9 M solution of KI with 10% per volume starch and at CCl_4 saturation upon sonication in a glass reaction vessel with the 1/2–in. direct immersion horn at 20 kHz, 75 W/cm^2. The volume of the sonicated solution was 30 ml. Although sonoluminescence experiments have suggested that the ultrasonic field is more intense in the vicinity of the titanium tip (see Chapter 7), no obvious inhomogeneities were observed. This suggests that even though the cavitation events may not be homogeneously distributed in our experimental setup, rapid mixing induced by the moving bubbles results in macroscopically homogeneous chemistry. The KI–CCl_4–starch solution was used subsequently for qualitative screening of different reactor systems. If a sonication set–up produces a field that is adequate to 'do chemistry', a rapid change in the color of that solution should be observed.

Solutions of 1M KI were sonicated under the same experimental conditions of the p–NP and S(–II) ultrasonic irradiation experiments as discussed in Chapters 3 and 4 (i.e., Branson CD200 sonifier, 75 W/cm^2, stainless steel cell, 25 ml solution). Figure 6.2 shows the observed linear increase of the absorbance at 350 nm. The absorbance at 350 nm is due to the I_3^- ion [$\epsilon_{350} = 2.6 \cdot 10^4$ M^{-1}sec^{-1}, (5)]. The

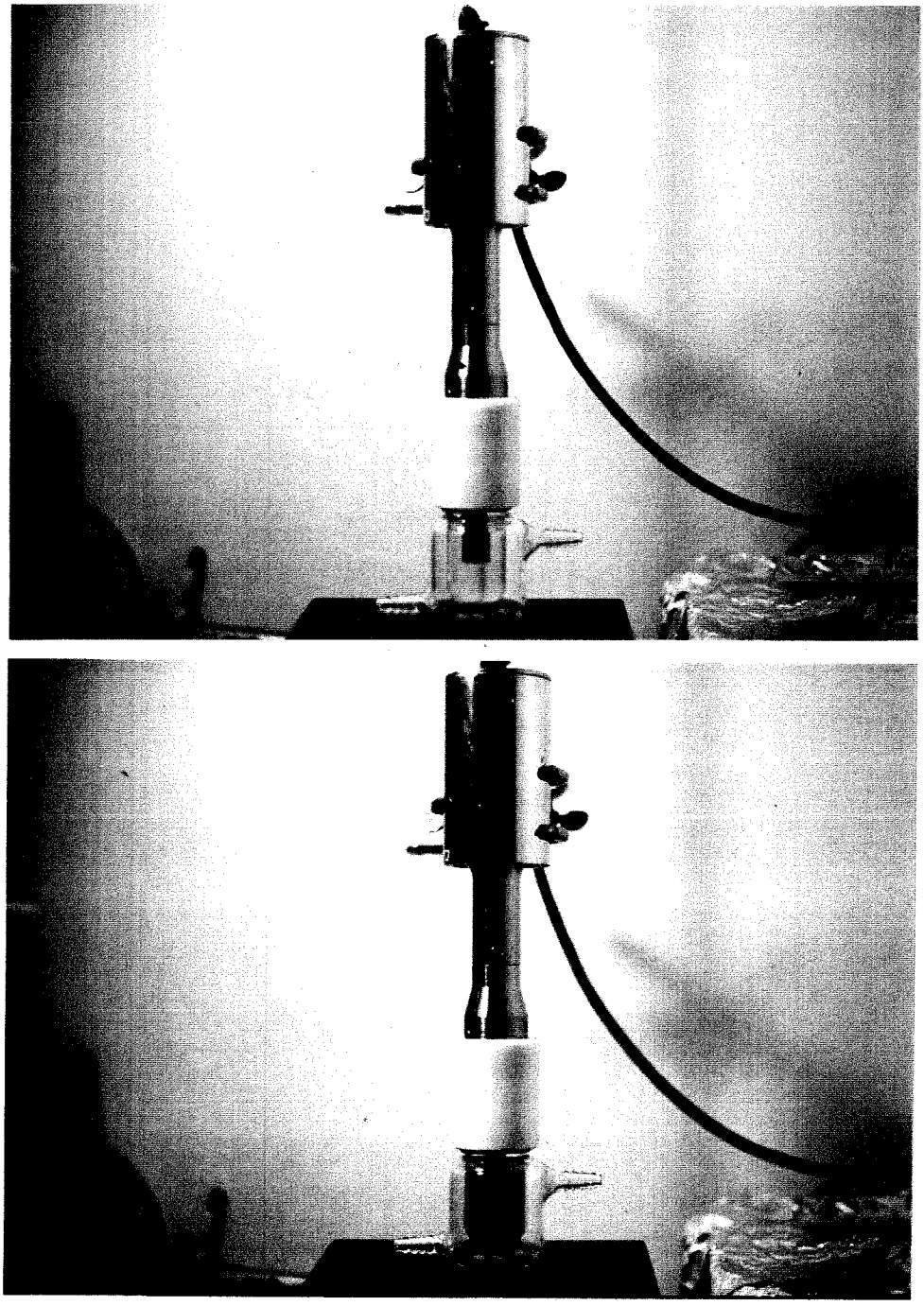

Figure 6.1. "Weissler's solution" (0.9 M KI, 10% starch, CCl_4) before (top) and after (bottom) sonication at 20 kHz, and 75 W/cm^2 for $\simeq$ 10 seconds.

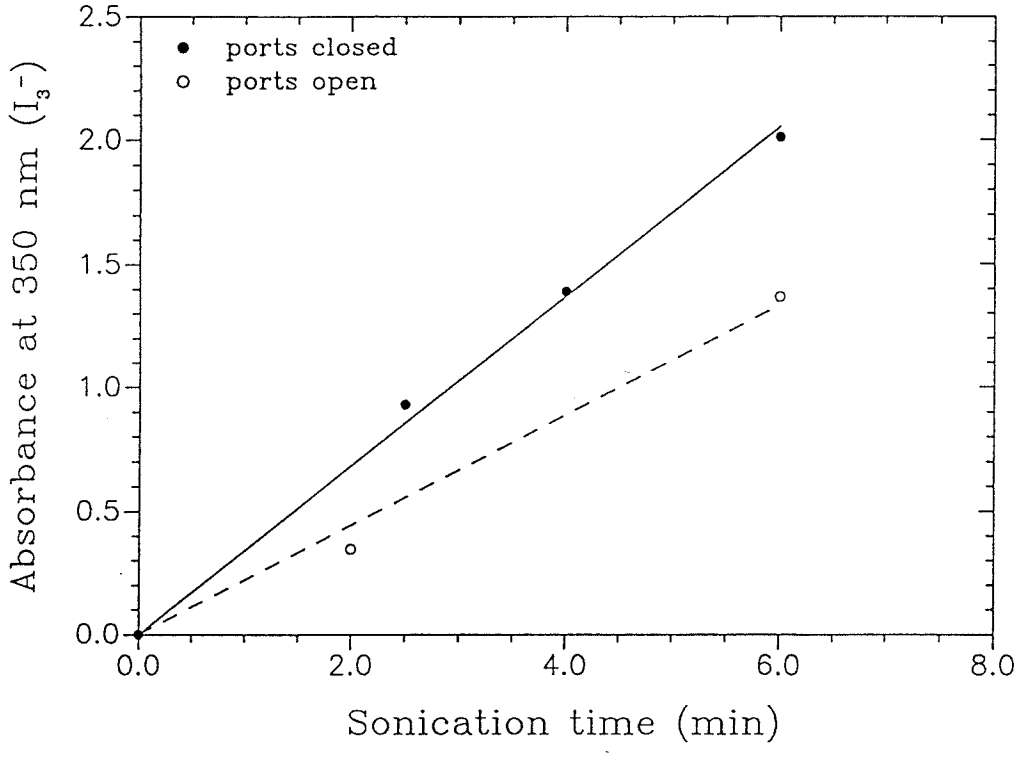

Figure 6.2. Absorption at 350 nm with sonication time; 1 M KI, 20 kHz, 75 W/cm^2, SS cell, 25 ml, $T_b \simeq 28$ °C.

increase in the absorbance is proportional to the release of iodine into solution, since the equilibrium reaction E1 (Table 6.1) is shifted substantially to the right for $[I^-] \simeq 1M$. The corresponding I_2 yield ($\simeq$ increase in I_3^-) is $\simeq 12.9\ \mu M \cdot min^{-1}$. It is noted that the reproducibility of I_2 sonolysis yields was very good ($\pm$ 5%).

The rate of I_3^- formation decreased by about 1/3 (Figure 6.1, $d[I_3^-]/dt = 8.6\ \mu M \cdot min^{-1}$) when the ports of the stainless steel cell were open, indicating a considerable iodine degassing. It is possible that the decrease in the iodine yield is partly related to the lower pressure in the headspace. When the ports are closed, iodine that is released into the headspace may increase the total gas pressure. Increased pressure is expected to lead to more intense cavitation and thus higher sonochemical yields (7).

The initial pH of 1M KI solution is $\simeq$ 6.9. If no buffer is used, pH increases gradually during sonication and stabilizes at $\simeq$ 8.8. This is in agreement with the increase of pH from neutral to about 8.2 reported by Renaud (3) for sonication of 1M KI solutions (and indicated by the stoichiometries of equations E2, E4, and E6 and reactions R6 and R15). Figure 6.3 compares the increase in A_{350} in the absence of buffer with that observed when pH was kept constant at 10 with borate buffer. It can be seen that no change in the iodine yield was observed. Gueguen (4) has reported that H_2O_2 yield in sonicated water (at 960 kHz) increased with increasing pH from pH 0.3 to pH 3.0 and remained constant thereafter (up to 6.5 that was the highest pH value that he studied). Assuming that this trend continues into the alkaline region and H_2O_2 yield does not depend on pH, our result is not surprising. Experimental results of Hart & Henglein (5) have indicated that sonolysis yields of H_2O_2 and I_2 are closely related and follow the same trends.

A series of experiments was conducted with a water–jacketed glass vessel in

Table 6.1
Equilibrium reactions

id#	Reaction	k	Reference
E1	$I_2 + I^- \rightleftharpoons I_3^-$	770	(12)
E2	$I_{2(aq)} + H_2O \rightleftharpoons I^- + H^+ + HIO$	$3.0 \cdot 10^{-13}$	(13)
E3	$I^\cdot + I^- \rightleftharpoons I_2^{\cdot -}$	$1.1 \cdot 10^{5}$	(14)
E4	$HOI \rightleftharpoons H^+ + OI^-$	$1.0 \cdot 10^{-11}$	(15)
E5	$O^{\cdot -} + IO_3^- \rightleftharpoons IO_4^{2-}$	$1.0 \cdot 10^{6}$	(15)
E6	$HIO_3 \rightleftharpoons H^+ + IO_3^-$	0.17	(24)

Table 6.2
Free radical iodide chemistry

id#	Reaction	k $M^{-1}s^{-1}$	Reference
R1	$^{\cdot}OH + {}^{\cdot}OH \longrightarrow H_2O_2$	$5.5 \cdot 10^9$	(16)
R2	$I^- + {}^{\cdot}OH \longrightarrow I^{\cdot} + OH^-$	$1.2 \cdot 10^{10}$	(16)
R3	$I^{\cdot} + I^{\cdot} \longrightarrow I_2$	$8.0 \cdot 10^9$	(17)
R4	$I_2^{\cdot -} + I_2^{\cdot -} \longrightarrow I_3^- + I^-$	$3.0 \cdot 10^9$	(17)
R5	$^{\cdot}OH + I_2 \longrightarrow HOI + I^{\cdot}$	$1.1 \cdot 10^{10}$	(16)
R6	$I_2^{\cdot -} + HOI \longrightarrow 2\ I^- + H^+ + IO$	$1.0 \cdot 10^5$	(17)
R7	$^{\cdot}OH + HOI \longrightarrow HOIOH$	$7.0 \cdot 10^9$	(16)‡
R8	$HOIOH \longrightarrow IO + H_2O$	$1.3 \cdot 10^{6}$*	(17)
R9	$^{\cdot}OH + IO_3^- \longrightarrow HIO_4^-$	$1.3 \cdot 10^9$	(16)
R10	$IO_4^{2-} \longrightarrow IO_3 + O^{\cdot -}$	$3.3 \cdot 10^{3}$*	(17)
R11	$NO_2^- + I^{\cdot} \longrightarrow I^- + NO_2^{\cdot}$	$8.8 \cdot 10^9$	(17)
R12	$I^- + NO_2^{\cdot} \longrightarrow I^{\cdot} + NO_2^-$	$1.1 \cdot 10^5$	(17)
R13	$I_2 + O_2^{\cdot -} \longrightarrow I_2^{\cdot -} + O_2$	$5.5 \cdot 10^9$	(18)
R14	$I_3^- + O_2^{\cdot -} \longrightarrow I_2^{\cdot -} + I^- + O_2$	$8.0 \cdot 10^8$	(18)
R15	$NO_2^{\cdot} + NO_2^{\cdot} \xrightarrow{H_2O} NO_2^- + NO_3^- + 2\ H^+$	$1.0 \cdot 10^8$	(17)
R16	$NO_2^- + OH \longrightarrow NO_2^{\cdot} + OH^-$	$1.0 \cdot 10^{10}$	(16)
R17	$5IOH \longrightarrow HIO_3 + 2\ I_2 + 2\ H_2O$	very fast	(23)
R18	$H_2O_2 + 2\ I^- + 2\ H^+ \longrightarrow I_2 + 2\ H_2O$	moder. rapid(13) hastened by molybdate	

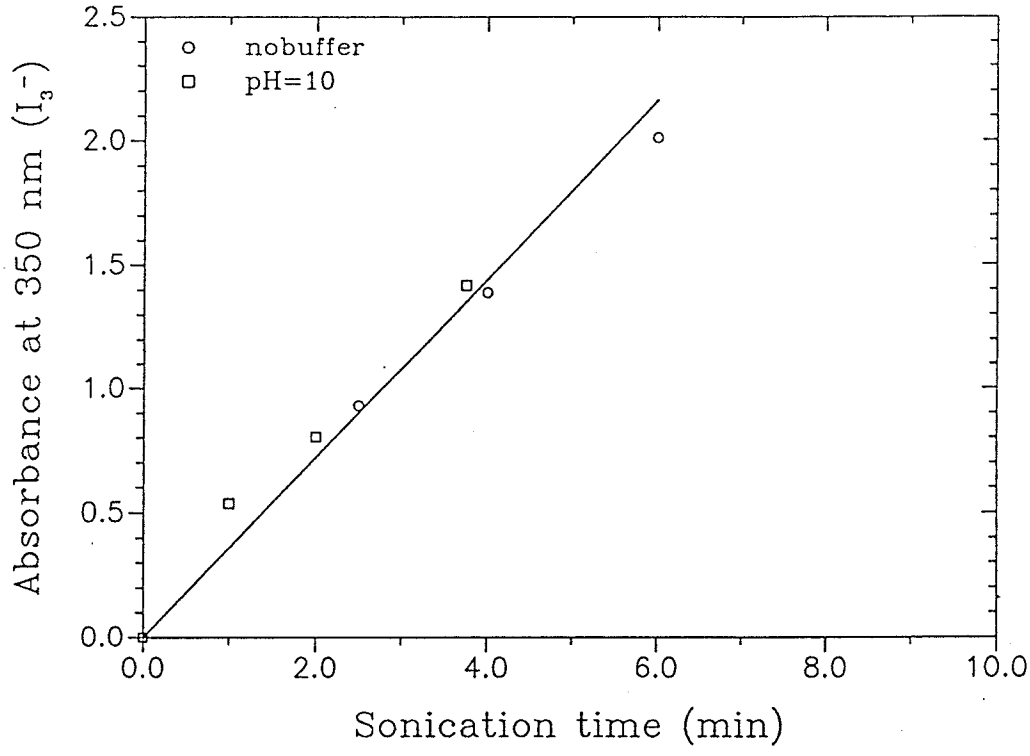

Figure 6.3. Comparison of I_3^- yields in the presence of borate buffer (pH 10) and in the absence of buffer (pH_{in} 6.9, pH_{final} 8.8).

order to study the effect of dissolved gases on the I_2 sonolysis yields. The vessel is connected to the nodal point of the horn with a teflon part; the configuration is similar to "Suslick's glass cell" (7) The volume of the sonicated solution was 100 ml. Similarly to the stainless steel cell, two side ports and a bottom port allowed for the dispersion of different gases into the solution before sonication: all ports were closed with rubber septa; the desired gas was bubbled into the bulk of the solution using a syringe through the bottom port, and air was removed from the headspace with the use of a second syringe from one of the side ports (volume of headspace $\simeq$ 60 ml). Bubbling times varied between 40 and 90 minutes. Repeated experiments showed that 40 minutes of bubbling gave the same results as extended bubbling for the gases used. Therefore, most of the experiments shown in Figure 6.4 were conducted after 40 minutes of bubbling of the appropriate gas.

The effect of different gases on the iodine yields is shown in Figure 6.4. It can be seen that the highest yield is obtained in sonication under oxygen, but this yield is comparable to that obtained under argon. Table 6.3 presents the absolute and relative yields of I_2 for the four gases that were studied, and compares our findings with previous related studies. Given the differences in the experimental conditions, our results are in general agreement with those reported by Hart and Henglein (5) and Gueguen (11). Weissler's results (2) seem to indicate that under his experimental conditions dissolved gases were not critical. Nevertheless, the same investigator found zero I_2 yield under helium and carbon dioxide. It has to be noted that he measured iodine by titration with sodium thiosulfate and the concentrations that he reports for the experiments without CCl_4 may have been close to his analytical limit of detection.

While the overall effect of ultrasound on KI could be viewed as reaction of

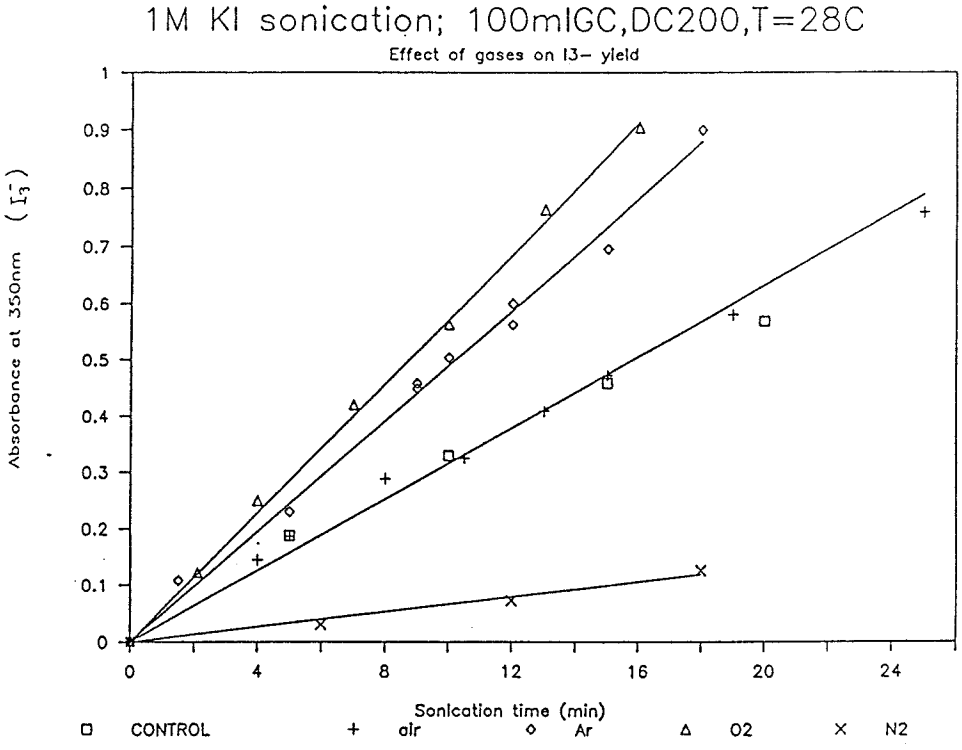

Figure 6.4. Effect of dissolved gas on iodine yield; 1 M KI, 100 ml glass cell, $T_b \simeq 28$ °C, 20 kHz, 75 W/cm^2.

Table 6.3
Effect of dissolved gases on KI sonolysis

Gas	k_o $\mu M \cdot min^{-1}$	Yields relative to that under O_2			
		This work	(2)	(5)	(11)
O_2	2.20	1.00	1.00	1.00	1.00
Ar	1.88	0.85	–	0.59	–
Air	1.21	0.55	1.39	–	–
N_2	0.25	0.11	0.91	–	0.25

This work: 20 kHz, 80 W; (2) Weissler, 1950: 1000 kHz, 310 W; (5) Hart & Henglein, 1985: 300 kHz; (11) Gueguen *et al.*, 1957: 960 kHz

·OH radical with I^- to produce $I^\cdot$ and subsequent recombination of two iodine atoms to produce I_2 (R2 and R3 in Table 6.3), the free–radical chemistry of the system could be much more complicated. Table 6.1 and Table 6.2 present some of the equilibrium and free–radical reactions of the iodine system that may be relevant to I^- sonication. Based on the equilibrium constant for equation E3, $I^\cdot$ will be converted to $I_2^{\cdot-}$, and diiodine radical could either recombine to give I_3^- and I^- (R4) or oxidize HOI with formation of $IO^\cdot$ (R6). It must be noted that there are several forms of I(VI) in addition to HIO_4^- and IO_4^{2-} (i.e., $H_5IO_6^-$, $H_4IO_6^{2-}$, $H_2IO_5^{2-}$, HIO_5^{3-}) that could be important. Furthermore, reactions with O_2 or oxygen atoms, O, have not been included because of lack of appropriate data. Not enough information was found for high temperature gas phase reactions of I_2 in the gas phase of the cavities. It is expected that iodine atoms will be formed and it may be possible to have a radical chain mechanism involving additional oxidants (e.g., O_2, O, $NO_2^\cdot$).

The observed increase of I_2 formation under argon can be explained by increased temperature during collapse. As discussed in Chapter 2, the presence of monoatomic gases in the imploding cavity results in higher T because of their higher ratio of specific heats, γ ($\gamma \simeq 1.7$ for Ar, and $\simeq 1.4$ for O_2, N_2, air). The fact that the thermal conductivity of Ar is about 70% lower than that of the other three gases should also favor higher local temperature upon collapse.

Comparing the effect of the three gases that have approximately the same γ (i.e, O_2, N_2, and air) it becomes clear that oxygen promotes the oxidation rate. The importance of O_2 has been reported before (5) and those researchers actually found that a mixture of 30% oxygen and 70% argon gives the highest I_2 yield. The addition of oxygen results in higher ·OH yields because of its high temperature reaction with hydrogen atoms to give ·OH and O [i.e., $H + O_2 \longrightarrow {}^\cdot OH + O$

(19)]. In the absence of O_2, about 80% of the ·OH and H· radicals originally formed from thermal dissociation of water are lost due to recombination (20). Oxygen atoms are also formed by direct thermal decomposition of O_2 in the hot regions of the bubble and their reaction with OH_2 leads to additional ·OH ($O + OH_2 \longrightarrow$ ·OH + ·OH). On the other hand, increasing concentrations of oxygen in the gas phase lower the γ value of the mixture and result in less intense cavitation.

The lower yields under nitrogen can be explained by scavenging of ·OH and O in the gas phase by N_2 with formation of N_2O, NO initially and then HNO_2, HNO_3 (21). Hart *et al.* (22) observed that H_2O_2 formation upon sonication of water was ≃ 7.6 times higher under Ar than under N_2 (13 $\mu M \cdot min^{-1}$: ≃ 1.7 $\mu M \cdot min^{-1}$). We found that I_2 yield under Ar was ≃ 7.5 times more than under N_2. This confirms that I_2 formation is closely related to the formation of H_2O_2.

It is easy to see that the I_2 yield under air is not simply the superposition of the iodine yields under O_2 and N_2 (i.e., $d[I_2]/dt|_{air} > \{0.29 \cdot d[I_2]/dt|_{O_2} + 0.71 \cdot d[I_2]/dt|_{N_2}\}$). This result could be due to the fact that when both O_2 and N_2 are present in the cavities, N_2 scavenges oxygen atoms to form nitrogen oxides that will eventually result in increased concentrations of nitrogen dioxide radical into solution. This radical can oxidize I^- to $I^\cdot$ (R12). Therefore, more O or ·OH that would be otherwise 'lost' to HO_2 or H_2O_2 through recombination reactions is used to oxidize I^- in the presence of nitrogen. It is noted that HO_2 does not oxidize I^-; but actually it is reducing I_2 or I_3^- back to I^- (R13, R14). H_2O_2 on the other hand can oxidize I^- (R18) but that reaction is fast only in acidic solution and in the presence of catalyst (molybdate + I^- in acid solution is the standard method for measuring H_2O_2). Therefore, H_2O_2 is not expected to contribute significantly to I^- oxidation; Hart & Henglein's results collaborate that argument (5).

The disproportional enhancement of I_2 formation under air, as compared to that under nitrogen, suggests that gas phase reactions of iodine species with O_2, O or $^{\cdot}OH$ are not very important. If they were, the additional scavenging of those oxygen species by N_2 should not be that important. It has to be stressed, however, that no effort was made to measure oxidized iodide species other than I_2. It is therefore conceivable that the relative yields of I_2 do not represent relative rates of overall I^- oxidation. Detailed study of the free–radical–ultrasound–induced chemistry of the iodide system was not within the scope of this work.

Samples taken immediately after bubbling showed no oxidation of I^- upon aeration or even oxygenation of the solution. This is in agreement with the known slow rate of I^- oxidation by molecular oxygen (23) and with simple observations made in this lab; the observed iodine in 1M KI solutions left in the dark was $\leq$ 3.0 μM after 24 hours.

The agreement between control experiments, where KI solutions were sonicated without any prior bubbling, and air experiments, with 40 minutes bubbling of compressed air, shows that bubbling did not affect sonochemical yields. That suggests that under our experimental conditions, we are not limited in the number of available 'cavitation nuclei' or pre–existing gas bubbles. Additional evidence supporting that conclusion is presented in Chapter 7 (effect of fine sand on sonication).

Conclusions

The mechanism of KI sonolysis could be more complicated than the simple reaction of I^- with $^{\cdot}OH$. Molecular oxygen clearly plays an important role in this free radical oxidation. High temperature reactions of I_2 in the gas phase were

suspected but the effect of dissolved gases on I_2 yield seems to indicate otherwise.

Potassium iodide can be used as an overall sonochemical dosimeter but a closed system is necessary. Considerable amounts of the I_2 produced can be lost through evaporation (as much as 33% for the commercial Branson CD200 system with the 1/2–in. horn and the 50 ml total volume stainless steel cell). The I_2 yield is independent of pH in the neutral to alkaline region.

Ultrasonic Irradiation of Parathion

Introduction

Parathion (O, O diethyl–O–p–nitrophenyl thiophosphate) is one of the organic pesticides that are used in large quantities all over the world. Organic esters used to be considered as a "safer" alternative to DDT and other chlorinated hydrocarbons. Nevertheless, there has been evidence presented that suggests that organophosphates can be quite persistent under environmental conditions of natural waters (25). For example, at 20 °C and pH 7.4 parathion was reported to have a half–life of 108 days; its most toxic metabolite, paraoxon, had a half–life of 144 days (25).

Ultrasonic irradiation may present an alternative treatment method for the destruction of organics present in water systems (e.g., groundwater or surface waters contaminated by pesticides). In this section, the effect of ultrasonic irradiation on parathion–saturated aqueous solutions is reported.

Experimental

The ultrasonic irradiation of parathion–saturated deionized water was conducted with the experimental setup and under the same conditions that were used for the p–nitrophenol experiments (Chapter 3).

P–nitrophenol concentrations were measured spectrophotometrically as described in Chapter 3. Nitrite, nitrate, sulfate, phosphate, and oxalate ions were determined with a Dionex 2020i ion chromatograph and a Dionex AS4–A column. The eluent consisted of a mixture of 14.7 mM Ethylenediamine, 10 mM NaOH, 10 mM H_3BO_3, and 1 mM Na_2CO_3.

Results and discussion

Sulfate, nitrite, nitrate, p–nitrophenol (p–NP), phosphate, and oxalate were identified as products of parathion sonolysis. Figure 6.5 shows the evolution of these species with sonication time for an initially saturated parathion solution. The solubility of parathion in water is 82 μM (24 μg/ml) at 25 °C (26).

Since the observed $[SO_4^{2-}]$ was $\simeq$ 82 μM after two hours of sonication, we can conclude that all of the initial parathion was decomposed in $\leq$ 2 hours under our experimental conditions. Furthermore, $[SO_4^{2-}]$ increased linearly with sonication time with a zero–order rate of $\simeq$ 0.68 $\mu M \cdot min^{-1}$. Figure 6.5 shows that $[NO_y]$ + [p–NP], where $[NO_y] = [NO_2^-] + [NO_3^-]$, were formed at the same rate. PO_4^{3-} and $C_2O_4^{2-}$ were formed at a lower rate.

No buffers were used and the pH of the solution changed during sonication. The pH of the initial solution was 6.1. After half hour of sonication the pH dropped at 4.1 and remained close to that value thereafter (3.9 at 1 hr, and 3.7 at 2 hr).

At any pH, p–nitrophenol is found to be the major product of the hydrolysis of parathion (25). When hydrolysis is catalyzed by heavy metal ions, deethylation of parathion can also take place and a secondary ester of phosphoric acid appears as an additional product (27). The equations describing these two pathways of hydrolysis are as follows:

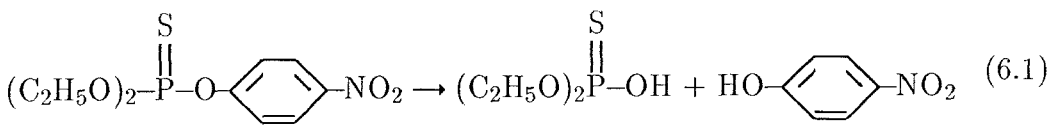

(6.1)

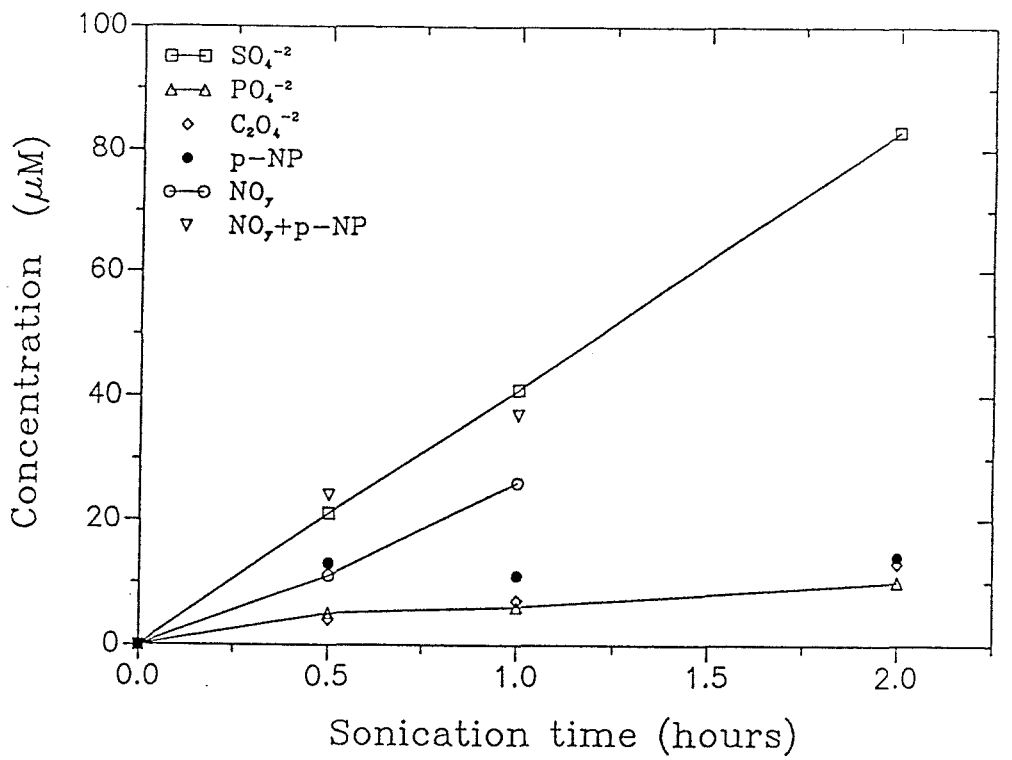

Figure 6.5. Products of parathion sonication at 75 W/cm^2, $T_b \simeq 28$ °C, $pH_{in} \simeq 6.0$, and initial parathion concentration of $\simeq 82$ μM.

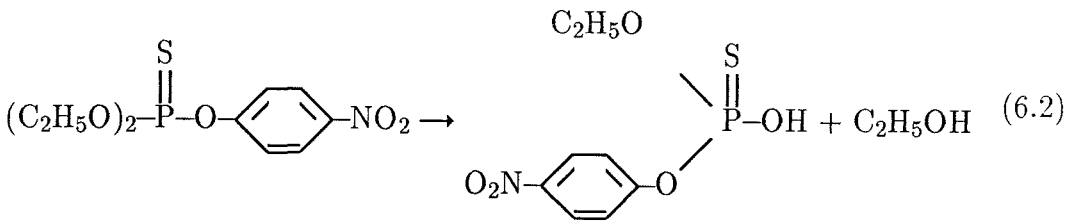

(6.2)

It is believed that at alkaline pH reaction (6.1) proceeds via nucleophilic substitution of the nitrophenolate group by OH^-, while rupture of the O – C bond apparently occurs in the acidic pH region (28).

Our experimental results suggest that when parathion is subjected to ultrasonic irradiation both the P = S and the P – nitrophenolate bonds break and SO_4^{2-} and p–NP are formed. Deethylation of the resulting diethyl–phosphate moiety leading to the formation of PO_4^{3-} and $C_2O_4^{2-}$ seems to follow at a slower rate. P–NP, which is the only toxic compound among these initial products, will decompose further during sonication (see Chapter 3) to NO_y, benzoquinone, 4–nitrocatechol and organic acids (formate, acetate, oxalate), and eventually to NO_y and CO_2. The overall effect of sonication on parathion is shown schematically in Figure 6.6.

Parathion has a low vapor pressure (26) and it is not expected to enter the cavities during sonication. It can be argued that the pathways for parathion sonolysis are the same as those accepted for the sonolysis of pNP, i.e., thermal decomposition in the interfacial region and reaction with ·OH radicals (see Chapter 3). Further experimental work could provide enough data to assess the relative importance of those two pathways.

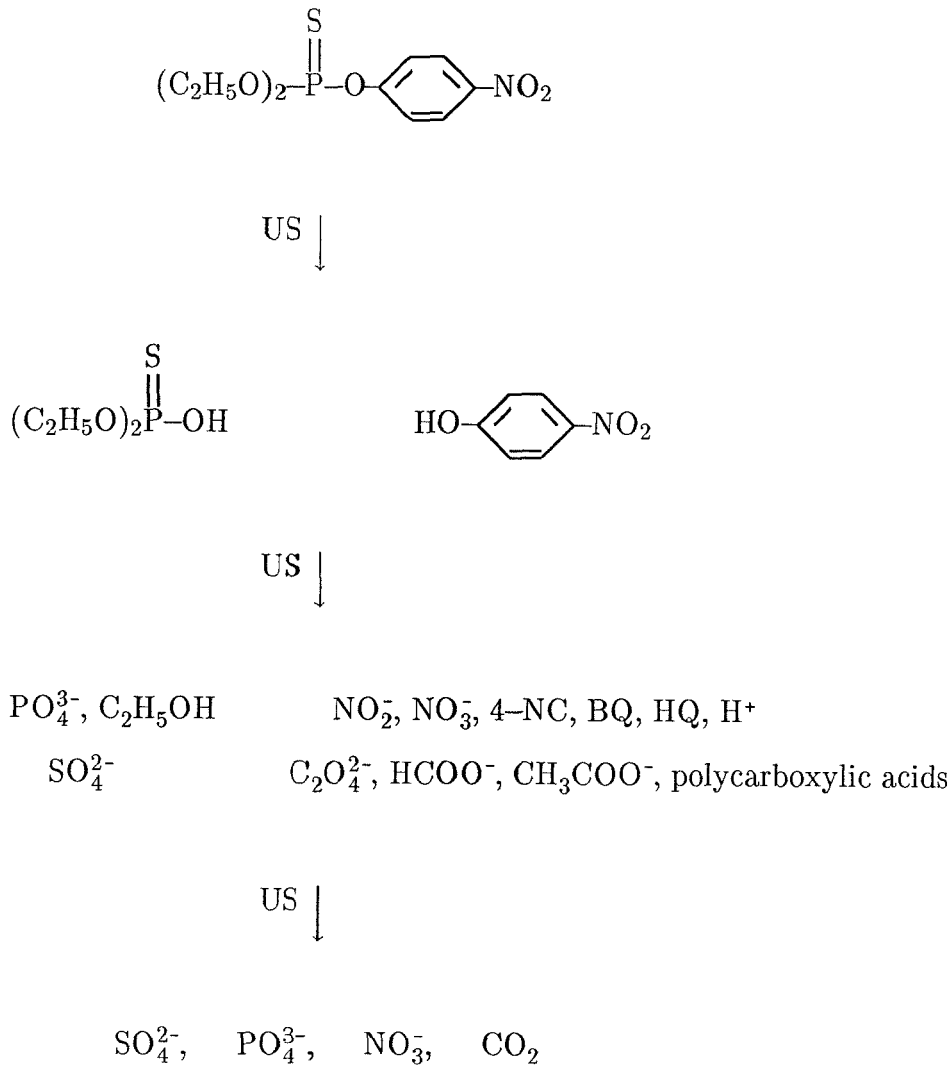

Figure 6.6. Schematic presentation of the effect of ultrasonic irradiation on parathion.

Conclusion

Ultrasonic irradiation of a parathion–saturated aqueous solution at 20 kHz and 75 W/cm^2 resulted in complete destruction of parathion within 2 hours. The observed products included inorganic species (sulfate, nitrate, phosphate) and simpler organics (mainly pNP and organic acids) that are known to degrade further under the action of ultrasound. Clearly, ultrasonic irradiation (US) has an advantage versus catalyzed hydrolysis of organophosphates; US results in harmless products, while many of the hydrolytic products (e.g., substituted phenols) may be toxic or cause taste and odor problems in water systems.

References

1. Schmitt, F. O.; Johnson, C. H.; Olson, A. R. *J. Am. Chem. Soc.* 1929, *51*, 370.
2. Weissler, A.; Cooper, H. W.; Snyder, S. *J. Am. Chem. Soc.* 1950, *72*, 1769.
3. Renaud, P. *J. Chim. Phys.* 1955, 339.
4. Gueguen, H. *Ann. Chim.* 1963, *8*, 667.
5. Hart, E. J.; Henglein, A. *J. Phys. Chem.* 1985, *89*, 4342.
6. Liu, S. C.; Wu, H. *J. Am. Chem. Soc.* 1934, *56*, 1005.
7. Suslick, K. S. In *Ultrasound: Its Chemical, Physical and Biological Effects;* Suslick, K. S., Ed., VCH: New York (1988).
8. Henglein, A. *Ultrasonics* 1987, *25*, 6.
9. Suslick, K. S.; Schubert, P. F.; Goodale, J. W. *IEEE Ultrason. Symp. Proc.* 1981, 612.
10. Henglein, A.; Gutierez, M. *J. Phys. Chem.* 1990, *94*, 5169.
11. Gueguen, H.; Renaud, P.; Segard, N. *Compt. rend.* 1957, *244*, 200.
12. Henz, R. R.; Clarence, G. J. *J. Chem. Phys.* 1969, *51*, 1236.
13. Kahn, M; Kleinberg, J. In *Radiochemistry of Iodine*; NAS–NS–3062, ERDA, Oak Ridge, Tennessee, 1977.
14. Schwarz, H. A.; Bielski, B. H. *J. Phys. Chem.* 1986, *90*, 1445.
15. Stanbury, D. M. *Adv. Inorg. Chem.* 1989, *33*, 69.
16. Buxton, G. V.; Greestock, C. L.; Helman, W. P.; Ross, A. B. *J. Phys. Chem. Ref. Data* 1988, *17*, 513.
17. Neta, P.; Huie, R. E.; Ross, A. B. *J. Phys. Chem. Ref. Data* 1988, *17*, 1027.
18 Bielski, B. H. J.; Cabelli, D. E.; Arudi, R. L.; Ross, A. *J. Phys. Chem. Ref. Data* 1985, *14*, 1041.

19. Fischer, Ch.–H.; Hart, E. J.; Henglein, A. *J. Phys. Chem.* 1986, *90*, 1954.

20. Fischer, Ch.–H.; Hart, E. J.; Henglein, A. *J. Phys. Chem.* 1986, *90*, 222.

21. Hart, E. J.; Henglein, A. *J. Phys. Chem.* 1986, *90*, 5992.

22. Hart, E. J.; Fischer, C. H.; Henglein, A. *J. Phys. Chem.* 1986, *90*, 5989.

23. Durrant, P. J.; Durrant, B. In *Introduction to Advanced Inorganic Chemistry*, 2nd Ed., William Clowes & Sons Ltd, London, 1970.

24. Smith, R. M.; Martell, A. E. *Critical Stability Constants*; Plenum: New York, 1976.

25. Faust, S. D.; Gomaa, H. M. *Environ. Lett.* 1972, *3*, 171.

26. Williams, E. F. *Indust. & Eng. Chem.* 1951, *43*, 950.

27. Hilgetag, G.; Teichmann, H. *Angew. Chem.* 1965, *77*, 1001.

28. Blumental, E.; Helbert, J. B. *Trans. Faraday Soc.* 1945, *41*, 611.

CHAPTER 7

EFFECT OF PHYSICAL AND CHEMICAL PARAMETERS ON SONOLYSIS OF CHEMICAL COMPOUNDS

Introduction

The effects of different parameters on the sonolysis yields of the chemicals studied are presented in this chapter. The observed effects are discussed in view of the sonolysis mechanisms proposed in the previous chapters. The parameters studied included: ionic strength and specific ions, input power, bulk solution temperature, dissolved gases, particles, sonication setup (reaction vessel and sonication unit type), and operation mode (flow through vs batch operation). Sonolysis of S(–II) in wastewater is also compared to that observed in clean water.

Results and discussion

Ionic strength and specific ions

No significant effect of the ionic strength on p–NP sonolysis yields was observed; sonolysis rates were the same in the presence or absence of nitrate or sulfate ions. On the other hand, p–NP sonolysis rates decreased in the presence of nitrite ions (Chapter 3).

Figure 7.1 presents the effect of NaCl and $CaCl_2$ on the sonolysis of S(–II) at alkaline pH. It can be seen that S(–II) decomposition rate increases with increasing electrolyte concentration. A plot of the logarithm of the observed initial zero–order rate, k_o, as a function of the square root of the ionic strength of the solution, I, is shown in Figure 7.2. This plot would seem to suggest that there is an effect of the cation too, i.e., that S(–II)sonolysis is enhanced by the presence of Ca^{2+}. Nevertheless, when k_o is plotted versus chloride concentration (Figure 7.3) the experimental results obtained with both NaCl and $CaCl_2$ fall on the same line,

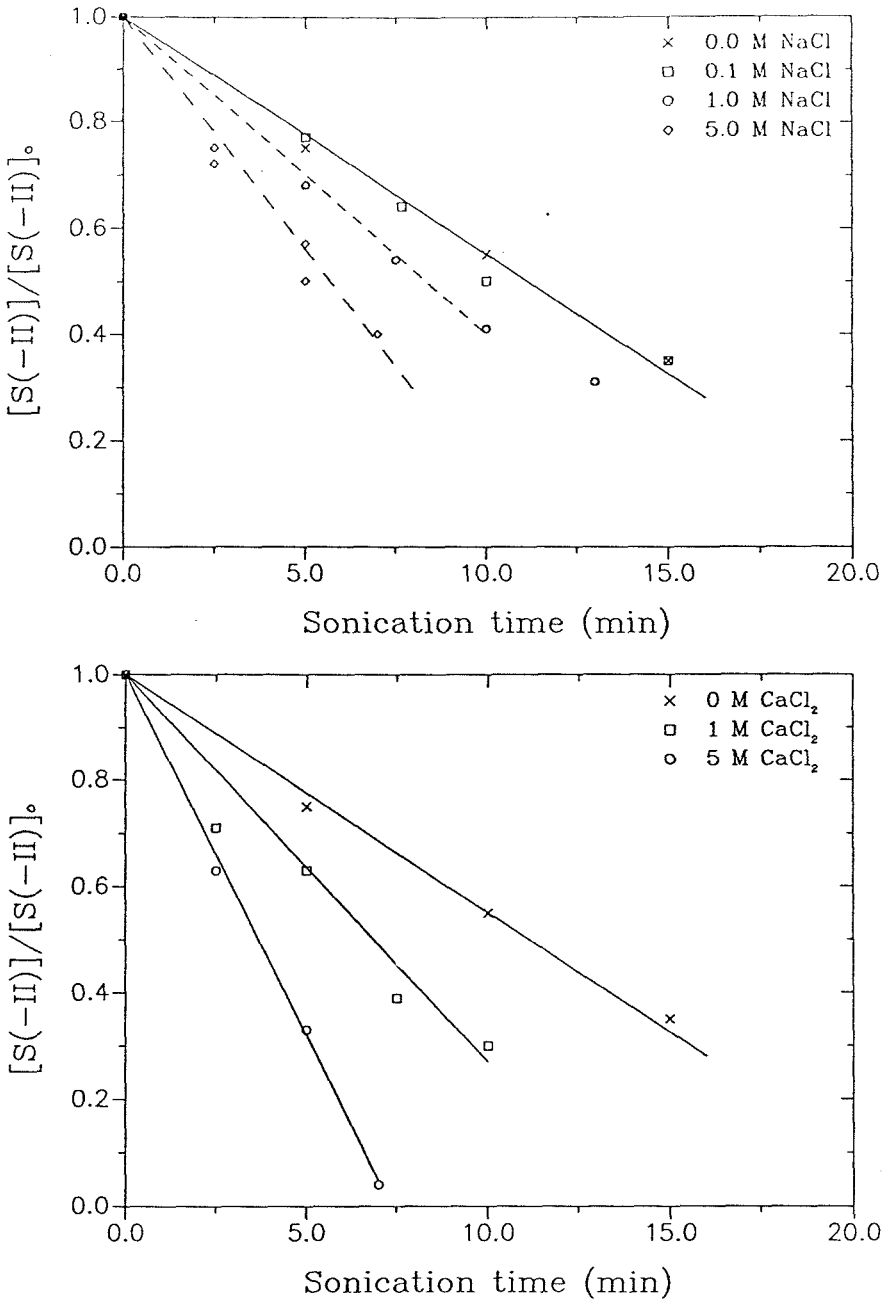

Figure 7.1 Effect of a) NaCl and b) $CaCl_2$ on the sonolysis of S(–II); $[S(-II)]_o \simeq 200\ \mu M$, pH 10, SS cell.

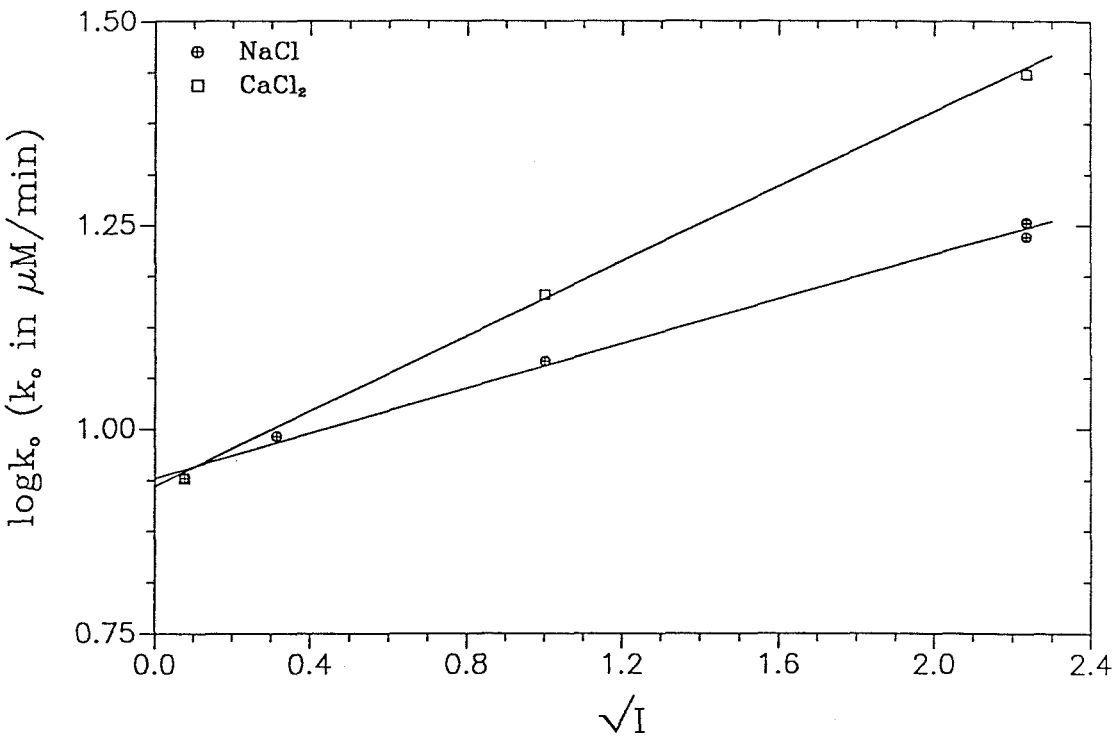

Figure 7.2 Plot of $\log k_o$ vs $\sqrt{I}$, using data of Figure 7.1.

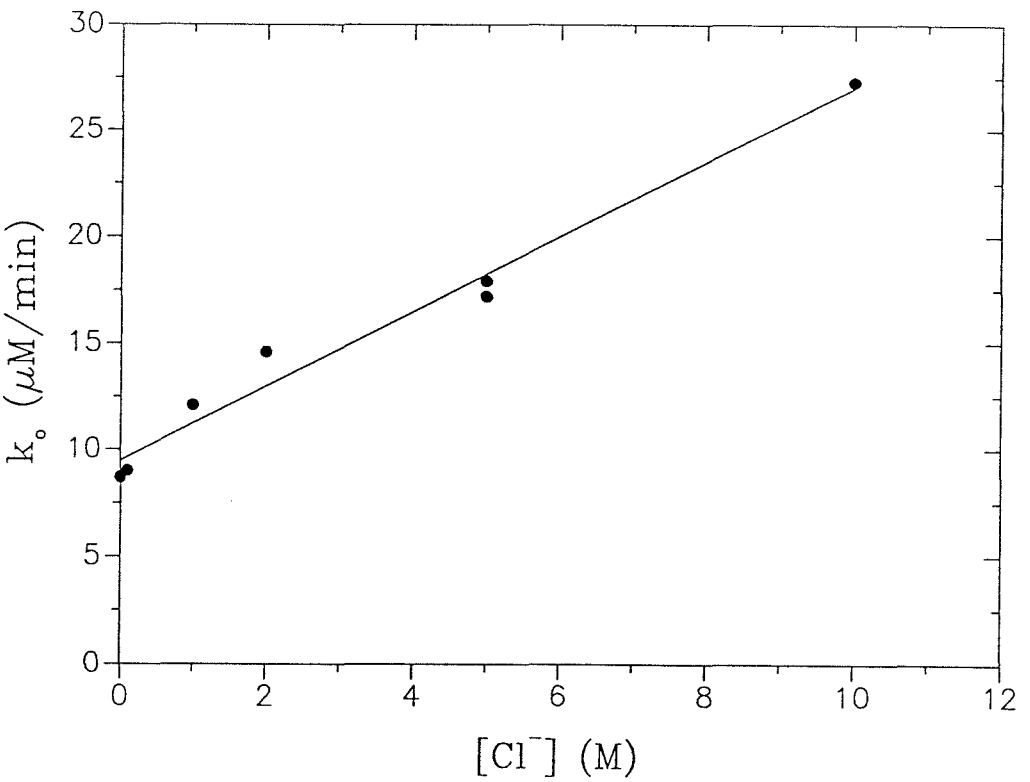

Figure 7.3 Plot of k_o vs [Cl^-], using data of Figure 7.1.

suggesting that the observed increase in k_o is due to the presence of the Cl^- ions and not to a general ionic strength effect.

Further evidence for a specific effect of halogen ions on the sonolysis of S(–II) were obtained when S(–II) was sonicated in the presence of I^-. Figure 7.4 shows the enhancement of S(–II) decomposition at pH 10 in the presence of 1M KI. Only trace amounts of iodine (I_2) were observed until practically all S(–II) was oxidized. This suggests that the intermediate species of the sonolysis of I^- (Chapter 6) are used for the oxidation of S(–II) instead of forming I_2. The E^o for the $I_2^{\cdot-}/2I^-$ couple is reported as 1.03 V, i.e., very close to the 1.08 V suggested for the HS/HS^- couple (1). It is therefore plausible that $I_2^{\cdot-}$, which is expected to be the main intermediate of the I^- oxidation to I_2 (see Chapter 6), is reduced back to I^- while oxidizing HS^- to $HS^{\cdot}$. I^- is thus acting as a catalyst that enhances the rate of S(–II) sonolysis.

Comparing Figure 7.1 and Figure 7.4 it becomes clear that I^- has a more significant 'catalytic' effect on S(–II) sonolysis than Cl^-. Since $Cl_2^{\cdot-}$ is a much stronger oxidant than $I_2^{\cdot-}$ [E^o for the $Cl_2^{\cdot-}/2Cl^-$ couple is 2.09 V (1)], the experimental results suggest that larger amounts of oxidized iodide species are formed. It seems reasonable to assume that this is due to the fact that iodide is a softer and less polar species than chloride and therefore goes preferably in the interfacial region of the bubble. As discussed in Chapter 3, cavitation bubbles are essentially hydrophobic, thus hydrophobic compounds can accumulate in the hot surroundings of the interfacial region where they subsequently undergo high temperature reactions.

Further evidence for the suggested role of halide ions on the sonolysis of chemical compounds was obtained when p–NP was sonicated in the presence of 1M KI. Figure 7.5 shows that I^- acts as an inhibitor in the case of p–NP. That is in

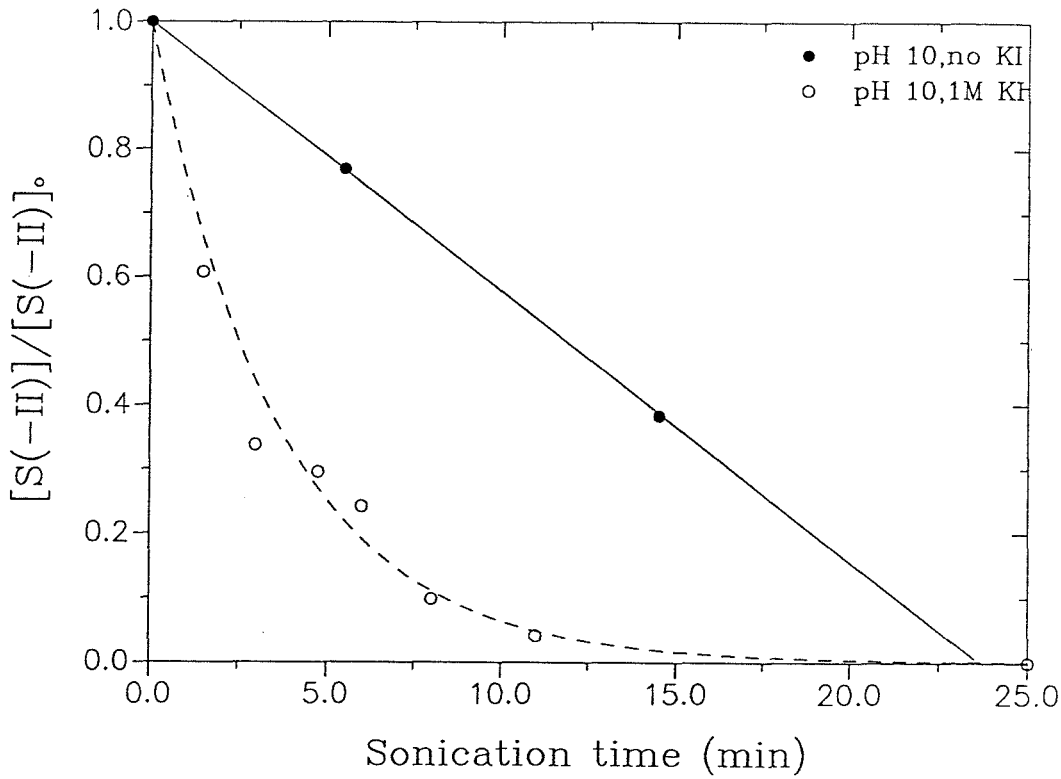

Figure 7.4 Effect of KI on S(–II) sonolysis at pH 10.

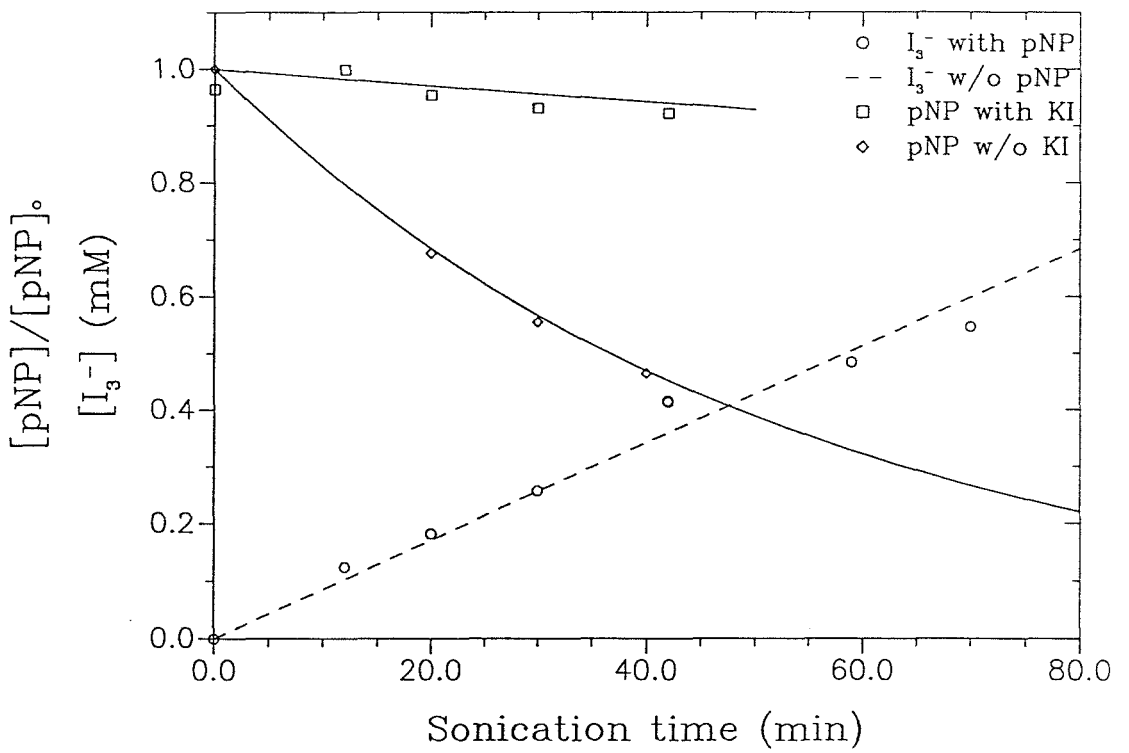

Figure 7.5 Effect of KI on p-NP sonolysis.

line with the proposed mechanism for p–NP sonolysis. As discussed in Chapter 3, p–NP is also expected to undergo high temperature reactions in the interfacial region. The presence of the smaller I^- ions in the same region inhibits the thermal decomposition of p–NP. Furthermore, $^{\cdot}OH$ radicals are scavenged by I^- at or near the interfacial region thus preventing the secondary mechanism of p–NP sonolysis (i.e., reaction with $^{\cdot}OH$).

Phosphate and borate ions had no effect on the sonolysis of S(–II) (see Chapter 4). On the other hand, carbonate and bicarbonate ions were shown to have an inhibitory effect on the sonolysis of $S_2O_3^{2-}$ (Figure 7.6). These results can be explained by the fact that the first–order rate constants for the reaction of carbonate/bicarbonate with $^{\cdot}OH$ are at least 2 orders of magnitude higher than the corresponding first–order constants for phosphate or borate (see Chapter 4).

Input power and temperature

The effect of input power of the sonifier (P) and bulk temperature of the solution (T_b) on S(–II) sonolysis yields in alkaline pH are presented in Chapter 4 (Figures 4.11 and 4.12). S(–II) sonolysis in the alkaline pH region is attributed to free–radical oxidation (see Chapters 4, 5), and the negligible effect of T_b can be easily explained by the low activation energies of free–radical reactions. The zero–order rate of S(–II) oxidation increased linearly with P, for P up to $\simeq$ 100 W (upper limit of the CD200 sonication unit). It is noted that care was taken to separate the effects of T_b and P: the temperature of the cooling system was varied so as to keep T_b constant. It is also noted that P values were calculated using calorimetry (Chapter 4). This method has been shown to give similar results to those obtained by measurement of the radiation pressure (2).

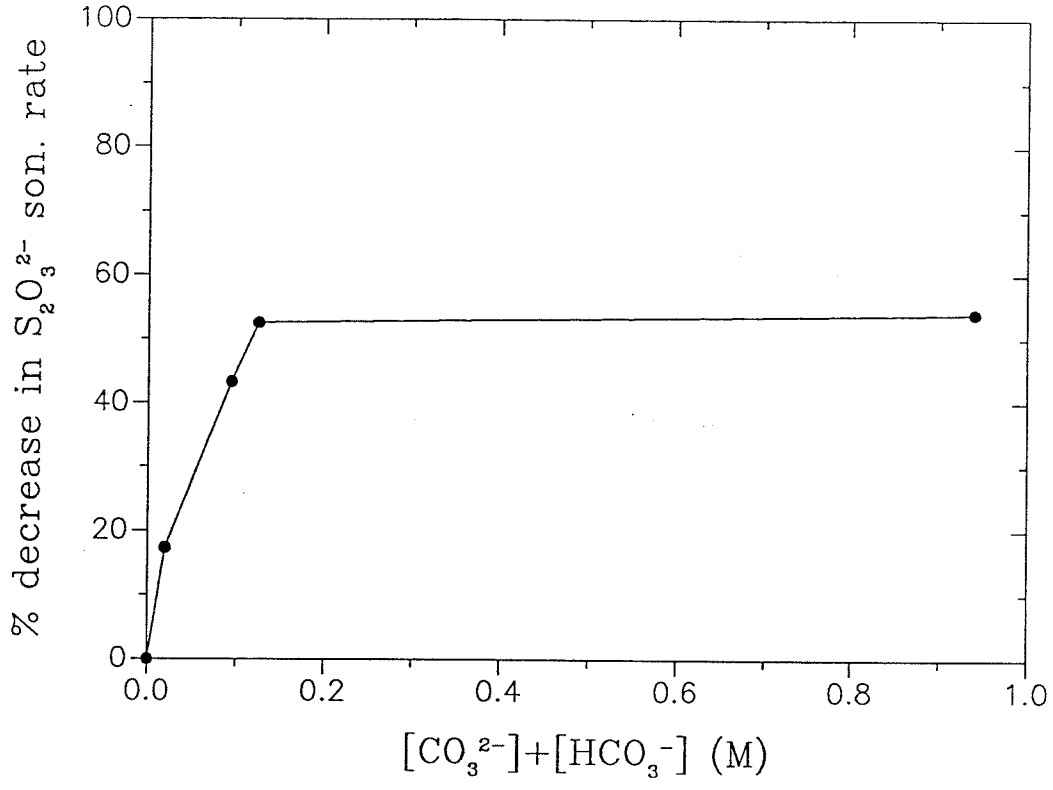

Figure 7.6 Effect of CO_3^{2-}/HCO_3^- on the sonolysis of $S_2O_3^{2-}$.

Dissolved gases

The two important properties that determine the effect of a particular gas on sonochemical reactions are its ratio of specific heats, γ, and its chemical reactivity. The higher γ values of monoatomic gases result in more intense cavitation (i.e., higher T, P upon collapse). On the other hand, a diatomic gas, such as O_2, that can participate in high temperature reactions inside the hot cavity enhances oxidative destruction of solutes by scavenging radical species that would otherwise recombine before reaching the solution phase and/or by providing additional excited species as a result of its thermal decomposition. The investigation of the ultrasonic oxidation of S(–II) has shown that dissolved molecular oxygen in particular can also play an important role by propagating a free–radical chain reaction initiated by $^{\cdot}OH$. The production of I_2 upon sonication of a KI solution in the presence of various gases is presented and discussed in Chapter 6.

Vessel type

In addition to the stainless steel cell (Chapters 3, 4, and 6), several glass vessels (total volume $\simeq 40 - 200$ ml) were used for some experiments so as to allow for visual observation of the sonicated solution. All vessels were water–jacketed and temperature of the sonicated solution was controlled using a water recirculation system. Calorimetry showed that the power delivered to the solution from the commercial CD200 sonicator with the 1/2–in. immersion–horn increased with increasing horn immersion, but was practically independent of the volume of the vessel. For example, for immersion depth of 1 cm and power dial set to 9 the input power ranged only from $\simeq$ 74 W to $\simeq$ 78.5 W for a small glass cell with 30 ml of

solution to a larger cell with 200 ml of solution. For the latter reaction vessel, the input power increased to ≃ 89 and ≃ 98.5 W for immersion depth 2.4 and 3.9 cm respectively.

Sonoluminesce experiments showed that cavitation intensity (as indicated by the light emitted from a luminol solution sonicated in the dark) is not uniform over the whole volume of the solution. Depending on the reaction vessel, solution volume, and horn immersion depth one or more regions of intense sonoluminescence were observed with the naked eye. The main region was always near the tip of the horn and extended down to the bottom of the reaction vessel when the distance between the tip and the bottom was less than ≃ 1.5 cm. Sonoluminesce patterns were similar with those observed by Reynolds *et al.* (3) with the use of a high–gain image intensifier system (3, Figure 7.7). Unfortunately, the appropriate experimental set–up for the recording of these patterns was not available in our laboratory (i.e., photomultiplier or image intensifier system).

The cavitation–induced damage of simple commercially available aluminum foil was used as a qualitative probe of the ultrasonic field inside the stainless steel cell. The inside of the stainless steel cell was covered with aluminum foil and 25 ml of deionized water were sonicated for a few seconds. The aluminum foil covering the bottom part of the cell was shredded to pieces practically instantaneously while the aluminum foil covering the wall near the liquid/headspace interface sustained only minor damage. These observations suggested that the more intense cavitation region is between the tip of the sonicator and the bottom of the reactor cell.

The observed initial S(–II) sonolysis rate at pH 10 and in a small glass cell (total volume ≃ 40 ml) was similar to that obtained in the stainless steel (SS) cell under similar conditions (i.e., solution volume, bulk temperature, solution

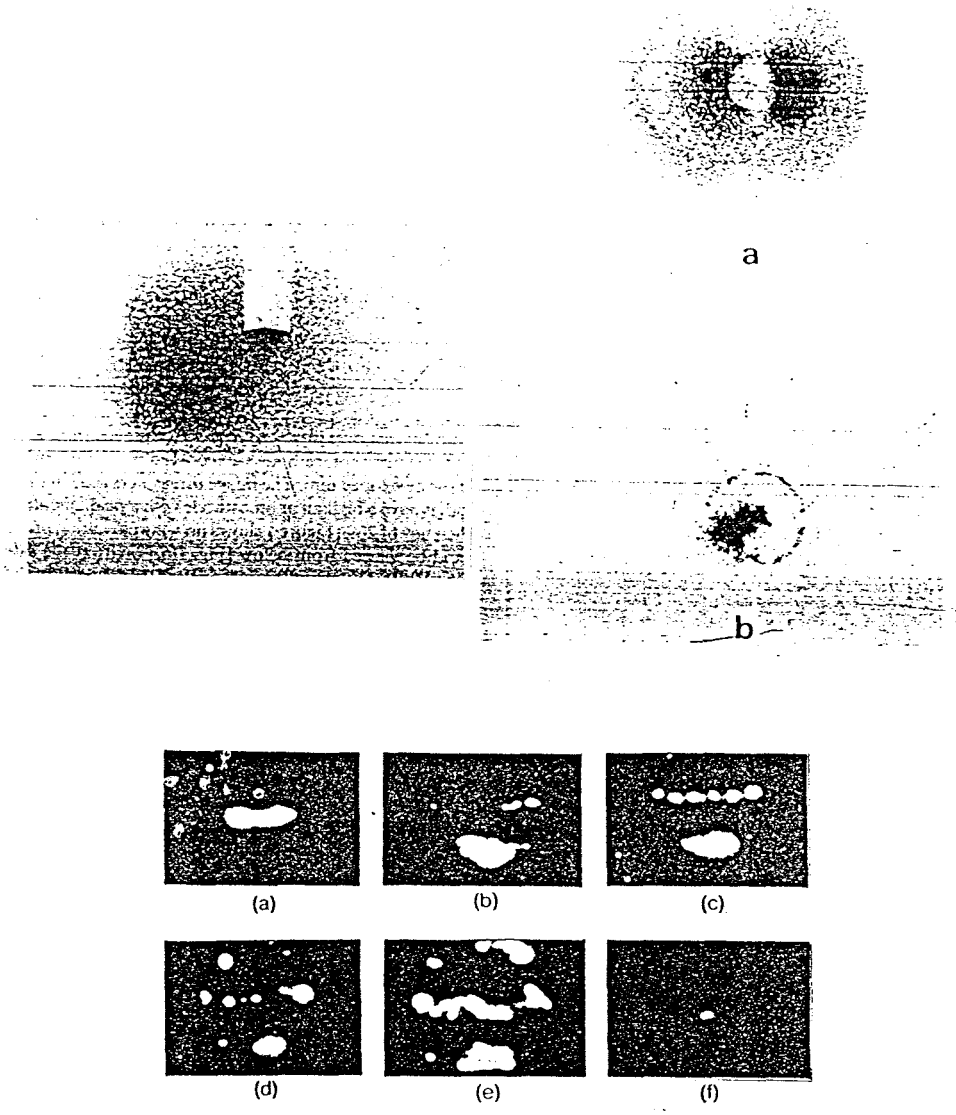

Figure 7.7 Sonoluminescence patterns observed by (top) Reynolds *et al.* (1982), and (bottom) Crum & Reynolds (1985) with a direct immersion horn (reproduced from refs. 3 and 4, respectively).

composition). Nevertheless, the decrease of S(–II) in the glass cell did not remain linear with sonication time (see Figure 7.8). The available headspace was considerably lower in the glass cell as compared to the SS cell and one possible explanation is oxygen depletion that would result in a slower oxidation rate as discussed in Chapter 4.

Particles

The effect of two different sizes of silica particles was studied in the 40 ml glass vessel. Large sand particles (500 μm average size OTTAWA 30) were used to determine whether the presence of these particles would have an adverse effect on the sonication rate because of sound attenuation. No such effect was observed even at very high solids concentration (Figure 7.9). Fine particles (7 nm average size AEROSIL 380, Degussa) were used in an attempt to enhance cavitation by providing additional nuclei for bubble formation and thus result in an increased S(–II) oxidation rate. Figure 7.9 shows that these fine particles did not have an effect on the sonochemical rate of S(–II) oxidation in air–saturated water solutions at a concentration of 100 $mg \cdot l^{-1}$.

The insignificant effect of sand particles at the sizes and concentration studied can be explained by the fact that air–saturated solutions already contain a large number of 'weak spots' that act as nuclei for the formation of cavities. This argument is strengthened by the absence of any observable effect of air bubbling on the sonolysis of iodide (Chapter 6).

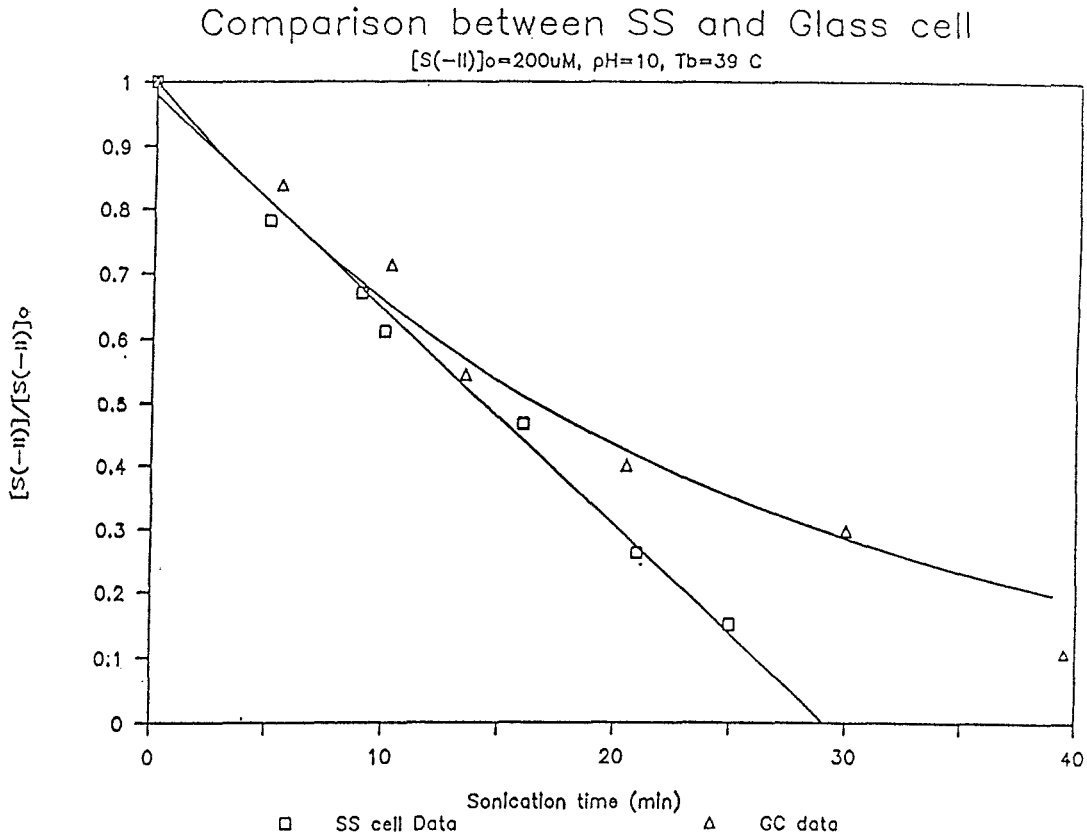

Figure 7.8 Comparison between a glass sonication reactor (30 ml) and the stainless steel (SS) cell (25 ml); $[S(-II)]_o = 200\ \mu M$, pH = 10 °C, $T_b = 39$ °C.

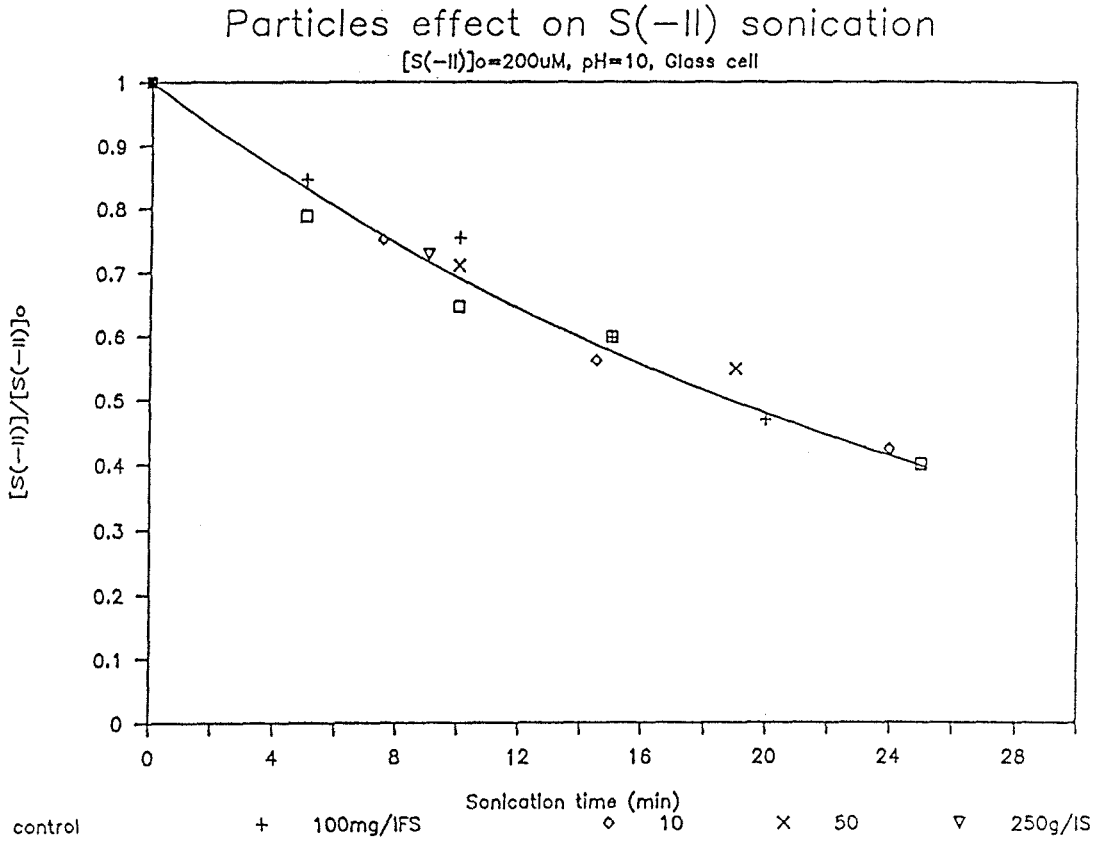

Figure 7.9 Effect of silica particles on S(–II) sonication. IS: Sand particles (0.5 mm), IFS: fine amorphous silica particles (7nm).

Continuous flow operation

A continuous flow experimental set–up that involves recycle of the solution to be sonicated (i.e., multiple passes through the sonicator and a holding reservoir where sampling is performed) was designed. S(–II) and KI solutions were sonicated in that set–up in order to compare the efficiency of the ultrasonic apparatus during flow–through operation to that of the batch mode operation. A schematic representation of the system is shown in Figure 7.10. Both the sonication vessel and the reservoir were closed to the atmosphere. The contents of the sonication cell are vigorously mixed due to the action of the ultrasound, and the reservoir is continuously mixed with a mechanical mixer. Therefore, both systems are CSTR's. The mathematical representation of the system is as follows:

Reservoir mass balance: $$V_r \cdot dC_r/dt = Q \cdot C_s - Q \cdot C_r - k_{1r} C_r V_r \qquad (7.1)$$

Sonication cell mass balance: $$V_s \cdot dC_s/dt = Q \cdot C_r - Q \cdot C_s - k_{os} V_s \qquad (7.2)$$

B.C. $$C_r = C_s = C_o \quad \text{at } t=0 \qquad (7.3)$$

where:

Q	= flow rate
V_r, V_s	= reservoir and sonication cell volume respectively
C_r, C_s	= reservoir and sonication cell S(–II) concentration respectively
k_{1r}	= first–order rate constant for S(–II) removal while in the reservoir
k_{os}	= zero–order rate constant for S(–II) removal due to sonication

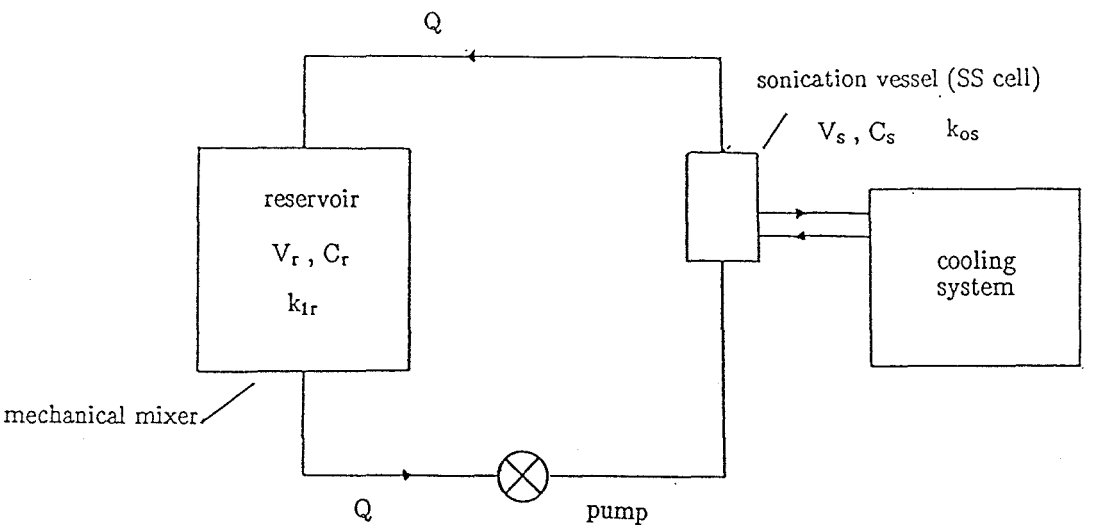

Continuous Flow Sonication

Figure 7.10 Schematic representation of the continuous system used.

The solution of the system of the two ODE's (7.1) and (7.2) with the initial condition (7.3) is as follows:

$$C_r = (C_o/b)\cdot A+(C_o/b)(D_r+D_s)\cdot B-[(D_r k_{os})/(D_s k_{1s} b)]\cdot C \qquad (7.4)$$

$$C_s = (C_o/b)\cdot A+[C_o c-k_{o2})/b]\cdot B-[(D_r k_{os}+k_{1r}k_{os})/(D_s k_{1s} b)]\cdot C \qquad (7.5)$$

where

$A = \lambda_1 e^{\lambda_1 t}-\lambda_2 e^{\lambda_2 t}$

$B = e^{\lambda_1 t}-e^{\lambda_2 t}$

$C = \lambda_2 e^{\lambda_1 t}-\lambda_1 e^{\lambda_2 t}+b$

$b = [(D_r+D_s+k_{1r})^2-4D_s k_{1r}]^{0.5}$

$c = D_r+D_s+k_{1r}$

$\lambda_1 = -c/2+b/2$

$\lambda_2 = -c/2-b/2$

$D_r = Q/V_r$ = 1/retention time in reservoir

$D_s = Q/V_s$ = 1/retention time in sonication cell

The zero–order rate constant for the decrease of [S(–II)] due to sonication, k_{os}, can be calculated by fitting the experimental C_r values ([S(–II)] profile with time in the reservoir) to equation (7.4). The other parameters are all known. The rate constant for the removal of S(–II) in the reservoir, k_{1r}, is found from control experiments where a S(–II) solution (from the same stock that is used for the sonication experiment) is stirred in an identical reservoir under the same conditions (headspace, lighting etc.).

When $k_{1r} \simeq 0$, equation (7.4) is simplified to :

$$C_r = C_o - [(k_{os}D_r)/(D_r+D_s)]\cdot t - [(k_{os}D_r)/(D_r+D_s)^2](e^{-(D_r+D_s)t}-1)t \qquad (7.6)$$

and for $t >> 1/(D_r+D_s)$ the concentration in the reservoir is given by:

$$C_r = [C_o+(k_{os}D_r)/(D_r+D_s)^2] - [(k_{os}D_r)/(D_r+D_s)]\cdot t \qquad (7.7)$$

In that case, k_{os} can be easily calculated from the slope or the intercept of C_r vs t.

Experimental k_{1r} values were in agreement with the first–order rate constants expected for S(–II) uncatalyzed oxidation by molecular oxygen (see Appendix A). Although these k_{1s} values are low ($k_{1r} \leq 5\cdot10^{-4}$ min^{-1}), the use of (7.7) instead of (7.4) would involve an error of ~ 8% for the particular experimental setup (V_s = 40 ml, V_r = 200–1000 ml, Co = $[S(-II)]_o$ = 200 μM).

Figure 7.11 shows the fraction of S(–II) remaining in the reservoir vs time for typical experiments where the sonication unit is the same as the one used for most of the experiments, i.e., CD200 sonifier, output power = 80 W (intensity at the tip 75 $W\cdot cm^{-2}$, 1/2–in. horn, SS cell. The sonicated volume was V_s = 40 ml (determined by the flow–through capacity of the cell). The flow rate was 165 ml/min and $[S(-II)]_o$ was 200 μM for all three experiments but V_r was 200, 280 and 1000 ml respectively. The solid lines in Figure 7.11 are the best fit of the experimental data with equation (7.4). All three experiments were in agreement and gave k_{os} = 5 $\mu M\cdot min^{-1}$. Control experiments gave a first–order rate constant for S(–II) removal in the reservoir $k_{1r} = 5\cdot10^{-4}$ min^{-1}. As expected, k_{os} values do not change when the flow changes (not shown). The flow rate only affects the rate

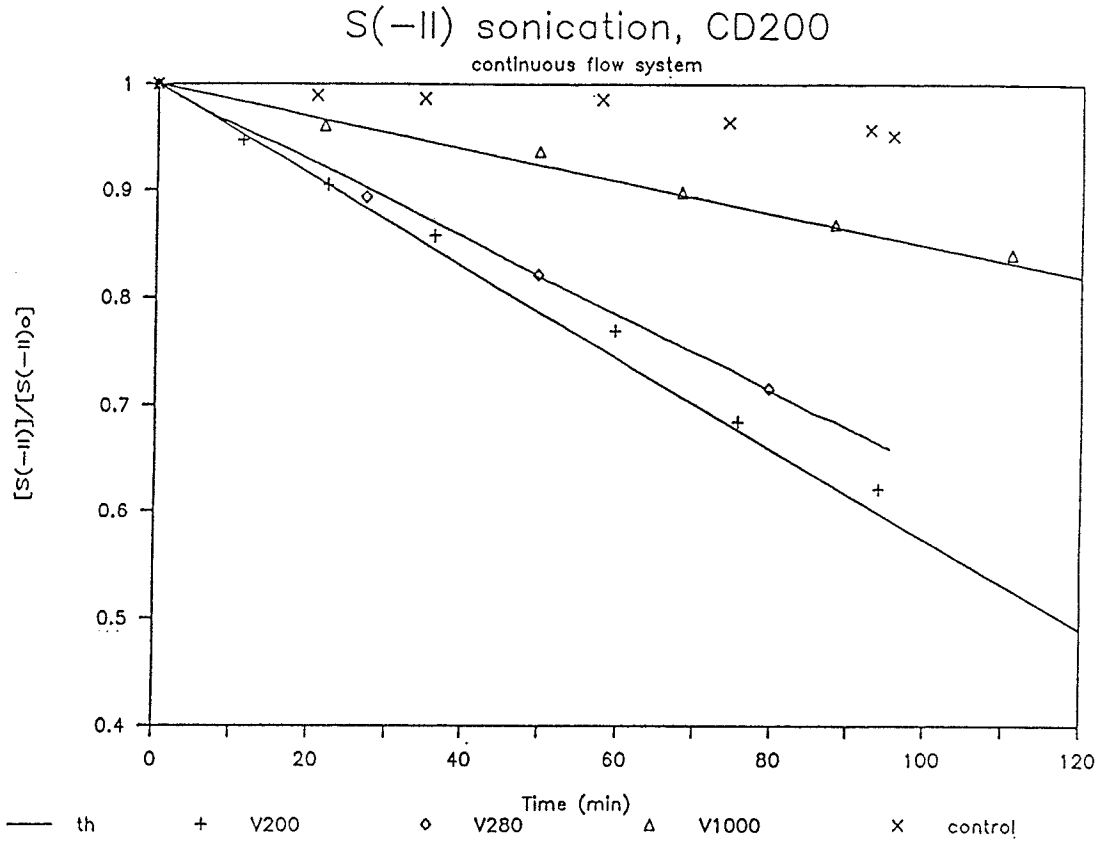

Figure 7.11 Fraction of S(–II) remaining in the holding reservoir; Q=165 ml/min, 1/2–in. horn, 80 W, $[S(-II)]_o$ = 200 μ,M, pH=10, SS cell (V_S=40 ml), V_r = 200, 280, and 1000 ml.

of sulfide decrease in the reservoir, not the rate at which it is destroyed at the sonication unit. This rate of S(–II) oxidation in the sonication cell is 37% lower than the corresponding rate for batch sonication of a 25 ml solution. Continuous flow experiments where 1 M solutions of KI were sonicated with the same system at $Q = 860$ ml/min and $V_r = 280$ ml gave $k_{os} = 8$ μM/min, i.e., a reduction of 38% as compared to the batch experiments (again, performed with a 25 ml solution). This is in perfect agreement with the S(–II) results. It can be therefore concluded that operation of this type of sonifiers in the flow–through mode does not greatly change the efficiency of the unit (in terms of the total amount of the chemical of interest destroyed per unit of total energy input). It must be noted that during batch operation filling the SS cell near maximum capacity with 40 ml of solution results in decrease of the observed reaction rate (about 17% decrease as compared to sonication of 25 ml; see Figure 4.10). Therefore, the $\simeq$ 37% decrease mentioned above corresponds to an actual $\simeq$ 24% [= (0.63/0.83) × 100] decrease in the efficiency of the unit under flow–through operation.

Sonication unit

A larger sonifier (VC1500) was tested with a power supply of up to 1500 W, and with a horn of 3/4–in. diameter. A special stainless steel flow–through chamber (FTC) was also acquired for continuous flow operation with VC1500. Initial experiments showed that continuous sonication of S(–II) using the new chamber and the larger unit was only ~ 60% faster than the smaller unit with the 1/2–in. horn and the stainless steel cell. Figure 7.12 shows this difference; for $[S(-II)]_o = 200$ μM and $V_r = 280$ ml the k_{os} in the FTC/VC1500 system is 8 $\mu M \cdot min^{-1}$ as compared to 5 $\mu M \cdot min^{-1}$ in the SS/CD200. It must be noted that V_s

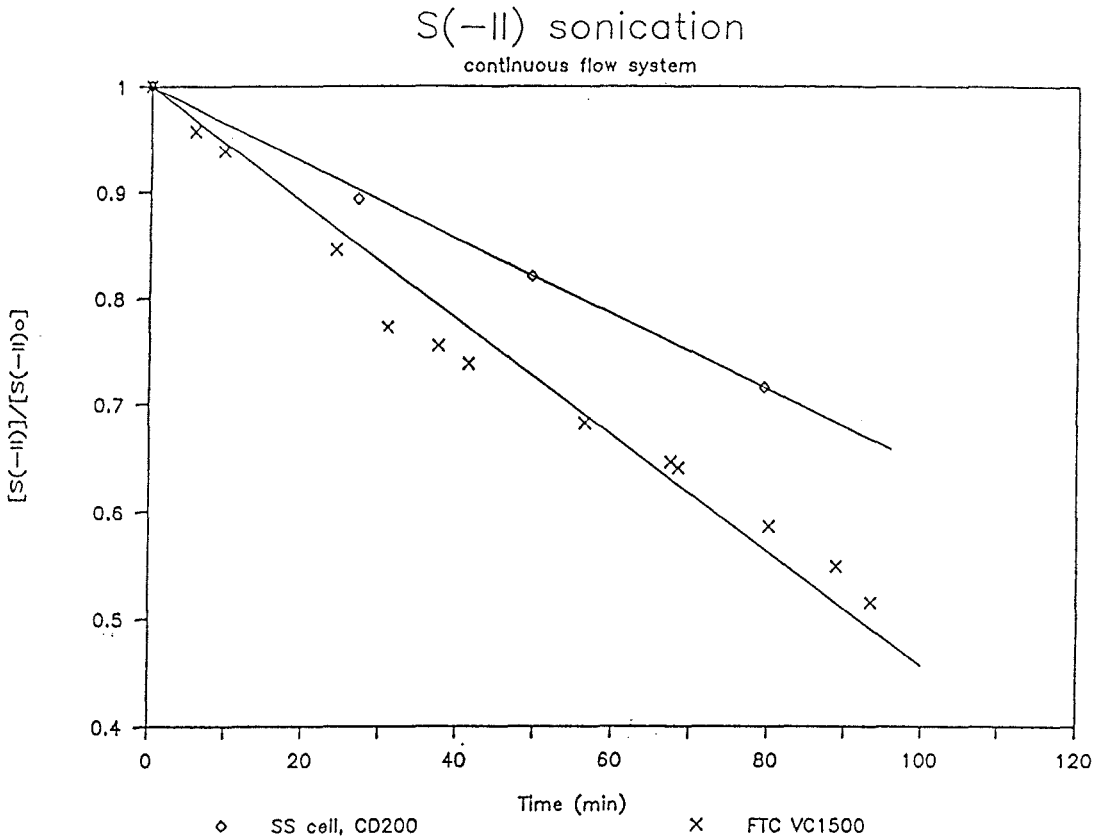

Figure 7.12 Continuous flow sonication; comparison of the effect of two different sonication units on the fraction of S(–II) remaining in the reservoir; $V_r = 280$ ml, $[S(-II)]_o = 200$ μM, pH 10.

for FTC was 36 ml which is close to the 40 ml capacity of the stainless steel cell.

Experiments with the VC1500 but the 1/2–in. horn and the stainless steel cell gave identical results as the smaller unit (CD200) for both S(–II) and KI. Figure 7.13 shows the increase in the absorbance at 350 nm (directly proportional to the concentration of iodine) for the two power supply units CD200 and VC1500 both with the SS cell. The actual input power, as calculated from temperature data, was not much different and it seems that there is a limit to the energy that can be taken by a liquid from the 'direct immersion horn' type of sonicators. In that case the sonochemical efficiency is not affected by the use of a larger power supply since the 1/2–in. horn is not drawing more power even though it is available to it. Figure 7.14 shows again the results of the batch sonication of 1 M KI solution in the SS cell with the CD200 unit and the VC1500 unit now operating under three different nominal power outputs. It can be seen that increasing the nominal power output (i.e., turning the power dial of the unit at 60%, 40% and 20% of the maximum available power of 1500 W) does not increase the rate of KI formation even though the temperature data (see Figure 7.15) show that the energy transferred to the solution increases with increasing power. This latter result can be due to increased mechanical stress on the titanium horn/tip resulting in overheating of the horn and subsequent heating of the sonicated liquid.

In an attempt to achieve full benefit from the larger power unit, a 'cup–horn' type sonicator was used. Figure 7.16 shows a schematic diagram of that ultrasonic apparatus; it is connected to the power supply in a similar way as the direct immersion horn used previously. The main difference is that there is a much larger radiating surface (of 7.5 cm diameter) instead of the 1/2–in. or 3/4–in. titanium tip and there need be no coupling of a transducer with a tip (which was suspected to be

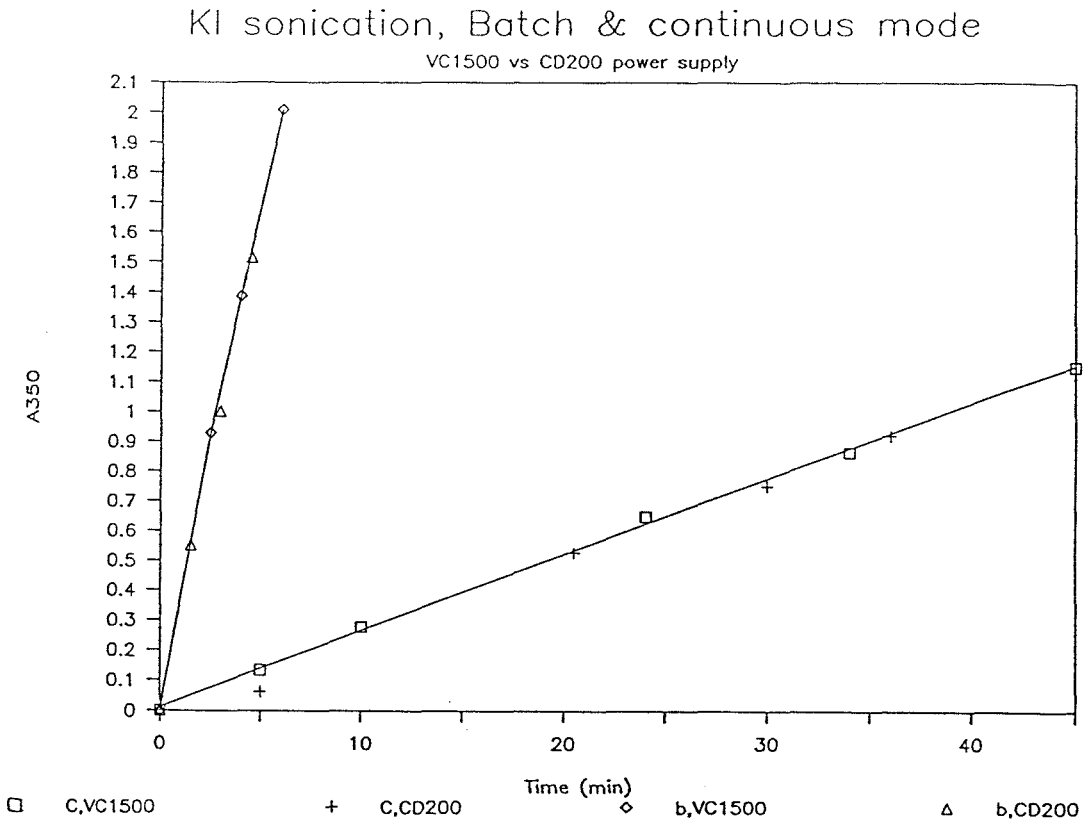

Figure 7.13 Sonication of 1 M KI solution. Continuous flow (C) and batch (b) operation using two different power supplies with the same SS cell and 1/2–in. horn.

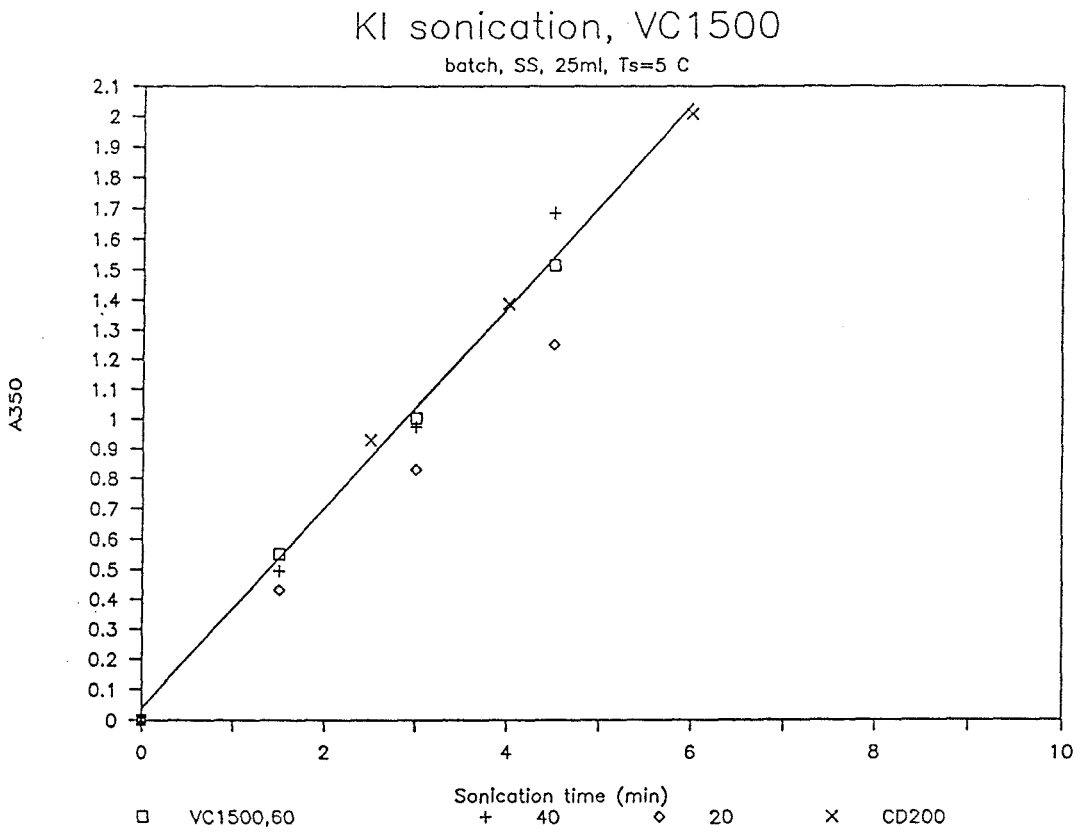

Figure 7.14 Sonication of 1 M KI using SS/VC1500 at different nominal output powers.

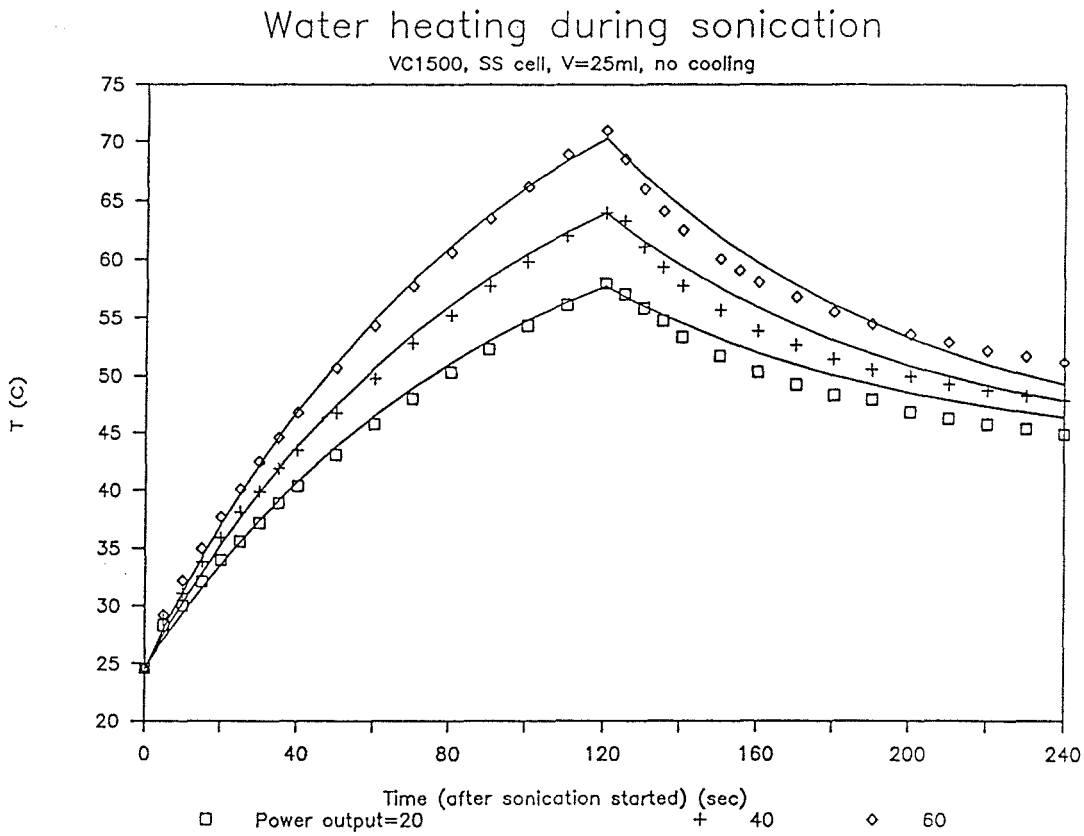

Figure 7.15 Rise in temperature of 25 ml water with sonication time; SS/VC1500, different nominal power (e.g., power output = 20 means that maximum nominal power is 20% of 1500 W). Sonication stopped at t=120 sec.

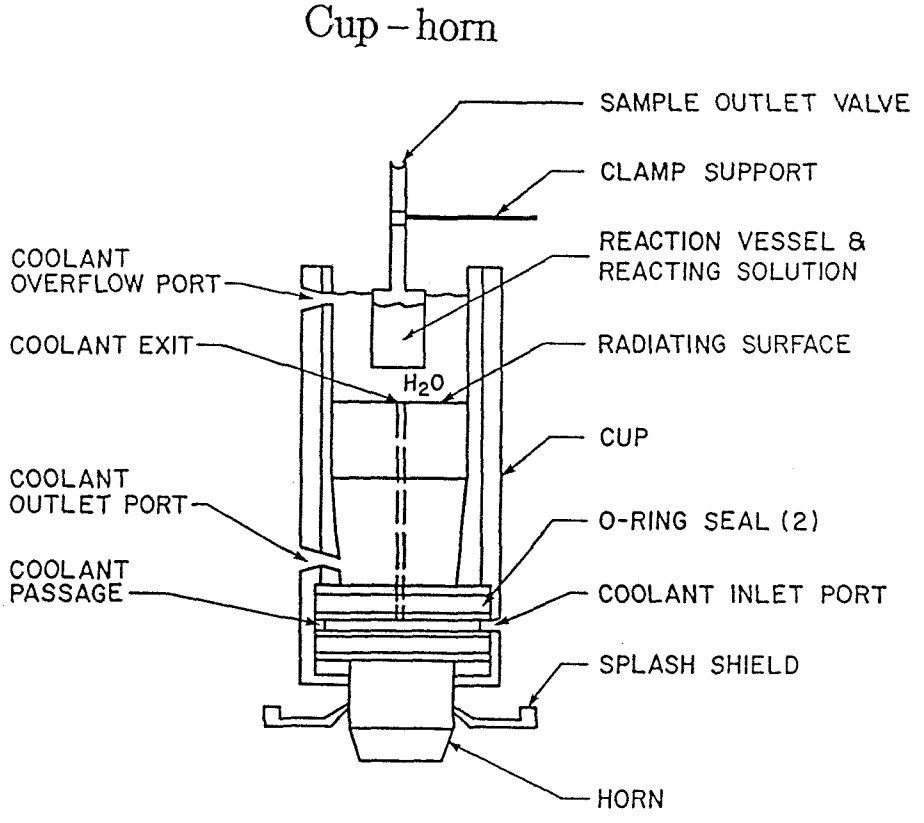

Figure 7.16 Schematic diagram of cup–horn sonication reactor configuration.

the problem with the direct immersion horn). An important point is that because of the larger surface area of the radiating surface of the cup–horn (44.2 cm^2 as compared to $\simeq$ 1.2 cm^2 for the 1/2–in. titanium tip) the intensity of the sound field delivered to the solution is much lower (intensity = power/vibrating area). If the solution to be irradiated is placed in a reaction vessel inside the water that is in contact with the radiating surface (as shown in Figure 7.16) the ultrasonic intensity inside the reaction vessel is even lower because of sound attenuation due to the bottom of the vessel. The height of the liquid above the radiating surface (h) is also very important; h must be an integer multiple of the wavelength of the sound waves (λ) in order for a stable sound field to be established.

Preliminary experiments with the configuration shown in Figure 7.16 were successful in establishing a sound field that would result in observable sonochemical effects. Figure 7.17 illustrates the change in color of an initially clear KI – CCl_4 – starch solution sonicated in a 50 ml flask inside the cup horn. Figure 7.18 compares the sonochemical yield of iodine in the flask/cup horn system to that observed with the direct immersion horn and different reaction vessels. It can be seen that sonochemical yields in the former system were rather low and results were not always reproducible. Therefore, that type of experimental set–up was not used further. A series of experiments were performed in the cup horn using the membrane surface for direct sonication of the solution of interest. This practice can result in damage of the radiating surface in the long–run but did not have any obvious short–term effects. Of course, the cup horn was washed repeatedly after each experiment and it was 'self–cleaned' by sonicating deionized water for a prolonged time.

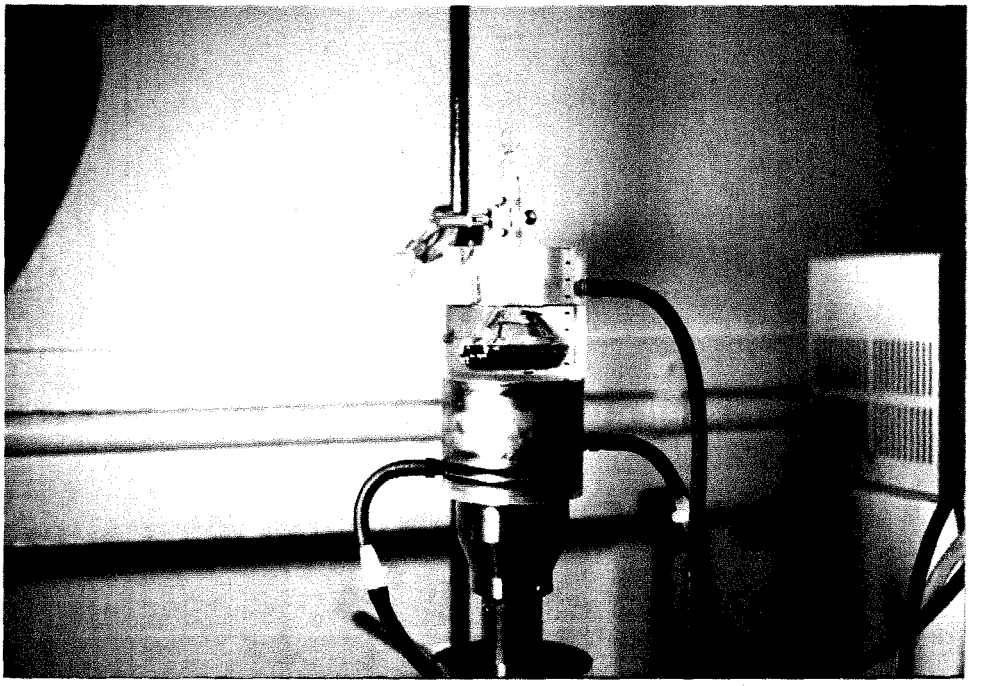

Figure 7.17 KI – CCl_4 – starch solution sonicated inside a flask in the cup horn.

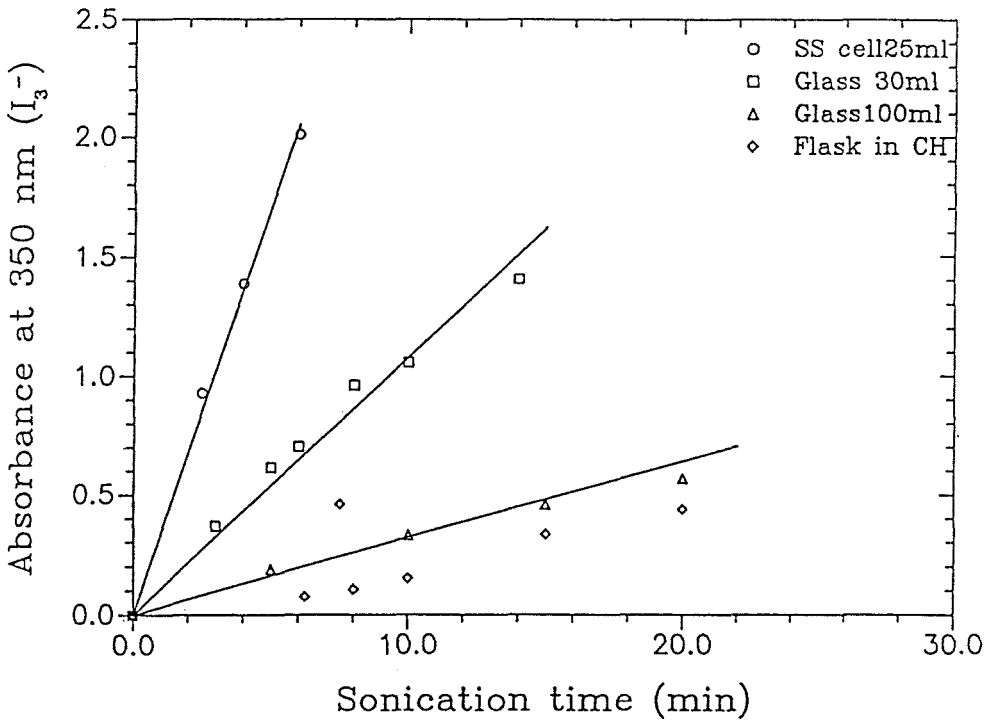

Figure 7.18 Comparison of the I_3^- release during sonication of a 1M KI solution with the direct immersion horn (and different reaction vessels) and the cup horn with a 50 ml flask.

Figure 7.19 shows the results of continuous flow sonication experiments for S(–II) and KI respectively with the VC1500 power supply unit connected to the cup–horn and operating at 50% nominal power. The solution to be sonicated was introduced through the coolant inlet and left the system via the coolant overflow port (shown in Figure 7.16). The height of the irradiated solution was 5.8 cm (irradiated volume = $V_s \simeq 270$ ml) and Q = 320 ml/min, V_r = 1500 ml for both experiments. From temperature data the input power was calculated to be 330 W giving an ultrasonic intensity at the radiating surface of 7.5 $W \cdot cm^{-2}$ and an energy input of 3.2 $J \cdot ml^{-1} \cdot s^{-1}$. The zero–order sonolysis rate constants, k_{os}, calculated from the experimental data were 10 and 16 μM/min for S(–II) and KI, respectively. These rates are twofold faster than the continuous flow experiments performed with the unit connected to the 1/2–in. 'direct immersion horn' [for both S(–II) and KI]. In the latter case, the power input was $\simeq 3.2$ $W \cdot ml^{-1}$ and the ultrasonic intensity at the horn tip was 75 $W \cdot cm^{-2}$. The total amount of S(–II) or I^- oxidized per unit of input energy during direct sonication in the cup–horn is 5.2 [= 2 × (3.2/1.2)] times higher than in the case of the direct immersion horn. Therefore, a reactor configuration in which the solution is directly sonicated by relatively large surface area membranes seems to be more efficient as compared to the direct immersion horn configuration. It must be noted that those experiments gave increased k_{1r} values, especially for iodide [$6 \cdot 10^{-3}$ and $7.5 \cdot 10^{-2}$ min^{-1} for S(–II) and KI respectively] which accounts for the loss of linearity of the concentration vs time profiles (Figure 7.19). For KI this could mean that part of the iodine that is formed upon sonication escapes from the solution (larger open surface in the sonication vessel in this configuration).

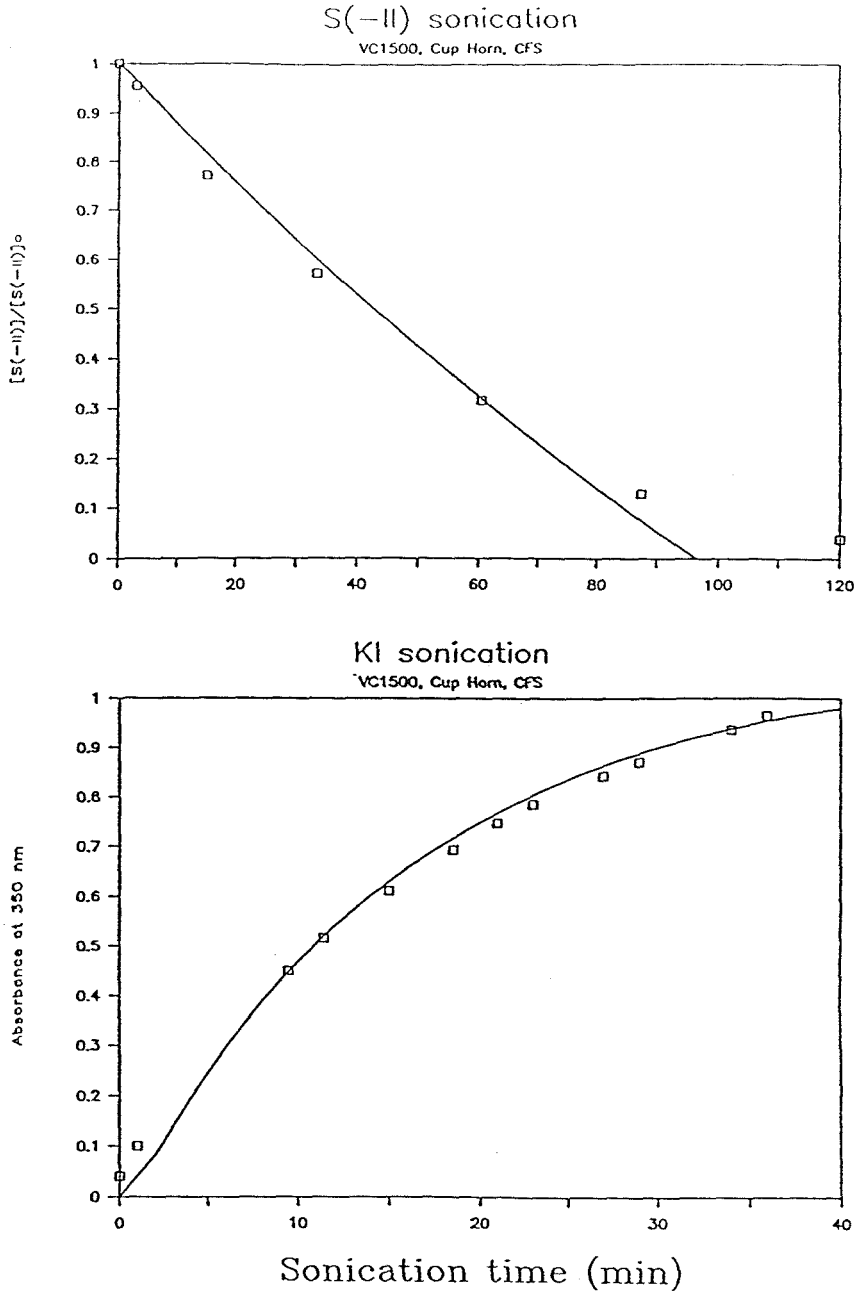

Figure 7.19 Continuous flow sonication with Cup–Horn/VC1500, Q=300 ml/l, V_s=270ml, V_r=1500ml. (a, top) $[S(-II)]_o$=200 μM, pH=10; solid line for k_{os}=10μM/min, k_{1r}=0.006min^{-1} (b, bottom) 1M KI; solid line for k_{os}=16μM/min, k_{1r}=0.075min^{-1}

Wastewater

Wastewater collected from the inlet of San Jose Creek Water Reclamation Plant was used for a series of batch sonication experiments. The raw wastewater was spiked with S(–II) and was diluted with borate buffer (20% of buffer per volume in the final solution) to raise the pH at a value of $\simeq$ 10. Under the same experiments conditions that were used for the deionized water sulfide experiments described in Chapter 4 (i.e., CD200 sonication unit at 20 kHz, 75 $W \cdot cm^{-2}$, 25 ml solution in stainless steel cell) the initial rates of S(–II) oxidation were similar to those observed in deionized water.

Figure 7.20 shows the profile of [S(–II)] with sonication time for a typical experiment at pH 10 (20% borate buffer). The straight line represents the linear S(–II) decrease observed in deionized water under the same experimental conditions. It can be seen that in the case of wastewater there is a divergence from this line at longer sonication times. This is most likely due to oxygen depletion (see Chapter 5). It is also possible that other oxidizable species present in wastewater interfere with S(–II) sonolysis at low sulfide concentrations by competing for the available oxidants (mainly $^{\cdot}OH$, O_2, $O_2^{\cdot -}$).

Repeated experiments confirmed that the depletion of S(–II) during sonication in alkaline pH was best described by a first order reaction. The effect of initial sulfide concentration, $[S(-II)]_o$, on the first–order reaction constant, k_1, is shown in Figure 7.21. It can be seen that the rate of S(–II) oxidation increases with increasing $[S(-II)]_o$. The following experimental expression was obtained:

$$k_1 = 9.1 \cdot 10^{-4} \cdot [S(-II)]_o^{0.535}, \quad r^2 = 0.9 \tag{7.8}$$

where k_1 is in min^{-1} and [S(–II)] in M.

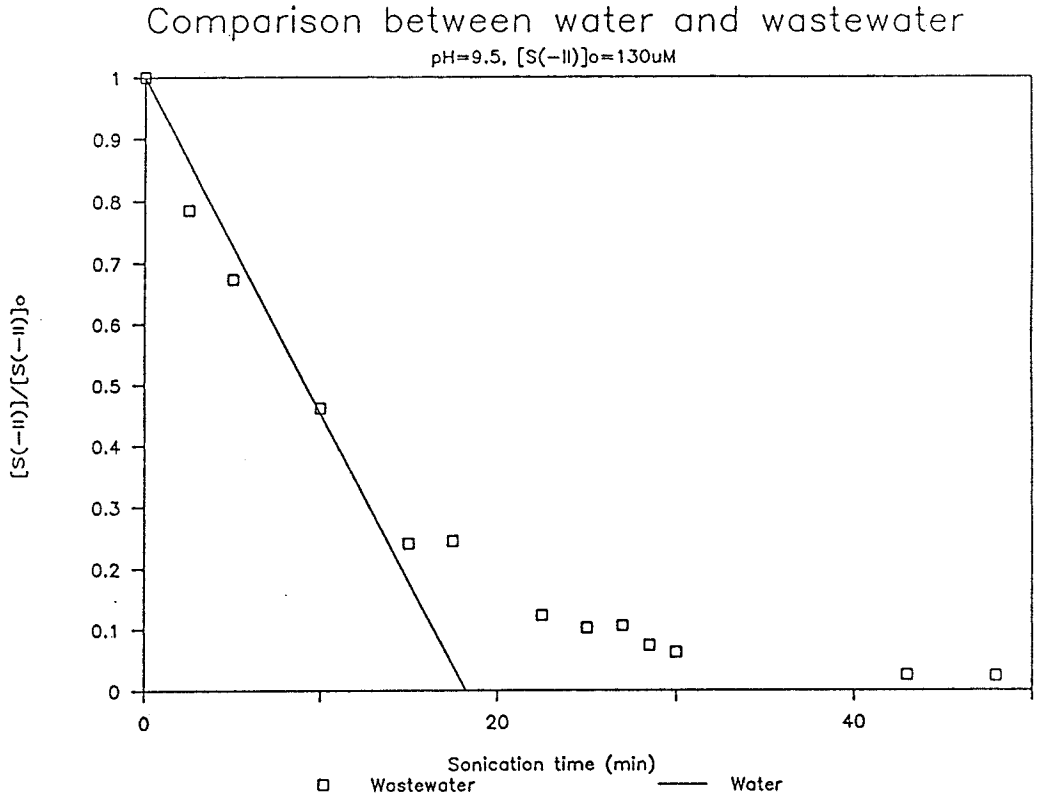

Figure 7.20 S(–II) sonication in wastewater (20% borate buffer); pH=9.5, T_b = 39 °C.

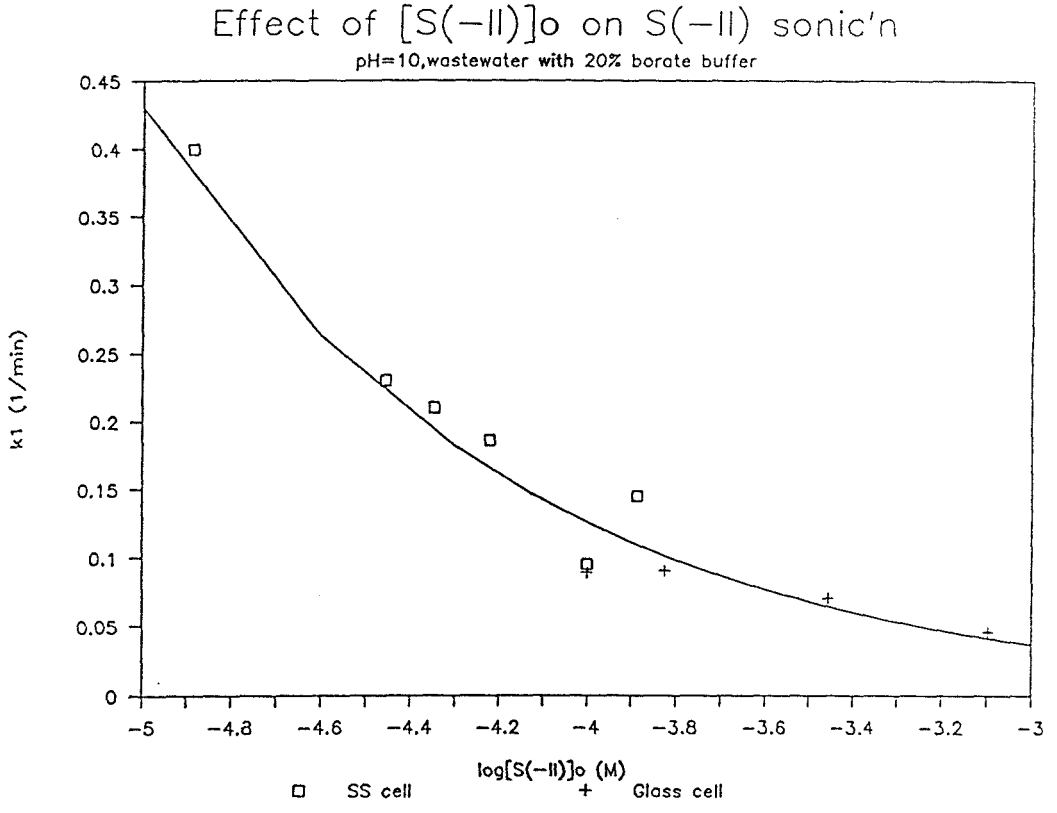

Figure 7.21 S(–II) sonication in wastewater; Effect of $[S(-II)]_o$ on first–order reaction rate constant.

Conclusions

The observed effects of bulk solution temperature and dissolved gases on the sonolysis of the chemicals studied are in agreement with the sonolytic mechanisms proposed for these chemicals and the existing acoustic cavitation theory. General ionic strength effects do not appear to be important for the sonolysis of chemicals, but specific ions (e.g. halogens) can have significant catalytic or inhibitory effects. These ions can react with ·OH radicals or can be involved in high temperature reactions at or near the interfacial region of cavitating bubbles. In either case, they can either interfere with the reactions of the chemical of interest, or provide additional oxidants for its destruction.

Sonication of S(–II) in wastewater produces similar results as sonication of aqueous S(–II) solutions. The experimental results obtained for the S(–II) system suggest that the free–radical oxidation reactions were not affected significantly by the complex wastewater matrix. This result is an encouraging sign for the potential of ultrasound as an alternative method of wastewater treatment.

Experimental results obtained with the use of two different power supply units and three different reactor configurations showed that *i)* the nominal power output of a sonication unit is not a good indication of its sonochemical efficiency, *ii)* sonication units with larger radiating surfaces are a better choice than localized application of high intensity ultrasound; there is a limit to the 'acoustical energy' that can be delivered to a solution with the direct–immersion–horn type of sonicators, and *iii*) commercial sonicators of the direct–immersion–horn type have similar sonochemical efficiency for both batch and flow–through operation. Scale–up of the sonication process is not evident and more work in this area is needed.

References

1. Stanbury, D. M. *Adv. Inorg. Chem.* 1989, *33*, 69.

2. Gueguen, H. *Ann. Chim.* 1963, *8*, 667.

3. Reynolds, G. T.; Walton, A. J.; Gruner, S. M. *Rev. Sci. Instrum.* 1982, *53*, 1673.

4. Crum, L. A.; Reynolds, G. T. *J. Acoust. Soc. Am.* 1985, *78*, 137.

CHAPTER 8

CONCLUSIONS

Conclusions

- Oxidizable inorganic and organic chemical compounds decompose rapidly when exposed to ultrasonic irradiation. Sonodegradation time scales range from minutes to hours with the ultrasonic devices used in this study. For example, $\tau_{1/2}$ for 100 μM H_2S at neutral pH sonicated with an immersion horn at 20 kHz and 75 $W \cdot cm^{-2}$ is $\simeq$ 2 minutes. In the same ultrasonic apparatus, $\tau_{1/2}$ for p–nitrophenol (p–NP) and parathion degradation is about 30 minutes and 1 hour, respectively.

- Sonolytic decomposition mechanisms are similar to those observed in radiolysis and combustion chemistry. The ultrasonic degradation of H_2S, p–NP and parathion can be explained, in part, by reaction with $^{\cdot}OH$ radicals generated from dissociation of water upon sonication and by thermal decomposition. The relative importance of those two degradation pathways depends mainly on the ability of the chemical of interest to enter into the gas phase of the cavitating bubbles or to accumulate in the interfacial region of the cavities.

The observed reaction kinetics and product distributions suggest that reaction with $^{\cdot}OH$ is the principal pathway for the sonolysis of H_2S at pH $\geq$ 10 (where H_2S is mainly present in the form of HS^-) but thermal decomposition of H_2S within or near collapsing cavitation bubbles is the predominant pathway at pH $\leq$ 8.5.

The sonochemical degradation of p–nitrophenol appears to proceed via high–temperature pyrolytic reactions in the hot surroundings of the cavitation bubbles. The main reaction pathway appears to be carbon–nitrogen bond cleavage. Reaction with $^{\cdot}OH$ appears to be a secondary reaction pathway. Thus, we have

shown that thermal decomposition can be the dominant sonodegradation pathway even for non–volatile organic compounds. These chemicals were previously thought to degrade primarily via reaction with ·OH. Based on the reaction products and the kinetic observations during p–nitrophenol sonolysis and with the use of chemical thermometry, the average effective temperature of the interfacial region surrounding the cavitation bubbles has been estimated to be $\simeq$ 800 K (direct immersion probe, at 20 kHz and 75 W·cm^2).

- The sonolytic oxidation of H_2S at pH $\geq$ 10 was successfully modeled with an aqueous–phase free–radical chemistry mechanism. This model development assumed a continuous and uniform ·OH input into solution from the imploding cavitation bubbles. This result suggests that the use of simplified approaches for modeling the liquid–phase sonochemistry of a well–mixed solution may be justified when ·OH radical reactions predominate. For the immersion probe at 20 kHz and 75 W·cm^{-2}, the effective ·OH uniform release into the bulk solution was estimated to be 3.5 μM·min^{-1} with a corresponding steady–state ·OH concentration of $\leq$ 0.1 μM.

- Sonolytic reaction yields and overall reaction rates depend on various physical and chemical parameters. The observed effects of the parameters studied in this work are in qualitative agreement with the sonolysis mechanisms proposed for the chemicals of interest and the existing hydrodynamic theories of acoustic cavitation.

We have shown that the presence of other chemical constituents can influence significantly the outcome of the sonolysis of the chemicals of interest. For

instance, halogen ions promote the sonolytic degradation of S(–II) at alkaline pH while the same ions inhibit the sonolysis of p–nitrophenol. However, the ionic strength of the solution does not appear to have a direct effect on sonochemical reactions (i.e., the presence of 'sonochemically inert' ions such as sulfate or nitrate did not affect sonolytic yields).

A direct linear relationship between the applied power at 20 kHz and the observed rate of S(–II) sonodegradation has been found. However, bulk solution temperature did not have a pronounced effect on the oxidative destruction of that chemical.

Sonication of a KI solution in the presence of different gases showed that the nature of the dissolved gases plays an important role in aqueous sonochemistry. The relative iodine yields are 1.00 : 0.85 : 0.55 : 0.11 in the presence of O_2, Ar, air, and N_2, respectively.

The study of S(–II) sonolysis showed that oxygen can also play an important role by propagating a free–radical chain reaction initiated by $^{\cdot}OH$. Furthermore, sonication seems to enhance the oxygen transfer to solution from the atmosphere.

The ultrasonic degradation of p–NP and S(–II) were shown to depend on the pH of the solution; in both cases oxidation rates increased with decreasing pH. However, iodide sonolysis was not affected by pH. It appears that pH does not affect the primary sonochemistry of water (i.e., intensity of cavitation, formation of excited species), but can have a significant effect on the sonochemistry of the solute especially if it has a pH–dependent speciation.

Addition of fine particles in the sonicated solution or air bubbling prior to sonication did not affect sonochemical yields. That suggests that the efficiency of sonolysis with an immersion probe in deionized water is not limited in the number

of available 'cavitation nuclei' or pre–existing bubbles.

Sonication of S(–II) in wastewater indicates that sonochemical free–radical reactions are not significantly affected by the complex wastewater matrix.

- Sonication with an ultrasonic device with a larger radiating surface (cup–horn type) resulted in faster and more efficient oxidation than localized application of high intensity ultrasound (direct–immersion–horn type). The operation of the direct–immersion–horn type sonicator with the commercial stainless steel cell in the flow–through mode resulted in only a modest decrease in the sonochemical efficiency of the unit ($\simeq$ 24 % decrease in the amount of chemical oxidized per unit energy supplied to the system). Results obtained from batch experiments with that configuration can therefore be extrapolated to continuous flow operation.

- Sonolysis is relatively inefficient with respect to utilization of the gross input energy. Less than 1% of of the total energy supplied to the system is used in the actual production of free–radical reactions with the ultrasonic setups used in this work. Even so, the relative efficiency of ultrasound in terms of the total power consumed per mole of p–nitrophenol degraded per liter of water is superior to photolysis.

- Ultrasound has the potential to become a viable alternative for the destruction of chemical contaminants in water and wastewater. Its low energy utilization efficiency would currently limit its potential use to relatively low–flow specific applications such as groundwater remediation, or pretreatment of industrial

wastes where, despite the high cost, this method could still compete with alternative technologies for the treatment of hazardous and persistent chemicals mainly because of its high effectiveness and its relatively easy and flexible operation. There is room for improvement of sonochemical efficiency by optimizing reactor design and physical/chemical operation conditions.

Recommendations for future research

- A model that includes both gas and liquid–phase chemistry and incorporates the physics of bubble collapse and bubble clouds dynamics would offer a more realistic and comprehensive mathematical representation of sonochemistry.

However, the development of such a model is not feasible at this stage because of lack of enough information about the number and size distribution of cavitation bubbles under intense sonication, about the dynamics of bubble clouds and about the physical conditions inside the bubble and its surrounding region upon collapse. Research in the above areas is necessary before mathematical models coupling the chemistry and physics involved in sonochemistry can be developed.

- The overall mechanisms involved in the ultrasonic decomposition of chemical compounds are now relatively well understood. However, more research is needed in order to gain an insight into the chemical and physical phenomena occurring in microscopic scale. Minimal information exists concerning the physical and chemical conditions inside and in the vicinity of imploding bubbles and the temporal and spatial concentration profiles of excited species and solute molecules.

- Ultrasound has the potential to become a competitive technology for water and wastewater treatment. However, more research is needed to address issues such as optimal reactor design and ultrasound–induced mixing, degassing, and cavitation damage before large–scale applications can be considered. The effects of temperature, ionic strength, and ultrasonic intensity should be studied further with different substrates. The effects of frequency and pressure should also be addressed.

It is recommended that a high intensity flow–through sonication system that uses sound reverberation between two flat plates (Near–field Acoustical Processor) be tested. This system is expected to have a higher efficiency and it should be relatively easy to scale–up.

APPENDIX A

Catalytic Autoxidation of Hydrogen Sulfide in Wastewater

(*Environmental Science & Technology*, 1991, *25*, 1153)

ABSTRACT

The catalytic effectiveness of cobalt(II)–4,4',4'',4'''–tetrasulfophthalocyanine [Co(II)TSP] for the autoxidation of hydrogen sulfide, S(–II), in wastewater was investigated. At pH 7 and 25°C the rate of S(–II) oxidation is first–order with respect to [S(–II)]. A fractional order on the catalyst was observed. At oxygen concentrations 15 to 200 μM the oxygen dependence can be described by simple Michaelis–Menten kinetics with K = 63 μM. The uncatalyzed oxidation of sulfide by molecular oxygen was found to be faster in wastewater than in clean water. This difference was attributed to microbial oxidation of S(–II) and to catalytic action of transition metals present in wastewater.

INTRODUCTION

Corrosion of concrete structures by sulfuric acid generated due to the presence of hydrogen sulfide is a problem often encountered in wastewater collection systems (1–3). Domestic sewage contains sulfates and other sulfur compounds, which under anaerobic conditions can be reduced to sulfides. Various industries may also discharge sulfur in the form of sulfides (e.g. tanneries, abattoirs, fell morgering works, coal–gas works, oil refineries, sulfur dye works). In partially filled sewers, hydrogen sulfide may be transferred from the liquid phase to the gas phase and finally to the crown of the sewer where it is oxidized in the presence of thiobacilli to H_2SO_4. The generation of acidity on the crown results in the corrosion of the concrete (1).

The problem of corrosion of concrete pipes due to the presence of hydrogen sulfide has been a focus of attention for many years (1–3). Aeration of wastewater, by compressed air or pure oxygen, is one of the control measures commonly employed in sewers to oxidize sulfides while still in the liquid phase (1–2).

In general, the oxidation of reductants such as H_2S by O_2 proceeds slowly in the absence of catalysts (4–13) because of unfavorable spin state symmetries that result from the differences in the electronic configurations of the reactants. Transition metal ions and complexes are usually effective catalysts because they are able to alter the electronic structure of either H_2S or O_2 in order to surmount the activation energy barrier imposed on the reaction by spin–state symmetry restrictions.

The oxidation of S(–II) {i.e., H_2S, HS^-, S^{2-}} by oxygen has a complicated stoichiometry because of the wide array of products and metastable intermediates

produced during the course of the reaction. Products and intermediates which have been identified (4–13) include: S_n (colloidal sulfur), S_8 (elemental sulfur – orthorombic), $S_2O_3^{2-}$ (thiosulfate), SO_3^{2-} (sulfite), S_4^{2-} and S_5^{2-} (polysulfide ions), $S_4O_6^{2-}$ (tetrathionate) and SO_4^{2-} (sulfate). The major products and intermediates, S_8, SO_3^{2-}, $S_2O_3^{2-}$, and SO_4^{2-} are formed according to the following stoichiometries:

$$8\,H_2S + 4\,O_2 \longrightarrow S_8 + 8\,H_2O \qquad (1)$$

$$H_2S + \tfrac{3}{2}\,O_2 \longrightarrow 2\,H^+ + SO_3^{2-} \qquad (2)$$

$$SO_3^{2-} + \tfrac{1}{8}\,S_8 \longrightarrow S_2O_3^{2-} \qquad (3)$$

$$H_2S + 2\,O_2 \longrightarrow 2\,H^+ + SO_4^{2-} \qquad (4)$$

The actual time–dependent distribution of products and intermediates depends on pH and the concentrations of the catalyst, S(–II) and oxygen employed (4, 6).

Previous studies (5, 9–10) have shown that cobalt(II) and nickel(II) are the most effective catalysts for oxidation of H_2S. Cobalt(II) 4,4',4'',4'''–tetrasulfophthalocyanine has also been reported to be an effective catalyst for the homogeneous and heterogeneous autoxidation of reduced sulfur compounds (4, 14–16). However, its effectiveness in complicated matrices such as wastewater had not been established.

The catalytic effectiveness of cobalt(II) 4,4',4'',4'''–tetrasulfophthalocyanine [Co(II)TSP] for H_2S oxidation was studied in wastewater obtained from a tertiary wastewater treatment plant in Los Angeles County. The kinetics of S(–II)

oxidation in the influent were investigated and empirical rate laws were determined.

EXPERIMENTAL SECTION

Preparation of Cobalt(II)–tetrasodium–tetrasulfophthalocyanine

Cobalt(II) 4,4',4'',4'''–tetrasulfophthalocyanine, Co(II)TSP, is a square–planar complex in which the metal center is bonded to the four pyrrole nitrogens of the ligand. The tetrasodium salt $CoNa_4C_{32}H_{12}N_8O_{12}S_4 \cdot 6H_2O$ was prepared based on the procedure described originally by Weber (17–18) and subsequently modified by Boyce *et al.* (14). In our preparation the following modifications to the original procedure were made: The monosodium salt of 4–sulfophthalic acid was prepared from 4–sulfophthalic acid and an equimolar concentration of sodium hydroxide. Sulfophthalic acid is usually a 50% water mixture; most of the water was evaporated to give a yellow/brown oil. Addition of excess ethanol and then equimolar sodium hydroxide as a solid with stirring to prevent overheating results in the precipitation of an almost white solid of the 4–sulfophthalate. The salt was washed with ethanol and dried in a desiccator overnight. Cobalt(II) in the form of cobalt(II) chloride hexahydrate was added and carefully mixed but not ground (grinding leads to a purple hygroscopic solid) to the prescribed mixture of 4–sulfophthalate, ammonium chloride, urea and ammonium molybdate. After the prescribed treatment with nitrobenzene and methanol excess Co(II) was extracted from the product by dissolving the solvent–free product in a solution of 1N HCl/75% ethanol, saturated with NaCl at 4 °C. Heating to 60 –

80°C accelerates the process and cooling in the refrigerator overnight precipitates most of the solid as a very fine powder (slimy), which was separated by filtration. The resulting precipitate was dissolved in 150 ml solution of 50% ethanol/0.1N NaOH, saturated with NaCl at 4 °C, and heated for 1 hour at 80 °C. After cooling the solution in the refrigerator overnight, the almost clean dark blue product was filtered. Excess chloride was washed out by heating the solid with 100 ml 70% ethanol for 1 hour to 60 °C, followed by filtration of the hot mixture. This process was repeated (3–6 times) until no Cl^- could be detected in the solution (no white AgCl precipitate upon addition of $AgNO_3$). Organic impurities were extracted by refluxing the pure product 3 times with absolute ethanol for 1 hour, followed by filtration of the hot mixture. The blue pure product was dried overnight in a desiccator. The elemental analysis (theoretical values in given brackets) for the final product was as follows: C: 35.52% (35.34%); H: 2.59% (2.23%); N: 9.93% (10.30%); S: 11.79% (11.43%); Na 7.76% (8.45%); Co 5.09% (5.42%). UV/VIS spectra were identical to those described in a previous report (4).

Reagents

All reagents were of analytical grade. Doubly–distilled (18 MΩ–cm) deionized water was used for the preparation of all solutions. S(–II) stock solutions were prepared from $Na_2S \cdot 9H_2O$ crystals (Aldrich) that had been washed with deionized water and dried. The actual concentrations were determined by potentiometric titration with $Pb(ClO_4)_2$ (Orion). Stock solutions were stored in a refrigerator and no significant decrease in sulfide concentration was detected during a period of approximately 10 days. Mixtures of mono and disodium phosphate salts (Mallinckrodt) were used as buffers. Sodium perchlorate (EM Science) was used to

adjust the ionic strength of the reaction solutions.

Experimental Apparatus

Experimental techniques and apparatus used in this study were similar to those described previously (4, 6–8). Experiments were conducted in sealed water–jacketed, glass reaction vessels with a total volume of 1.5 to 2.0 l. The design and operation of the batch reactor system have been described previously (4, 15). An aluminum cover was used to protect the reaction solution against light. To minimize the potential catalytic effect of trace–metal contaminants, all glassware was washed with phosphate free detergent (Alconox), soaked in dilute HNO_3, and then rinsed several times with deionized water.

Two types of Dissolved Oxygen (DO) probes were used in order to measure oxygen concentrations. Concentrations above 0.4 mM were measured with an INGOLD type 531 oxygen electrode with coupled amplifier, linked to a RADIOMETER ion 83 ionmeter, while for concentrations below 0.4 mM an ORION 97–08–00 oxygen electrode was used. Sulfide concentrations were measured with a sulfide ion electrode (ORION 94–16 Ag/Ag_2S with double junction reference electrode) coupled to an ORION 801–A ion analyzer. pH measurements were performed with a RADIOMETER pH electrode and a PHM84 pH meter. An automatic titration system (autoburette ABU12 and titrator TTT60) was utilized to control pH in the absence of a buffer. The temperature was maintained constant at 25°C with the use of a HAAKE A80 water circulation and temperature controlling system. Spectrophotometric measurements were performed on an HP 8450A UV/VIS spectrophotometer. An AMSCO 2022 autoclaving apparatus was used to autoclave wastewater at temperature 120 °C and pressure

20 psi. All instruments were interfaced to an IBM–AT computer for data collection. During an experiment, data from all but the sulfide electrodes were taken continuously (every 10 seconds) and stored for later analysis.

All electrodes were calibrated at regular time intervals and showed no significant drift with time. The sulfide ion specific electrode (ISE) was calibrated both for clean water and wastewater. The EMF versus concentration response of the electrode was found to follow the Nernst equation with similar slopes in both systems.

Kinetic Data

Control experiments in Milli–Q water were conducted in buffered solutions (mono/disodium phosphate buffer, pH=6.6, I=0.4M), at constant temperature (T=25°C), under oxygen saturation, and in the presence of various catalysts [Co(II)TSP, $NiCl_2$ $CuCl_2$]. The buffer/catalyst mixture was purged with pure oxygen gas (PO_2 = 1 atm) until oxygen saturation was established (initial oxygen concentration 1.2 mM). Reactions were initiated by adding a known volume of sulfide stock solution. Initial experiments with the sulfide electrodes immersed in the reaction medium gave inconsistent results. Intermediates such as polysulfides and elemental sulfur were found to interfere with the Ag_2S electrode measurements. These interferences were overcome by taking samples periodically from the reaction vessel, using a syringe through a septum in one of the reaction vessel openings, and analyzing for sulfide after dilution 1:1 with SAOB (sulfide antioxidant buffer: a mixture of 67g Na_2EDTA, 35g ascorbic acid, 80g NaOH in 1000 ml). In selected experiments, UV/VIS spectra of samples were also taken during the course of the reaction.

Wastewater experiments were performed at pH 7 and T=25°C in the presence or absence of Co(II)TSP and at various initial oxygen concentrations. Oxygen concentrations were established by dispersing oxygen gas, compressed air, or a mixture of oxygen and nitrogen gas into the wastewater. At the end of aeration, pH was adjusted to 7.0 using perchloric acid and the appropriate amount of sulfide stock was added. Even though no buffer was added the pH of the medium remained constant during the experiment. Sampling and measurement techniques were the same as those used in the control water experiments.

For a reaction that is first order with respect to total sulfide (i.e. pseudo–first–order conditions of constant pH, T, and ionic strength with $[O_2] >> [S(-II)]$ or $[O_2]$ held constant, $d[S(-II)]/dt = - k_{obs} \cdot [S(-II)]$), a plot of the sulfide–specific electrode potential, E_h, versus time should yield a straight line with a positive slope equal to $\frac{RT}{nF} \cdot k_{obs}$ (7). In that case the pseudo–first–order constant k_{obs} can be readily obtained from

$$k_{obs} = \frac{2F}{RT} \frac{dE_h}{dt} \qquad (5)$$

where $\frac{2F}{RT} = 7.785 \times 10^{-2}\ mV^{-1}$ at 25 °C.

The empirical rate law was deduced from data sets accumulated for the observed pseudo–first–order rate constants under a variety of initial conditions, using the principle of the initial rates method (19). It is noted that the order obtained by this method deals with initial slopes (in this case initial k_{obs}'s) and the change in concentrations of reactants is small in the initial stage of the reaction. Therefore, the validity of the method does not change materially even if the concentrations of the reactants that are assumed to remain constant are not in

excess, as long as these initial concentrations are kept the same for all experiments of a particular data set (10, 23).

RESULTS AND DISCUSSION

Kinetic results in water

Kinetic measurements of the sulfide autoxidation in the control experiments with clean water were performed in near neutral oxygen saturated water (pH 6.7, $[O_2]_o$=1.2 mM) at T = 25 °C, using Co(II)TSP, Cu(II) and Ni(II) as catalysts. The catalyst concentrations ranged from 0.01 to 100 μM. Initial sulfide concentrations varied between $6.25 \cdot 10^{-5}$ and $2.0 \cdot 10^{-3}$ M (2 to 64 mg/l).

The plots of E_h versus time remained linear for more than 95% of the reaction (i.e. 95% depletion of the initial [S(–II)]). The corresponding $[O_2]$ decrease was consistent with the decrease of [S(–II)] and showed a 1:1 relation ($[O_2]_{utilized}$: $[S(-II)]_{oxidized}$) at the completion of the reaction in cases where initial concentrations of sulfide and oxygen were practically the same, and a 2:1 ratio in cases where $[O_2]_o >> [S(-II)]$. The observed stoichiometry indicates that sulfate is the final product when oxygen is in excess (eq. 4), while elemental sulfur is one of the final products when sulfide is present in excess (eq. 1). In the latter case, formation of elemental sulfur was also observed visually as an increase in turbidity during the course of the reaction and isolated as a yellowish white precipitate at completion of the experiment. The linearity of the E_h versus t confirmed previous observations that the reaction was first order with respect to [S(–II)] (4). The pseudo–first–order rate constants, k_{obs}, were calculated for each kinetic run from the slope of the potential curve (eq. 5); they are summarized in Table A.1.

Table A.1

Pseudo–first–order rate constants (k_{obs}) for the catalytic oxidation of sulfide in oxygen saturated deionized water

Catalyst (M)	[S(–II)] (M)	electrode slope mV/min	k_{obs} min^{-1}
Cu^{2+}			
$1.0 \cdot 10^{-4}$	$1.0 \cdot 10^{-3}$	$1.33 \cdot 10^{-1}$	$1.01 \cdot 10^{-2}$
$1.0 \cdot 10^{-5}$	$1.0 \cdot 10^{-3}$	$9.20 \cdot 10^{-2}$	$7.16 \cdot 10^{-3}$
$1.0 \cdot 10^{-6}$	$1.0 \cdot 10^{-3}$	–	$< 1 \cdot 10^{-3}$
Ni^{2+}			
$3.0 \cdot 10^{-5}$	$1.0 \cdot 10^{-3}$	$2.28 \cdot 10^{-1}$	$1.78 \cdot 10^{-2}$
$3.0 \cdot 10^{-5}$	$1.0 \cdot 10^{-3}$		$1.69 \cdot 10^{-2}$ *
$1.0 \cdot 10^{-5}$	$1.0 \cdot 10^{-3}$	$1.12 \cdot 10^{-1}$	$8.71 \cdot 10^{-3}$
$1.0 \cdot 10^{-5}$	$1.0 \cdot 10^{-3}$		$8.50 \cdot 10^{-3}$ *
$1.0 \cdot 10^{-6}$	$1.0 \cdot 10^{-3}$	$6.00 \cdot 10^{-2}$	$4.67 \cdot 10^{-3}$
Co(II)TSP			
$1.0 \cdot 10^{-8}$	$1.0 \cdot 10^{-3}$	$3.50 \cdot 10^{-2}$	$2.78 \cdot 10^{-3}$
$5.0 \cdot 10^{-8}$	$1.0 \cdot 10^{-3}$	$1.82 \cdot 10^{-1}$	$1.42 \cdot 10^{-2}$
$1.0 \cdot 10^{-7}$	$1.0 \cdot 10^{-3}$	$3.30 \cdot 10^{-1}$	$2.55 \cdot 10^{-2}$
$1.0 \cdot 10^{-7}$	$1.0 \cdot 10^{-3}$	$2.47 \cdot 10^{-1}$	$1.93 \cdot 10^{-2}$ **
$1.0 \cdot 10^{-7}$	$1.0 \cdot 10^{-3}$		$1.82 \cdot 10^{-2}$ *
$3.0 \cdot 10^{-7}$	$1.0 \cdot 10^{-3}$	$4.34 \cdot 10^{-1}$	$3.38 \cdot 10^{-2}$
$5.0 \cdot 10^{-7}$	$1.0 \cdot 10^{-3}$	$6.02 \cdot 10^{-1}$	$4.68 \cdot 10^{-2}$
$1.0 \cdot 10^{-7}$	$6.25 \cdot 10^{-5}$	$2.50 \cdot 10^{-1}$	$1.95 \cdot 10^{-2}$
$1.0 \cdot 10^{-7}$	$2.0 \cdot 10^{-4}$	$2.30 \cdot 10^{-1}$	$1.75 \cdot 10^{-2}$
$1.0 \cdot 10^{-7}$	$5.0 \cdot 10^{-4}$	$2.60 \cdot 10^{-1}$	$2.02 \cdot 10^{-2}$
$1.0 \cdot 10^{-7}$	$2.0 \cdot 10^{-3}$	$2.90 \cdot 10^{-1}$	$2.26 \cdot 10^{-2}$
$1.0 \cdot 10^{-7}$	$2.0 \cdot 10^{-3}$	$2.20 \cdot 10^{-1}$	$1.71 \cdot 10^{-2}$

* From absorbance data
** $h\nu$ experiment

Figure A.1 shows the non–linear dependence of k_{obs} on [Co(II)TSP]. At low concentrations k_{obs} has a stronger dependence on the catalyst concentration than at higher concentrations. This behavior can be attributed in part to the monomer/dimer equilibrium of Co(II)TSP, where the dimeric species (i.e., $[Co(II)TSP)_2]$ is catalytically less active (4, 15). At pH 6.7 an observed fractional–order dependence of 0.498 was determined for [Co(II)TSP] $\geq 5 \cdot 10^{-8}$ M (i.e., $k_{obs} = 62.934 \cdot [Co(II)TSP]^{0.498}$ with $r^2 = 0.929$). This value is close to the 0.5 order that is predicted theoretically (15) when the dimeric form of the catalyst predominates.

In one experiment the reaction solution was irradiated with low–intensity light during the entire kinetic run. The resulting rate constant is slightly lower but similar to those of the thermal reactions. Thus activation of the catalyst by light as reported earlier (14) for the case of S(IV) oxidation does not appear to be important.

The dependence of k_{obs} on [S(–II)] is shown in Figure A.2 (pH = 6.7, phosphate buffer, T = 25°C, oxygen saturation, [Co(II)TSP] = 0.1 μM). Varying the initial [S(–II)] from 6.25×10^{-5} M to 2.0×10^{-3} M does not change the observed rate constant ($k_{obs} \simeq 0.02$ min^{-1}). This observation reconfirms the first–order dependence of the reaction on [S(–II)] and shows that our analysis based on the initial rate constant k_{obs} is valid even when $[O_2]_o$ is of the same order as $[S(-II)]_o$.

Experiments performed with Cu^{2+} or Ni^{2+} as catalysts showed a dramatic decrease in catalytic activity compared to the activity of Co(II)TSP. At 1.0 μM Cu^{2+} $k_{obs} < 10^{-4}$ min^{-1}, while at $[Cu^{2+}] = 100$ μM k_{obs} was 0.01 min^{-1}. In the latter case however the actual $[Cu^{2+}]$ in solution was probably lower than the calculated value due to the formation of a dark brown precipitate (CuS, pK_{so}=37) after the

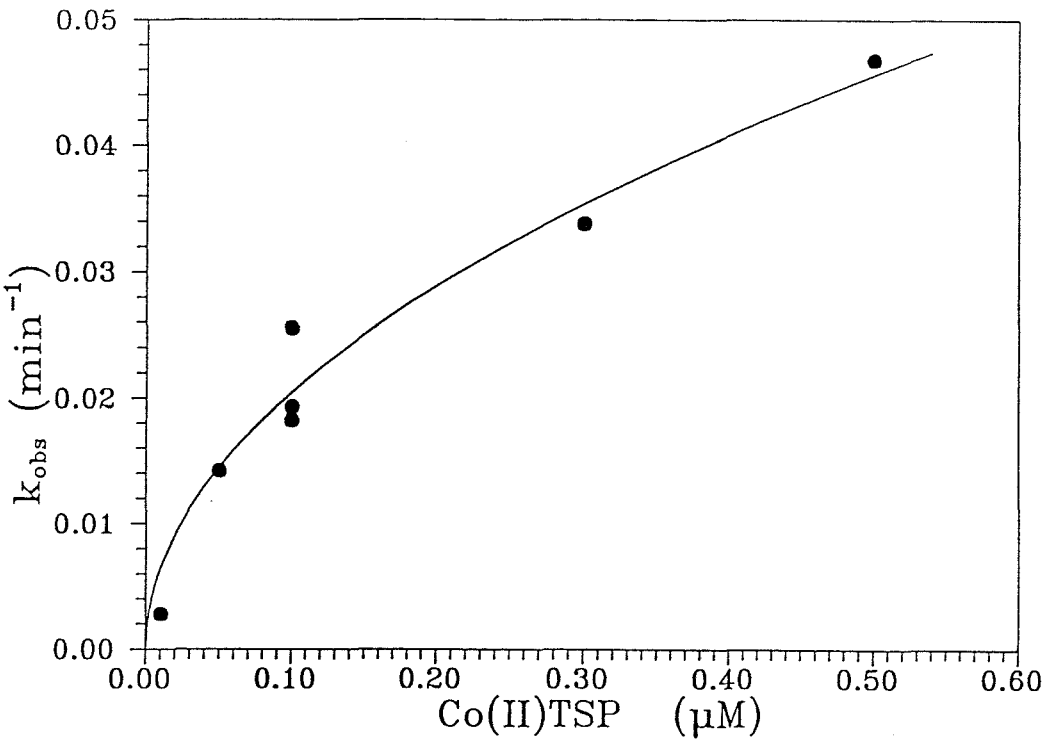

Figure A.1 k_{obs} dependence on [Co(II)TSP] for Co(II)TSP–catalyzed sulfide oxidation in water; T=25°C, pH=6.7 (phosphate buffer), oxygen saturation ($[O_2]=1.2\cdot10^{-3}$ M)

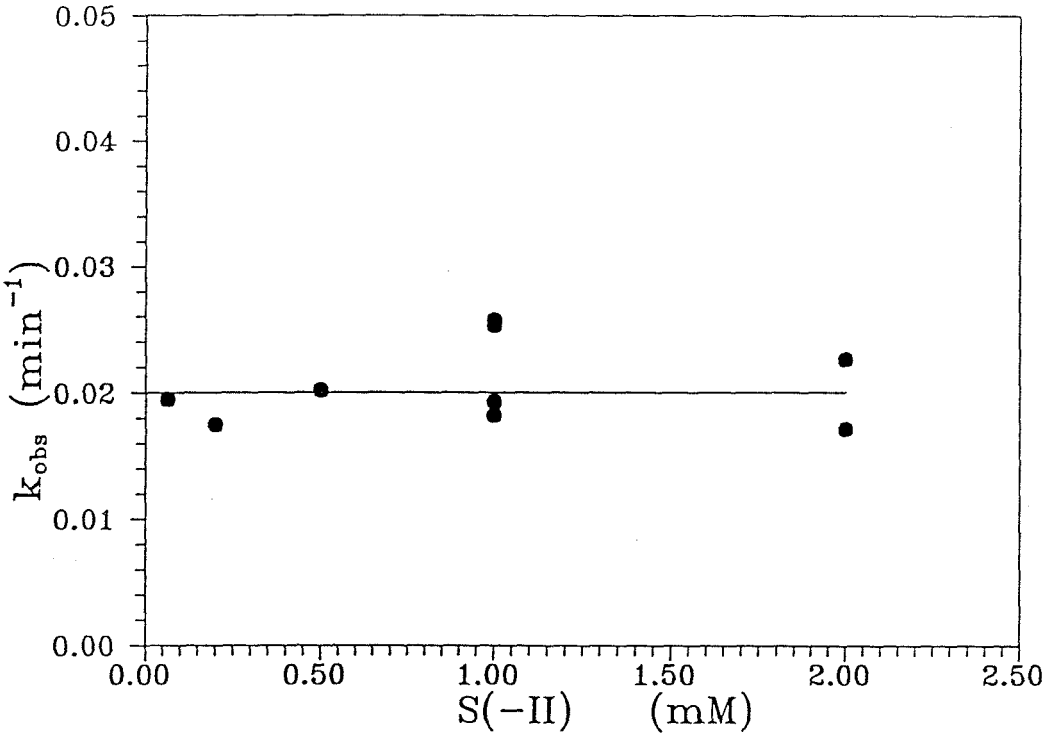

Figure A.2 k_{obs} dependence on [S(–II)] for Co(II)TSP catalyzed sulfide oxidation in water; T=25°C, pH=6.7 (phosphate buffer), oxygen saturation, [Co(II)TSP]=10^{-7} M

addition of sulfide. This effect was not observed at lower [Cu^{2+}]. At these lower concentrations Cu^{2+} may form soluble complexes with polysulfides. These initial intermediate oxidation products of sulfide autoxidation are expected to be excellent complexing ligands with the ability to form water soluble metal–polysulfide species (10–11). Polysulfides are formed during all control clean water experiments where $[S(-II)]_o \geq 1$ mM (*vide infra*). In all cases ([S(–II)] $\simeq$ 1.0 mM) the concentrations of total S_n^{2-} exceeds 10^{-6} M and can be as high as 100 μM.

The Ni(II)–catalyzed autoxidation of sulfide leads to higher k_{obs} values than for Cu(II) catalysis. For example, at 1 μM catalyst, $k_{obs}(Ni^{2+}) = 5 \times 10^{-3}$ min^{-1} as compared to $k_{obs}(Cu^{2+}) \leq 1 \times 10^{-4}$ min^{-1}. The superior catalytic effect of Ni^{2+} has been reported previously (6, 12). A comparison of the observed rate constants for the catalytic oxidation of S(–II) is given in Figure A.3. The graphic relationships show that Co(II)TSP is a significantly better catalyst than either Cu^{2+} or Ni^{2+} with a pronounced catalytic activity even at concentrations as low as 0.01 μM (k_{obs} = 2.8×10^{-3} min^{-1}). The much higher k_{obs} values, reported for even much lower concentrations (e.g. at [Co(II)TSP]= 2.5×10^{-9} M, k_{obs} = 0.36 min^{-1} (1)) are believed to be artifacts due to the electrode interferences (*vide supra*).

Because of the strong absorbance of hydrogen sulfide and its oxidation products (e.g. polysulfides) in the UV range, spectrophotometric measurements are a convenient way to follow their concentration changes during the reaction. Thus spectra of the ongoing reaction were taken at different time intervals. Typical spectra are shown in Figure A.4 for Ni^{2+}–catalyzed oxidation. The sequential spectra show a continuous decrease of [HS^-] at λ = 230 nm and an initial increase in absorption at $\lambda > 260$ nm for the first 20 – 30 min reaction time due to the production of polysulfides (peaks) and elemental sulfur (turbidity with broad

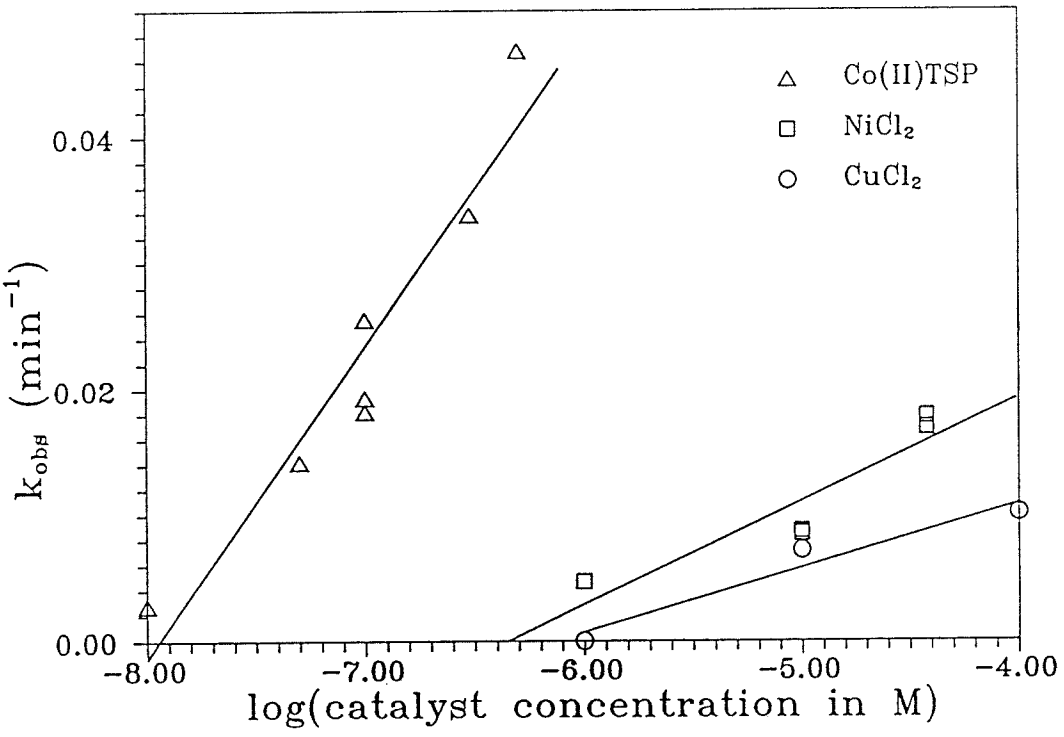

Figure A.3 k_{obs} values for different catalysts; T=25°C, pH=6.7, oxygen saturation

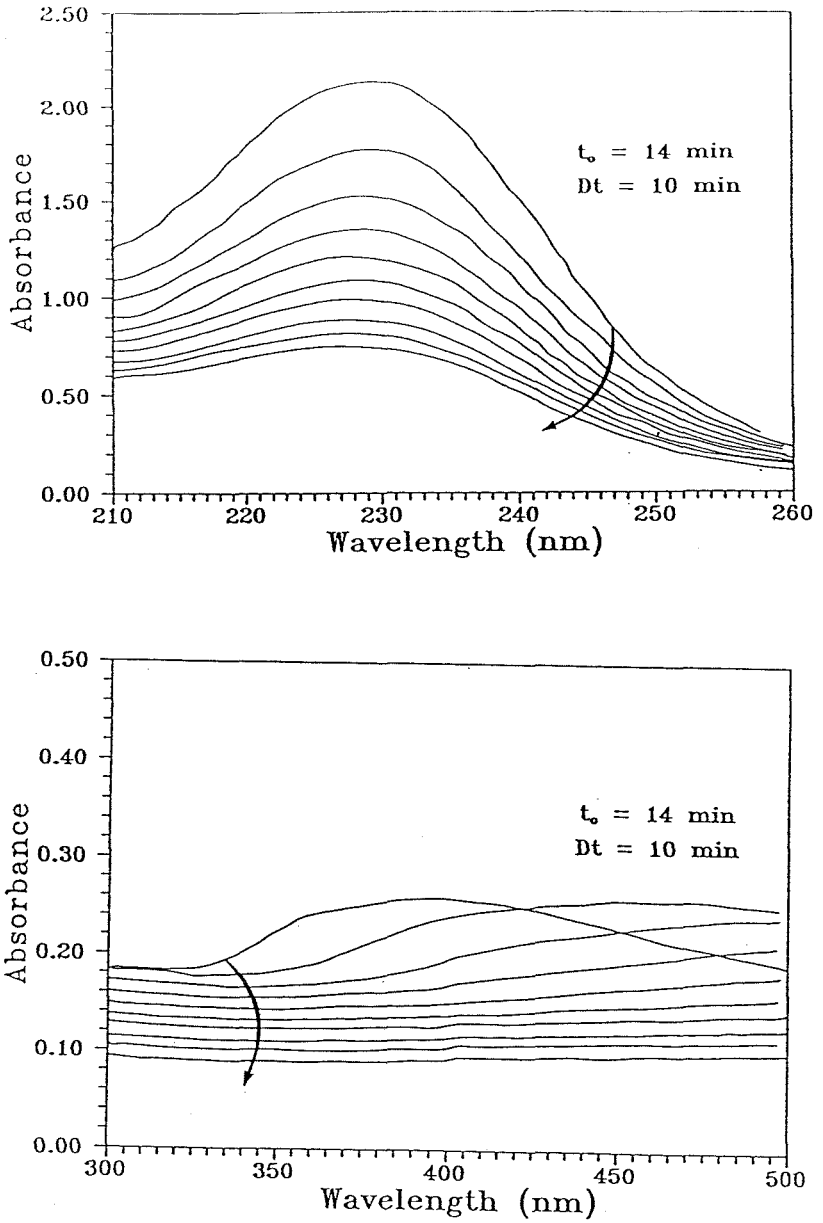

Figure A.4 UV/VIS spectra during a kinetic run in water; $[Ni^{2+}]=3 \cdot 10^{-5}M$, $[S(-II)]=10^{-3}M$, $[O_2]=1.2 \cdot 10^{-3}M$ (oxygen saturation), pH=6.7, T=25 °C; t_o = time corresponding to the first curve, Dt = time increment, arrows indicate direction of reaction.

absorbance into the visible region, no characteristic maxima). During the reaction, this latter absorption decreases suggesting the dissolution (i.e. further oxidation) of the colloidal elemental sulfur.

The decrease in the HS^- absorbance can be correlated to the change in [S(–II)], using the acid/base sulfide equilibria:

$$H_2S \xleftarrow{pK_{a1}} HS^- \xleftarrow{pK_{a2}} S^{2-}$$

$$[S(-II)] = \alpha_1^{-1}[HS^-] \qquad (6)$$

where

$$\alpha_1 = \frac{K_{a1}[H^+]}{([H^+]^2 + K_{a1}[H^+] + K_{a1}K_{a2})} \qquad (7)$$

and K_{a1}, K_{a2} are the first (pK_{a1} = 7.00) and second ($pK_{a2} \geq 14.00$) acid–dissociation constants for H_2S, respectively. The value of pK_{a2} was previously accepted to be about 14.00 (20) but a later spectrophotometric study (21) reports it as 17.00. In any case, $K_{a2} << K_{a1}$ and equation (7) can be simplified to:

$$\alpha_1 = \frac{K_{a1}}{[H^+] + K_{a1}} \qquad (7a)$$

Under the experimental conditions used in this study, pseudo–first–order rate constants can be calculated from linear plots of ln $(A_{HS^-} - A_\infty)$ versus time. These rates (included in Table 1) agree well with those found from the Ag_2S electrode measurements, indicating that both methods respond linearly to the same species (i.e. HS^- or S^{2-}). However, the spectrophotometric analysis at λ = 230 nm leads to slightly lower k_{obs} values, which could be due to interferences by polysulfide ions.

These unstable intermediates have well defined spectra at $\lambda \geq 300$ nm (22–23), but no information about their exact absorbance at $\lambda < 300$ nm is available (22).

Polysulfides are in equilibrium with elemental sulfur (a stable oxidation product in neutral to acidic solutions) and sulfide. They form as intermediates during the autoxidation of sulfide, mainly at neutral pH and high [S(–II)] concentrations (4, 7). The maximum yield of polysulfides at pH 7 with $[O_2] = 1.2$ mM and [S(–II)] = 1.0 mM has been reported to be 14% (23). The most stable species in neutral solutions saturated with S^o have been reported to be the tetra– and pentasulfides, S_4^{2-} and S_5^{2-}, respectively. The ratio of S_4^{2-} : S_5^{2-} was calculated to be 1:5 (23) or 1:1 (22). Lowering the $[S_8]/[S(-II)]$ ratio leads to the formation of tri– or disulfides (22). This behavior is reflected in the spectra shown in Figure 4. Our calculations suggest a conversion of less than 16% of the initial [S(–II)] to tetra– and pentasulfides after 30 minutes of reaction time.

From the experimental results reported by Hong *et al.* (14), an initial rate constant $k_{obs} \simeq 1.5 \cdot 10^{-2}$ min^{-1} can be calculated for the Co(II)TSP catalyzed sulfide autoxidation at pH=9.2, $[S(-II)]_o$=1 mM, $[O_2]_o$=0.25 mM, T=25°C, I=0.4 M, [Co(II)TSP]=0.17 μM. This value is of the same order of magnitude with our results, but lower, as could be expected from the fact that they were working at a higher pH. Experimental results of Hoffmann and Lim (4) indicated that the rate of the reaction is maximum around neutral pH.

Snavely and Blount (5) have studied sulfide autoxidation catalyzed by metal ions in sour water (3.5% NaCl), $[S(-II)]_o$=6.25 mM, $[O_2]_o$=0.19 mM, and at various pH values. A direct comparison of experimental rates is not easy, since they worked at higher sulfide concentrations and $[S(-II)] >> [O_2]$, and they also reported the rate in terms of the zero order decrease in oxygen concentration. Nevertheless,

the rate constants that can be calculated from their data are within the same order of magnitude with ours in the case of Ni^{2+} (about $4 \cdot 10^{-2}$ min^{-1} for $[Ni^{2+}]$=18 μM, pH=6.8, as compared to $1.8 \cdot 10^{-2}$ min^{-1} for $[Ni^{2+}]$=30 μM, pH=6.7), while being one order of magnitude lower for Cu^{2+} (about 10^{-3} min^{-1} for $[Cu^{2+}]$=172 μM, pH=6.4, as compared to 10^{-2} min^{-1} for $[Cu^{2+}]$=100 μM, pH=6.7).

Kinetic results in wastewater

Initial experiments were conducted at 25 °C, pH=7.0, at two different O_2 concentrations 1.2×10^{-3} M (PO_2 = 1 atm) and 2.5×10^{-4} M (PO_2 = 0.21 atm) and initial sulfide concentrations 10^{-4} M and 1.5×10^{-4} M (3.2 and 5 mg/l). Several experiments were performed with autoclaved wastewater to determine the importance of biological sulfide oxidation in situ by microorganisms. Autoclaving was selected as sterilization procedure after comparing the oxidation rates in autoclaved and 0.45μ filtered primary sewage (the latter was faster).

Samples were taken periodically, by syringe, and the [S(–II)]'s were determined with the sulfide ISE (measurements were performed in SAOB). The plots of potential vs time were linear for more than 90% of the reaction. The decrease in $[O_2]$ was directly proportional to the decrease of [S(–II)] in a 2:1 ratio ($[O_2]$ used]:[S(–II) oxidized]) at the completion of the reaction. This indicates that the final oxidation product was sulfate (as expected, since O_2 was in excess).

The pseudo–first–order rate constants (k_{obs}) for different experiments, under oxygen and air saturation are given in Table A.2. The uncatalyzed sulfide oxidation was faster in wastewater than in clean water. The enhanced oxidation rate can be attributed to the activity of the microorganisms and to the catalytic activity of transition metals present in wastewater. The uncatalyzed oxidation

Table A.2

Pseudo first–order rate constants (k_{obs}) for Co(II)TSP catalyzed sulfide oxidation in sewage, under air and oxygen saturation

	Co(II)TSP (μM)	S(–II) (mM)	pH	k_{obs} (min^{-1})	
a) Oxygen saturation ($[O_2]$=1.2 mM)					
primary effluent	0.00	0.1	7.00	$1.97 \cdot 10^{-3}$	a
"	0.00	0.1	7.00	$1.37 \cdot 10^{-3}$	b
"	0.00	0.1	7.00	$3.34 \cdot 10^{-3}$	c
"	0.10	0.1	7.00	$1.18 \cdot 10^{-2}$	c
"	0.10	0.1	7.00	$2.21 \cdot 10^{-2}$	
raw sewage	0.00	0.1	7.00	$1.34 \cdot 10^{-2}$	
"	0.00	0.1	7.00	$1.74 \cdot 10^{-2}$	
"	0.05	0.1	7.00	$2.69 \cdot 10^{-2}$	
"	0.10	0.1	7.00	$2.85 \cdot 10^{-2}$	
"	0.30	0.1	7.00	$3.83 \cdot 10^{-2}$	
"	0.50	0.1	7.00	$4.94 \cdot 10^{-2}$	
"	0.75	0.1	7.00	$6.45 \cdot 10^{-2}$	
"	1.00	0.1	7.00	$7.36 \cdot 10^{-2}$	
b) Air saturation ($[O_2]$=0.25 mM)					
raw sewage	0.00	0.15	7.00	$2.02 \cdot 10^{-2}$	
"	0.10	0.15	7.00	$2.41 \cdot 10^{-2}$	
"	0.40	0.15	7.00	$3.88 \cdot 10^{-2}$	
"	0.75	0.15	7.00	$4.78 \cdot 10^{-2}$	
"	1.00	0.15	7.00	$5.08 \cdot 10^{-2}$	
"	0.00	0.15	7.00	$5.60 \cdot 10^{-3}$	d
"	0.10	0.15	7.00	$1.12 \cdot 10^{-2}$	d
"	0.40	0.15	7.00	$2.75 \cdot 10^{-2}$	d
"	0.75	0.15	7.00	$3.00 \cdot 10^{-2}$	d
"	1.00	0.15	7.00	$4.01 \cdot 10^{-2}$	d

[a] filtered sewage, diluted 1:3
[b] autoclaved, diluted 1:3
[c] diluted 1:3
[d] autoclaved

rates are in good agreement with the rates reported by Wilmot *et al.* (24) for Australian wastewaters (typical k_{obs}'s $\simeq$ 0.02 min^{-1}). They also reported a 12 – 56% reduction in oxidation rate after sterilization, which also agrees with our results.

Co(II)TSP was seen to catalyze S(–II) autoxidation in wastewater and k_{obs} values were similar to those in clean water, as shown in Figure A.5. However, the biological contribution to the net oxidation had to be taken into consideration. Figure A.6 shows that the rate constants for fresh and autoclaved wastewater differ by a constant amount. This difference, 0.0132 min^{-1}, was attributed to the biological component and the fact that it remains constant indicated that the presence of the catalyst does not affect the sulfide–oxidizing microorganisms. When this component is subtracted from the overall rate, a slight loss of catalytic activity of Co(II)TSP compared to clean systems is noted (Figure 5). This is in agreement with findings of Hong *et al.* (14) that Co(II)TSP is a less efficient catalyst for the oxidation of HS^- in heterogeneous systems than in homogeneous solutions. The dependence of the corrected Co(II)TSP–catalyzed oxidation rate, $k_{obs}' = k_{obs} - 0.0132$, on [Co(II)TSP] was found to be non–linear. Double logarithmic plots of k_{obs}' versus [Co(II)TSP] show an apparent reaction order, β,

$$k_{obs}' = k_i \cdot [\text{Co(II)TSP}]^{\beta} \qquad (8)$$

of 0.60 (r^2 = 0.982) and 0.55 (r^2 = 0.991) in wastewater at oxygen and air saturation respectively. The order was 0.53 (r^2 = 0.965) for air–saturated autoclaved wastewater. All these values are quite close to the expected value of 0.5 for clean water.

In the case of filtered primary effluent, the sulfide concentration was followed spectrophotometrically and pseudo–first–order rate constants were obtained from linear plots of $\ln(A_{HS^-} - A_\infty)$ versus time and were found to be in agreement with

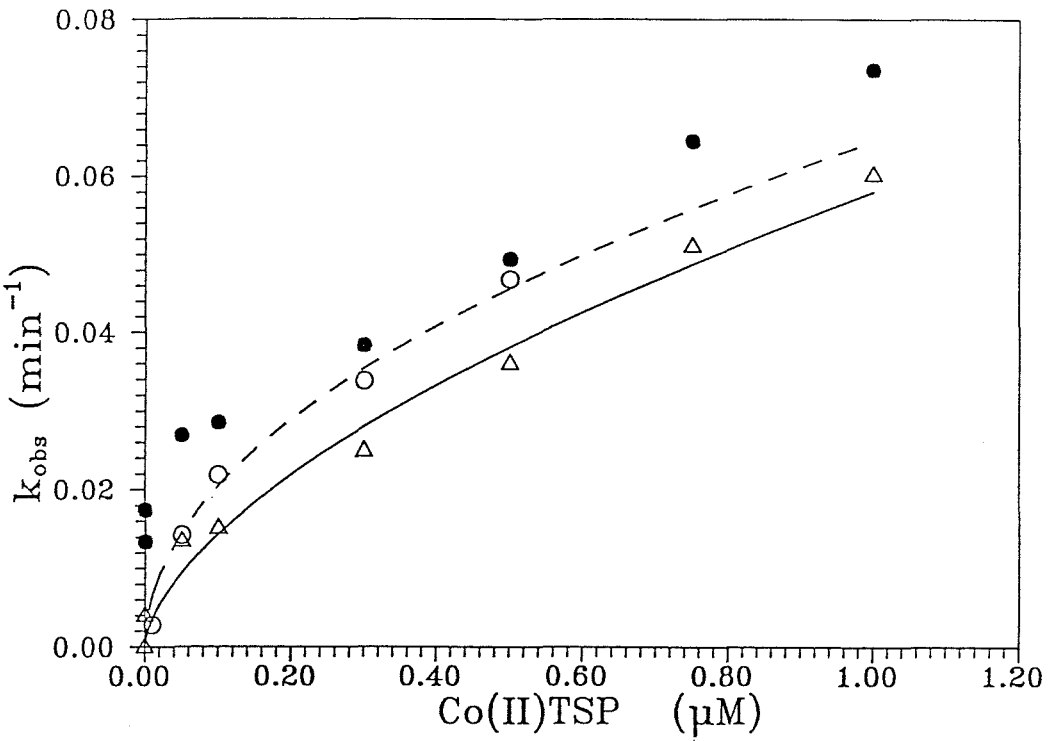

Figure A.5 Co(II)TSP–catalyzed sulfide oxidation; comparison between water and wastewater; open circles, dashed line: water data, closed circles: wastewater raw data, open triangles, solid line: wastewater data corrected for biological component. T=25°C, neutral pH, oxygen saturation, $[S(-II)]_o = 100\ \mu M$.

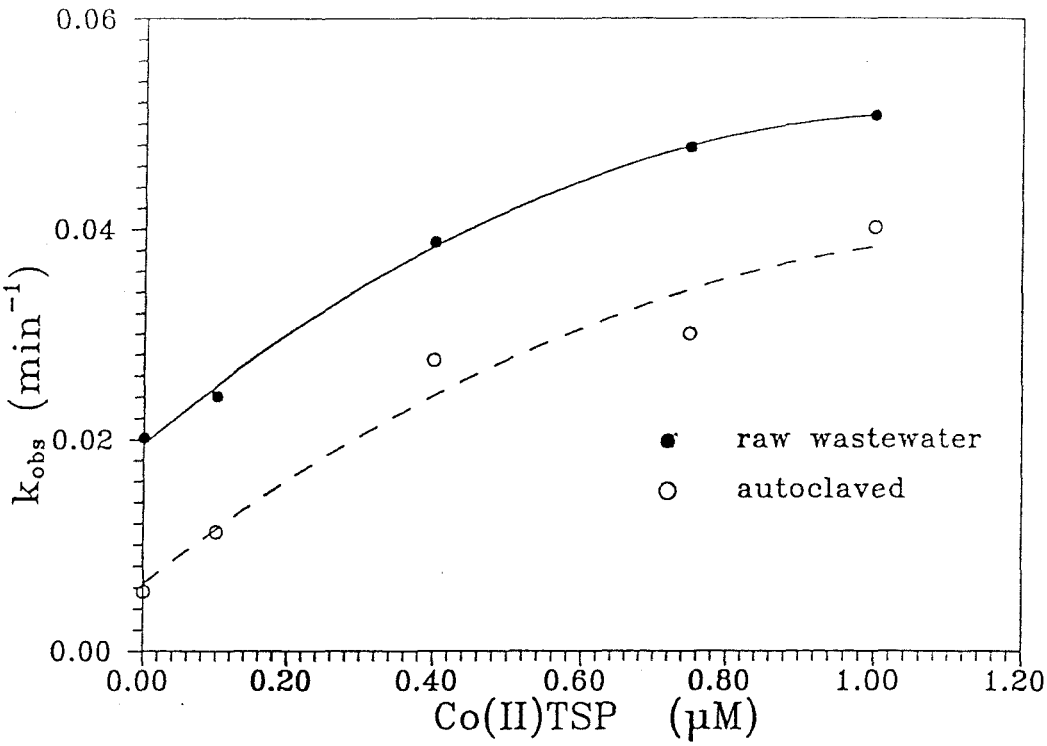

Figure A.6 Co(II)TSP–catalyzed sulfide oxidation; comparison between raw and autoclaved wastewater. T=25°C, neutral pH, air saturation, $[S(-II)]_o = 150\ \mu M$.

those obtained from the ISE measurements. However, the spectrophotometric analysis was not possible in the case of fresh or autoclaved sewage due to the high turbidity of the solution.

A series of experiments was conducted at lower oxygen concentrations (below air saturation). Figure A.7 shows the dependence of k_{obs} on the oxygen concentration at T = 25 °C, pH = 7.0, $[S(-II)]_o = 1.5 \cdot 10^{-4}$ M, [Co(II)TSP] = 1 μM (0.059 mg/l as Co^{+2}). In the few experiments where S(–II) was not in excess care was taken to determine k_{obs} within the initial stage of the reaction so as to minimize the error inherent in assuming constant [S(–II)]. As expected, the oxidation of sulfide was faster in fresh wastewater as compared to autoclaved wastewater. For the catalyzed oxidation, the oxidation rate increased with increasing initial oxygen concentration for $[O_2] < 3$ ppm but was essentially constant at higher $[O_2]$. A similar trend was also observed for the uncatalyzed reaction.

If a dependence of the form

$$k_{obs} = k_m [O_2]^{\gamma} \qquad (9)$$

is assumed, γ can be found from a double–logarithmic plot of k_{obs} against initial $[O_2]$. Using this approach a fractional reaction order (γ) of 0.55 ($r^2 = 0.97$) and 0.58 ($r^2 = 0.90$) was found for the uncatalyzed and catalyzed sulfide oxidation, respectively. These values are consistent with the value of 0.56 reported by Chen and Morris (6) for sulfide oxidation in buffered water.

Alternatively, a bisubstrate Michaelis–Menton rate law can be used (4, 24) and then,

$$k_{obs} = \frac{k \cdot [O_2]}{K + [O_2]} \qquad (10)$$

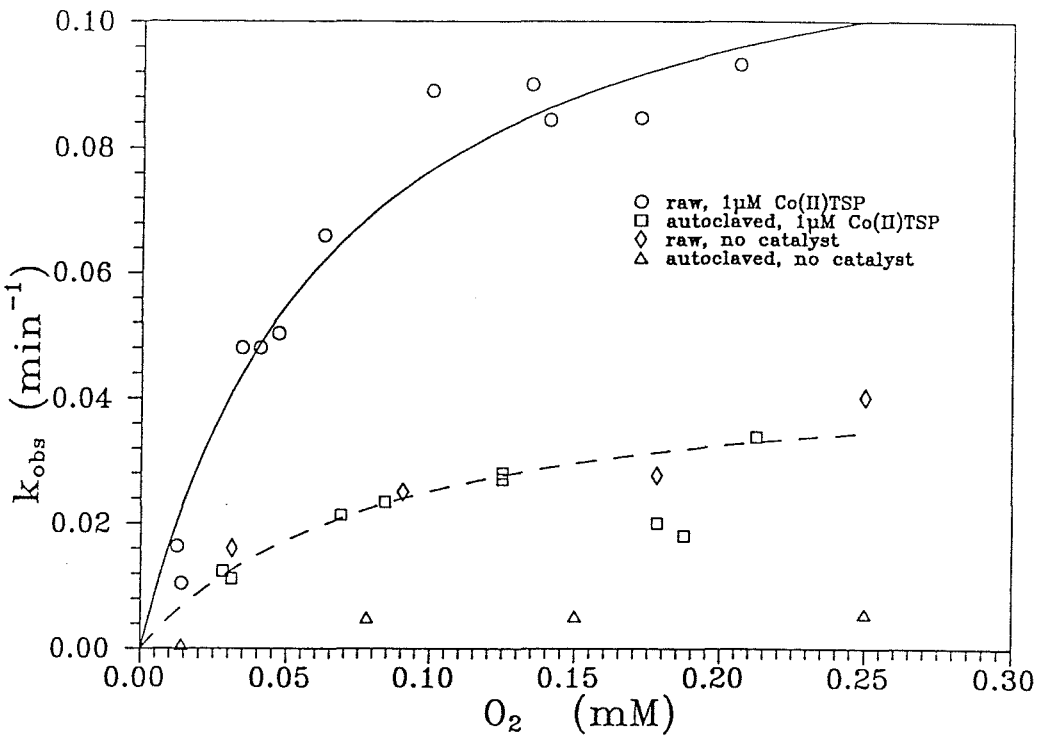

Figure A.7 Dependence of k_{obs} on $[O_2]$ for sulfide oxidation in wastewater; T=25°C, neutral pH, $[S(-II)]_o = 150\ \mu M$

k and K can be calculated by plotting k_{obs} vs $-k_{obs}/[O_2]$. Such a plot should give a straight line of slope K and intercept k. Using this approach, the following values were calculated:

uncatalyzed sulfide oxidation : $k = 0.0458\ min^{-1}$, $K = 74\ \mu M$ (2.64 ppm)

catalyzed ($1\mu M$ CoTSP) " : $k = 0.126\ min^{-1}$, $K = 65\ \mu M$ (2.07 ppm)

The values for the uncatalyzed S(–II) oxidation are in general agreement with the values reported by Wilmot *et al.* (24) (k ranging from 0.024 to 0.087, $K = 94\ \mu M$) for various Australian wastewaters. The curves shown in Figure A.7 have been calculated using the above constants (k and K). Table A.3 summarizes the pseudo–first–order rate constants for different oxygen concentrations.

Figure A.8 shows spectra of Co(II)TSP ($10\mu M$) in deionized water and in wastewater (after filtration with a 0.2 μ filter). The visible spectrum of Co(II)TSP has a characteristic double hump. The absorption bands at 625 nm and 670 nm have been attributed to the dimer and the summation of monomeric species (16, 25–26). The spectra of Fig. A.8 show that the catalyst adsorbs partially onto particles in wastewater (both peaks are lower for the latter case) but not to a great extent. Using $\epsilon_{625} = 1.9 \times 10^5\ M^{-1}cm^{-1}$ and $\epsilon_{663} = 1.03 \times 10^5\ M^{-1}cm^{-1}$ for the dimer $\{[Co(II)TSP]_2\}$ and the monomer $\{Co(II)TSP\}$, respectively (26), it can be calculated that approximately 80% of the total catalyst remains in solution.

Spectra taken at different times after the addition of sulfide in oxygenated, Co(II)TSP containing, deionized water solution showed an absorption shift from 636 nm to 670 nm. That can be explained by a shift in the monomer/dimer equilibrium, upon coordination of HS^- and O_2 at the Co(II) center. The monomer appears to be the catalytically active species as it is also indicated by the approximately half order dependence of the oxidation reaction on Co(II)TSP (15).

Table A.3

Pseudo first–order rate constants (k_{obs}) for Co(II)TSP catalyzed sulfide oxidation in raw sewage, and low oxygen concentrations

O_2 (ppm)	Co(II)TSP (μM)	k_{obs} (min^{-1})	Comments
0.1	0.0	< 0.001	A *
0.1	0.5	< 0.001	C
0.1	1.0	< 0.001	A
0.1	0.0	< 0.001	A [a]
0.1	1.0	< 0.001	A [a]
0.4	1.0	0.00945	B
0.45	1.0	0.01040	B
0.45	0.0	0.00055	A [a]
0.9	0.0	0.01240	B
1.0	0.5	0.03300	C
1.0	0.0	0.01120	A
1.0	1.0	0.01600	A [a]
1.1	1.0	0.04800	B
1.3	1.0	0.04800	B
1.5	1.0	0.05030	A
2.0	1.0	0.06600	B
2.0	0.5	0.07220	C
2.2	0.0	0.02130	B
2.5	0.0	0.00500	A [a]
2.7	0.0	0.02340	B
2.9	1.0	0.02500	A [a]
3.2	1.0	0.08900	B
4.0	0.0	0.02700	B
4.0	0.0	0.02800	B
4.3	1.0	0.09000	B
4.5	1.0	0.08440	B
4.8	0.0	0.00520	A [a]
5.5	1.0	0.08470	B
5.7	0.0	0.02000	B
5.7	1.0	0.02760	A [a]
6	0.0	0.01800	B
6.6	1.0	0.09320	B
6.8	0.0	0.03380	B
7.6	1.0	0.07750	A

* A, B, C represent different batches of raw sewage
[a] autoclaved
All experiments at $[S(-II)]_o = 150\ \mu M$

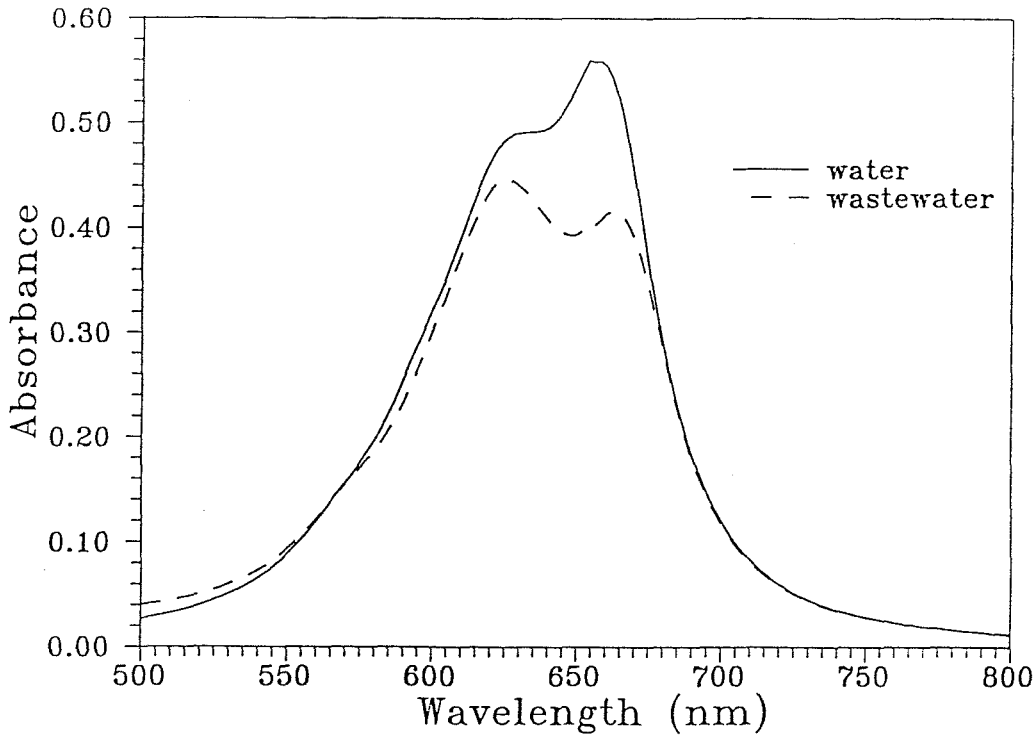

Figure A.8 UV/VIS spectra of Co(II)TSP in water and wastewater; [Co(II)TSP]= 10^{-5}M

Spectra taken during the experiments with wastewater at low oxygen concentrations indicate that there is no loss of the catalyst during the reaction.

The reproducibility of the experiments with wastewater was reasonable. Samples were collected from the inlet at the San Jose Creek Water Reclamation Plant and were kept refrigerated (at temperature near 0 °C) in sealed containers until they were used for experiments. The pH and DO remained constant for a period of 1 – 2 weeks. Most experiments were conducted within a week from the collection of the samples. Experimental rate constants exhibited some variability for different samples (i.e. samples collected on different occasions) but were consistent for all the experiments conducted with the same batch of wastewater. Furthermore, the general trends were the same even for samples from different batches of raw wastewater.

Mechanism

The mechanism of the Co(II)TSP–catalyzed oxidation of reduced sulfur compounds by dioxygen has been discussed previously (4, 14–16). The catalyzed autoxidation of S(–II) appears to proceed via the following ternary complex mechanism:

$$(\mathrm{Co(II)TSP})_2^{4-} \overset{K_d}{\rightleftharpoons} 2\ \mathrm{Co(II)TSP}^{2-} \qquad (11)$$

$$\mathrm{Co(II)TSP}^{2-} + \mathrm{HS}^- \overset{K_1}{\rightleftharpoons} \mathrm{(HS)Co(II)TSP}^{3-} \qquad (12)$$

$$\mathrm{(HS)Co(II)TSP}^{3-} + \mathrm{O_2} \underset{k_{-2}}{\overset{k_2}{\rightleftharpoons}} \mathrm{(HS)Co(III)TSP}(\mathrm{O_2}^{\cdot})^{3-} \qquad (13)$$

$$(HS)Co(III)TSP(O_2^{\cdot-})^{3-} + HS^- \underset{k_{-3}}{\overset{k_3}{\rightleftharpoons}} (HS)Co(III)TSP(O_2^{\cdot-})(HS)^{4-} \qquad (14)$$

$$(HS)Co(III)TSP(O_2^{\cdot-})(HS)^{4-} \xrightarrow[slow]{k_4} (HS)Co(II)TSP(O_2^{2-})^{5-} + S^0 + H^+ \qquad (15)$$

$$(HS)Co(II)TSP(O_2^{2-})^{5-} + 2\,H^+ \xrightarrow[fast]{k_5} (HS)Co(II)TSP^{3-} + H_2O_2 \qquad (16)$$

$$HS^- + H_2O_2 + H^+ \longrightarrow \tfrac{1}{8}S_8 + 2\,H_2O \qquad (17)$$

$$HS^- + 4\,H_2O_2 \longrightarrow SO_4^{2-} + 4\,H_2O + H^+ \qquad (18)$$

The catalytic activity of Co(II)TSP toward S(–II) autoxidation involves *1*) the dissociation of the dimeric form of the catalyst into the monomeric form (eq. 11), *2*) the complexation of the bisulfide ion (HS^-) in an open axial coordination site on the central metal atom (eq. 12), *3*) the binding of dioxygen in a position *trans* to the bound HS^-, and the simultaneous electron delocalization from the cobalt center to the bound dioxygen (superoxide formation, eq. 13), *4*) the formation of a ternary adduct with another HS^- molecule (eq. 14), *5*) the oxidative transfer of two electrons from HS^- to the Co(III)–O_2^- moiety resulting in the formation of elemental sulfur as S^o and the release of a proton (eq. 15), and *6*) the protonation of the bound O_2^{2-} to form hydrogen peroxide (eq. 16). Elemental sulfur can be further oxidized to thiosulfate and sulfate. Hydrogen peroxide, which is generated as an intermediate in the above reaction sequence, reacts with S(–II) according to the

stoichiometries reported previously (7) (eqs. 17–18).

The mechanism given in eqs. 11–16 leads to the following theoretical rate expression (15):

$$-\frac{d[S(-II)]}{dt} = \frac{k'K'\left[(Co(II)TSP)_2^{4-}\right]^{\frac{1}{2}}[O_2]\,[HS^-]}{K_A + K_B[O_2] + K_C[HS^-] + [O_2][HS^-]} \qquad (19)$$

where

$$k' = \frac{k_4 k_5}{k_4 + k_5}$$

$$K' = K_1 K_d^{\frac{1}{2}}[HS^-]$$

$$K_A = \frac{k_5(k_{-2}k_{-3} + k_{-2}k_4)}{k_2 k_3(k_4 + k_5)}$$

$$K_B = \frac{k_5(k_{-3} + k_4)}{k_3(k_4 + k_5)}$$

$$K_C = \frac{k_4 k_5}{k_2(k_4 + k_5)}$$

The theoretical rate expression can be simplified for pseudo–first–order conditions, and it is consistent with our empirical observation of eq. 10.

Two possible mechanisms have been suggested for the catalysis of S(–II) autoxidation by transition metal ions (10) *1*) electron transfer leading to free

radical formation, or *2*) formation of metal–sulfide complexes leading to sulfur precipitation. We believe that catalysis of S(–II) autoxidation by $Cu(H_2O)_6^{2+}$ and presumably by $Ni(H_2O)_6^{2+}$ is initiated by an outer–sphere electron transfer from HS^- to the hexaaquo metal ion to form $HS^\cdot$ radical. The $HS^\cdot$ radical is oxidized further by a free radical chain sequence involving oxygen as shown below:

$$Cu^{2+} + HS^- \longrightarrow Cu^+ + HS^\cdot \quad (20)$$

$$HS^- + O_2 \longrightarrow HS^\cdot + O_2^{-\cdot} \quad (21)$$

$$HS^\cdot + O_2 \longrightarrow HSO_2^\cdot \quad (22)$$

$$HSO_2^\cdot + O_2 \longrightarrow HSO_4^\cdot \quad (23)$$

$$HSO_4^\cdot + O_2 \longrightarrow HSO_4^- + O_2 \quad (24)$$

$$2\ HS^\cdot \longrightarrow H_2S_2 \quad (25)$$

$$H_2S_2 \rightleftharpoons 2\ H^+ + S_2^{2-} \quad (26)$$

$$HS^- + HS^\cdot \longrightarrow H_2S_2^{-\cdot} \quad (27)$$

$$H_2S_2^{-\cdot} + O_2 \longrightarrow H_2S_2 + O_2^{-\cdot} \quad (28)$$

$$H_2S_2 + O_2 \longrightarrow H_2O_2 + S_2 \quad (29)$$

A similar free radical pathway has been proposed by Chen and Morris (6).

CONCLUSIONS

Co(II)TSP is a substantially more effective catalyst for the autoxidation of sulfide than Ni^{2+} and Cu^{2+} ions. Spectrophotometric measurements provide evidence for the production of intermediates such as elemental sulfur (S_8) and polysulfides (S_2^{2-}, S_3^{2-}, S_4^{2-}, S_5^{2-}). When $[O_2] >> [S(-II)]$ the stoichiometry of the reaction is 2:1 ([O_2 used]:[S(–II) oxidized]) with SO_4^{2-} formed as the product. When $[O_2] \simeq [S(-II)]$ the reaction stoichiometry is 1:1 and elemental sulfur is formed as one of the products.

The uncatalyzed oxidation of sulfide by molecular oxygen was found to be faster in wastewater than in clean water. This difference was attributed to microbial oxidation of S(–II) and to catalytic action of transition metals present in wastewater. Co(II)TSP has been shown to catalyze the autoxidation of sulfide in wastewater. The reaction rate is first order with respect to total sulfide and has a fractional (0.55) dependency on the catalyst.

Our results suggest that Co(II)TSP can be used for H_2S control in sewers in conjunction with oxygen or compressed air injection. Because of the relatively high value of the Michaelis–Menton rate constant K, maximum advantage of the catalyst is taken when dissolved oxygen levels are about 4 ppm or higher. On the other hand, even at the low oxygen concentrations typically encountered in sewers ($\leq$ 1 ppm) sulfide oxidation rates more than double in the presence of 1μM of Co(II)TSP.

Acknowledgments

Many thanks to Dr. Jochen Kraft for the preparation of the catalyst and his valuable contribution in the initial stage of this work. We gratefully acknowledge the financial support of the County Sanitation Districts of Los Angeles County (CDS Contract No. 2966). We also thank the reviewers of this manuscript for useful comments and suggestions.

References

1. "Sulfide in Wastewater Collection and Treatment Systems"; ASCE Manuals and Reports on Engineering Practice No. 69. American Society of Civil Engineers: New York, 1989.
2. Thistlethwayte, D. K. *The control of sulphides in Sewerage Systems.* Butterworth, Sydney, 1972.
3. Pomeroy, R.; Bowlus, F. D. *J. Sewage Works* 1946, *18, 4*, 597.
4. Hoffmann, M. R.; Lim, C. H. *Environ. Sci. Technol.* 1979, *13*, 1406.
5. Snavely, E. S.; Blount, F.E. *Corrosion* 1969, *25*, 397.
6. Chen, K. Y.; Morris, J. C. *Environ. Sci. Technol.* 1972, *6*, 529.
7. Hoffmann, M. R. *Environ. Sci. Technol.* 1977, *11*, 61.
8. Hoffmann, M. R.; Edwards, J. O. *Inorg. Chem.* 1977, *16*, 3333.
9. McArdle, J. V.; Hoffmann, M. R. *J. Phys. Chem.* 1983, *87*, 5425.
10. Chen, K. Y.; Morris, J. G. *Journal of the San. Eng. Div., Proc. ASCE* 1972, *SA1*, 215.
11. Weres, O.; Tsao, L.; Chatre, R. M. *Corrosion* 1985, *41*, 307.
12. Dohnalek, D. A.; FitzPatrick, J. A. *J. Am. Water Works Assoc.* 1983, *65*, 298.
13. O'Brien, D. J.; Birkner, F. B. *Environ. Sci. Technol.* 1977, *11*, 1114.
14. Hong, A. P.; Boyce, S. D.; Hoffmann, M. R. *Environ. Sci. Technol.* 1989, *23*, 533.
15. Boyce, S.D.; Hoffmann, M. R.; Hong, P. A.; Moberly, L. M. *Environ. Sci. Technol.* 1983, *17*, 602.
16. Leung, K.; Hoffmann, M. R. *Environ. Sci. Technol.* 1988, *22*, 275.
17. Weber, J. H.; Busch, D. H. *Inorg. Chem.* 1965, 4, 469.

18. Baumann, F.; Bienert, B. U.S. Patent No. 2,613,128, 1952.

19. Moore, J. W.; Pearson, R. G. *Kinetics and Mechanism,* 3rd ed.; Wiley, New York, 1981.

20. Ellis, A. J.; Golding, R. M. *J. Chem. Soc.* (London) 1959, 127.

21. Giggenbach, W. *Inorg. Chem.* 1971, *7*, 1333.

22. Giggenbach, W. *Inorg. Chem.* 1972, *5*, 1201.

23. Chen, K. Y.; Gupta, S. K. *Environmental Letters* 1973, *4,3*, 187.

24. Wilmot, P. D., *et al. Journal WPCF* 1988, *60*, 7, 1264.

25. Bernauer, K.; Fallab, S. *Helv. Chim. Acta* 1961, *44*, 1287.

26. Wagnerova, D. M.; Blanck, J.; Veprek–Siska, J. *Collection Czechoslov. Chem. Commun.* 1982, *47*, 755.

APPENDIX B

Peroxymonosulfate: An alternative to hydrogen peroxide for the control of hydrogen sulfide

(***Research Journal of Water Pollution Control Federation***, *in print*)

ABSTRACT

The oxidation of total dissolved sulfide, where S(–II) = H_2S + HS^- + S^{2-}, by peroxymonosulfate, HSO_5^-, has been studied in wastewater. Peroxymonosulfate was found a more rapid and efficient oxidant of S(–II) than either H_2O_2 or Fe(II). The combination of peroxymonosulfate and hydrogen peroxide was additive in terms of S(–II) oxidation, while the combination of peroxymonosulfate and Fe(II) resulted in a decrease in the effectiveness of Fe(II) as an oxidant. Peroxymonosulfate has been shown to be a viable alternative to H_2O_2 for the control of sulfide–induced corrosion in concrete sewers.

KEYWORDS

corrosion, hydrogen sulfide, oxidation, peroxymonosulfate, sewers, wastewater.

INTRODUCTION

Hydrogen sulfide (H_2S) gas generation in sewers, the subsequent production of sulfuric acid (H_2SO_4) on concrete sewer crowns and the resultant corrosion of the structural components are problems often encountered in wastewater collection systems (ASCE, 1989; Thistlethwayte, 1972; Pomeroy and Bowlus, 1949). Current strategies for the control of hydrogen sulfide gas in sewers involve chemical, biochemical, and physical treatment schemes that are designed to suppress H_2S generation, to retard or prevent H_2S oxidation to H_2SO_4 on sewer crowns, to trap H_2S in the flowing wastewater, or to oxidize H_2S in the liquid phase in order to prevent its transfer into the gas phase.

Aeration of wastewater, by compressed air or pure oxygen, is one of the control measures commonly employed in sewers to oxidize sulfides while still in the liquid phase (ASCE, 1989). Nevertheless, the oxidation of reductants such as H_2S by O_2 proceeds slowly in the absence of catalysts (Chen and Morris, 1972a,b; Snavely and Blount, 1969; Weres *et al.*, 1985) because of unfavorable spin state symmetries that result from the differences in the electronic configurations of the reactants (Hoffmann and Lim, 1979). More powerful (i.e. $E^o > 1.29$ V) oxidants than O_2 can be used to achieve a faster rate of oxidation of H_2S (Hoffmann, 1977; Dohnalek and FitzPatrick, 1983). The oxidant that is most commonly used for the control of sulfides in wastewater collection systems is hydrogen peroxide. The effectiveness of H_2O_2 depends on the degree of sulfide control required and the concentration of compounds, other than sulfide, that are present in the wastewater in a reduced state and will compete for H_2O_2. Large scale applications of H_2O_2 for S(–II) control in sewers have shown that stoichiometric ratios of $\geq$ 6:1

($[H_2O_2]$:[S(–II)]) are required to keep [S(–II)] ≤ 0.2 ppm (ASCE, 1989).

Peroxymonosulfate ion, a monosubstituted derivative of hydrogen peroxide, ($HOOSO_3^-$) is often more reactive kinetically than HOOH, even though it is only slightly more powerful as an oxidant [$E^\circ_{HSO_5^-/HSO_4^-}$ = + 1.82 V; $E^\circ_{H_2O_2/H_2O}$ = + 1.776 V (Balej, 1984; Steele, 1982; Spiro, 1979)]. In addition to its enhanced reactivity, HSO_5^- appears to be more stable than H_2O_2 with respect to spontaneous decomposition in water. Peroxymonosulfate is commercially available as a free–flowing powder known by the trade names Oxone (DuPont) or Curox (Interox). These products are triple salts with the composition $2KHSO_5 \cdot KHSO_4 \cdot K_2SO_4$. Simple peroxymonosulfate salts (i.e. $KHSO_5$) are difficult to prepare.

Betterton and Hoffmann (1990) have recently studied the kinetics of S(–II) oxidation by peroxymonosulfate, HSO_5^-, in pure water over the pH range of 2.0 to 6.3. They reported that the reaction of HSO_5^- with S(–II) is 3–4 orders of magnitude faster than the corresponding reaction with H_2O_2. Peroxymonosulfate could thus be a viable alternative to H_2O_2 for the control of sulfide–induced corrosion in concrete sanitary sewers and wastewater treatment facilities but its effectiveness and its specificity for oxidation of S(–II) in actual wastewater had not been studied before.

The effectiveness of HSO_5^- for H_2S oxidation was studied in wastewater obtained from the influent of a tertiary wastewater treatment plant in Los Angeles County and compared to that of H_2O_2. The effective molar stoichiometry of oxidant used to total sulfide oxidized, i.e., $[HSO_5^-]_{used}$:$[S(-II)]_{oxidized}$, as a function of the ratio of the initial concentrations of HSO_5^- and S(–II), $[HSO_5^-]_o$:$[S(-II)]_o$, was also examined. Combined reagent additions, where peroxymonosulfate was used

together with another chemical reagent (H_2O_2, $FeCl_2$, or $S_2O_8^{=}$), were investigated in water and wastewater in order to determine optimal conditions for HSO_5^- application. Control kinetic experiments following the oxidation of S(–II) in the presence of H_2O_2 and $FeCl_2$ were conducted in both clean water and wastewater.

EXPERIMENTAL

Reagents

All reagents were of analytical grade. Doubly–distilled (18 MΩ–cm) deionized water was used for the preparation of buffer solutions and for clean water experiments. S(–II) stock solutions were prepared from $Na_2S \cdot 9H_2O$ crystals (Aldrich) that had been cleaned with deionized water and lightly dried with absorbent paper. The actual concentrations were determined by potentiometric titration with $Pb(ClO_4)_2$ (Orion) or $AgNO_3$. Stock solutions were stored in a refrigerator and no significant decrease in sulfide concentration was detected during a period of approximately 10 days. Mono and disodium phosphate salts, acid phthalate salts (Mallinckrodt), borate (Spectrum), sodium hydroxide and hydrochloric acid (Baker) were used for the preparation of the buffers. A triple salt commercially available by the name of Oxone (Aldrich) was used as source of peroxymonosulfate ($2\ KHSO_5 \cdot KHSO_4 \cdot K_2SO_4$). Peroxymonosulfate solutions were prepared by dissolving Oxone in a portion of the appropriate buffer and adjusting the pH (if necessary) with NaOH before making up to the mark in a volumetric flask. Ferric and ferrous chloride and sodium persulfate were purchased from Baker, and hydrogen peroxide stocks were prepared from a 30% solution (Mallinckrodt).

Apparatus

Experimental techniques and apparatus used in this study were similar to those described previously (e.g., Chen and Morris, 1972; Hoffmann, 1977). Experiments were conducted in sealed water–jacketed, glass reaction vessels with total volumes ranging from 50 to 1600 ml. The design and operation of the batch reactor system have been described previously (Hoffmann and Lim, 1979; Kotronarou and Hoffmann, 1991).

Oxygen concentrations were measured with an ORION 97–08–00 oxygen electrode. Sulfide concentrations were measured with a sulfide ion electrode (ORION 94–16 Ag/Ag_2S with double junction reference electrode) coupled to an ORION 801–A ion analyzer. pH measurements were performed with a RADIOMETER pH electrode and a PHM84 pH meter. The temperature was maintained constant with the use of a HAAKE A80 water circulation and temperature controlling system. Hydrogen peroxide concentrations in stock solutions were determined iodometrically (Allen, 1952). Spectrophotometric measurements were performed on an HP 8450A UV/VIS spectrophotometer.

All instruments were interfaced to an IBM–AT computer for data collection. Oxygen concentration and pH were monitored continuously during the kinetic experiments. Samples from the reaction vessel were taken periodically (syringes, septa) and analyzed for sulfide after a 1:1 dilution with sulfide antioxidant buffer (SAOB; a mixture of 67 g of Na_2EDTA, 35 g ascorbic acid, and 80 g of NaOH in 1 L).

All electrodes were calibrated at regular time intervals and showed no significant drift with time. The sulfide ion specific electrode (ISE) was calibrated both for clean water and wastewater. The EMF versus concentration response of

the electrode was found to follow the Nernst equation with similar slopes in both systems.

RESULTS AND DISCUSSION

Sulfide oxidation in raw wastewater

Wastewater samples were collected from the inlet at the San Jose Creek Water Reclamation Plant. Raw wastewater was kept refrigerated (at temperatures near 0 °C) in sealed containers until it was used for experiments. The pH and DO remained constant for a period of 1 – 2 weeks and were around 7.5 and less than 1.5 ppm respectively. Most experiments were conducted within a week from the collection of the samples.

As we have reported previously (Kotronarou and Hoffmann, 1991), the oxidation of S(–II) in raw wastewater with no added catalyst or oxidant had an apparent first order rate with respect to S(–II) (i.e., $d[S(-II)]/dt = -k_{obs} \cdot [S(-II)]$) and was faster than in clean water. Table B.1 presents typical observed first–order reaction constants calculated from kinetic experiments where the disappearance of S(–II) in sulfide–spiked wastewater was followed with time. These constants are consistent with the oxidation rates observed in our previous work where wastewater from the same treatment plant was used (Kotronarou and Hoffmann, 1991). They are also in good agreement with the rates reported by Wilmot *et al.* (1988) for various Australian wastewaters (e.g., $k_{obs} \simeq 0.02$ min^{-1}).

Experimental rate constants exhibited a certain variability especially for different batches (i.e. samples collected on different occasions) but the general trends were the same and the oxidation rates for the same batch differed by less

Table B.1

Pseudo–first–order rate constants (k_{obs}) for the oxidation of sulfide in wastewater

Sample #	pH	$[S(-II)]_o$ (μM)	k_{obs} (min^{-1})	Comments
1	9.8	100	$2.76 \cdot 10^{-2}$	same day collection
2	9.8	100	$3.40 \cdot 10^{-3}$	sample #1 stored overnight at pH = 9.8
2	9.8	100	$7.14 \cdot 10^{-4}$ *	
3	7.5	200	$3.04 \cdot 10^{-2}$	sample #1 four days after collection
3	7.5	200	$2.20 \cdot 10^{-2}$	
3	7.5	200	$2.70 \cdot 10^{-2}$	
3	7.5	200	$2.30 \cdot 10^{-2}$	
4	9.4	200	$2.04 \cdot 10^{-2}$	same day collection
4	9.4	200	$2.27 \cdot 10^{-2}$	
4	9.4	400	$8.30 \cdot 10^{-3}$	
5	9.5	100	$2.40 \cdot 10^{-2}$	sample #4 stored overnight
5	9.5	100	$1.80 \cdot 10^{-2}$	
5	9.3	100	$1.53 \cdot 10^{-2}$	
5	9.3	100	$1.58 \cdot 10^{-2}$	
6	9.3	100	$2.42 \cdot 10^{-2}$	sample #5 stored overnight; supernatant
7	9.3	100	$2.86 \cdot 10^{-2}$	sample#5 stored overnight;contents mixe
8	9.3	100	$5.10 \cdot 10^{-2}$	sample #4 two days after collection
8	9.6	800	$6.40 \cdot 10^{-3}$	
9	9.3	100	$4.40 \cdot 10^{-2}$	sample #4 three days after collection
10	9.4	200	$4.90 \cdot 10^{-2}$	sample #9 stored for 5 days
11	7.3	100	$3.40 \cdot 10^{-2}$	same day collection
12	7.2	100	$3.10 \cdot 10^{-2}$	sample #11 stored overnight
13	7.1	100	$2.30 \cdot 10^{-2}$	sample #11 stored for 7 days

* reaction at T = 4 °C in dark

Samples were stored in dark, at T < 4 °C and unless it is stated otherwise no buffer was added during storage (typical pH of raw wastewater samples ≃ 7.5). To achieve pH ≃ 9.5 borate buffer was added (20% per solution volume for pH ≃ 9.4, 30% for pH ≃ 9.8) before the kinetic experiment. All kinetic experiments were performed at T = 25 °C.

than 20%. The observed uncatalyzed oxidation rates generally increased with time, even when wastewater was stored near T = 0 °C. A slow generation of S(–II) during storage was also noticed (less than 100 μM = 3.2 ppm in about 1 month). Uncatalyzed oxidation rates were lower for samples stored at pH 10 (30% borate buffer pH 10). Furthermore, the observed rate decreased with initial sulfide concentration, $[S(-II)]_o$. This can be explained by the fact that the biological component of the oxidation (i.e., oxidation of sulfide by microorganisms present in the wastewater) is not expected to increase continuously with increasing [S(–II)].

Peroxymonosulfate experiments

· ***Kinetics***

The total sulfide, S(–II), is present in the form of H_2S, HS^- or S^{2-}. The relative amounts of these three species depend on the pH of the solution based on the acid/base sulfide equilibria:

$$H_2S \xleftarrow{pK_{a1}} HS^- \xleftarrow{pK_{a2}} S^{2-} \qquad (1)$$

where K_{a1}, K_{a2} are the first (pK_{a1} = 7.00) and second (pK_{a2} = 17.00) acid–dissociation constants for H_2S, respectively. The value of pK_{a2} was previously accepted to be ~ 14 (Smith and Martell, 1976), but an earlier spectrophotometric study (Giggenbach, 1971) reported it to be 17.00. It now seems clear that pK_{a2} is much higher than 14 and that S^{2-} is not present at appreciable concentrations even in basic solutions (Myers, 1986). Therefore, the species S^{2-} can be neglected for all practical purposes, and the concentrations of H_2S and HS^- are given by:

$$[H_2S] = \alpha_0[S(-II)] \qquad (2)$$

$$[HS^-] = \alpha_1[S(-II)] \quad (3)$$

where

$$\alpha_0 = \frac{[H^+]^2}{([H^+]^2 + K_{a1}[H^+] + K_{a1}K_{a2})} \simeq \frac{[H^+]}{[H^+] + K_{a1}} \quad (4)$$

$$\alpha_1 = \frac{K_{a1}[H^+]}{([H^+]^2 + K_{a1}[H^+] + K_{a1}K_{a2})} \simeq \frac{K_{a1}}{[H^+] + K_{a1}} \quad (5)$$

Therefore, the fraction of the total sulfide, [S(–II)], that is in the form of HS^- increases with increasing pH. At pH around neutral, 50% of the total S(–II) is present in the form of HS^- and at pH 10 practically all S(–II) is present as HS^-.

A two–term rate law of the following form has been reported for the oxidation of S(–II) by HSO_5^- in water (Betterton and Hoffmann, 1990):

$$-d[S(-II)]/dt = k_1[H_2S][HSO_5^-] + k_2[HS^-][HSO_5^-] \quad (6)$$

where $k_1 = 19.8\ M^{-1}s^{-1}$ and $k_2 = 1.22 \cdot 10^4\ M^{-1}s^{-1}$ at 4.9 °C and $\mu = 0.2$ M. Based on the activation parameters reported by Betterton and Hoffmann (1990) ($\Delta H^{\neq}_{k1} = 2.8$ kJ mol^{-1}, $\Delta H^{\neq}_{k2} = 38.7$ kJ mol^{-1}) the reaction rate constants at 25 °C can be calculated to be: $k_1 = 21.5\ M^{-1}s^{-1} = 1.29 \cdot 10^3\ M^{-1}min^{-1}$ and $k_2 = 3.78 \cdot 10^4\ M^{-1}s^{-1} = 2.27 \cdot 10^6\ M^{-1}min^{-1}$. The fact that k_2 is more than 3 orders of magnitude higher than k_1 explains the observed steep increase in the overall reaction rate with increasing pH. At neutral pH the half life for the oxidation of aqueous S(–II) by 100 μM HSO_5^- can be calculated to be 0.4 second. Peroxymonosulfate is the only significant oxidant at neutral pH since its acidity constants are $pK_{a1} < 0$ and $pK_{a2} = 9.88$ (Spiro, 1979).

The oxidation of aqueous H_2S by H_2O_2 follows the same rate law (Hoffmann, 1977) with $k_1 = 8 \times 10^{-3}$ $M^{-1}s^{-1}$ and $k_2 = 4.8 \times 10^{-1}$ $M^{-1}s^{-1}$ at 25 °C and $\mu = 0.4$ M. Millero *et al.* (1989) report a value for k_2 of 5.1×10^{-1} $M^{-1}s^{-1}$ at 25 °C; they did not observe a two–term rate law and thus do not report a value for k_1.

A series of experiments was conducted where known amounts of HSO_5^- were added to sulfide–spiked wastewater. The pH of the solution was 7.0 – 7.5 and the temperature was kept constant at 25 ± 1 °C. Total sulfide concentrations were determined before and after the addition of the oxidant. Upon addition of HSO_5^- a sudden drop in the total sulfide concentration was observed followed by a slower oxidation of the same magnitude as in plain wastewater. The initial oxidation was completed in less than 2 minutes; that was the time required for mixing of the reactants and sampling for total sulfide. Figure B.1 shows the percentage of S(–II) oxidized after 2 min for different molar ratios of initial concentrations of peroxymonosulfate and sulfide, $[HSO_5^-]_o$:$[S(-II)]_o$. For molar ratios $\geq \simeq 2$ complete S(–II) oxidation was observed in less than 2 minutes.

Upon H_2O_2 addition in sulfide–containing wastewater an initial exponential decrease in [S(–II)] was observed. This initial decrease was the same for molar ratios $[H_2O_2]_o$:$[S(-II)]_o$ between 1 and 6 and $[S(-II)]_o = 200$ μM (6.4 ppm). The corresponding first–order rate was $k_{obs} = 0.18$ min^{-1}. At the later stage of the reaction, after the depletion of H_2O_2, the rate of sulfide oxidation was similar to that observed in plain wastewater. A molar ratio $[H_2O_2]_o$:$[S(-II)]_o$ = 6:1 was necessary in order to achieve complete oxidation of 200 μM S(–II) in 30 min.

It is noted that our kinetic observations for sulfide oxidation by H_2O_2 in wastewater are similar with those reported by Cadena & Peters (1988) for wastewater collected at a wastewater treatment plant in Albuquerque. These

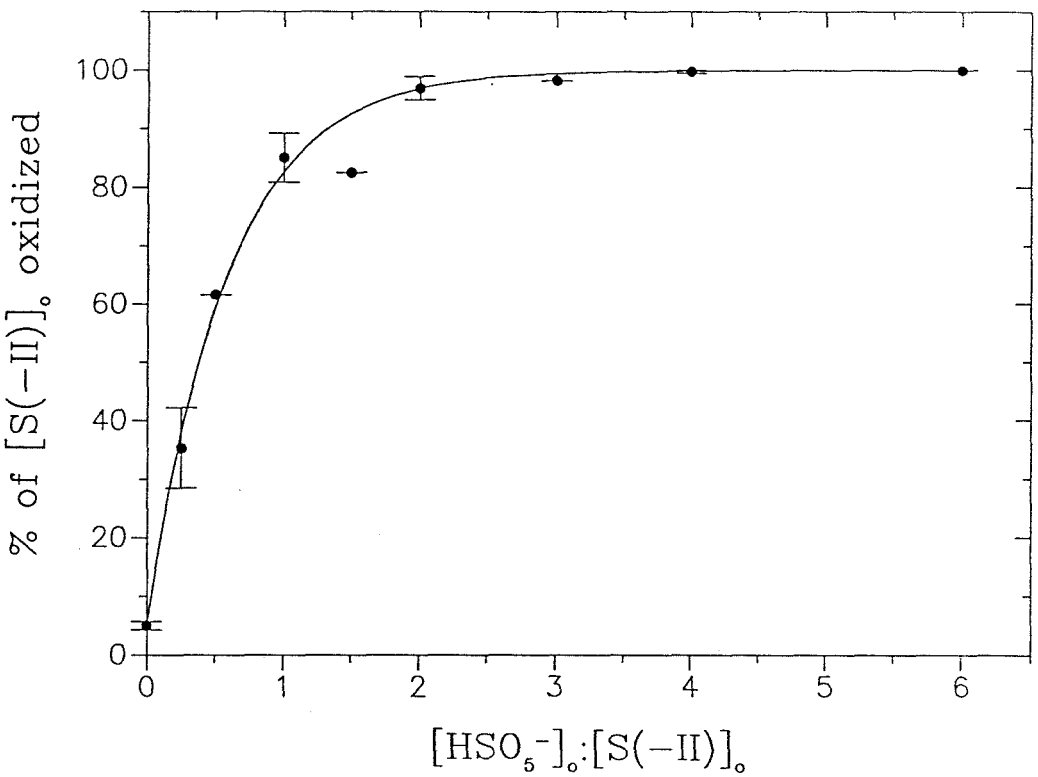

Figure B.1 S(–II) oxidation by HSO_5^- in wastewater. Percentage of $[S(-II)]_o$ oxidized after 2 minutes of HSO_5^- addition; pH $\simeq$ 7.5, $[O_2]_o \leq 1.5$ ppm, $[S(-II)]_o = 200\ \mu M$ (6.4 ppm), T = 25 °C.

researchers reported a value of 0.12 min^{-1} for the observed initial first–order rate. They also observed a 99% S(–II) oxidation after 30 min for $[H_2O_2]_o$:$[S(-II)]_o$ = 3:1. In our experiments, although we observed ≃ 96% oxidation for molar ratio of 3:1 we had to double the dosage (i.e., use $[H_2O_2]_o$:$[S(-II)]_o$ = 6:1) in order to achieve complete oxidation after 30 min of reaction time. This result is consistent with the results reported for large–scale field applications of H_2O_2 for the control of H_2S in sewers, where a dose close to 6:1 is usually necessary in order to remove sulfides completely (ASCE, 1989).

· ***Stoichiometry***

As reported earlier for clean water (Betterton and Hoffmann, 1990), the stoichiometry of the reaction of HSO_5^- with S(–II) depends on the pH of the solution and the initial molar ratio of the reactants. It was suggested that if there is a large excess of oxidant, especially at high pH, then sulfate and H^+ are produced,

$$HS^- + 4\ HSO_5^- \longrightarrow 5\ H^+ + 5\ SO_4^{2-} \qquad (7)$$

whereas if the oxidant and the reductant are present in approximately equimolar proportions (especially at low pH) then the products are elemental sulfur, sulfate and water.

$$HS^- + HSO_5^- \longrightarrow \tfrac{1}{8} S_8 + SO_4^{2-} + H_2O \qquad (8)$$

High pH appears to favor sulfate formation, while low pH appears to favor S^o formation (at high $[HSO_5^-]$). This behavior parallels that found for the oxidation of

H_2S by H_2O_2 (Hoffmann, 1977). It should be noted that reaction (7) results in the release of proton acidity whereas reaction (8) does not. This may have important implications for the application of HSO_5^- in the control of hydrogen sulfide.

For wastewater applications it is the 'effective stoichiometry' (*i.e.* the ratio of $[HSO_5^-]_{used}$ to $[S(-II)]_{oxidized}$) that is important. Figure B.2 presents the effective stoichiometry observed in experiments conducted in wastewater at different pH values and initial molar ratios of $[HSO_5^-]_o$:$[S(-II)]_o$. It was observed that at neutral pH and concentrations of interest ([S(–II)] around 5 ppm) the ratio of $[HSO_5^-]_{used}$ (assumed to be the initial concentration of oxidant added to the solution, $[HSO_5^-]_o$) to $[S(-II)]_{oxidized}$ increases linearly with the initial molar ratio from $[HSO_5^-]_o$:$[S(-II)]_o \simeq 0.5$ up to $[HSO_5^-]_o$:$[S(-II)]_o \simeq 3$. From linear regression of the experimental data for wastewater at neutral pH the following relationship was found to hold for $1 \leq [HSO_5^-]_o$:$[S(-II)]_o \leq 3$:

$$[HSO_5^-]_o:[S(-II)]_{oxidized} = 1.27 \cdot ([HSO_5^-]_o:[S(-II)]_o), \quad r^2 = 0.956 \quad (9)$$

For $[HSO_5^-]_o$:$[S(-II)]_o = 3$ the effective stoichiometry was $[HSO_5^-]_o$:$[S(-II)]_{oxidized}$ = 4:1, which is the maximum theoretically expected (from eq. 7) assuming that all of the HSO_5^- added is used for the oxidation of S(–II). For $[HSO_5^-]_o$:$[S(-II)]_o > 3$ complete S(–II) oxidation was observed, and since no analysis was done to determine residual HSO_5^-, it was not possible to confirm that the actual stoichiometry $[HSO_5^-]_{used}$:$[S(-II)]_{oxidized}$ was 4:1 as expected.

It is interesting to note that the effective stoichiometry in wastewater is similar to that observed in clean water experiments (see Figure B.2). The fact that the efficiency of HSO_5^- for sulfide oxidation is not reduced in wastewater indicates

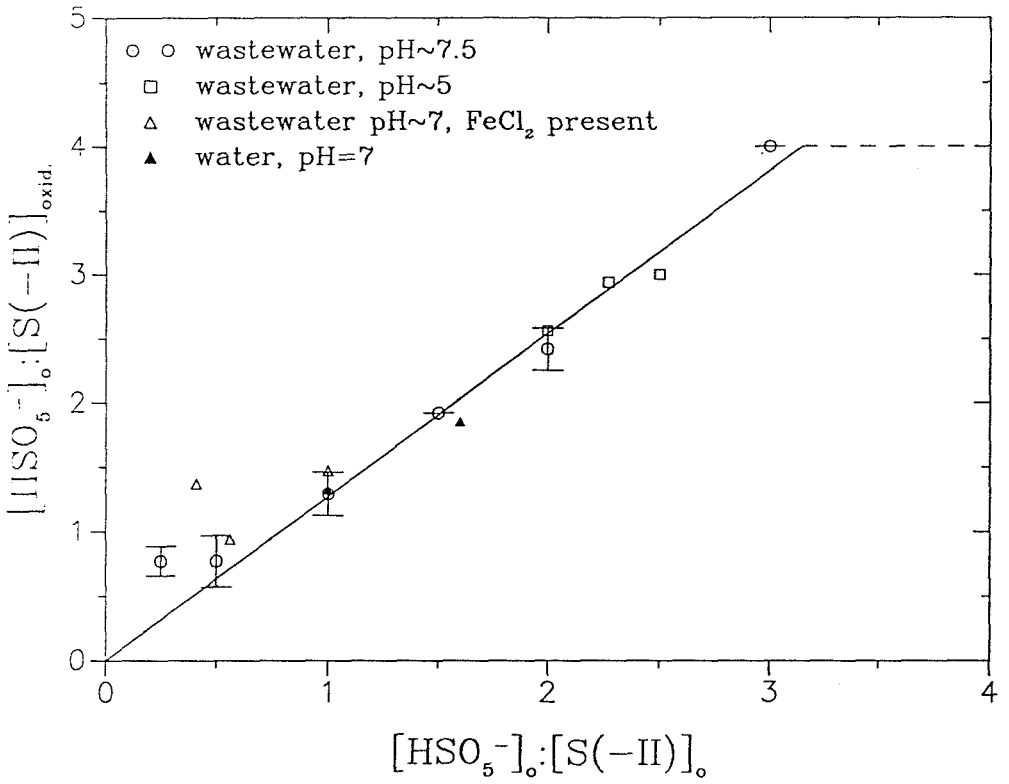

Figure B.2 S(–II) oxidation by HSO_5^- in wastewater. Effect of $[HSO_5^-]_o$:$[S(-II)]_o$ on effective reaction stoichiometry $[HSO_5^-]_o$:$[S(-II)]_{oxidized}$.

that HSO_5^- reacts preferentially with sulfide and not with other oxidizable substrates present in this complex matrix.

Our experimental results in wastewater indicate that a molar dosage of $[HSO_5^-]_o$:$[S(-II)]_o$ = 2:1 would lead to ≥ 95% instantaneous S(–II) oxidation, while a molar dosage of 1:1 would lead to an instantaneous oxidation of the order of 85%. Obviously, the appropriate dosage for a particular application would depend on the level of sulfide control desired. It must be noted that if HSO_5^- is added in the form of a salt (in our experiments the triple salt of Oxone that contains 2 molecules of HSO_5^- and has a molecular weight 614.78 gr/mole) the molecular weight of the salt must be used to calculate the corresponding weight ratio from the molar ratio. For the triple salt of Oxone, a molar dosage of $[HSO_5^-]_o$:$[S(-II)]_o$ = 1:1 corresponds to a weight dosage of 9.6:1.

Control experiments with iron salts

Iron salts are occasionally used in wastewater collection systems and anaerobic digesters to control hydrogen sulfide (ASCE, 1989; Pomeroy and Bowlus, 1949). We decided to investigate the effect of combined addition of ferrous chloride ($FeCl_2$) and peroxymonosulfate. Therefore, control experiments were conducted where a known amount of $FeCl_2$ was added to sulfide–spiked solutions and the disappearance of total dissolved sulfide, S(–II), was followed with time.

Initial experiments were conducted in water, at neutral pH, T = 25 °C and air saturation ($[O_2] = 2.4 \cdot 10^{-4}$ M = 7.7 ppm). The oxidation of S(–II) in the presence of $FeCl_2$ initially followed first–order kinetics, and typical observed first–order rates, k_1, can be seen in Table B.2. From linear regression of the data, the following expression was derived: $k_1 = 89.73 \cdot [FeCl_2]^{0.75}$, $r^2 = 0.986$; where k_1 in

Table B.2

Sulfide oxidation in the presence of $FeCl_2$

$[FeCl_2]$ (M)	$[S(-II)]_o$ (μM)	k_1 min^{-1}	% S(–II) oxidized in 30 minutes	Comments
Water, pH = 7.0				
$1.0 \cdot 10^{-5}$	100	$1.5 \cdot 10^{-2}$	36	$[O_2]_o$ = 240 μM
$5.0 \cdot 10^{-5}$	100	$6.4 \cdot 10^{-2}$	68	"
$1.0 \cdot 10^{-4}$	100	$8.4 \cdot 10^{-2}$	60	"
$5.0 \cdot 10^{-4}$	100	0.37	69	"
$1.0 \cdot 10^{-3}$	100	0.43	73	"
Wastewater, pH = 7.5				
$1.0 \cdot 10^{-3}$	125	1.00	87	
$1.0 \cdot 10^{-4}$	125	0.23	84	
$2.0 \cdot 10^{-5}$	61	$6.63 \cdot 10^{-2}$	86	$3.4 \cdot 10^{-5}$ M $FeCl_3$ present

All rates at T = 25°C

min^{-1} and [$FeCl_2$] in M. It must be noted that due to the low solubility of FeS ($FeS_{(s)} + H_2O \rightleftharpoons Fe^{2+} + HS^- + OH^-$, $K_{sp} = 6 \cdot 10^{-19}$, Myers, 1986) the concentration of free Fe^{2+} in solution is expected to be much lower than the concentration of total $FeCl_2$ that was used in the above experimental expression. For example, at neutral pH and total sulfide concentration 100 μM, the equilibrium [Fe^{2+}] calculated using the above K_{sp} is $\simeq$ 0.12 μM.

The fast initial oxidation of S(–II) was followed by a slower oxidation rate and tapered off at some point after which no further decrease in S(–II) was observed. This could not always be explained by oxygen depletion. It seems plausible that the fast initial S(–II) removal is associated with formation of iron–sulfide complexes and subsequent precipitation and physical S(–II) removal from the solution, while the later slower S(–II) removal is the result of chemical reactions due to the presence of Fe^{2+}. The percentage of initial [S(–II)] oxidized after 30 minutes is also given in Table B.2.

Experiments were subsequently conducted in wastewater. No oxygen was added, and the initial oxygen concentration was that of the wastewater, that was less than 1.5 ppm. Even after subtracting the observed first–order oxidation rate constant for S(–II) oxidation in plain wastewater the initial oxidation rate of S(–II) in the presence of $FeCl_2$ was about twofold higher in wastewater than the corresponding one for clean water. Nevertheless, the final percentage of S(–II) oxidized was the same for [$FeCl_2$] ranging between 50 μM and 1 mM and it was about 85%.

In one experiment, a combination of $FeCl_2$ and $FeCl_3$ was used, but no enhancement of the initial oxidation rate or the final S(–II) removal was observed. It must be noted that Fe^{2+} gets oxidized to Fe^{3+} rather readily in the presence of

oxygen. The following experimental rate law is known for pH $\geq$ 4.5 (Stumm and Morgan, 1981):

$$d[Fe^{2+}]/dt = k[OH^-]^2[Fe^{2+}]P_{O_2} \qquad (10)$$

where $k = 8 \cdot 10^{13}$ $M^{-2}atm^{-1}min^{-1}$. From the above expression and at neutral pH the half–life of Fe^{2+} can be calculated to be 4 minutes under air saturation and 22 minutes at $[O_2]$ = 1.5 ppm. Therefore, it is possible that at least some of the iron present in the solution is effectively in the form of Fe^{3+} and not Fe^{2+} and our experimental results present the effect of mixtures of Fe^{3+} and Fe^{2+}.

Combined additions of HSO_5^- and other chemicals

Several experiments were conducted in water where peroxymonosulfate and hydrogen peroxide were added together in solutions containing S(–II), at neutral pH and T = 25 °C. An initial sudden drop in [S(–II)] was observed, followed by a slower decrease afterwards (see Figure B.3). The initial [S(–II)] oxidation was attributed to peroxymonosulfate while the later slower reaction was assigned to hydrogen peroxide. The ratio of $[HSO_5^-]_o$ to [S(–II)] initially oxidized was practically the same as that observed when only $[HSO_5^-]$ was present except at low $[S(-II)]_o$ values where it was somewhat higher. The first–order rates observed after the initial steep sulfide decrease were in agreement with the rates obtained when only hydrogen peroxide was present. These results indicate that when peroxymonosulfate is used in conjunction with hydrogen peroxide for the oxidation of sulfide the effects of those reagents are simply added together.

Combined additions of $FeCl_2$ and peroxymonosulfate in S(–II) containing

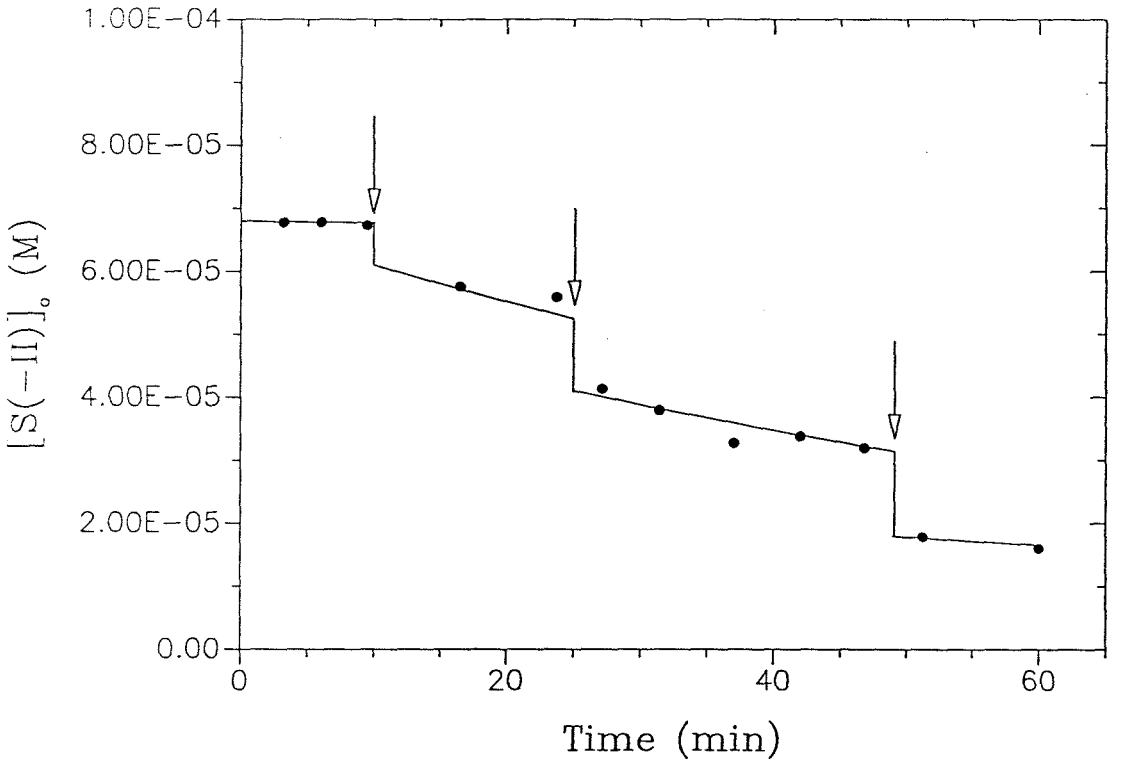

Figure B.3 Combined addition of HSO_5^- and H_2O_2 in water; $[S(-II)]_o = 68\ \mu M$, pH = 6.3; arrows indicate additions of HSO_5^-; $[HSO_5^-] = 25\ \mu M$ after each addition; $[H_2O_2] = 200\ \mu M$ added at t = 10 min; first–order S(–II) decrease between HSO_5^- additions same as for control experiment when only H_2O_2 was present.

wastewater at pH around neutral and T = 25 °C gave similar results as described above for H_2O_2 and HSO_5^-. The stoichiometry for the initial reaction was not really affected, but the later reaction rate was much lower than that observed in wastewater experiments when only $FeCl_2$ was present. These experiments showed that the combined application of peroxymonosulfate and $FeCl_2$ in wastewater does not affect much the oxidation by peroxymonosulfate but decreases considerably the effect of $FeCl_2$ on S(–II) oxidation.

Persulfate ($S_2O_8^{2-}$) was added to sulfide–containing deionized water at neutral pH and T = 25 °C. No change in [S(–II)] was observed over a period of about half an hour for $[S_2O_8^{2-}]$ up to about 1 mM. A few experiments showed that the addition of $S_2O_8^{2-}$ together with peroxymonosulfate at neutral pH and T = 25 °C had no effect on the oxidation of S(–II) by peroxymonosulfate. Work on $S_2O_8^{2-}$ was not pursued further.

CONCLUSIONS

Peroxymonosulfate is an efficient oxidant for S(–II) control in wastewater. At neutral pH HSO_5^- reacts with S(–II) in less than 2 minutes contact time and complete oxidation is achieved at molar dosages $[HSO_5^-]:[S(-II)]_o \geq \simeq 2:1$. Hydrogen peroxide on the other hand, requires higher molar ratios ($[H_2O_2]:[S(-II)]_o \simeq 6$) and longer times ($\simeq$ 30 minutes) to achieve complete oxidation. Peroxymonosulfate is not only more efficient than hydrogen peroxide but also presents advantages with respect to storage and handling since it is available in the form of a powder.

It has to be noted, however, that if peroxymonosulfate is added in the form of a triple salt the weight ratio, [total weight of oxidant]:[weight of total sulfide],

required is higher than the molar ratio. For example, for the commercially available Curox or Oxone ($2 \cdot KHSO_5 \cdot KHSO_4 \cdot K_2SO_4$, FW = 614.78 gr) a molar ratio of $[HSO_5^-]$:$[S(-II)]_o$ = 1:1 corresponds to a weight ratio of Oxone:sulfide = 9.6:1. The cost of Oxone or Curox per weight is currently similar to that of H_2O_2 (there is no wide market for Oxone/Curox at present). Therefore, the use of HSO_5^- as an alternative to H_2O_2 does not present an economic advantage at the moment. Combined addition of peroxymonosulfate and hydrogen peroxide can reduce the required cost for sulfide control and could be advantageous in cases where an instantaneous partial control of sulfide is desired while a slower rate for subsequent complete oxidation can be tolerated.

Another point that has to be stressed is that the use of a triple salt like Oxone or Curox results in sulfate concentrations that are higher than those corresponding to the oxidation of the sulfide present in the system; one additional mole of SO_4^{2-} is added per mole of HSO_5^-. This fact precludes the use of these salts in cases where sulfate is the limiting factor for sulfide generation. Nevertheless, oxidized sulfur is usually not limiting with respect to sulfide production in sewers (ASCE, 1989) and this factor is not expected to be critical for applications in sewers.

Full–scale testing of peroxymonosulfate in sewers is recommended. Recommended molar ratios of $[HSO_5^-]$ to $[S(-II)]$ for initial testing is between 1:1 and 2:1. Use of excess HSO_5^- should be avoided and operation at low pH are preferable.

ACKNOWLEDGMENTS

The authors wish to thank Isabel Chen, Martha Shaw and Joel Pedersen for

their contribution to the experimental work. This work was funded by the County Sanitation Districts of Los Angeles County under CSD Contract No. 3082.

Authors. A. Kotronarou is a Ph.D. candidate and M. R. Hoffmann is a Professor in Environmental Engineering Science at the California Institute of Technology. Correspondence should be addressed to M. R. Hoffmann, Environmental Engineering Science, W. M. Keck Laboratories, California Institute of Technology, Pasadena, California 91125.

REFERENCES

Allen, A.O., Hochanadel, C. J., Ghormley, J.A., and Davis, T. W. (1952). Decomposition of Water and Aqueous Solutions under Mixed Fast Neutron and Gamma Radiation. *J. Phys. Chem.*, **56**, 575.

ASCE (1990). Sulfide in Wastewater Collection and Treatment Systems. Manuals and reports on Engineering Practice No. 69, ASCE, New York.

Balej, J. (1984) Thermodynamics of reactions during the electrosynthesis of peroxodisulphates. *Electrochim. Acta*, **29**, 1239.

Betterton, E. A., and Hoffmann, M. R. (1990). Kinetics and Mechanism of the Oxidation of Aqueous Hydrogen–Sulfide by Peroxymonosulfate. *Environ. Sci. Technol.*, **24**, *12*, 1819.

Cadena, F., and Peters, R. W. (1988). Evaluation of Chemical Oxidizers for Hydrogen Sulfide Control. *J. Water Pollut. Control Fed.*, **60**, 7, 1259.

Chen, K. Y., and Morris, J. C. (1972a). Kinetics of Oxidation of Aqueous Sulfide by O_2. *Environ. Sci. Technol.*, **6**, 529.

Chen, K. Y., and Morris, J. C. (1972b). Oxidation of Sulfide by O_2: Catalysis and Inhibition. *Journal of the San. Eng. Div., Proc. ASCE, SA1*, 215.

Dohnalek, D. A., and FitzPatrick, J. A. (1983). The Chemistry of reduced sulfur species and their removal from Groundwater supplies. *J. Am. Water Works Assoc.*, **65**, 298.

Giggenbach, W. (1971). Optical Spectra of Highly Alkaline Sulfide Solutions and the Second Dissociation Constant of Hydrogen Sulfide. *Inorg. Chem.*, **7**, 1333.

Hoffmann, M. R. (1977). Kinetics and Mechanism of Oxidation of Hydrogen Sulfide by Hydrogen Peroxide in Acidic Solution. *Environ. Sci. Technol.*, **11**, 61.

Hoffmann, M. R., and Lim, C. H. (1979). Kinetics and Mechanism of the Oxidation of Sulfide by Oxygen: Catalysis by Homogeneous Metal–Phthalocyanine Complexes. *Environ. Sci. Technol.*, **13**, 1406.

Kotronarou, A., and Hoffmann, M. R. (1991). Catalytic Autoxidation of Hydrogen Sulfide in Wastewater. *Environ. Sci. Technol.*, **25**, 1153.

Millero, F. J., LeFerriere, A., Fernandez, M., Hubinger, S., and Hershey, J. P. (1989). Oxidation of H_2S with H_2O_2 in Natural–waters. *Environ. Sci. Technol.*, **23**, 209.

Myers, R. J. (1986). The New Low Value for the Second Dissociation Constant for H_2S. *J. Chem. Educ.*, **63**, 8, 687.

Pomeroy, R., and Bowlus, F. D. (1949). Progress Report on Sulfide Control Research. *J. Sew. Wks.*, 18, *4*, 597.

Smith, R. M., and Martell, A. E. (1976). Critical Stability Constants, vol. 4: Inorganic Complexes. Plenum, New York.

Snavely, E. S., and Blount, F.E. (1969). Rates of Reaction of Dissolved Oxygen with Scavengers in Sweet and Sour Brines. *Corrosion*, **25**, 397.

Spiro, M. (1979). The standard potential of the peroxosulphate/sulphate couple. *Electrochim. Acta*, 24, 313.

Steele, W. V., and Appleman, E. H. (1982). The standard enthalpy of formation of peroxymonosulfate (HSO_5^-) and the standard electrode potential of the peroxymonosulfate–bisulfate couple. *J. Chem. Thermodyn.*, **14**, 337.

Stumm, W., and Morgan, J. J. (1981). Aquatic Chemistry, 2nd ed., Wiley & Sons, pp. 465–468.

Thistlethwayte, D. K., ed. (1972). The Control of Sulphides in Sewerage Systems. Butterworth, Sydney.

Weres, O., Tsao, L., and Chhatre, R. M. (1985). Catalytic Oxidation of Aqueous Hydrogen Sulfide in the Presence of Sulfite. *Corrosion*, **41**, 307.

Wilmot P. D., Cadee, K., Katinic, J.J., and Kavanagh, B. V. (1988). Kinetics of Sulfide Oxidation by Dissolved Oxygen. *J. Water Pollut. Control Fed.*, **60**, 7, 1264.

APPENDIX C

USMODEL AND EPIS COMPUTER CODES

USMODEL

```
      program hsmodel
c**********************************************************************
c
c     This is a program written by Natasha Kotronarou (June 1991)
c     to model the S(-II) + OH system in the aqueous phase and at
c     neutral to alkaline pH in the presence of oxygen
c
c     The chemical mechanism includes 22 species and 47 reactions;
c     The 22 ODE's are solved by subroutine EPIS
c
c**********************************************************************
      character*30 optitle
      character*1 op
      character*20 inputs, outputs
      dimension x(22), dxdtt(22), rk(47),rr(47)
      real NO2min
c
c     common for EPIS
c
      common/epcomy/ymin,hmax
      common/int1/rele,ho
      common/int2/ktol,mfepi
c
      common/rxnr/nr,rk
      common/rxns/dxdtt,rr
      common/vdata/Sm2o,O2o,S2O3o
      common/flags/flag1
      common/ohinp/OHin,Ohminus,OHo,H2O2in,O2kl,Hplus,NO2min
      common/alpha/al02,al12,al18,al28
c
c     Set up parameters for EPIS
c
      neq=22
      nr=47
      rele=1.0e-2
      ktol=5
      mfepi=22
      tout=0.
      flag1=0.
c
   1  continue
c
c     input names of input and output files
c     not active at the moment for output files
c     Results are written in pre-specified files
c
       write(*,100)
 100   format(' input the name of the data file')
       read(*,110) inputs
 110   format(a20)
       open(1,file=inputs,status='old')
       open(11,file='error.res',status='unknown')
c      write(*,120)
 120   format(' input the name of the output file')
c      read(*,110) outputs
c
c      pH is treated as a fixed parameter.
c      [OH-], [H+], and alphas are calculated here
c
       write(*,*) ' input pH'
       read(*,*) pH
       Hplus=10.**(-pH)
```

```
      a102=Hplus/(Hplus+10.**(-7.02))
      OHminus=10.**(-14.)/10.**(-pH)
      a112=10.**(-7.02)/(Hplus+10.**(-7.02))
      a118=Hplus/(Hplus+10.**(-7.18))
      a128=10.**(-7.18)/(Hplus+10.**(-7.18))
c
c     Input of OH, H2O2, NO2- into the aqueous phase
c     is treated as a constant and is read here
c
      write(*,*) ' input OHin (uM/min)'
      read(*,*) OHin
      write(*,*) ' input OHo (uM)'
      read(*,*) OHo
      write(*,*) ' input H2O2in (uM/min)'
      read(*,*) H2O2in
      write(*,*) ' input NO2min (uMmin)'
      read(*,*) NO2min
c
c     Read rate constants from input file
c
      call input(neq,x,nr,rk)
c
c     Specify names of output files
c
      open(2,file='gen.res',status='new')
      open(3,file='sulf.res',status='new',recl=250)
     open(4,file='rad.res',status='new',recl=250)
     open(5,file='ox.res',status='new',recl=250)
c
c     write titles in result files
c
      write(2,401) pH, OHin,OHo,H2O2in
     +,NO2min,neq,nr,Sm2o,O2o,O2kl,S2O3o
 401  format(5x,'S(-II) + OH in aqueous phase'
     */5x,'temperature = 25 C, pH = ',f5.2/
     +/5x,'OHinput = ',f7.2,' uM/min'/
     +/5x,'OHo =',f7.2,' uM'/
     +5x,'H2O2input =',f7.2/5x,'NO2-input =',f7.2/
     +/5x,'# of species =',i3
     +/5x,'# of reactions =',i3//5x
     +,'[S(-II)]o=',f7.2/5x,'[O2]o=',f7.2/5x,
     +'Kl(O2) =',e10.4/5x,'[S2O3--]o=',f7.2)
       write(*,*) ' H+ =', Hplus,' OH- =', OHminus
       write(2,411) a102,a112,a118,a128
 411  format(1x//1x,'S(-II)a0 =',e10.4,'  S(-II)a1 =',e10.4/
     +1x,'S(IV)a1 =',e10.4,'  S(IV)a2 =',e10.4)
c
c     convert uM/min to M/s (units used in DIFFUN)
c
      OHin=Ohin*1.e-6/60.
      NO2min=NO2min*1.e-6/60.
      H2O2in=H2O2in*1.e-6/60.
       write(3,402)
 402  format(1x,'t (min)',3x,'S(-II)',5x,'SO4',5x,'SO3'
     +,5x,'S2O3',5x,'NOy',5x,'H2O2')
       write(4,403)
 403  format(1x,'t (min)',5x,'HS',5x,'H2S2-',5x,'HSOH-',
     +5x,'SO2-',5x,'S2O3OH2-',5x,'S4O63-',5x,'SO3-',5x,'SO4-')
       write(5,404)
 404  format(1x,'O2',5x,'OH',5x,'H2O2',5x,'O2-',5x,'NO2-',5x,'NO3-'
     +,5x,'NO2')
      tout=0.
```

```
c
c      Call subroutine OUT to write initial values
c
       call out(neq,x,tout,dxdtt,rr)
c
c      input time step and total # of steps
c      calculate parameters needed for EPIS
c
       write(*,140)
  140  format(' input time increment in secs')
       read(*,*) tdelt
       ho=1.0e-4*tdelt
       ymin=1.0e-12
       hmax=0.1*tdelt
       write(*,150)
  150  format(' input # of time steps')
       read(*,*) iter
       write(*,*) ' input tprint (in secs)'
       read(*,*) tprint
c
c      last chance to change ho, ymin, hmax
c      (parameters used in EPIS)
c
       write(*,*) ' do you want to change ho/ymin/hmax?'
       read(*,56) op
       if(op.ne.'y') go to 777
       write(*,*)'ho=',ho
       write(*,55)
   55  format(' do you want to change it? (Y/N)')
       read(*,56) op
       if(op.eq.'y') read(*,*) ho
       write(*,*) 'ymin=',ymin
       write(*,55)
       read(*,56) op
   56  format(a1)
       if(op.eq.'y') read(*,*) ymin
       write(*,*) 'hmax=',hmax
       write(*,55)
       read(*,56) op
       if(op.eq.'y') read(*,*) hmax
  777  continue
c
c      Last chance to change rate constants
c
       write(*,*) ' do you want to change a rate constant? (y/n)'
       read(*,56) op
       if(op.ne.'y') go to 77
  800  continue
       write(*,*) 'input #id of the k (1-47) or 0 to terminate'
       read(*,*) idk
       if(idk.gt.47) go to 800
       if(idk.eq.0) go to 77
       write(*,*) ' old value: ',rk(idk)
       write(*,*) ' input new value'
       read(*,*) rk(idk)
       go to 800
   77  tin=tout
       index=1
c
c      Loop for EPIS starts here
c
       do 200 i=1,iter
```

```
      tout=tin+i*tdelt
c       write(*,*) 'starts Loop ',i
      call drive(neq,t,ho,x,tout,rele,ktol,mfepi,index)
c
c     if index is not 0, results cannot be trusted!
c
       if(index.ne.0)then
       write(*,*) 't',t,'tout',tout,'ho',ho,'index',index
       end if
c       write(*,*) 'end Loop ',i
c      write(*,*) (x(k),k=1,neq)
c
c     At the specified time intervals, write concentrations
c     in result files
c
      tindex=tout/tprint
      itindex=tindex
      dif=tindex-float(itindex)
      if(dif.eq.0.) then
      call out(neq,x,tout,dxdtt,rr)
      write(*,*) ' completed:', tout,' secs, Loop:',i
      endif
c
c     use Warren's option for calculation of derivatives in EPIS
c     after each step
c
      index=7
 200  continue
c
c     end of Loop
c
      close(1)
      close(2)
      close(3)
      close(4)
      close(5)
      close(11)
      write(*,*) ' do you want to start a new run? (Y/N)'
      read(*,56) op
      if(op.ne.'y') go to 88
      flag1=1.
      go to 1
 88   continue
      stop
      end
c
c
c     END OF MAIN PROGRAM
c
c ***********************************************************************
c
c     SUBROUTINE INPUT
c
c     initialize vector x and read rate constants
c
      subroutine input(neq,x,nr,rk)
      character*1 op
      dimension x(neq),rk(nr)
      real NO2min
c
c     common parameters
c
```

```
      common/flags/flag1
      common/vdata/Sm2o,O2o,S2O3o
      common/int1/rele,ho
      common/int2/ktol,mfepi
      common/ohinp/OHin,Ohminus,OHo,H2O2in,O2kl,Hplus,NO2min
c
c      give a chance to change data related to EPIS
c
       write(*,*) 'do you want to check/change data?'
       read(*,99) op
       if(op.ne.'y') go to 98
 99    format(a1)
       write(*,*)'rele=',rele,'do you want to change it? (Y/N)'
       read(*,99) op
       if(op.eq.'y') read(*,*) rele
       write(*,*)'ktol=',ktol,'do you want to change it? (Y/N)'
       read(*,99) op
       if(op.eq.'y') read(*,*) ktol
       write(*,*)'mfepi=',mfepi,'do you want to change it? (Y/N)'
       read(*,99) op
       if(op.eq.'y') read(*,*) mfepi
  98   continue
c
c     initialize vector x
c
c
c      X(1) : OH                          (R)
c      X(2) : S(-II) = H2S + HS-
c      X(3) : HS                          (R)
c      X(4) : O2
c      X(5) : H2S2-                       (R)
c      X(6) : HSOH-                       (R)
c      X(7) : H2S2t = H2S2 + HS2- + S2--
c      X(8) : S(IV) = HSO3- + SO3--
c      X(9) : SO2-                        (R)
c      X(10): S2O3--
c      X(11): S2O3OH--                    (R)
c      X(12): S4O6---                     (R)
c      X(13): O2-                         (R)
c      X(14): SO3-                        (R)
c      X(15): SO4-                        (R)
c      X(16): H2O2
c      X(17): SO4--
c      X(18): NO2-
c      X(19): NO3-
c      X(20): NO2                         (R)
c      X(21): HS2                         (R)
c      X(22): H2S2O                       (R)
c
      write(*,*) ' reading input'
      do 1 i=1,neq
   1  x(i)=0.
c
c     Read initial concentrations of selected species
c     and oxygen transfer coefficient, O2kl
c     ([O2] addition is O2kl*([O2]s-[O2])
c
      write(*,*) ' input initial [S(-II)] (uM)'
      read(*,*) Sm2o
      write(*,*) ' input initial [O2] (uM)'
      read(*,*) O2o
      write(*,*) ' input O2 tranfer coef (1/s)'
```

```
      read(*,*) O2kl
      write(*,*) ' input initial [S2O3] (uM)'
      read(*,*) S2O3o
      write(*,*) ' input initial [NO2-] (uM)'
      read(*,*) NO2o
      write(*,*) ' input initial [NO3-] (uM)'
      read(*,*) NO3o
      write(*,*) Sm2o,o2o,oho,NO2o,NO3o
c
c     convert concentrations to M
c
      x(1)=OHo*1.e-6
      x(2)=Sm2o*1.e-6
      x(4)=O2o*1.e-6
      x(10)=S2O3o*1.e-6
      x(18)=NO2o*1.e-6
      x(19)=NO3o*1.e-6
c
c     read rate constants (unless this is not the first run)
c
      if(flag1.eq.0.) then
      do 2 i=1,nr
      read(1,*) rk(i)
  2   continue
      endif
      write(*,*) ' finished reading data'
      return
      end
c
c ***********************************************************************
c
c     SUBROUTINE OUTPUT (writes results in output files)
c
      subroutine out(neq,x,tout,dxdtt,rr)
      dimension x(22),xs(22),rr(47),dxdtt(22)
c
      ttt=tout/60.
      do 555 j=1,neq
 555      xs(j)=x(j)*1.e6
      xNOy=xs(18)+xs(19)
      write(3,161) ttt,xs(2),xs(17),xs(8),xs(10),xNOy
     +,xs(16)
 161  format(1x,f6.2,6(1x,e9.3))
      write(4,162) ttt,xs(3),xs(5),xs(6),xs(9),xs(11),xs(12),
     +xs(14),xs(15)
 162  format(1x,f6.2,8(1x,e9.3))
      write(5,163) ttt,xs(4),xs(1),xs(16),xs(13)
     +,xs(18),xs(19),xs(20)
 163  format(1x,f6.2,7(1x,e9.3))
c      do 999 kk=1,neq
c      write(*,*) 'species#',kk,' is ',xs(kk),'his rate is',dxdtt(kk)
c 999  continue
c      do 888 kk=1,47
c      write(*,*) 'rate of rxn#',kk,' is ',rr(kk)
c 888  continue
      return
      end
c
c***********************************************************************
c
c     SUBROUTINE DIFFUN
c
```

```
c      the derivatives of the ODE's solved by EPIS
c      are defined here
c
       subroutine diffun(neq,t,xxx,dxdt)
       dimension x(22),dxdt(22),xxx(22)
       dimension rk(47),rr(47),dxdtt(22)
       real NO2min
c
c      common for EPIS
c
       common/epcomy/ymin,hmax
c      common/epco99/ncstep,ncfe,ncje
c
c      common for input, etc
c
       common/rxnr/nr,rk
       common/rxns/dxdtt,rr
       common/ohinp/OHin,OHminus,OHo,H2O2in,O2kl,Hplus,NO2min
       common/alpha/al02,al12,al18,al28
c
c      This DO LOOP can be used to set negative values to zero
c      (not recommended for normal runs!)
c
       do 55 kk=1,neq
       x(kk)=xxx(kk)
       dxdtt(kk)=dxdt(kk)
c      if(x(kk).lt.0.) x(kk)=0.
 55    continue
c
c      calculate the rates of the reactions
c      X(1:22) are species as defined in INPUT
c
       rr(1)=rk(1)*x(1)*x(1)
       rr(2)=rk(2)*x(1)*x(2)*al02
       rr(3)=rk(3)*x(1)*x(2)*al12
       rr(4)=rk(4)*x(3)*x(3)
       rr(5)=rk(5)*x(3)*x(2)*al02
       rr(6)=rk(6)*x(3)*x(2)*al12
       rr(7)=rk(7)*x(3)*x(4)
       rr(8)=rk(8)*x(3)*x(5)
       rr(9)=rk(9)*x(6)*x(2)*al12
       rr(10)=rk(10)*x(6)*x(2)*al02
       rr(11)=rk(11)*x(6)*x(4)
       rr(12)=rk(12)*x(5)*x(5)
       rr(13)=rk(13)*x(5)*x(4)
       rr(14)=rk(14)*x(7)*x(8)*al28
       rr(15)=rk(15)*x(7)*x(4)
       rr(16)=rk(16)*x(9)*x(4)
       rr(17)=rk(17)*x(1)*x(8)*al28
       rr(18)=rk(18)*x(1)*x(8)*al18
       rr(19)=rk(19)*x(1)*x(10)
       rr(20)=rk(20)*x(11)*x(10)
       rr(21)=rk(21)*x(12)
       rr(22)=rk(22)*x(1)*x(13)
       rr(23)=rk(23)*x(4)*x(14)
       rr(24)=rk(24)*x(15)*x(8)*al18
       rr(25)=rk(25)*x(15)*x(8)*al28
       rr(26)=rk(26)*x(15)*x(13)
       rr(27)=rk(27)*x(15)*OHminus
       rr(28)=rk(28)*x(15)*x(16)
       rr(29)=rk(29)*x(8)*x(13)
       rr(30)=rk(30)*x(8)*x(16)*al28+
```

```
     +7.45e7*Hplus*x(16)*x(8)*al18
      rr(31)=rk(31)*x(2)*x(16)
      rr(32)=rk(32)*x(10)*x(16)
      rr(33)=rk(33)*x(2)*x(13)
      rr(34)=rk(34)*x(14)*x(14)
      rr(35)=rk(35)*x(1)*x(16)
      rr(36)=rk(36)*x(1)*x(18)
      rr(37)=rk(37)*x(1)*x(20)
      rr(38)=rk(38)*x(20)*x(8)
      rr(39)=rk(39)*x(2)*x(15)
      rr(40)=rk(40)*x(5)
      rr(41)=rk(41)*x(2)*al12*x(9)
      rr(42)=rk(42)*x(14)*x(2)*al12
      rr(43)=rk(43)*x(13)*x(10)
      rr(44)=rk(44)*x(7)*x(1)
      rr(45)=rk(45)*x(21)*x(1)
      rr(46)=rk(46)*x(21)*x(6)
      rr(47)=rk(47)*x(22)*x(1)
c
c
c     calculate the derivatives for EPIS
c
      dxdt(1)=OHin-2.*rr(1)-rr(2)-rr(3)-rr(17)-rr(18)-rr(19)-rr(22)
     ++rr(27)+rr(29)-rr(35)-rr(36)-rr(37)-rr(44)-rr(45)-4.*rr(47)
      dxdt(2)=-rr(2)-rr(3)-rr(5)-rr(6)+rr(8)+2.*rr(12)+rr(14)
     ++rr(15)-rr(9)-rr(10)-rr(31)-rr(33)-rr(39)
     ++rr(40)-rr(41)-rr(42)
      dxdt(3)=rr(2)-2.*rr(4)-rr(5)-rr(6)-rr(7)-rr(8)+rr(39)
     ++rr(40)+rr(41)+rr(42)+rr(46)
      dxdt(4)=-rr(7)-rr(11)-rr(13)-rr(15)-rr(16)+rr(22)+rr(26)
     ++O2kl*(2.4e-4-x(4))-rr(41)
      dxdt(5)=+rr(5)+rr(6)-rr(8)+rr(9)+rr(10)-2.*rr(12)-rr(13)
     +-rr(40)
      dxdt(6)=rr(3)-rr(9)-rr(10)-rr(11)-rr(46)
      dxdt(7)=rr(4)+rr(8)+rr(12)+rr(13)-rr(14)-rr(15)-rr(44)
      dxdt(8)=-rr(14)+rr(16)-rr(17)-rr(18)-rr(24)-rr(25)-rr(29)
     +-rr(30)+0.5*rr(21)+rr(34)-rr(38)+rr(42)+rr(43)
      dxdt(9)=rr(7)+rr(11)+rr(15)-rr(16)-rr(41)
      dxdt(10)=rr(14)-rr(19)-rr(20)+(7./4.)*rr(21)-rr(32)-rr(43)
     ++rr(47)
      dxdt(11)=rr(19)-rr(20)
      dxdt(12)=rr(20)-rr(21)
      dxdt(13)=rr(13)+rr(16)-rr(22)-rr(26)+rr(28)-rr(29)-3.*rr(33)
     ++rr(35)-2.*rr(43)
      dxdt(14)=rr(17)+rr(18)-rr(23)+rr(24)+rr(25)-2.*rr(34)-rr(42)
      dxdt(15)=0.5*rr(23)-rr(24)-rr(25)-rr(26)-rr(27)-rr(28)-rr(39)
      dxdt(16)=H2O2in+rr(1)-rr(28)-rr(30)-4.*rr(31)-4*rr(32)
     +-rr(35)
      dxdt(17)=0.5*rr(23)+rr(24)+rr(25)+rr(26)+rr(27)+rr(39)
     ++rr(28)+rr(29)+rr(30)+rr(31)+2.*rr(32)+rr(33)+rr(34)+rr(38)
     ++rr(41)+rr(43)
      dxdt(18)=NO2min-rr(36)+2.*rr(38)
      dxdt(19)=rr(37)
      dxdt(20)=rr(36)-rr(37)-2.*rr(38)
      dxdt(21)=rr(44)-rr(45)-rr(46)
      dxdt(22)=rr(46)-rr(47)
c
      return
      end
```

EPIS

```
      SUBROUTINE DRIVE (N, T0, H0, Y0, TOUT, EPS, IERROR, MF, INDEX)
C
C***********************************************************************
*
C
C  PURPOSE:
C  To Solve a System of Stiff ODEs, with custom modifications to
C   handle a non-negativity constraint and to keep error limited
C   where neither simple relative nor absolute error bounds
C   are appropriate.
C
C  ON ENTRY:
C  See original documentation below.
C
C  ON RETURN:
C  See original documentation below.
C
C  COMMENTS:
C  This is the November 1982 Modification (called EPIS)
C   by Dale Warren (Caltech) of the EPISODE program.
C  Adapted in February 1986 for the IBM AT running
C   MICROSOFT FORTRAN-77 v3.20.
C  The ability to convert to DOUBLE PRECISION has been
C   removed (for conciseness and readability).
C
C***********************************************************************
*
C      THE JUNE 24, 1975  VERSION OF
C EPISODE..  EXPERIMENTAL PACKAGE FOR INTEGRATION OF
C SYSTEMS OF ORDINARY DIFFERENTIAL EQUATIONS,
C    DY/DT = F(Y,T),  Y = (Y(1),Y(2),...,Y(N)) TRANSPOSE,
C GIVEN THE INITIAL VALUE OF Y.
C THIS CODE IS FOR THE IBM 370/195 AT ARGONNE NATIONAL LABORATORY
C AND IS A MODIFICATION OF EARLIER VERSIONS BY G.D.BYRNE
C AND A.C.HINDMARSH.
C                  REFERENCES
C 1.  G. D. BYRNE AND A. C. HINDMARSH, A POLYALGORITHM FOR THE
C       NUMERICAL SOLUTION OF ORDINARY DIFFERENTIAL EQUATIONS,

C       UCRL-75652, LAWRENCE LIVERMORE LABORATORY, P. O. BOX 808,
C       LIVERMORE, CA 94550, APRIL 1974. ALSO IN ACM TRANSACTIONS
C       ON MATHEMATICAL SOFTWARE, 1 (1975), PP. 71-96.
C
C 2.  A. C. HINDMARSH AND G. D. BYRNE, EPISODE.. AN EXPERIMENTAL
C       PACKAGE FOR THE INTEGRATION OF SYSTEMS OF ORDINARY
C       DIFFERENTIAL EQUATIONS, UCID-30112, L.L.L., MAY, 1975.
C
C 3.  A. C. HINDMARSH, GEAR.. ORDINARY DIFFERENTIAL EQUATION
C       SYSTEM SOLVER, UCID-30001, REV. 3, L.L.L., DECEMBER, 1974.
C
C----------------------------------------------------------------------
-
C DRIVE IS A DRIVER SUBROUTINE FOR THE EPISODE PACKAGE.
C DRIVE IS TO BE CALLED ONCE FOR EACH OUTPUT VALUE OF T.
C IT THEN MAKES REPEATED CALLS TO THE CORE INTEGRATOR
C SUBROUTINE, TSTEP.
C
C THE INPUT PARAMETERS ARE AS FOLLOWS.
C   N      =  THE NUMBER OF DIFFERENTIAL EQUATIONS (USED ONLY ON
C               FIRST CALL, UNLESS INDEX = -1).  N MUST NEVER BE
```

```
C                 INCREASED DURING A GIVEN PROBLEM.
C    T0     =   THE INITIAL VALUE OF T, THE INDEPENDENT VARIABLE
C                 (USED FOR INPUT ONLY ON FIRST CALL).
C    H0     =   THE STEP SIZE IN T (USED FOR INPUT ONLY ON THE
C                 FIRST CALL, UNLESS INDEX = 3 ON INPUT).  WHEN
C                 INDEX = 3, H0 IS THE MAXIMUM ABSOLUTE VALUE OF
C                 THE STEP SIZE TO BE USED.
C    Y0     =   A VECTOR OF LENGTH N CONTAINING THE INITIAL VALUES OF
C                 Y (USED FOR INPUT ONLY ON FIRST CALL).
C    TOUT   =   THE VALUE OF T AT WHICH OUTPUT IS DESIRED NEXT.
C                 INTEGRATION WILL NORMALLY GO BEYOND TOUT AND
C                 INTERPOLATE TO T = TOUT.  (USED ONLY FOR INPUT.)
C    EPS    =   THE RELATIVE ERROR BOUND (USED ONLY ON FIRST CALL,
C                 UNLESS INDEX = -1).  THIS BOUND IS USED AS FOLLOWS.
C                 LET R(I) DENOTE THE ESTIMATED RELATIVE LOCAL ERROR
C                 IN Y(I), I.E. THE ERROR RELATIVE TO YMAX(I), AS
C                 MEASURED PER STEP (OF SIZE H) OR PER SS UNITS OF T.
C                 THEN EPS IS A BOUND ON THE ROOT-MEAN-SQUARE NORM
C                 OF THE VECTOR R, I.E.
C                          N
C                 SQRT ( SUM ( R(I)**2 )/N ) .LT. EPS.
C                         I=1
C                 THE VECTOR YMAX IS COMPUTED IN DRIVE AS DESCRIBED
C                 UNDER IERROR BELOW.
C                 IF ERROR CONTROL PER SS UNITS OF T IS DESIRED, SET SS
C                 TO A POSITIVE NUMBER AFTER STATEMENT 10 (WHERE IT IS
C                 NOW SET TO ZERO) AND UPDATE IT AFTER STATEMENT 60.
C                 SEE ALSO THE COMMENTS ON SS AND YMAX BELOW.
C  IERROR =   THE ERROR FLAG WITH VALUES AND MEANINGS AS FOLLOW.
C         1     ABSOLUTE ERROR IS CONTROLLED.  YMAX(I) = 1.0.
C         2     ERROR RELATIVE TO ABS(Y) IS CONTROLLED.  IF Y(I) = 0.0
C               A DIVIDE ERROR WILL Not OCCUR.  YMAX(I) = ABS(Y(I)).
C         3     ERROR RELATIVE TO THE LARGEST VALUE OF ABS(Y(I)) SEEN
C               SO FAR IS CONTROLLED.  IF THE INITIAL VALUE OF Y(I) IS
C               0.0, THEN YMAX(I) IS SET TO 1.0 INITIALLY AND REMAINS
C               AT LEAST 1.0.
C         4     SAME AS 2 EXCEPT IF Y(I) INITIALLY <YMIN, YMAX(I)=YMIN
C         5     SAME AS 3 EXCEPT IF Y(I) CURRENTLY <YMIN, YMAX(I)=YMIN
C         6     SAME AS 4 EXCEPT IF Y(I) < 0., Error Criteria Not Met
C         7     SAME AS 5 EXCEPT IF Y(I) < 0., Error Criteria Not Met
C         8     SAME AS 4 EXCEPT IF Y(I) < -YMIN, Error Criteria Not Met
C         9     SAME AS 5 EXCEPT IF Y(I) < -YMIN, Error Criteria Not Met
C       Note: For 6-9, Special Modification so Y(N)<0. rejected
C             4 & 5 were added for problems when
C              IERROR=2 fails because of divide by zero and
C              IERROR=3 scales poorly to ONE  -DRW
C         Note 4 & 5 require user to set YMIN reasonably in DRIVES
C    MF     =   THE METHOD FLAG (USED ONLY ON FIRST CALL, UNLESS
C                 INDEX = -1).  ALLOWED VALUES ARE 10, 11, 12, 13,
C                 20, 21, 22, 23.  MF IS AN INTEGER WITH TWO DECIMAL
C                 DIGITS, METH AND MITER (MF = 10*METH + MITER).  (MF
C                 CAN BE THOUGHT OF AS THE ORDERED PAIR (METH,MITER).)
C                 METH IS THE BASIC METHOD INDICATOR.
C                   METH = 1 INDICATES VARIABLE-STEP SIZE, VARIABLE-
C                            ORDER ADAMS METHOD, SUITABLE FOR NON-
C                            STIFF PROBLEMS.
C                   METH = 2 INDICATES VARIABLE-STEP SIZE, VARIABLE-
C                            ORDER BACKWARD DIFFERENTIATION METHOD,
C                            SUITABLE FOR STIFF PROBLEMS.
C                 MITER INDICATES THE METHOD OF ITERATIVE CORRECTION
```

```
C                (NONLINEAR SYSTEM SOLUTION).
C                MITER = 0 INDICATES FUNCTIONAL ITERATION (NO
C                          PARTIAL DERIVATIVES NEEDED).
C                MITER = 1 INDICATES A CHORD OR SEMI-STATIONARY
C                          NEWTON METHOD WITH CLOSED FORM (EXACT)
C                          JACOBIAN, WHICH IS COMPUTED IN THE
C                          USER SUPPLIED SUBROUTINE
C                          PEDERV(N,T,Y,PD,N0) DESCRIBED BELOW.
C                MITER = 2 INDICATES A CHORD  OR SEMI-STATIONARY
C                          NEWTON METHOD WITH AN INTERNALLY
C                          COMPUTED FINITE DIFFERENCE APPROXIMATION
C                          TO THE JACOBIAN.
C                MITER = 3 INDICATES A CHORD OR SEMI-STATIONARY
C                          NEWTON METHOD WITH AN INTERNALLY
C                          COMPUTED DIAGONAL MATRIX APPROXIMATION
C                          TO THE JACOBIAN, BASED ON A DIRECTIONAL
C                          DERIVATIVE.
C   INDEX =  INTEGER USED ON INPUT TO INDICATE TYPE OF CALL,
C              WITH THE FOLLOWING VALUES AND MEANINGS..
C         1    THIS IS THE FIRST CALL FOR THIS PROBLEM.
C         0    THIS IS NOT THE FIRST CALL FOR THIS PROBLEM,
C              AND INTEGRATION IS TO CONTINUE.
C        -1    THIS IS NOT THE FIRST CALL FOR THE PROBLEM,
C              AND THE USER HAS RESET N, EPS, AND/OR MF.
C         2    SAME AS 0 EXCEPT THAT TOUT IS TO BE HIT
C              EXACTLY (NO INTERPOLATION IS DONE).
C              ASSUMES TOUT .GE. THE CURRENT T.
C         3    SAME AS 0 EXCEPT CONTROL RETURNS TO CALLING
C              PROGRAM AFTER ONE STEP.  TOUT IS IGNORED.
C         7    THIS IS NOT THE FIRST CALL, BUT THE Y ARRAY
C              HAS CHANGED SLIGHTLY, SO THE DERIVATIVES
C              MUST BE RECOMPUTED (NEW by DRW)
C            SINCE THE NORMAL OUTPUT VALUE OF INDEX IS 0,
C            IT NEED NOT BE RESET FOR NORMAL CONTINUATION.
C            SINCE THE NORMAL OUTPUT VALUE OF INDEX IS 0,
C            IT NEED NOT BE RESET FOR NORMAL CONTINUATION.
C
C AFTER THE INITIAL CALL, IF A NORMAL RETURN OCCURRED AND A NORMAL
C CONTINUATION IS DESIRED, SIMPLY RESET TOUT AND CALL AGAIN.
C ALL OTHER PARAMETERS WILL BE READY FOR THE NEXT CALL.
C A CHANGE OF PARAMETERS WITH INDEX = -1 CAN BE MADE AFTER
C EITHER A SUCCESSFUL OR AN UNSUCCESSFUL RETURN.
C
C THE OUTPUT PARAMETERS ARE AS FOLLOWS.
C   T0     =  THE OUTPUT VALUE OF T.  IF INTEGRATION WAS SUCCESSFUL,
C             T0 = TOUT.  OTHERWISE, T0 IS THE LAST VALUE OF T
C             REACHED SUCCESSFULLY.
C   H0     =  THE STEP SIZE H USED LAST, WHETHER SUCCESSFULLY OR NOT.
C   Y0     =  THE COMPUTED VALUES OF Y AT T = T0.
C   INDEX =  INTEGER USED ON OUTPUT TO INDICATE RESULTS,
C              WITH THE FOLLOWING VALUES AND MEANINGS..
C         0    INTEGRATION WAS COMPLETED TO TOUT OR BEYOND.
C        -1    THE INTEGRATION WAS HALTED AFTER FAILING TO PASS THE
C              ERROR TEST EVEN AFTER REDUCING H BY A FACTOR OF
C              1.E10 FROM ITS INITIAL VALUE.
C        -2    AFTER SOME INITIAL SUCCESS, THE INTEGRATION WAS
C              HALTED EITHER BY REPEATED ERROR TEST FAILURES OR
C              BY A TEST ON EPS.  POSSIBLY TOO MUCH ACCURACY HAS
C              BEEN REQUESTED, OR A BAD CHOICE OF MF WAS MADE.
C        -3    THE INTEGRATION WAS HALTED AFTER FAILING TO ACHIEVE
```

```
C               CORRECTOR CONVERGENCE EVEN AFTER REDUCING H BY A
C               FACTOR OF 1.E10 FROM ITS INITIAL VALUE.
C         -4    IMMEDIATE HALT BECAUSE OF ILLEGAL VALUES OF INPUT
C               PARAMETERS.  SEE PRINTED MESSAGE.
C         -5    INDEX WAS -1 ON INPUT, BUT THE DESIRED CHANGES OF
C               PARAMETERS WERE NOT IMPLEMENTED BECAUSE TOUT
C               WAS NOT BEYOND T.  INTERPOLATION TO T = TOUT WAS
C               PERFORMED AS ON A NORMAL RETURN.  TO CONTINUE,
C               SIMPLY CALL AGAIN WITH INDEX = -1 AND A NEW TOUT.
C         -6    INDEX WAS 2 ON INPUT, BUT TOUT WAS NOT BEYOND T.
C               NO ACTION WAS TAKEN.
C    -7     INTEGRATION SUSPENDED BECAUSE A Y(I)<0 FOUND,
C               WITH NRMIN<=I<=NRMAX, AND IERROR OF 6 OR 7
C               HAD PROSCRIBED AGAINST NEGATIVE VALUES --DRW
C
C IN ADDITION TO DRIVE, THE FOLLOWING SUBROUTINES ARE USED BY AND
C PROVIDED IN THIS PACKAGE:
C   INTERP(TOUT,Y,N0,Y0)  INTERPOLATES TO GIVE OUTPUT VALUES AT
C                         T = TOUT  BY USING DATA IN THE Y ARRAY.
C   TSTEP(Y,N0)  IS THE CORE INTEGRATION SUBROUTINE, WHICH INTEGRATES
C                OVER A SINGLE STEP AND DOES ASSOCIATED ERROR
C                CONTROL.
C   COSET  SETS COEFFICIENTS FOR USE IN TSTEP.
C   ADJUST(Y,N0)  ADJUSTS THE HISTORY ARRAY Y ON REDUCTION OF ORDER.
C   PSET(Y,N0,CON,MITER,IER)  COMPUTES AND PROCESSES THE JACOBIAN
C                             MATRIX, J = DF/DY.
C   DEC(N,N0,A,IP,IER)  PERFORMS THE LU DECOMPOSITION OF A MATRIX.
C   SOL(N,N0,A,B,IP)  SOLVES A LINEAR SYSTEM A*X = B, AFTER DEC
C                     HAS BEEN CALLED FOR THE MATRIX A.
C NOTE:  PSET, DEC, AND SOL ARE CALLED IF AND ONLY IF MITER = 1
C        OR MITER = 2.
C
C THE USER MUST FURNISH THE FOLLOWING SUBROUTINES:
C   DIFFUN(N,T,Y,YDOT)  COMPUTES THE FUNCTION  YDOT = F(Y,T),
C                       THE RIGHT HAND SIDE OF THE ORDINARY
C                       DIFFERENTIAL EQUATION SYSTEM, WHERE Y
C                       AND YDOT ARE VECTORS OF LENGTH N.
C   PEDERV(N,T,Y,PD,N0)  COMPUTES THE N BY N JACOBIAN MATRIX OF
C                        PARTIAL DERIVATIVES AND STORES IT IN PD AS
C                        AN N0 BY N0 ARRAY.   PD(I,J) IS TO BE SET
C                        TO THE PARTIAL DERIVATIVE OF YDOT(I) WITH
C                        RESPECT TO Y(J).  PEDERV IS CALLED IF AND
C                        ONLY IF MITER = 1. FOR OTHER VALUES OF
C                        MITER, PEDERV CAN BE A DUMMY SUBROUTINE.
C
C CAUTION:  AT THE PRESENT TIME THE MAXIMUM NUMBER OF DIFFERENTIAL
C           EQUATIONS, WHICH CAN BE SOLVED BY EPISODE, IS 20.  TO
C           CHANGE THIS NUMBER TO A NEW VALUE, SAY NMAX, CHANGE
C           Y(20,13) TO Y(NMAX,13), YMAX(20) TO YMAX(NMAX),
C           ERROR(20) TO ERROR(NMAX), SAVE1(20) TO SAVE1(NMAX),
C           SAVE2(20) TO SAVE2(NMAX), PW(400) TO PW(NMAX*NMAX),
C           AND IPIV(20) TO IPIV(NMAX) IN THE COMMON AND DIMENSION
C           STATEMENTS BELOW.  ALSO CHANGE THE ARGUMENT IN THE
C           IF...GO TO 440 STATEMENT (AFTER THE COMMON STATEMENTS)
C           FROM 20 TO NMAX.  NO OTHER CHANGES NEED TO BE MADE TO
C           ANY OTHER SUBROUTINE IN THIS PACKAGE WHEN THE MAXIMUM
C           NUMBER OF EQUATIONS IS CHANGED.  ELSEWHERE, THE COLUMN
C           LENGTH OF THE Y ARRAY IS N0 INSTEAD OF 20.  THE ROW
C           LENGTH OF Y CAN BE REDUCED FROM 13 TO 6 IF METH = 2.
C           THE ARRAY IPIV IS USED IF AND ONLY IF MITER = 1 OR
```

```
C            MITER = 2.  THE SIZE OF THE PW ARRAY CAN BE REDUCED
C            TO 1 IF MITER = 0 OR TO N IF MITER = 3.
C
C THE COMMON BLOCK EPCOM9 CAN BE ACCESSED EXTERNALLY BY THE USER,
C IF HE DESIRES.  IT CONTAINS THE STEP SIZE LAST USED SUCCESSFULLY
C (HUSED), THE ORDER LAST USED SUCCESSFULLY (NQUSED), THE
C NUMBER OF STEPS TAKEN SO FAR (NSTEP), THE NUMBER OF FUNCTION
C EVALUATIONS (DIFFUN CALLS) SO FAR (NFE), AND THE NUMBER OF
C JACOBIAN EVALUATIONS SO FAR (NJE).
C
C IN A DATA STATEMENT BELOW, LOUT IS SET TO THE LOGICAL UNIT NUMBER
C FOR THE OUTPUT OF MESSAGES DURING INTEGRATION.  CURRENTLY, LOUT
C = 3.
C-----------------------------------------------------------------------
-
C$ THIS IS THE SINGLE PRECISION VERSION OF SUBROUTINE DRIVE.
C
C               Set Maximum number of dif. eqs.
      PARAMETER ( NMAX =120 )
      PARAMETER ( NMAXSQ = NMAX*NMAX )
C*
C  All the Explicit Variable Type Definitions are Unnecessary
C  Simply insert the following card in the each module
C       IMPLICIT REAL*#(A-H,O-Z) , INTEGER(I-N)
C  Where # is 8 for Double Precision and 4 for Single Precision
C*
      INTEGER IERROR, INDEX, MF, N
      INTEGER IPIV, JSTART, KFLAG, MFC, NC, NFE, NJE,
     1        NQUSED, NSQ, NSTEP
      INTEGER I, KGO, NHCUT, N0
      INTEGER LOUT
      INTEGER NFLAG
      REAL EPS, H0, TOUT, T0, Y0
      REAL EPSC, EPSJ, ERROR, HMAX, H, HMIN, HUSED,
     1     PW, SAVE1, SAVE2, SS, T, UROUND, YMAX
      REAL AYI, D, T0P, Y
      REAL HCUT
      REAL FOUR, HUNDRD, ONE, TEN, ZERO
      REAL*4 YMIN,YCUT
      DIMENSION Y(NMAX,13)
      DIMENSION Y0(N)
C
      COMMON /EPCOM1/T,H,HMIN,HMAX,EPSC,SS,UROUND,NC,MFC,KFLAG,JSTART
      COMMON /EPCOM2/ YMAX(NMAX)
      COMMON /EPCOM3/ ERROR(NMAX)
      COMMON /EPCOM4/ SAVE1(NMAX)
      COMMON /EPCOM5/ SAVE2(NMAX)
      COMMON /EPCOM6/ PW(NMAXSQ)
      COMMON /EPCOM7/ IPIV(NMAX)
      COMMON /EPCOM8/ EPSJ,NSQ
      COMMON /EPCOM9/ HUSED,NQUSED,NSTEP,NFE,NJE
C                  For # of Evaluations
      COMMON /EPCO99/ NCSTEP,NCFE,NCJE
C                  Set by calling prog - DRW
      COMMON /EPCOMR/ NRMIN,NRMAX
C                  Set by calling prog - DRW
      COMMON /EPCOMY/ YMIN,HMAXMX
C
C               Messages to Unit # 3, or FOR003.DAT
      DATA LOUT /11/
```

```
      DATA HCUT /0.1E0/
      DATA FOUR /4.0E0/, HUNDRD /1.0E2/, ONE  /1.0E0/,
     1     TEN  /1.0E1/, ZERO   /0.0E0/
C           Convenient for Nucleation Tests - DRW
C     DATA YMIN /1.0E-17/
C               Normal Continuation
      IF (INDEX .EQ. 0) GOTO 20
C               Continue & Hit Exactly
      IF (INDEX .EQ. 2) GOTO 25
C               Integration Mode Reset
      IF (INDEX .EQ. -1) GOTO 30
C               Single Step Integration
      IF (INDEX .EQ. 3) GOTO 40
C               NEW -- Continue with Y modified
      IF (INDEX .EQ. 7) GOTO 27
C               Bad Input; 1 is First Call
      IF (INDEX .NE. 1) GOTO 430
C
      IF (EPS .LE. ZERO) GOTO 400
      IF (N .LE. 0) GOTO 410
      IF (N .GT. NMAX) GOTO 440
      IF ((T0-TOUT)*H0 .GE. ZERO) GOTO 420
      WRITE(LOUT,999) T0,H0,TOUT
  999 FORMAT(1H ,2X,'T0=',E12.5,2X,'H0=',E12.5,2X,'TOUT=',E12.5)
C-----------------------------------------------------------------------
-
C IF INITIAL VALUES FOR YMAX OTHER THAN THOSE BELOW ARE DESIRED,
C THEY SHOULD BE SET HERE.  ALL YMAX(I) MUST BE POSITIVE.  IF
C VALUES FOR HMIN OR HMAX, THE BOUNDS ON THE ABSOLUTE VALUE OF H,
C OTHER THAN THOSE BELOW, ARE DESIRED, THEY ALSO SHOULD BE SET HERE.
C IF ERROR PER SS UNITS OF T IS TO BE CONTROLLED, SS SHOULD BE SET
C TO A POSITIVE VALUE BELOW.  ERROR PER UNIT STEP IS CONTROLLED
C WHEN SS = 1.  THE DEFAULT VALUE FOR SS IS 0 AND YIELDS CONTROL
C OF ERROR PER STEP.
C-----------------------------------------------------------------------
-
C SET UROUND, THE MACHINE ROUNDOFF CONSTANT, HERE.
C USE STATEMENT BELOW FOR SHORT PRECISION ON IBM 360 OR 370.
C     UROUND = 9.53674E-7
C USE STATEMENT BELOW FOR SINGLE PRECISION ON CDC 7600 OR 6600.
C     UROUND = 7.105427406E-15
C USE STATEMENT BELOW FOR LONG PRECISION ON IBM 360 OR 370.
C-----------------------------------------------------------------------
-
C               Set for VAX Single Precision
      UROUND = 5.960E-8
      IF (IERROR.LE.5) GOTO 3
C               Default check for negative Y(I)
      IF (NRMIN.LE.0) NRMIN=1
C               or, for all values of I
C      IF (NRMAX.LE.0) NRMAX=N
C               Special for MAEROS with Vapor
      IF (NRMAX.LE.0) NRMAX=N-1
C
C
  3   DO 10 I = 1,N
C
   GOTO (5, 6, 7, 8, 8, 8, 8, 8, 8), IERROR
C IERROR  =   1, 2, 3, 4, 5, 6, 7, 8, 9 ------Six Extra by DRW---------
-
```

```
C
C                    For ABSOLUTE Error
  5      YMAX(I) = ONE
   GOTO 10
  6      YMAX(I) = ABS(Y0(I))
C                    To Avoid Automatic /0
         IF (YMAX(I).EQ.ZERO) YMAX(I)=YMIN
         GOTO 10
  7      YMAX(I) = ABS(Y0(I))
C                    For SEMI-RELATIVE to 1.
    IF (YMAX(I) .EQ. ZERO) YMAX(I) = ONE
         GOTO 10
C                    For RELATIVE Error
  8      YMAX(I) = ABS(Y0(I))
C      WRITE(LOUT,998) I,YMAX(I),ABS(Y0(I)),YMIN
C 998 FORMAT(1H ,2X,'I=',I2,2X,'YMAX=',E12.5,2X,'ABY=',E12.5,2X,
C     $'YMIN=',E12.5)
         IF (YMAX(I) .LT. YMIN) YMAX(I) = YMIN
 10      Y(I,1) = Y0(I)
       NC = N
       T = T0
       H = H0
       WRITE(LOUT,997) NC,T,H
  997 FORMAT(1H ,2X,'NC=',I2,2X,'T=',E12.5,2X,'H=',E12.5)
       IF ((T+H) .EQ. T) WRITE(LOUT,15) T
CO 15    FORMAT(/46H---  MESSAGE FROM SUBROUTINE DRIVE IN EPISODE,,
CO      1       24H THE O.D.E. SOLVER.  ---/22H WARNING.. T + H = T =,
CO      2       E18.8,18H IN THE NEXT STEP./)
 15    FORMAT(' WARNING... T + H = T =',1PE16.7,' IN THE NEXT STEP.')
       HMIN = ABS(H0)
       HMAX = ABS(T0 - TOUT)*TEN
       HMAX = AMIN1(HMAX,HMAXMX)
       EPSC = EPS
       MFC = MF
       JSTART = 0
       SS = ZERO
       N0 = N
       NSQ = N0*N0
       EPSJ = SQRT(UROUND)
       NHCUT = 0
       YCUT= ZERO
       IF (IERROR.GE.8) YCUT=-YMIN
       GOTO 50
C T0P IS THE PREVIOUS OUTPUT VALUE OF T0 FOR USE IN HMAX. ------------
-
  20   HMAX = ABS(TOUT - T0P)*TEN
       HMAX = AMIN1(HMAX,HMAXMX)
       GOTO 80
  25   HMAX = ABS(TOUT - T0P)*TEN
       HMAX = AMIN1(HMAX,HMAXMX)
C
        IF ((T-TOUT)*H .GE. ZERO) GOTO 460
        GOTO 85
C
C           Throw out old derivative information
 27    JSTART = 0
C?       H=H0    ! Use New Step Size (if MAIN changed it)?
       IF ((T0-TOUT)*H0 .GE. ZERO) GOTO 420
       GOTO 45
C
```

```
 30    IF ((T-TOUT)*H .GE. ZERO) GOTO 450
       IF (MF .NE. MFC) JSTART = -1
       NC = N
       EPSC = EPS
       MFC = MF
       GOTO 45
C
 40    HMAX = H0
       HMAX = AMIN1(HMAX,HMAXMX)
C
C                    Round-off Warning
 45    IF ((T+H) .EQ. T) WRITE(LOUT,15) T
C
 50    CALL TSTEP (Y, N0)
C
       KGO = 1 - KFLAG
C      WRITE(LOUT,996) KFLAG
C 996 FORMAT(1H ,2X,'KFLAG='I3)
       GOTO (60, 100, 200, 300), KGO
C KFLAG  =   0,  -1,  -2,  -3  ----------------------------------------
-
C
 60    CONTINUE
C-------------------------------------------------------------------
-
C NORMAL RETURN FROM TSTEP.
C
C THE WEIGHTS YMAX(I) ARE UPDATED.  IF DIFFERENT VALUES ARE DESIRED,
C THEY SHOULD BE SET HERE.  IF SS IS TO BE UPDATED FOR CONTROL OF
C ERROR PER SS UNITS OF T, IT SHOULD ALSO BE DONE HERE.  A TEST IS
C MADE TO DETERMINE IF EPS IS TOO SMALL FOR MACHINE PRECISION.
C
C ANY OTHER TESTS OR CALCULATIONS THAT ARE REQUIRED AFTER EACH STEP
C SHOULD BE INSERTED HERE.
C
C IF INDEX = 3, Y0 IS SET TO THE CURRENT Y VALUES ON RETURN.
C IF INDEX = 2, H IS CONTROLLED TO HIT TOUT (WITHIN ROUNDOFF
C ERROR), AND THEN THE CURRENT Y VALUES ARE PUT IN Y0 ON
C RETURN.  FOR ANY OTHER VALUE OF INDEX, CONTROL RETURNS TO
C THE INTEGRATOR UNLESS TOUT HAS BEEN REACHED.  THEN
C INTERPOLATED VALUES OF Y ARE COMPUTED AND STORED IN Y0 ON
C RETURN.
C IF INTERPOLATION IS NOT DESIRED, THE CALL TO INTERP SHOULD
C BE DELETED AND CONTROL TRANSFERRED TO STATEMENT 500 INSTEAD
C OF 520.
C-------------------------------------------------------------------
-
C
C      DO 990 I=1,N
C      IF(Y(I,1).LE.1.0E-20) Y(I,1)=1.0E-20
C 990 CONTINUE
C
       D = ZERO
C           Initialize to no negative problem
       NFLAG = 0
       DO 70 I = 1,N
         AYI = ABS(Y(I,1))
    GOTO (70, 62, 68, 64, 68, 63, 67, 63, 67), IERROR
C IERROR  =     1,  2,  3,  4,  5,  6,  7,  8,  9 --------DRW --------
-
```

```
C
C               Relative Error
   62     YMAX(I) = AYI
C               No sense in permitting /0.
          IF (AYI.EQ.ZERO) YMAX(I)=YMIN
    GOTO 70
   63   IF (Y(I,1).LT.YCUT.AND.I.GE.NRMIN.AND.I.LE.NRMAX) NFLAG=I
C             Relative Error not below YMIN -DRW
   64     YMAX(I) = AMAX1(AYI,YMIN)
          GOTO 70
   67   IF (Y(I,1).LT.YCUT.AND.I.GE.NRMIN.AND.I.LE.NRMAX) NFLAG=I
C               SemiRelative Error
   68     YMAX(I) = AMAX1(YMAX(I), AYI)
          GOTO 70
   70   D = D + (AYI/YMAX(I))**2
        D = D*(UROUND/EPS)**2
C                     Halt Condition
        IF (D .GT. FLOAT(N)) GOTO 250
        IF (INDEX .EQ. 3) GOTO 500
        IF (INDEX .EQ. 2) GOTO 85
C                     Integration Passed TOUT
  80    IF ((T-TOUT)*H .GE. ZERO) GOTO 82
C               Negative Value Error
        IF (NFLAG.GT.0) GOTO 275
C               Keep Going in Time
        GOTO 45
C               Passed TOUT, set Y0
  82    CALL INTERP (TOUT, Y, N0, Y0)
C               Done, so T0=TOUT
        T0 = TOUT
        GOTO 520
  85    IF (((T+H)-TOUT)*H .LE. ZERO) GOTO 45
        IF (ABS(T-TOUT) .LE. HUNDRD*UROUND*HMAX) GOTO 500
        IF ((T-TOUT)*H .GE. ZERO) GOTO 500
        H = (TOUT - T)*(ONE - FOUR*UROUND)
        JSTART = -1
        GOTO 45
C-----------------------------------------------------------------------
-
C ON AN ERROR RETURN FROM TSTEP, AN IMMEDIATE RETURN OCCURS IF
C KFLAG = -2, AND RECOVERY ATTEMPTS ARE MADE OTHERWISE.
C TO RECOVER, H AND HMIN ARE REDUCED BY A FACTOR OF .1 UP TO 10
C TIMES BEFORE GIVING UP.
C-----------------------------------------------------------------------
-
  100   WRITE (LOUT,101)
  101   FORMAT (/46H---  MESSAGE FROM SUBROUTINE DRIVE IN EPISODE,,
       1        24H THE O.D.E. SOLVER.   ---/)
        WRITE(LOUT,105) T,HMIN
  105   FORMAT(//35H KFLAG = -1 FROM INTEGRATOR AT T = ,1PE16.6/
       1       40H  ERROR TEST FAILED WITH ABS(H) = HMIN =,1PE16.6/)
  110   IF (NHCUT .EQ. 10) GOTO 150
        NHCUT = NHCUT + 1
        HMIN = HCUT*HMIN
        H = HCUT*H
        WRITE (LOUT,115) H
  115   FORMAT(24H  H HAS BEEN REDUCED TO ,1PE16.6,
       1       26H  AND STEP WILL BE RETRIED//)
        JSTART = -1
        GOTO 45
```

```
C
 150  WRITE (LOUT,155)
 155  FORMAT(//44H PROBLEM APPEARS UNSOLVABLE WITH GIVEN INPUT//)
      GOTO 500
C
 200  WRITE (LOUT,101)
      WRITE (LOUT,205) T,H,EPS
 205  FORMAT(//14H KFLAG= -2  T=,1PE17.7,4H H =,E16.6,6H EPS =,E16.6/
     1       50H  THE REQUESTED ERROR IS TOO SMALL FOR INTEGRATOR.//)
      GOTO 500
C
 250  WRITE (LOUT,101)
      WRITE (LOUT,255) T,EPS
 255  FORMAT(//46H INTEGRATION HALTED BY SUBROUTINE DRIVE AT T =,
     1     1PE17.8/43H EPS IS TOO SMALL FOR MACHINE PRECISION AND/
     2     29H PROBLEM BEING SOLVED.  EPS =,1PE16.6//)
      KFLAG = -2
      GOTO 500
C
 275  WRITE (LOUT,280) T,NFLAG,Y(NFLAG,1)
 280  FORMAT(' INTEGRATION SUSPENDED BY NEGATIVE CONCENTRATION AT',
     $' T=',1PE10.3/' ELEMENT #',I3,' WAS',1PE12.3,6X,'(DRIVES)')
      KFLAG=-7
C              INDEX for Negative Value
      GOTO 500
C
 300  WRITE (LOUT,101)
      WRITE (LOUT,305) T
 305  FORMAT(//34H KFLAG = -3 FROM INTEGRATOR AT T =,1PE18.8/
     1       45H  CORRECTOR CONVERGENCE COULD NOT BE ACHIEVED/)
      GOTO 110
C
 400  WRITE (LOUT,101)
      WRITE (LOUT,405) EPS
 405  FORMAT(//35H ILLEGAL INPUT.. EPS .LE. 0. EPS = ,E16.6//)
      INDEX = -4
      RETURN
C
 410  WRITE (LOUT,101)
      WRITE (LOUT,415) N
 415  FORMAT(//31H ILLEGAL INPUT.. N .LE. 0. N = ,I8//)
      INDEX = -4
      RETURN
C
 420  WRITE (LOUT,101)
      WRITE (LOUT,425) T0,TOUT,H0
 425  FORMAT(//39H ILLEGAL INPUT.. (T0 - TOUT)*H0 .GE. 0./
     1       5H T0 =,1PE18.8,7H TOUT =,E18.8,5H H0 =,E16.6//)
      INDEX = -4
      RETURN
C
 430  WRITE (LOUT,101)
      WRITE (LOUT,435) INDEX
 435  FORMAT(//24H ILLEGAL INPUT.. INDEX =,I8//)
      INDEX = -4
      RETURN
C
 440  WRITE (LOUT,101)
      WRITE (LOUT,445) N
 445  FORMAT (//39H ILLEGAL INPUT.  THE NUMBER OF ORDINARY/
```

```
     1        43H DIFFERENTIAL EQUATIONS BEING SOLVED IS N =, I6/
     2        42H STORAGE ALLOCATION IN SUBROUTINE DRIVE IS/
     3        46H TOO SMALL.  SEE COMMENTS IN SUBROUTINE DRIVE./)
      INDEX = -4
      RETURN
C
 450  WRITE (LOUT,101)
      WRITE (LOUT,455) T,TOUT,H
 455  FORMAT(//46H INDEX = -1 ON INPUT WITH (T - TOUT)*H .GE. 0./
     1        44H INTERPOLATION WAS DONE AS ON NORMAL RETURN./
     2        41H DESIRED PARAMETER CHANGES WERE NOT MADE./
     3        4H T =,E18.8,7H TOUT =,E18.8,4H H =,E16.6//)
      CALL INTERP (TOUT, Y, N0, Y0)
      T0 = TOUT
      INDEX = -5
      RETURN
C
 460  WRITE (LOUT,101)
      WRITE (LOUT,465) T,TOUT,H
 465  FORMAT(//45H INDEX = 2 ON INPUT WITH (T - TOUT)*H .GE. 0./
     1        4H T =,E18.8,7H TOUT =,E18.8,4H H =,E16.6//)
      INDEX = -6
      RETURN
C
 500  T0 = T
      DO 510 I = 1,N
 510    Y0(I) = Y(I,1)
 520  INDEX = KFLAG
      T0P = T0
      H0 = HUSED
      IF (KFLAG .NE. 0) H0 = H
      RETURN
      END
C
C=====================================================================
=
C
      SUBROUTINE INTERP (TOUT, Y, N0, Y0)
C---------------------------------------------------------------------
-
C SUBROUTINE INTERP COMPUTES INTERPOLATED VALUES OF THE DEPENDENT
C VARIABLE Y AND STORES THEM IN Y0.  THE INTERPOLATION IS TO THE
C POINT T = TOUT AND USES THE NORDSIECK HISTORY ARRAY Y AS FOLLOWS..
C                             NQ
C                 Y0(I)  =  SUM  Y(I,J+1)*S**J ,
C                           J=0
C WHERE S = -(T-TOUT)/H.
C---------------------------------------------------------------------
-
C$ THIS IS THE SINGLE PRECISION VERSION OF SUBROUTINE INTERP.
C---------------------------------------------------------------------
-
C CAUTION:  NOT ALL MEMBERS OF EPCOM1 ARE USED IN THIS SUBROUTINE.
C---------------------------------------------------------------------
-
      INTEGER N0
      INTEGER JSTART, KFLAG, MF, N
      INTEGER I, J, L
      REAL TOUT, Y, Y0
      REAL EPS, H, HMAX, HMIN, SS, T, UROUND
```

```
      REAL S, S1
      REAL ONE
      DIMENSION Y0(N0),Y(N0,13)
C
      COMMON /EPCOM1/ T,H,HMIN,HMAX,EPS,SS,UROUND,N,MF,KFLAG,JSTART
      DATA ONE /1.0E0/
      DO 10 I = 1,N
 10     Y0(I) = Y(I,1)
      L = JSTART + 1
      S = (TOUT - T)/H
      S1 = ONE
      DO 30 J = 2,L
        S1 = S1*S
        DO 20 I = 1,N
 20       Y0(I) = Y0(I) + S1*Y(I,J)
 30     CONTINUE
      RETURN
      END
C
C=====================================================================
=
C
      SUBROUTINE TSTEP (Y, N0)
C---------------------------------------------------------------------
-
C TSTEP PERFORMS ONE STEP OF THE INTEGRATION OF AN INITIAL VALUE
C PROBLEM FOR A SYSTEM OF ORDINARY DIFFERENTIAL EQUATIONS.
C COMMUNICATION WITH TSTEP IS VIA THE FOLLOWING VARIABLES..
C
C    Y        AN N0 BY LMAX ARRAY CONTAINING THE DEPENDENT VARIABLES
C               AND THEIR SCALED DERIVATIVES.  LMAX IS CURRENTLY 6 FOR
C               THE VARIABLE STEP BACKWARD DIFFERENTIATION FORMULAS,
C               AND 13 FOR THE VARIABLE STEP ADAMS FORMULAS.
C               (LMAX -1) = MAXDER, THE MAXIMUM ORDER USED.
C               SEE SUBROUTINE COSET.  Y(I,J+1) CONTAINS THE
C               J-TH DERIVATIVE OF Y(I), SCALED BY H**J/FACTORIAL(J)
C               FOR J = 0,1,...,NQ, WHERE NQ IS THE CURRENT ORDER.
C    N0       A CONSTANT INTEGER .GE. N, USED FOR DIMENSIONING
C               PURPOSES.
C    T        THE INDEPENDENT VARIABLE, UPDATED ON EACH STEP TAKEN.
C    H        THE STEP SIZE TO BE ATTEMPTED ON THE NEXT STEP.
C               H IS ALTERED BY THE ERROR CONTROL ALGORITHM DURING
C               THE SOLUTION OF THE PROBLEM. H CAN BE EITHER POSITIVE
C               OR NEGATIVE, BUT ITS SIGN MUST REMAIN CONSTANT
C               THROUGHOUT THE PROBLEM RUN.
C    HMIN,    THE MINIMUM AND MAXIMUM ABSOLUTE VALUES OF THE STEP
C     HMAX      SIZE TO BE USED FOR THE STEP. THESE MAY BE CHANGED AT
C               ANY TIME, BUT THE CHANGE WILL NOT TAKE EFFECT UNTIL THE
C               NEXT CHANGE IN H IS MADE.
C    EPS      THE RELATIVE ERROR BOUND.  SEE DESCRIPTION IN
C               SUBROUTINE DRIVE.
C    SS       THE SIZE OF THE TIME INTERVAL TO BE USED FOR ERROR
C               CONTROL.  A DEFAULT VALUE OF 0 IS USED TO PRODUCE
C               CONTROL OF ERROR PER STEP.  SEE SUBROUTINE DRIVE.
C    UROUND   THE UNIT OF ROUNDOFF FOR THE COMPUTER BEING USED.
C    N        THE NUMBER OF FIRST ORDER ORDINARY DIFFERENTIAL
C               EQUATIONS BEING SOLVED.
C    MF       THE METHOD FLAG.  SEE DESCRIPTION IN SUBROUTINE DRIVE.
C    KFLAG    A COMPLETION CODE WITH THE FOLLOWING MEANINGS..
C                      0  THE STEP WAS SUCCESFUL.
```

```
C                     -1  THE REQUESTED ERROR COULD NOT BE ACHIEVED
C                         WITH ABS(H) = HMIN.
C                     -2  THE REQUESTED ERROR IS SMALLER THAN CAN
C                         BE HANDLED FOR THIS PROBLEM.
C                     -3  CORRECTOR CONVERGENCE COULD NOT BE
C                         ACHIEVED FOR ABS(H) = HMIN.
C               ON A RETURN WITH KFLAG NEGATIVE, THE VALUES OF T AND
C               THE Y ARRAY ARE AS OF THE BEGINNING OF THE LAST
C               STEP AND H IS THE LAST STEP SIZE ATTEMPTED.
C    JSTART   AN INTEGER USED ON INPUT AND OUTPUT.
C               ON INPUT, IT HAS THE FOLLOWING VALUES AND MEANINGS..
C                        0  PERFORM THE FIRST STEP.
C                    .GT.0  TAKE A NEW STEP CONTINUING FROM THE LAST.
C                    .LT.0  TAKE THE NEXT STEP WITH A NEW VALUE OF
C                         H AND/OR MF.
C               ON EXIT, JSTART IS SET TO NQ, THE CURRENT ORDER OF THE
C               METHOD.
C    YMAX       AN ARRAY OF N ELEMENTS WITH WHICH THE ESTIMATED LOCAL
C                 ERRORS IN Y ARE COMPARED.
C    ERROR      AN ARRAY OF N ELEMENTS.  ERROR(I)/TQ(2) IS THE
C                 ESTIMATED LOCAL ERROR IN Y(I) PER SS UNITS OF
C                 T OR PER STEP (OF SIZE H).
C    SAVE1,     TWO ARRAYS FOR WORKING STORAGE,
C      SAVE2      EACH OF LENGTH N.
C    PW         A BLOCK OF LOCATIONS USED FOR THE PARTIAL DERIVATIVES
C                 OF F WITH RESPECT TO Y, IF MITER IS NOT 0.  SEE
C                 DESCRIPTION IN SUBROUTINE DRIVE.
C    IPIV       AN INTEGER ARRAY OF LENGTH N, WHICH IS USED FOR PIVOT
C                 INFORMATION FOR THE LINEAR ALGEBRAIC SYSTEM IN THE
C                 CORRECTION PROCESS, WHEN MITER = 1 OR 2.
C
C THE COMMON BLOCK EPCM10, DECLARED BELOW, IS PRIMARILY INTENDED
C FOR INTERNAL USE, BUT IT CAN BE ACCESSED EXTERNALLY.
C-----------------------------------------------------------------------
-
C$ THIS IS THE SINGLE PRECISION VERSION OF SUBROUTINE TSTEP.
C-----------------------------------------------------------------------
-
      PARAMETER ( NMAX =120 )
      PARAMETER ( NMAXSQ = NMAX*NMAX )
      INTEGER N0
      INTEGER IPIV, JSTART, KFLAG, L, LMAX, METH, MF, N, NFE, NJE,
     1        NQ, NQINDX, NQUSED, NSTEP
      INTEGER I, IBACK, IER, IREDO, J, J1, J2, M, MFOLD, MIO,
     1        MITER, MITER1, NEWJ, NSTEPJ
      INTEGER ISTEPJ, KFC, KFH, MAXCOR
      REAL Y
      REAL EL, EPS, ERROR, H, HMAX, HMIN, HUSED, PW,
     1     SAVE1, SAVE2, SS, T, TAU, TQ, UROUND, YMAX
      REAL BND, CNQUOT, CON, CONP, CRATE, D, DRC,
     1     D1, E, EDN, ETA, ETAMAX, ETAMIN, ETAQ, ETAQM1,
     2     ETAQP1, EUP, FLOTL, FLOTN, HOLD, HRL1, PHRL1,
     3     PRL1, R, RC, RL1, R0, R1, TOLD
      REAL ADDON, BIAS1, BIAS2, BIAS3, CRDOWN, DELRC,
     1     ETACF, ETAMXF, ETAMX1, ETAMX2,
     2     ETAMX3, ONEPSM, SHORT, THRESH
      REAL ONE, PT5, ZERO
C* Multiple Declaration of ETAMIN fixed - DRW
      DIMENSION Y(N0,13)
C
```

```
      COMMON /EPCOM1/ T,H,HMIN,HMAX,EPS,SS,UROUND,N,MF,KFLAG,JSTART
      COMMON /EPCOM2/ YMAX(NMAX)
      COMMON /EPCOM3/ ERROR(NMAX)
      COMMON /EPCOM4/ SAVE1(NMAX)
      COMMON /EPCOM5/ SAVE2(NMAX)
      COMMON /EPCOM6/ PW(NMAXSQ)
      COMMON /EPCOM7/ IPIV(NMAX)
      COMMON /EPCOM9/ HUSED,NQUSED,NSTEP,NFE,NJE
      COMMON /EPCM10/ TAU(13),EL(13),TQ(5),LMAX,METH,NQ,L,NQINDX
      COMMON /EPCO99/ NCSTEP,NCFE,NCJE
C
      DATA ISTEPJ /20/, KFC /-3/, KFH /-7/, MAXCOR /3/
      DATA ADDON  /1.0E-6/,    BIAS1  /2.5E1/, BIAS2  /2.5E1/,
     1     BIAS3  /1.0E2/,     CRDOWN /0.1E0/, DELRC  /0.3E0/,
     2     ETACF  /0.25E0/,    ETAMIN /0.1E0/, ETAMXF /0.2E0/,
     3     ETAMX1 /1.0E4/,     ETAMX2 /1.0E1/, ETAMX3 /1.5E0/,
     4     ONEPSM /1.00001E0/, SHORT  /0.1E0/, THRESH /1.3E0/
      DATA ONE /1.0E0/, PT5 /0.5E0/, ZERO /0.0E0/
      KFLAG = 0
      TOLD = T
      FLOTN = FLOAT(N)
      IF (JSTART .GT. 0) GOTO 200
      IF (JSTART .NE. 0) GOTO 150
C-----------------------------------------------------------------------
-
C ON THE FIRST CALL, THE ORDER IS SET TO 1 AND THE INITIAL
C DERIVATIVES ARE CALCULATED.  ETAMAX IS THE MAXIMUM RATIO BY
C WHICH H CAN BE INCREASED IN A SINGLE STEP.  IT IS 1.E04 FOR THE
C FIRST STEP TO COMPENSATE FOR THE SMALL INITIAL H, THEN 10 FOR
C THE NEXT 10 STEPS, AND THEN 1.5 THEREAFTER.  IF A FAILURE
C OCCURS (IN CORRECTOR CONVERGENCE OR ERROR TEST), ETAMAX IS SET AT 1
C FOR THE NEXT INCREASE.  ETAMIN = .1 IS THE MINIMUM RATIO BY WHICH
C H CAN BE REDUCED ON ANY RETRY OF A STEP.
C-----------------------------------------------------------------------
-
      CALL DIFFUN (N, T, Y, SAVE1)
      DO 110 I = 1,N
 110    Y(I,2) = H*SAVE1(I)
      METH = MF/10
      MITER = MF - 10*METH
      MITER1 = MITER + 1
      MFOLD = MF
      NQ = 1
      L = 2
      TAU(1) = H
      PRL1 = ONE
      RC = ZERO
      ETAMAX = ETAMX1
      NQINDX = 2
C      For unknown reasons, these variables are sometimes
C      unitialized and cause the program to crash under
C      Microsoft FORTRAN, despite a BLOCK DATA initialization.
C     WRITE(99,789) NSTEP,NCSTEP
C789  FORMAT(' NSTEP=',I8,'   NCSTEP=',I8)
C               Cumulative Values
      NCSTEP=NCSTEP+NSTEP
      NCFE=NCFE+NFE
      NCJE=NCJE+NJE
      NSTEP = 0
      NSTEPJ = 0
```

```
      NFE = 1
      NJE = 0
      GOTO 200
C-----------------------------------------------------------------------
-
C IF THE USER HAS CHANGED H, THEN Y MUST BE RESCALED.  IF THE
C USER HAS CHANGED MITER, THEN NEWJ IS SET TO MITER TO FORCE
C THE PARTIAL DERIVATIVEES TO BE UPDATED, IF THEY ARE BEING USED.
C-----------------------------------------------------------------------
-
 150  IF (MF .EQ. MFOLD) GOTO 170
      MIO = MITER
      METH = MF/10
      MITER = MF - 10*METH
      MFOLD = MF
      IF (MITER .EQ. MIO) GOTO 170
      NEWJ = MITER
      MITER1 = MITER + 1
 170  IF (H .EQ. HOLD) GOTO 200
      ETA = H/HOLD
      H = HOLD
      IREDO = 3
      GOTO 185
  180 ETA = AMAX1(ETA,HMIN/ABS(H),ETAMIN)
  185 ETA = AMIN1(ETA,HMAX/ABS(H),ETAMAX)
      R1 = ONE
      DO 190 J = 2,L
        R1 = R1*ETA
        DO 190 I = 1,N
 190      Y(I,J) = Y(I,J)*R1
      H = H*ETA
      RC = RC*ETA
      IF (IREDO .EQ. 0) GOTO 690
C-----------------------------------------------------------------------
-
C THIS SECTION COMPUTES THE PREDICTED VALUES BY EFFECTIVELY
C MULTIPLYING THE Y ARRAY BY THE PASCAL TRIANGLE MATRIX.  THEN
C COSET IS CALLED TO OBTAIN EL, THE VECTOR OF COEFFICIENTS OF
C LENGTH NQ + 1.  RC IS THE RATIO OF NEW TO OLD VALUES OF THE
C COEFFICIENT H/EL(2).  WHEN RC DIFFERS FROM 1 BY MORE THAN
C DELRC, NEWJ IS SET TO MITER TO FORCE THE PARTIAL DERIVATIVES
C TO BE UPDATED, IF USED.  DELRC IS 0.3.  IN ANY CASE, THE PARTIAL
C DERIVATIVES ARE UPDATED AT LEAST EVERY 20-TH STEP.
C-----------------------------------------------------------------------
-
 200  T = T + H
      DO 210 J1 = 1,NQ
        DO 210 J2 = J1,NQ
          J = (NQ + J1) - J2
          DO 210 I = 1,N
 210        Y(I,J) = Y(I,J) + Y(I,J+1)
      CALL COSET
      BND = FLOTN*(TQ(4)*EPS)**2
      RL1 = ONE/EL(2)
      RC = RC*(RL1/PRL1)
      PRL1 = RL1
      IF (NSTEP .GE. NSTEPJ+ISTEPJ) NEWJ = MITER
      DRC = ABS(RC-ONE)
      IF (DRC .LE. DELRC) GOTO 215
      NEWJ = MITER
```

```
      CRATE = ONE
      RC = ONE
      GOTO 220
  215 IF ((MITER .NE. 0) .AND. (DRC .NE. ZERO)) CRATE = ONE
C-----------------------------------------------------------------------
-
C UP TO 3 CORRECTOR ITERATIONS ARE TAKEN.  A CONVERGENCE TEST IS MADE
C ON THE ROOT MEAN SQUARE NORM OF EACH CORRECTION, USING BND, WHICH
C IS DEPENDENT ON EPS.  THE SUM OF THE CORRECTIONS IS ACCUMULATED IN
C THE VECTOR ERROR.  THE Y ARRAY IS NOT ALTERED IN THE CORRECTOR
C LOOP.  THE UPDATED Y VECTOR IS STORED TEMPORARILY IN SAVE1.
C-----------------------------------------------------------------------
-
 220  DO 230 I = 1,N
 230    ERROR(I) = ZERO
      M = 0
      CALL DIFFUN (N, T, Y, SAVE2)
      NFE = NFE + 1
      IF (NEWJ .LE. 0) GOTO 290
C-----------------------------------------------------------------------
-
C IF INDICATED, THE MATRIX P = I - H*RL1*J IS REEVALUATED BEFORE
C STARTING THE CORRECTOR ITERATION.  NEWJ IS SET TO 0 AS AN
C INDICATOR THAT THIS HAS BEEN DONE.  IF MITER = 1 OR 2, P IS
C COMPUTED AND PROCESSED IN PSET.  IF MITER = 3, THE MATRIX  IS
C P = I - H*RL1*D, WHERE D IS A DIAGONAL MATRIX.  RL1 IS 1/EL(2).
C-----------------------------------------------------------------------
-
      NEWJ = 0
      RC = ONE
      NJE = NJE + 1
      NSTEPJ = NSTEP
      GOTO (250, 240, 260), MITER
 240  NFE = NFE + N
 250  CON = -H*RL1
      CALL PSET(Y, N0, CON, MITER, IER)
      IF (IER .NE. 0) GOTO 420
      GOTO 350
 260  R = RL1*SHORT
      DO 270 I = 1,N
 270    PW(I) = Y(I,1) + R*(H*SAVE2(I) - Y(I,2))
      CALL DIFFUN(N, T, PW, SAVE1)
      NFE = NFE + 1
      HRL1 = H*RL1
      DO 280 I = 1,N
        R0 = H*SAVE2(I) - Y(I,2)
        PW(I) = ONE
        D = SHORT*R0 - H*(SAVE1(I) - SAVE2(I))
        SAVE1(I) = ZERO
        IF (ABS(R0) .LT. UROUND*YMAX(I)) GOTO 280
        IF (ABS(D) .EQ. ZERO) GOTO 420
        PW(I) = SHORT*R0/D
        SAVE1(I) = PW(I)*RL1*R0
 280    CONTINUE
      GOTO 370
 290  GOTO (295, 350, 350, 310), MITER1
C-----------------------------------------------------------------------
-
C IN THE CASE OF FUNCTIONAL ITERATION, Y IS UPDATED DIRECTLY FROM
C THE RESULT OF THE LAST DIFFUN CALL.
```

```
C-----------------------------------------------------------------------
-
 295  D = ZERO
      DO 300 I = 1,N
C
C        WRITE(LOUT,999) I,YMAX(I)
C 999    FORMAT(1H 2X,'I=',I2,2X,'YMAX=',E12.5)
C
         R = RL1*(H*SAVE2(I) - Y(I,2))
C
C  The next line often gave an Undefined Real Error.
C  Let's try to fix it without changing anything else.  - DRW
C
C        D = D + ((R - ERROR(I))/YMAX(I))**2
C
         DTERM = ABS ( (R-ERROR(I)) / YMAX(I) )
         IF (DTERM.LT.1.E15) DTERM = DTERM*DTERM
         D = D + DTERM
         SAVE1(I) = Y(I,1) + R
 300     ERROR(I) = R
      GOTO 400
C-----------------------------------------------------------------------
-
C IN THE CASE OF A CHORD METHOD, THE RESIDUAL -G(Y SUB N(M))
C IS COMPUTED AND THE LINEAR SYSTEM WITH THAT AS RIGHT-HAND SIDE
C AND P AS COEFFICIENT MATRIX IS SOLVED, USING THE LU DECOMPOSITION
C OF P IF MITER = 1 OR 2.  IF MITER = 3 THE SCALAR H*RL1 IS UPDATED.
C-----------------------------------------------------------------------
-
 310  PHRL1 = HRL1
      HRL1 = H*RL1
      IF (HRL1 .EQ. PHRL1) GOTO 330
      R = HRL1/PHRL1
      DO 320 I = 1,N
        D = ONE - R*(ONE - ONE/PW(I))
        IF (ABS(D) .EQ. ZERO) GOTO 440
 320    PW(I) = ONE/D
 330  DO 340 I = 1,N
 340    SAVE1(I) = PW(I)*(RL1*H*SAVE2(I) - (RL1*Y(I,2) + ERROR(I)))
      GOTO 370
 350  DO 360 I = 1,N
 360    SAVE1(I) = RL1*H*SAVE2(I) - (RL1*Y(I,2) + ERROR(I))
      CALL SOL (N, N0, PW, SAVE1, IPIV)
 370  D = ZERO
      DO 380 I = 1,N
        ERROR(I) = ERROR(I) + SAVE1(I)
 380    SAVE1(I) = Y(I,1) + ERROR(I)
C-----------------------------------------------------------------------
-
C TEST FOR CONVERGENCE.  IF M .GT. 0, AN ESTIMATE OF THE SQUARE OF
C THE CONVERGENCE RATE CONSTANT IS STORED IN CRATE, AND THIS IS USED
C IN THE TEST.
C-----------------------------------------------------------------------
-
  400 IF (M .NE. 0) CRATE = AMAX1(CRDOWN*CRATE,D/D1)
      IF (D*AMIN1(ONE,CRATE) .LE. BND) GOTO 450
      D1 = D
      M = M + 1
      IF (M .EQ. MAXCOR) GOTO 410
      CALL DIFFUN (N, T, SAVE1, SAVE2)
```

```
      GOTO (295, 350, 350, 310), MITER1
C-----------------------------------------------------------------------
-
C THE CORRECTOR ITERATION FAILED TO CONVERGE IN 3 TRIES. IF PARTIAL
C DERIVATIVES ARE INVOLVED BUT ARE NOT UP TO DATE, THEY ARE
C REEVALUATED FOR THE NEXT TRY.  OTHERWISE THE Y ARRAY IS RESTORED
C TO ITS VALUES BEFORE PREDICTION, AND H IS REDUCED,
C IF POSSIBLE.  IF NOT, A NO-CONVERGENCE EXIT IS TAKEN.
C-----------------------------------------------------------------------
-
 410  NFE = NFE + MAXCOR - 1
      IF (NEWJ .EQ. -1) GOTO 440
 420  T = TOLD
      ETAMAX = ONE
      DO 430 J1 = 1,NQ
        DO 430 J2 = J1,NQ
          J = (NQ + J1) - J2
          DO 430 I = 1,N
 430        Y(I,J) = Y(I,J) - Y(I,J+1)
      IF (ABS(H) .LE. HMIN*ONEPSM) GOTO 680
      ETA = ETACF
      IREDO = 1
      GOTO 180
 440  NEWJ = MITER
      GOTO 220
C-----------------------------------------------------------------------
-
C THE CORRECTOR HAS CONVERGED.  NEWJ IS SET TO -1 IF PARTIAL
C DERIVATIVES WERE USED, TO SIGNAL THAT THEY MAY NEED UPDATING ON
C SUBSEQUENT STEPS.  THE ERROR TEST IS MADE AND CONTROL PASSES TO
C STATEMENT 500 IF IT FAILS.
C-----------------------------------------------------------------------
-
 450  IF (MITER .NE. 0) NEWJ = -1
      NFE = NFE + M
      D = ZERO
      DO 460 I = 1,N
 460    D = D + (ERROR(I)/YMAX(I))**2
      E = FLOTN*(TQ(2)*EPS)**2
      IF (D .GT. E) GOTO 500
C-----------------------------------------------------------------------
-
C AFTER A SUCCESSFUL STEP, THE Y ARRAY, TAU, NSTEP, AND NQINDX ARE
C UPDATED, AND A NEW VALUE OF H AT ORDER NQ IS COMPUTED.
C THE VECTOR TAU CONTAINS THE NQ + 1 MOST RECENT VALUES OF H.
C A CHANGE IN NQ UP OR DOWN BY 1 IS CONSIDERED IF NQINDX = 0.
C IF NQINDX = 1 AND NQ .LT. MAXDER, THEN ERROR IS SAVED
C FOR USE IN A POSSIBLE ORDER INCREASE ON THE NEXT STEP.
C A CHANGE IN H OR NQ IS MADE ONLY OF THE INCREASE IN H
C IS BY A FACTOR OF AT LEAST 1.3.
C IF NOT, NQINDX IS SET TO 2 TO PREVENT TESTING FOR THAT MANY
C STEPS.  IF NQ IS CHANGED, NQINDX IS SET TO NQ + 1 (NEW VALUE).
C-----------------------------------------------------------------------
-
      KFLAG = 0
      IREDO = 0
      NSTEP = NSTEP + 1
      HUSED = H
      NQUSED = NQ
      DO 470 IBACK = 1,NQ
```

```
        I = L - IBACK
 470    TAU(I+1) = TAU(I)
      TAU(1) = H
      DO 480 J = 1,L
        DO 480 I = 1,N
 480      Y(I,J) = Y(I,J) + ERROR(I)*EL(J)
      NQINDX = NQINDX - 1
      IF ((L .EQ. LMAX) .OR. (NQINDX .NE. 1)) GOTO 495
      DO 490 I = 1,N
 490    Y(I,LMAX) = ERROR(I)
      CONP = TQ(5)
 495  IF (ETAMAX .NE. ONE) GOTO 520
      IF (NQINDX .LT. 2) NQINDX = 2
      GOTO 690
C-----------------------------------------------------------------------
-
C THE ERROR TEST FAILED.  KFLAG KEEPS TRACK OF MULTIPLE FAILURES.
C T AND THE Y ARRAY ARE RESTORED TO THEIR PREVIOUS VALUES.  A NEW
C H FOR A RETRY OF THE STEP IS COMPUTED.  THE ORDER IS KEPT FIXED.
C-----------------------------------------------------------------------
-
 500  KFLAG = KFLAG - 1
      T = TOLD
      DO 510 J1 = 1,NQ
        DO 510 J2 = J1,NQ
          J = (NQ + J1) - J2
          DO 510 I = 1,N
 510        Y(I,J) = Y(I,J) - Y(I,J+1)
      NEWJ = MITER
      ETAMAX = ONE
      IF (ABS(H) .LE. HMIN*ONEPSM) GOTO 660
      IF (KFLAG .LE. KFC) GOTO 630
      IREDO = 2
C COMPUTE RATIO OF NEW H TO CURRENT H AT THE CURRENT ORDER. -----------
-
  520 FLOTL = FLOAT(L)
      ETAQ = ONE/((BIAS2*D/E)**(PT5/FLOTL) + ADDON)
      IF ((NQINDX .NE. 0) .OR. (KFLAG .NE. 0)) GOTO 580
      ETAQM1 = ZERO
      IF (NQ .EQ. 1) GOTO 540
C COMPUTE RATIO OF NEW H TO CURRENT H AT THE CURRENT ORDER LESS ONE. --
-
      D = ZERO
      DO 530 I = 1,N
 530    D = D + (Y(I,L)/YMAX(I))**2
      EDN = FLOTN*(TQ(1)*EPS)**2
      ETAQM1 = ONE/((BIAS1*D/EDN)**(PT5/(FLOTL - ONE)) + ADDON)
 540  ETAQP1 = ZERO
      IF (L .EQ. LMAX) GOTO 560
C COMPUTE RATIO OF NEW H TO CURRENT H AT CURRENT ORDER PLUS ONE. ------
-
      CNQUOT = (TQ(5)/CONP)*(H/TAU(2))**L
      D = ZERO
      DO 550 I = 1,N
 550    D = D + ((ERROR(I) - CNQUOT*Y(I,LMAX))/YMAX(I))**2
      EUP = FLOTN*(TQ(3)*EPS)**2
      ETAQP1 = ONE/((BIAS3*D/EUP)**(PT5/(FLOTL + ONE)) + ADDON)
 560  NQINDX = 2
      IF (ETAQ .GE. ETAQP1) GOTO 570
      IF (ETAQP1 .GT. ETAQM1) GOTO 600
```

```
      GOTO 590
 570  IF (ETAQ .LT. ETAQM1) GOTO 590
 580  IF ((ETAQ .LT. THRESH) .AND. (KFLAG .EQ. 0)) GOTO 690
      ETA = ETAQ
      IF ((KFLAG .LE. -2) .AND. (ETA .GT. ETAMXF)) ETA = ETAMXF
      GOTO 180
 590  IF (ETAQM1 .LT. THRESH) GOTO 690
      CALL ADJUST (Y, N0)
      L = NQ
      NQ = NQ - 1
      ETA = ETAQM1
      NQINDX = L
      GOTO 180
 600  IF (ETAQP1 .LT. THRESH) GOTO 690
      NQ = L
      ETA = ETAQP1
      L = L + 1
      DO 610 I = 1,N
 610    Y(I,L) = ZERO
      NQINDX = L
      GOTO 180
C-----------------------------------------------------------------------
-
C CONTROL REACHES THIS SECTION IF 3 OR MORE CONSECUTIVE FAILURES
C HAVE OCCURRED.  IT IS ASSUMED THAT THE ELEMENTS OF THE Y ARRAY
C HAVE ACCUMULATED ERRORS OF THE WRONG ORDER.  THE ORDER IS REDUCED
C BY ONE, IF POSSIBLE.  THEN H IS REDUCED BY A FACTOR OF 0.1 AND
C THE STEP IS RETRIED.  AFTER A TOTAL OF 7 CONSECUTIVE FAILURES,
C AN EXIT IS TAKEN WITH KFLAG = -2.
C-----------------------------------------------------------------------
-
 630  IF (KFLAG .EQ. KFH) GOTO 670
      IF (NQ .EQ. 1) GOTO 640
      ETA = ETAMIN
      CALL ADJUST (Y, N0)
      L = NQ
      NQ = NQ - 1
      NQINDX = L
      GOTO 180
  640 ETA = AMAX1(ETAMIN,HMIN/ABS(H))
      H = H*ETA
      CALL DIFFUN (N, T, Y, SAVE1)
      NFE = NFE + 1
      DO 650 I = 1,N
 650    Y(I,2) = H*SAVE1(I)
      NQINDX = 10
      GOTO 200
C-----------------------------------------------------------------------
-
C ALL RETURNS ARE MADE THROUGH THIS SECTION.  H IS SAVED IN HOLD
C TO ALLOW THE CALLER TO CHANGE H ON THE NEXT STEP.
C-----------------------------------------------------------------------
-
 660  KFLAG = -1
      GOTO 700
 670  KFLAG = -2
      GOTO 700
 680  KFLAG = -3
      GOTO 700
 690  ETAMAX = ETAMX3
```

```
      IF (NSTEP .LE. 10) ETAMAX = ETAMX2
 700  HOLD = H
      JSTART = NQ
      RETURN
      END
C
C=======================================================================
=
C
      SUBROUTINE COSET
C-----------------------------------------------------------------------
-
C COSET IS CALLED BY TSTEP AND SETS COEFFICIENTS FOR USE THERE.
C
C FOR EACH ORDER NQ, THE COEFFICIENTS IN EL ARE CALCULATED BY USE OF
C  THE GENERATING POLYNOMIAL LAMBDA(X), WITH COEFFICIENTS EL(I):
C      LAMBDA(X) = EL(1) + EL(2)*X + ... + EL(NQ+1)*(X**NQ).
C FOR THE BACKWARD DIFFERENTIATION FORMULAS,
C                          NQ
C      LAMBDA(X) = PRODUCT (1 + X/XI(I) ) .
C                        I = 1
C FOR THE ADAMS FORMULAS,
C                                  NQ-1
C      (D/DX) LAMBDA(X) = C * PRODUCT (1 + X/XI(I) ) ,
C                                   I = 1
C      LAMBDA(-1) = 0,    LAMBDA(0) = 1,
C WHERE C IS A NORMALIZATION CONSTANT.
C IN BOTH CASES, XI(I) IS DEFINED BY
C      H*XI(I) = T SUB N  -  T SUB (N-I)
C              = H + TAU(1) + TAU(2) + ... TAU(I-1).
C
C COSET ALSO SETS MAXDER, THE MAXIMUM ORDER OF THE FORMULAS
C AVAILABLE. CURRENTLY THIS IS 5 FOR THE BACKWARD DIFFERENTIATION
C FORMULAS, AND 12 FOR THE ADAMS FORMULAS.  TO USE DIFFERENT
C VALUES (.LE. 13),  CHANGE THE NUMBERS IN STATEMENTS 1 AND 2 BELOW.
C
C IN ADDITION TO VARIABLES DESCRIBED PREVIOUSLY, COMMUNICATION
C WITH COSET USES THE FOLLOWING..
C   TAU    = A VECTOR OF LENGTH 13 CONTAINING THE PAST NQ VALUES
C            OF H.
C   EL     = A VECTOR OF LENGTH 13 IN WHICH COSET STORES THE
C            COEFFICIENTS FOR THE CORRECTOR FORMULA.
C   TQ     = A VECTOR OF LENGTH 5 IN WHICH COSET STORES CONSTANTS
C            USED FOR THE CONVERGENCE TEST, THE ERROR TEST, AND
C            SELECTION OF H AT A NEW ORDER.
C   LMAX   = MAXDER + 1, WHERE MAXDER IS THE MAXIMUM ORDER
C            AVAILABLE.  LMAX IS THE MAXIMUM NUMBER OF COLUMNS
C            OF THE Y ARRAY TO BE USED.
C   METH   = THE BASIC METHOD INDICATOR.
C   NQ     = THE CURRENT ORDER.
C   L      = NQ + 1, THE LENGTH OF THE VECTOR STORED IN EL, AND
C            THE NUMBER OF COLUMNS OF THE Y ARRAY BEING USED.
C   NQINDX = A COUNTER CONTROLLING THE FREQUENCY OF ORDER CHANGES.
C            AN ORDER CHANGE IS ABOUT TO BE CONSIDERED IF
C            NQINDX = 1.
C-----------------------------------------------------------------------
-
C$ THIS IS THE SINGLE PRECISION VERSION OF SUBROUTINE COSET.
C-----------------------------------------------------------------------
-
```

```
C CAUTION:  NOT ALL MEMBERS OF EPCOM1 ARE USED IN THIS SUBROUTINE.
C-----------------------------------------------------------------------
-
      INTEGER JSTART, KFLAG, L, LMAX, METH, MF, N, NQ, NQINDX
      INTEGER I, IBACK, J, JP1, MAXDER, LMAXN, NQM1
      REAL EL, EPS, H, HAX, HMIN, SS, T, TAU, TQ,
     1     UROUND
      REAL AHDSS, CNQM1, CSUM, ELP, EM, EM0, FLOTI,
     1     FLOTL, FLOTNQ, HSUM, HSUM1, PROD, RXI, S, XI
      REAL CORTES
      REAL ONE, SIX, TWO, ZERO
C* Multiple Declaration of JSTART,KFLAG,L,METH,MF,NQ,NQINDX, fixed - DR
W
      DIMENSION EM(13)
C
      COMMON /EPCOM1/ T,H,HMIN,HMAX,EPS,SS,UROUND,N,MF,KFLAG,JSTART
      COMMON /EPCM10/ TAU(13),EL(13),TQ(5),LMAX,METH,NQ,L,NQINDX
      DATA CORTES /0.1E0/
      DATA ONE  /1.0E0/, SIX /6.0E0/, TWO /2.0E0/, ZERO /0.0E0/
      AHDSS = ONE
      IF (SS .NE. ZERO) AHDSS = ABS(H)/SS
      FLOTL = FLOAT(L)
      NQM1 = NQ - 1
      GOTO (1, 2), METH
 1    MAXDER = 12
      GOTO 100
C
 2    MAXDER = 5
      GOTO 200
C
 100  IF (NQ .NE. 1) GOTO 110
      EL(1) = ONE
      EL(2) = ONE
      TQ(1) = ONE
      TQ(2) = TWO*AHDSS
      TQ(3) = SIX*TQ(2)
      TQ(5) = ONE
      GOTO 300
 110  HSUM = H
      EM(1) = ONE
      FLOTNQ = FLOTL - ONE
      DO 115 I = 2,L
 115    EM(I) = ZERO
      DO 150 J = 1,NQM1
        IF ((J .NE. NQM1) .OR. (NQINDX .NE. 1)) GOTO 130
        S = ONE
        CSUM = ZERO
        DO 120 I = 1,NQM1
          CSUM = CSUM + S*EM(I)/FLOAT(I+1)
 120      S = -S
        TQ(1) = AHDSS*EM(NQM1)/(FLOTNQ*CSUM)
 130    RXI = H/HSUM
        DO 140 IBACK = 1,J
          I = (J + 2) - IBACK
 140      EM(I) = EM(I) + EM(I-1)*RXI
 150    HSUM = HSUM + TAU(J)
C COMPUTE INTEGRAL FROM -1 TO 0 OF POLYNOMIAL AND OF X TIMES IT. ------
-
      S = ONE
      EM0 = ZERO
```

```
      CSUM = ZERO
      DO 160 I = 1,NQ
        FLOTI = FLOAT(I)
        EM0 = EM0 + S*EM(I)/FLOTI
        CSUM = CSUM + S*EM(I)/(FLOTI+1)
 160    S = -S
C IN EL, FORM COEFFICIENTS OF NORMALIZED INTEGRATED POLYNOMIAL. -------
-
      S = ONE/EM0
      EL(1) = ONE
      DO 170 I = 1,NQ
  170   EL(I+1) = S*EM(I)/FLOAT(I)
      XI = HSUM/H
      TQ(2) = AHDSS*XI*EM0/CSUM
      TQ(5) = XI/EL(L)
      IF (NQINDX .NE. 1) GOTO 300
C FOR HIGHER ORDER CONTROL CONSTANT, MULTIPLY POLYNOMIAL BY 1+X/XI(Q).
-
      RXI = ONE/XI
      DO 180 IBACK = 1,NQ
        I = (L + 1) - IBACK
 180    EM(I) = EM(I) + EM(I-1)*RXI
C COMPUTE INTEGRAL OF POLYNOMIAL. -------------------------------------
-
      S = ONE
      CSUM = ZERO
      DO 190 I = 1,L
      CSUM = CSUM + S*EM(I)/FLOAT(I+1)
 190    S = -S
      TQ(3) = AHDSS*FLOTL*EM0/CSUM
      GOTO 300
C
 200  DO 210 I = 3,L
 210    EL(I) = ZERO
      EL(1) = ONE
      EL(2) = ONE
      HSUM = H
      HSUM1 = ZERO
      PROD = ONE
      RXI = ONE
      IF (NQ .EQ. 1) GOTO 240
      DO 230 J = 1,NQM1
C IN EL, CONSTRUCT COEFFICIENTS OF (1+X/XI(1))*...*(1+X/XI(J+1)). -----
-
        HSUM = HSUM + TAU(J)
        HSUM1 = HSUM1 + TAU(J)
        PROD = PROD*(HSUM/HSUM1)
        RXI = H/HSUM
        JP1 = J + 1
        DO 220 IBACK = 1,JP1
          I = (J + 3) - IBACK
 220      EL(I) = EL(I) + EL(I-1)*RXI
 230    CONTINUE
 240  TQ(2) = AHDSS*EL(2)*(ONE + PROD)
      TQ(5) = (ONE + PROD)/EL(L)
      IF (NQINDX .NE. 1) GOTO 300
      CNQM1 = RXI/EL(L)
      ELP = EL(2) - RXI
      TQ(1) = AHDSS*ELP/CNQM1
      HSUM = HSUM + TAU(NQ)
```

```
      RXI = H/HSUM
      ELP = EL(2) + RXI
      TQ(3) = AHDSS*ELP*RXI*(ONE + PROD)*(FLOTL + ONE)
 300  TQ(4) = CORTES*TQ(2)
      LMAX = MAXDER + 1
      RETURN
      END
C
C=======================================================================
=
C
      SUBROUTINE ADJUST (Y, N0)
C-----------------------------------------------------------------------
-
C THIS SUBROUTINE ADJUSTS THE Y ARRAY ON REDUCTION OF ORDER.
C SEE REFERENCE 1 FOR DETAILS.
C-----------------------------------------------------------------------
-
C$ THIS IS THE SINGLE PRECISION VERSION OF SUBROUTINE ADJUST.
C-----------------------------------------------------------------------
-
C CAUTION:  NOT ALL MEMBERS OF EPCOM1 ARE USED IN THIS SUBROUTINE.
C-----------------------------------------------------------------------
-
      INTEGER N0
      INTEGER JSTART, KFLAG, L, LMAX, METH, MF, N, NQ, NQINDX
      INTEGER I, IBACK, J, JP1, NQM1, NQM2
      REAL Y
      REAL EL, EPS, H, HMAX, HMIN, SS, T, TAU, TQ, UROUND
      REAL HSUM, XI
      REAL ONE, ZERO
      DIMENSION Y(N0,13)
C
      COMMON /EPCOM1/ T,H,HMIN,HMAX,EPS,SS,UROUND,N,MF,KFLAG,JSTART
      COMMON /EPCM10/ TAU(13),EL(13),TQ(5),LMAX,METH,NQ,L,NQINDX
      DATA ONE /1.0E0/, ZERO /0.0E0/
      IF (NQ .EQ. 2) RETURN
      NQM1 = NQ - 1
      NQM2 = NQ - 2
      GOTO (100, 200), METH
C
 100  DO 110 J = 1,LMAX
 110    EL(J) = ZERO
      EL(2) = ONE
      HSUM = ZERO
      DO 130 J = 1,NQM2
C CONSTRUCT COEFFICIENTS OF X*(X+XI(1))*...*(X+XI(J)). ----------------
-
        HSUM = HSUM + TAU(J)
        XI = HSUM/H
        JP1 = J + 1
        DO 120 IBACK = 1,JP1
          I = (J + 3) - IBACK
 120      EL(I) = EL(I)*XI + EL(I-1)
 130    CONTINUE
C CONSTRUCT COEFFICIENTS OF INTEGRATED POLYNOMIAL. --------------------
-
      DO 140 J = 2,NQM1
  140   EL(J+1) = FLOAT(NQ)*EL(J)/FLOAT(J)
      GOTO 300
```

```
C
 200  DO 210 J = 1,LMAX
 210    EL(J) = ZERO
      EL(3) = ONE
      HSUM = ZERO
      DO 230 J = 1,NQM2
C CONSTRUCT COEFFICIENTS OF X*X*(X+XI(1))*...*(X+XI(J)). --------------
-
        HSUM = HSUM + TAU(J)
        XI = HSUM/H
        JP1 = J + 1
        DO 220 IBACK = 1,JP1
          I = (J + 4) - IBACK
 220      EL(I) = EL(I)*XI + EL(I-1)
 230    CONTINUE
C
C SUBTRACT CORRECTION TERMS FROM Y ARRAY. ----------------------------
-
 300  DO 320 J = 3,NQ
        DO 310 I = 1,N
 310      Y(I,J) = Y(I,J) - Y(I,L)*EL(J)
 320    CONTINUE
      RETURN
      END
C
C=======================================================================
=
C
      SUBROUTINE PSET (Y,N0,CON,MITER,IER)
C-----------------------------------------------------------------------
-
C PSET IS CALLED BY TSTEP TO COMPUTE AND TO PROCESS THE MATRIX
C P = I - (H/EL(2))*J, WHERE J IS AN APPROXIMATION TO THE
C JACOBIAN.  J IS COMPUTED BY EITHER THE USER SUPPLIED
C SUBROUTINE PEDERV, WHEN MITER = 1, OR BY FINITE DIFFERENCES,
C WHEN MITER = 2.  J IS STORED IN PW AND REPLACED BY P, USING
C CON = -H/EL(2).  THEN P IS SUBJECTED TO AN LU DECOMPOSITION
C FOR LATER SOLUTION OF LINEAR ALGEBRAIC SYSTEMS WITH P AS THE
C COEFFICIENT MATRIX.
C
C IN ADDITION TO VARIABLES DESCRIBED PREVIOUSLY, COMMUNICATION
C WITH PSET USES THE FOLLOWING..
C   EPSJ = SQRT(UROUND), USED IN THE NUMERICAL JACOBIAN INCREMENTS.
C   NSQ  = N0**2.
C-----------------------------------------------------------------------
-
C CAUTION:  NOT ALL EPCOM1 VARIABLES ARE USED INTHIS SUBROUTINE.
C-----------------------------------------------------------------------
-
C$ THIS IS THE SINGLE PRECISION VERSION OF SUBROUTINE PSET.
C-----------------------------------------------------------------------
-
      PARAMETER ( NMAX =120 )
      PARAMETER ( NMAXSQ = NMAX*NMAX )
      INTEGER IER, MITER, N0
      INTEGER IPIV, JSTART, KFLAG, MF, N, NSQ
      INTEGER I, J, J1
      REAL CON, Y
      REAL EPS, EPSJ, H, HMAX, HMIN, PW, SAVE1, SAVE2,
     1     SS, T, UROUND, YMAX
```

```
      REAL D, R, R0, YJ
      REAL ONE, REP, ZERO
C* Multiple Declaration of IER, T, N fixed - DRW
      DIMENSION Y(N0,1)
C
      COMMON /EPCOM1/ T,H,HMIN,HMAX,EPS,SS,UROUND,N,MF,KFLAG,JSTART
      COMMON /EPCOM2/ YMAX(NMAX)
      COMMON /EPCOM4/ SAVE1(NMAX)
      COMMON /EPCOM5/ SAVE2(NMAX)
      COMMON /EPCOM6/ PW(NMAXSQ)
      COMMON /EPCOM7/ IPIV(NMAX)
      COMMON /EPCOM8/ EPSJ,NSQ
      DATA ONE /1.0E0/, REP /1.0E-3/, ZERO /0.0E0/
      IF (MITER .EQ. 2) GOTO 20
C IF MITER = 1, CALL PEDERV AND MULTIPLY BY A SCALAR.  ----------------
-
      CALL PEDERV (N, T, Y, PW, N0)
      DO 10 I = 1,NSQ
 10     PW(I) = PW(I)*CON
      GOTO 60
C IF MITER = 2, MAKE N CALLS TO DIFFUN TO APPROXIMATE J. --------------
-
 20   D = ZERO
      DO 30 I = 1,N
 30     D = D + SAVE2(I)**2
      R0 = ABS(H)*SQRT(D)*UROUND/REP
      J1 = 0
      DO 50 J = 1,N
        YJ = Y(J,1)
        R = EPSJ*YMAX(J)
        R = AMAX1(R,R0)
        Y(J,1) = Y(J,1) + R
        D = CON/R
        CALL DIFFUN (N, T, Y, SAVE1)
        DO 40 I = 1,N
 40       PW(I+J1) = (SAVE1(I) - SAVE2(I))*D
        Y(J,1) = YJ
        J1 = J1 + N0
 50     CONTINUE
C ADD ON THE IDENTITY MATRIX.  ---------------------------------------
-
 60   J = 1
      DO 70 I = 1,N
        PW(J) = PW(J) + ONE
 70     J = J + (N0 + 1)
C GET LU DECOMPOSITION OF P. -----------------------------------------
-
      CALL DEC (N, N0, PW, IPIV, IER)
      RETURN
      END
C
C=======================================================================
=
C
      SUBROUTINE DEC (N, NDIM, A, IP, IER)
C-----------------------------------------------------------------------
-
C MATRIX TRIANGULARIZATION BY GAUSSIAN ELIMINATION.
C INPUT..
C    N = ORDER OF MATRIX.
```

```
C     NDIM = DECLARED DIMENSION OF ARRAY  A .
C     A = MATRIX TO BE TRIANGULARIZED.
C OUTPUT..
C     A(I,J), I.LE.J = UPPER TRIANGULAR FACTOR, U .
C     A(I,J), I.GT.J = MULTIPLIERS = LOWER TRIANGULAR FACTOR, I - L.
C     IP(K), K.LT.N = INDEX OF K-TH PIVOT ROW.
C     IP(N) = (-1)**(NUMBER OF INTERCHANGES) OR O .
C     IER = 0 IF A NONSINGULAR, OR K IF A FOUND TO BE
C           SINGULAR AT STAGE K.
C USE  SOL  TO OBTAIN SOLUTION OF LINEAR SYSTEM.
C DETERM(A) = IP(N)*A(1,1)*A(2,2)*...*A(N,N).
C IF IP(N)=0, A IS SINGULAR, SOL WILL DIVIDE BY ZERO.
C INTERCHANGES FINISHED IN U , ONLY PARTLY IN L .
C
C REFERENCE..
C C. B. MOLER, ALGORITHM 423, LINEAR EQUATION SOLVER,
C COMM. ASSOC. COMPUT. MACH., 15 (1972), P. 274.
C---------------------------------------------------------------------
-
C$ THIS IS THE SINGLE PRECISION VERSION OF SUBROUTINE DEC.
C---------------------------------------------------------------------
-
      INTEGER IER, IP, N, NDIM
      INTEGER I, J, K, KP1, M, NM1
      REAL A
      REAL T
      REAL ONE, ZERO
      DIMENSION A(NDIM,N),IP(N)
      DATA ONE /1.0E0/, ZERO /0.0E0/
      IER = 0
      IP(N) = 1
      IF (N .EQ. 1) GOTO 70
      NM1 = N - 1
      DO 60 K = 1,NM1
        KP1 = K + 1
        M = K
        DO 10 I = KP1,N
 10       IF (ABS(A(I,K)) .GT. ABS(A(M,K))) M = I
        IP(K) = M
        T = A(M,K)
        IF (M .EQ. K) GOTO 20
        IP(N) = -IP(N)
        A(M,K) = A(K,K)
        A(K,K) = T
 20     IF (T .EQ. ZERO) GOTO 80
        T = ONE/T
        DO 30 I = KP1,N
 30       A(I,K) = -A(I,K)*T
        DO 50 J = KP1,N
          T = A(M,J)
          A(M,J) = A(K,J)
          A(K,J) = T
          IF (T .EQ. ZERO) GOTO 50
          DO 40 I = KP1,N
 40         A(I,J) = A(I,J) + A(I,K)*T
 50       CONTINUE
 60     CONTINUE
 70   K = N
      IF (A(N,N) .EQ. ZERO) GOTO 80
      RETURN
```

```
 80    IER = K
       IP(N) = 0
       RETURN
       END
C
C=====================================================================
=
C
       SUBROUTINE SOL (N, NDIM, A, B, IP)
C---------------------------------------------------------------------
-
C SOLUTION OF LINEAR SYSTEM, A*X = B .
C INPUT..
C    N = ORDER OF MATRIX.
C    NDIM = DECLARED DIMENSION OF ARRAY  A .
C    A = TRIANGULARIZED MATRIX OBTAINED FROM DEC.
C    B = RIGHT HAND SIDE VECTOR.
C    IP = PIVOT VECTOR OBTAINED FROM DEC.
C DO NOT USE IF DEC HAS SET IER .NE. 0.
C OUTPUT..
C    B = SOLUTION VECTOR, X .
C---------------------------------------------------------------------
-
C$ THIS IS THE SINGLE PRECISION VERSION OF SUBROUTINE SOL.
C---------------------------------------------------------------------
-
       INTEGER IP, N, NDIM
       INTEGER I, K, KB, KM1, KP1, M, NM1
       REAL A, B
       REAL T
       DIMENSION A(NDIM, N), B(N), IP(N)
C
       IF (N .EQ. 1) GOTO 50
       NM1 = N - 1
       DO 20 K = 1,NM1
         KP1 = K + 1
         M = IP(K)
         T = B(M)
         B(M) = B(K)
         B(K) = T
         DO 10 I = KP1,N
 10        B(I) = B(I) + A(I,K)*T
 20      CONTINUE
       DO 40 KB = 1,NM1
         KM1 = N - KB
         K = KM1 + 1
         B(K) = B(K)/A(K,K)
         T = -B(K)
         DO 30 I = 1,KM1
 30        B(I) = B(I) + A(I,K)*T
 40      CONTINUE
 50    B(1) = B(1)/A(1,1)
       RETURN
       END
C
C=====================================================================
=
C
       BLOCK DATA
       COMMON /EPCOM9/ HUSED,NQUSED,NSTEP,NFE,NJE
```

```
COMMON /EPCO99/ NCSTEP,NCFE,NCJE
COMMON /EPCOMR/ NRMIN,NRMAX
COMMON /EPCOMY/ YMIN,HMAXMX
DATA HUSED,NQUSED,NSTEP,NFE,NJE / 0.,0,0,0,0 /
DATA NCSTEP,NCFE,NCJE / 0,0,0 /
DATA NRMIN,NRMAX / 1,500 /
DATA YMIN,HMAXMX / 1.E-20,1.E6 /
END
```

PD0

```
C=======================================================================

      SUBROUTINE PEDERV(N,T,Y,PD,N0)

C This is presently intended to be a dummy subroutine in this applicati
on
C Used only in EPISODE versions of MAEROS ; not adequate if MF=11 or 21

      WRITE(*,10) T
   10 FORMAT(/5X,' Error -- PEDERV was called at time ',1PE10.2/)
      WRITE(*,20)
   20 FORMAT(' Hence MITER of MF was set equal to one'/)
      STOP 'STOP on bad MF to DRIVES for Dummy PEDERV'
      END
```